Thesis presented to the Instituto Tecnológico de Aeronáutica, in partial fulfillment of the requirements for the degree of Doctor of Science in the Graduate Program of Physics, Field of Atomic and Molecular Physics.

Julio Cesar Verli Chagas

ELECTRONIC STRUCTURE OF CONJUGATED ORGANIC MOLECULES: FROM AROMATICITY TO EXCITED-STATE DYNAMICS

Thesis approved in its final version by signatories below:

Prof. Dr. Francisco Bolivar Correto Machado

Advisor

Dr. Hans Lischka

Co-advisor

Campo Montenegro
São José dos Campos, SP - Brazil
2025

Cataloging-in Publication Data
Documentation and Information Division

Chagas, Julio Cesar Verli
Electronic Structure of Conjugated Organic Molecules: From Aromaticity to Excited-State Dynamics / Julio Cesar Verli Chagas.
São José dos Campos, 2025.
204f.

Thesis of Doctor of Science – Course of Physics. Area of Atomic and Molecular Physics – Instituto Tecnológico de Aeronáutica, 2025. Advisor: Prof. Dr. Francisco Bolivar Correto Machado. Co-advisor: Dr. Hans Lischka.

1. Electronic structure of molecules. 2. Atomic and molecular physics. 3. Computational and theoretical chemistry. I. Instituto Tecnológico de Aeronáutica. II. Title.

BIBLIOGRAPHIC REFERENCE

CHAGAS, Julio Cesar Verli. **Electronic Structure of Conjugated Organic Molecules: From Aromaticity to Excited-State Dynamics**. 2025. 204f. Thesis of Doctor of Science – Instituto Tecnológico de Aeronáutica, São José dos Campos.

CESSION OF RIGHTS

AUTHOR'S NAME: Julio Cesar Verli Chagas
PUBLICATION TITLE: Electronic Structure of Conjugated Organic Molecules: From Aromaticity to Excited-State Dynamics.
PUBLICATION KIND/YEAR: Thesis / 2025

Julio Cesar Verli Chagas
Rua Charles Diamond, 110
12221-150 – São José dos Campos–SP

ELECTRONIC STRUCTURE OF CONJUGATED ORGANIC MOLECULES: FROM AROMATICITY TO EXCITED-STATE DYNAMICS

Julio Cesar Verli Chagas

Thesis Committee Composition:

Prof. Dr.	Marcelo Marques	Chair	-	ITA
Prof. Dr.	Francisco Bolivar Correto Machado	Advisor	-	ITA
Dr.	Orlando Roberto Neto		-	IEAv
Dr.	Antonio Gustavo Sampaio de Oliveira Filho		-	USP
Dr.	Roberto Rivelino de Melo Moreno		-	UFBA

ITA

Acknowledgments

I would like to express my gratitude to my advisors, Prof. Dr. Francisco Bolivar Correto Machado and Prof. Dr. Hans Liscka, for their guidance throughout this journey. Their expertise, patience, and dedication not only shaped this thesis but also had a profound influence on my development as a researcher.

I am also thankful to all collaborators who contributed to the development and publication of the results presented in this thesis. Their insight and teamwork were essential to the success of this research.

I gratefully acknowledge the Instituto Tecnológico de Aeronáutica (ITA), my home institution, and the conferrer of this degree. I also extend my sincere gratitude to Texas Tech University (TTU) for hosting me during a six-month research exchange.

This work was made possible thanks to the financial support of the Brazilian funding agencies—Conselho Nacional de Desenvolvimento Científico e Tecnológico (CNPq), Fundação de Amparo à Pesquisa do Estado de São Paulo (FAPESP), and Coordenação de Aperfeiçoamento de Pessoal de Nível Superior (CAPES), including its institutional internationalization program (CAPES-PrInt).

I extend my appreciation to my family and friends for their unwavering encouragement and support.

To all who contributed, directly or indirectly, to this dissertation: thank you.

Abstract

This thesis presents a comprehensive investigation into the electronic structure of conjugated organic molecules, spanning from aromaticity in benzene derivatives to the complex excited-state dynamics of linear all-trans polyenes. In the first study, a detailed multicomponent analysis reveals how substituents influence the aromatic character of mono- and disubstituted benzene derivatives. The findings provide the reader with a conceptual toolkit to modulate aromaticity. We show that appropriate π-electron-donating and π-electron-accepting substituents, with suitable size and symmetry, can interact with the ring's π-system and significantly affect π-electron delocalization. The second and third studies focus on the spectroscopic properties of linear polyenes—structures that form the backbone of many chromophores. Particular attention is given to the covalent $2^1A_g^-$ and ionic $1^1B_u^+$ excited states. Using high-level multireference methods, we demonstrate in the second study that while nondynamic correlation is sufficient to describe the covalent state, accurately treating the ionic state requires addressing basis set effects, size-extensivity errors, and, most critically, σ–π electron correlation. This analysis offers the reader a clear prescription for the appropriate multireference treatment of covalent and ionic excited states. In the third study, analytic gradients based on a multireference wavefunction are employed to compute refined adiabatic transition and emission energies, allowing close comparison with experimental results. The insights deepen our understanding of the intricate electronic landscape of polyenes and underscore the challenges involved in bridging theoretical predictions with experimental spectroscopy. Taken together, the results offer detailed insight into how electronic structure evolves across different conjugated systems and electronic states, thereby fulfilling the central aim of this work: to explore the Electronic Structure of Conjugated Organic Molecules: From Aromaticity to Excited-State Dynamics.

Contents

1 Introduction

This thesis is composed of three main contributions in the fields of theoretical chemistry and molecular physics, with a focus on molecular electronic structure. The first contribution, whose full text can be found in Reference (1), presents a detailed multi-component analysis of aromaticity in benzene derivatives. In this work, we address how and why certain substituents are capable of affecting π-electron delocalization in a benzenoid ring. The insights from this study have supported, for example, the design of molecules with tailored properties by experimentalists seeking to tune conjugation through substitution.[2]

The second contribution investigates the electronic spectra of all-*trans* polyenes—linear systems that form the backbone of many chromophores, which inherit their spectroscopic properties from the underlying polyene structure. The complete text for this contribution is available in Reference (3). Here, we identify the key electronic effects that must be considered to properly describe the lowest excited states of these systems, with a particular focus on the ionic state, whose accurate characterization remains challenging even for advanced theoretical methods.

Building on the findings from Reference (3), the third contribution determines the minima of the potential energy surfaces for the ground state and the two lowest excited states of polyenes using analytic energy gradients based on a multireference wavefunction. This enables accurate calculations of adiabatic transitions and emission energies, offering valuable insights into the spectroscopic behavior of these systems. Together, the second and third contributions deepen our understanding of the intricate electronic landscape of polyenes and emphasize important considerations when bridging theoretical predictions with experimental spectroscopy.

In Chapter 2, a brief literature review is provided for each of these contributions individually. Chapter 3 introduces the theoretical framework underlying the computational methods employed. Chapters 4, 5, and 6 present the results and discussions corresponding to the three main contributions. Chapter 7 concludes the thesis with a summary of the main findings.

Bibliography

1 CHAGAS, Julio C. V. et al. A multi-descriptor analysis of substituent effects on the structure and aromaticity of benzene derivatives: π-Conjugation versus charge effects. **Journal of Computational Chemistry**, v. 45, n. 12, p. 863–877, May 2024.

2 HAN, Bo et al. Structure-performance relationship and molecular structure optimization design of acid phosphate ester extractants. **Chemical Engineering Journal**, v. 502, p. 157860, Dec. 2024.

3 CHAGAS, Julio C. V. et al. Low-lying excited states of linear all-trans polyenes: the σ–π electron correlation and the description of ionic states. **Physical Chemistry Chemical Physics**, v. 27, n. 15, p. 7916–7928, 2025.

2 Literature Review

2.1 A Multi-Descriptor Analysis of Substituent Effects on the Structure and Aromaticity of Benzene Derivatives: π-Conjugation vs. Charge Effects

Over the years, substituent effects have been extensively investigated in various classes of molecules, both experimentally and theoretically. Introducing appropriate electronic controller groups allows the adjustment of the properties and consequent extension of the range of possible applications of several materials. This strategy has wide applications in several research fields and has enabled, for example, molecular light emitters utilizing a simple benzene core,[1] the design of singlet fission materials,[2,3] and thermodynamic and kinetic stabilization of polycyclic aromatic hydrocarbons (PAHs).[4–7]

As widely known, aromaticity is a multidimensional phenomenon closely related to π-electron delocalization. The most common characteristics of aromatic compounds involve the decrease of bond length alternation, increased chemical stability, and unique magnetic properties. The benzene ring has been generally accepted as an archetype of aromatic systems.[8] The effect of substitution(s) on the structure and properties of benzene is one of the subjects that has received special attention. In particular, one of the most prominent subjects is the relationship between the effect of substituents and the aromaticity of benzene in the ground[9–14] and excited states.[15–17] With a few exceptions, which are the subject of this work, the π-electron delocalization is typically only slightly influenced by substituents attached to the benzene ring,[10,13] as briefly summarized below.

Krygowski and coworkers[9] studied the relation between the substituent effect and aromaticity by varying the electron donating/accepting character of substituents for 18 monosubstituted benzene derivatives. The changes of π-electron delocalization of the benzene fragment were estimated by the use of aromatic stabilization energy (ASE),[18–22] para-delocalization index (PDI),[23] harmonic oscillator model of aromaticity (HOMA),[24–27] nucleus-independent chemical shift (NICS),[28] and their variants.[29–32] Despite the substantial variation in the nature of the substituent (from strongly electron-donating to strongly

electron-accepting), no dramatic changes in the π-electron structure of the benzene ring are observed, i.e., comparing the modified systems to benzene, the aromaticity indices remain almost unchanged. In another work, Krygowski and coworkers investigated the geometry patterns of benzene derivatives.[10,33] The changes in π-electron delocalization were estimated in terms of the dependence between the geometry-based index Harmonic Oscillator Model of Aromaticity (HOMA) and *ipso* bond angle α, shown to suffer the largest variance in monosubstituted benzene derivatives.[34] In general, changes in HOMA values were almost negligible, remaining close to 0.9, the value found for the pristine benzene ring. However, significant deviations were found for substituents such as CH_2^+, CH_2^-, and O^+, which are known for their π-electron donating or accepting properties.

The slight variation in indices of aromaticity indicates a strong resistance of the system against changes in π-electron delocalization caused by the substituent, which is consistent with the tendency of the π-electron system in the benzene ring to maintain its structural integrity throughout chemical reactions, favoring substitution over addition.[10,13] However, some substituted cyclic π-electron systems involving π-electron donating and π-electron accepting substituents exhibit substantial changes in the cyclic π-electron delocalization when compared to benzene.

Numerous studies have been conducted on the relation between substituent effect and aromaticity; however, they primarily concentrate on substituents with similar electronic structures in terms of ring-substituent bonding or use a limited set of properties to characterize the π-electron delocalization. In this work, we study the effect of neutral, anionic, and cationic substituents that exhibit high π-electron donor or acceptor character. The effects of the substituent on the π-electron delocalization are assessed through a wide range of descriptors based on structural, vibrational, magnetic, and electronic properties using single-reference DFT and multireference CASSCF/MRCI approaches. We describe different aspects of aromaticity and how they provide complementary information regarding the electronic structure and reactivity of the systems.

2.2 Low-lying excited states of linear all-*trans* polyenes: the σ-π electron correlation and the description of ionic states

The study of linear all-trans polyenes has a long-standing tradition due to their distinctive spectral properties, which arise from the structure of their low-lying excited-state manifold. Polyenes serve as valuable models for chromophores in biological systems, such as carotenoids, which are crucial in photosynthetic processes. These processes include

light-harvesting, particularly in the blue region of the visible spectrum,[35,36] and photoprotection through dissipation of excitation energy into heat.[37–39] Moreover, polyenes constitute a traditional set of molecules for testing theoretical concepts and benchmarking electronic structure methods,[40–50] thereby deepening the understanding of their electronic structure. Finally, various chromophores are built around polyene backbones inheriting their spectroscopic properties from the underlying polyene.[51,52] The three lowest excited states, in particular, have attracted significant attention both experimentally[53–57] and theoretically.[49,58–60] This study will focus on their description from an electronic structure perspective.

The electronic states of linear all-*trans* polyenes are conveniently identified using the irreducible representations of the C_{2h} symmetry associated with their molecular framework. Additionally, the states are labeled according to the nomenclature introduced by Pariser, which is based on the alternance symmetry derived from the Pariser-Parr-Pople[61–63] model Hamiltonian. In this approach, the linear combinations of the two degenerate transitions yield antisymmetric (-) and symmetric (+) states relative to the interchange of conjugated pairs of orbitals. In valence bond theory, these states are referred to as covalent (-) and ionic (+) states, respectively.[64] Notably, within the molecular orbital picture, distinguishing between ionic and covalent states is less straightforward.[65]

The relative ordering of the two low-lying excited singlet excited states, $2^1A_g^-$ and $1^1B_u^+$, in small all-*trans* linear polyenes, remains a topic of ongoing debate.[58] It is generally agreed that, for the first members of the series, the ionic $1^1B_u^+$ state is the first vertically excited state. As the chain length increases, the covalent $2^1A_g^-$ state becomes the lowest excited state. However, there is no consensus in the literature on the exact point in the series where this change occurs. A brief review of this aspect is provided in the following paragraphs. The $2^1A_g^-$ state exhibits high covalent character and has the same symmetry as the ground state; thus, the transition dipole moment between these two states vanishes entirely due to symmetry constraints, rendering this state strictly dark in one-photon absorption experiments. In contrast, the $1^1B_u^+$ state is a strongly optically allowed "bright" state with ionic character. The third vertically excited valence singlet excited state is the $2^1B_u^-$, which has a small transition dipole moment and exhibits covalent character.[59]

The wave functions of ionic states are primarily composed of singly excited configurations, whereas those of covalent states are more intricate, with significant contributions from doubly excited configurations.[66] This complexity is one of the main reasons why uniformly describing the electronic spectra of linear all-*trans* polyenes remains challenging from a theoretical perspective. Due to their nature, ionic states are relatively straightforward to describe using single-reference quantum chemical methods, such as time-dependent density functional theory (TD-DFT),[67–69] algebraic diagrammatic construction of second order (ADC(2)),[70] and equation of motion coupled-cluster (EOM-

CCSD).[71] On the other hand, covalent states require the use of higher-level methods to capture static correlation effects effectively. Multiconfiguration self-consistent field (MCSCF) and multireference (MR) methods, in general, will be well suited for that purpose.

However, the MCSCF method and MR configuration interaction with singles and doubles (MR-CISD), which effectively capture static electron correlation effects and adequately describes covalent states, encounter notorious accuracy issues when applied to ionic states.[43,44,72] Specifically, excitation energies for ionic states are typically overestimated by about 1-2 eV when using an active space that includes only valence π-electrons and π-orbitals.[72] Several strategies have been proposed to mitigate this issue, such as expanding the active space to include additional unoccupied π-orbitals, including σ-orbitals into the active space, and modifying the one-electron basis set.[43,44,73–76] Indeed, a reasonable description of ionic states requires an extensive treatment of the σ-π electron correlation, which can in principle not be achieved by including correlation only in the π-space.[77]

Several methods have been employed to investigate the manifold of low-lying excited states in the series of all-trans polyenes. Here, we provide a brief review of key results. Hirao and co-workers,[78] using multireference Møller-Plesset (MRMP) theory, found that the $2^1B_u^-$ and $1^1B_u^+$ states are nearly degenerate in hexatriene. In longer polyenes, however, the covalent state becomes the first vertically excited state. This finding is corroborated by DFT/MRCI calculations performed by Marian and Gilka,[48] which also show that the covalent state is the lowest singlet excited state in polyenes longer than hexatriene.

Serrano-Andrés and coworkers,[79,80] employing complete active space second-order perturbation theory (CASPT2), suggested that in terms of vertical excitation, the $1^1B_u^+$ state is the lowest excited state in hexatriene, lying 0.18 eV below the covalent state. In octatetraene, their results indicate that these states are virtually degenerate, with the $2^1B_u^-$ state being 0.04 eV lower than the $1^1B_u^+$ state. This trend is further supported by CASPT2 benchmark calculations.[81] The near-degeneracy of these two states in octatetraene is also corroborated by N-electron valence state second-order perturbation theory (NEVPT2) calculations.[75]

The most recent database of highly accurate excitation energies for electronic structures (QUESTDB),[82] which includes results based on coupled-cluster CCSDT and CC3 methods, suggests that the bright $1^1B_u^+$ state is the first vertically excited state in both hexatriene and octatetraene, being 0.25 eV and 0.12 eV lower than the covalent $2^1B_u^-$ state, respectively. This ordering is also obtained using CCSD and CC2 methods.[81]

MR-CISD,[77,83] and multireference averaged quadratic coupled-cluster (MR-AQCC)[84,85] calculations have been performed for ethylene[43] and butadiene,[44] the first members of the series. In the present work, we aim to achieve an accurate and balanced treatment of both

static and dynamic electron correlation effects in all-trans linear polyenes, ranging from hexatriene up to dodecahexaene, using the variational MR-CISD and MR-AQCC methods. While nonvariational extensivity corrections are applied in the MR-CISD case, the MR-AQCC method inherently accounts for higher excitations, restoring size extensivity in an approximate yet considerably accurate manner.[86,87] We also seek to provide insights into the relative ordering of the excited states. A detailed analysis of the wave functions, based on the one-electron transition density matrix calculated with respect to the ground state, is presented. In particular, the ionic character of each state is assessed using the $Q_{\mathrm{a}}^{\mathrm{t}}$ diagnostic, which has recently been shown to associate large transition charges centered on individual atoms with ionic states.[72] Complementary analysis of the one-electron transition density matrix provides insights into how the wave functions of the excited states evolve across the series in terms of multiconfigurational and single-excitation character.

2.3 Low-lying excited states of linear All-*trans* polyenes: insights from analytical gradient calculations based on a multireference Wavefunction

The investigation of linear all-trans polyenes has long been a cornerstone of molecular photophysics due to their unique spectral properties, which stem from the intricate nature of their low-lying excited states. Among the manifold of excited states, the two lowest-lying singlet states—the covalent $2^1\mathrm{A}_\mathrm{g}^-$ state, and the ionic $1^1\mathrm{B}_\mathrm{u}^+$ state—are focal points for experimental[88–90,56,91–94,57,55,95] and computational[67–71,58,80,75,78,60,96,79,44] studies. Various chromophores are built around polyene backbones, inheriting their spectroscopic properties from the underlying polyene.[51,52] In this context, in naturally occurring carotenoids, the $2^1\mathrm{A}_\mathrm{g}^-$-analogous state is mostly responsible for driving non-photochemical quenching, dissipating excessive excitation energy in a harmless form,[39] while the $1^1\mathrm{B}_\mathrm{u}^+$-analogous state is responsible for the absorption of light energy and rapid excitation energy transfer to chlorophylls, enhancing photosynthetic efficiency.28 Hence, understanding the spectroscopic behavior of polyenes is of monumental importance. Beyond their biological relevance, polyenes provide a rigorous testing ground for theoretical frameworks and electronic structure methodologies.[51,40–43,45–50]

The focus of our work is on *trans*,*trans*-1,3,5-hexatriene, all-*trans*-1,3,5,7-octatetraene, and all-*trans*-1,3,5,7,9-decapentaene—hereafter referred to as hexatriene, octatetraene, and decapentaene. From the experimental standpoint, the $1^1\mathrm{B}_\mathrm{u}^+ \leftarrow 1^1\mathrm{A}_\mathrm{g}^-$ transition is dipole-allowed, which enables its detection in single-photon absorption experiments. The origin peak–which is also the strongest peak–has been unambiguously observed in the gas phase for hexatriene,[90,55] octatetraene,[56,92,93] and decapentaene.[57] On the other hand, the

$2^1A_g^-$ state is dipole forbidden, requiring more sophisticated detection techniques, such as two-photon absorption experiments in free jet expansions.[91] Nevertheless, it has been demonstrated that in octatetraene, the one-photon cross section is sufficiently large to allow the detection and study of the $2^1A_g^-$ state.[57,55]

From the theoretical point of view, ionic states are typically composed of singly excited configurations, whereas covalent states have substantial contributions from doubly excited configurations.[96,44,66] The differing characters of these states create theoretical challenges in uniformly describing the electronic spectra of these molecules: single-reference methods like time-dependent density functional theory (TD-DFT),[67–69] algebraic diagrammatic construction of second order (ADC(2)),[70] and equation of motion coupled-cluster (EOM-CCSD)[71] adequately describe ionic states but falter for covalent states. The multiconfiguration self-consistent field (MCSCF) method provides accurate results for capturing static correlation in covalent states but exhibits systematic limitations when applied to ionic states.[96,72,74] Indeed, a reasonable description of ionic states at the multireference (MR) level requires an extensive treatment of the σ-π electron correlation.[96,77] In this context, perturbative treatments via complete active space second-order perturbation theory (CASPT2) or N-electron valence perturbation theory (NEVPT2), and variational methods like multireference configuration interaction with singles and doubles (MR-CISD) or multireference averaged quadratic coupled-cluster (MR-AQCC) based on the MCSCF wavefunction are good alternatives to obtain a balanced description of the two lowest-lying excited states of polyenes with differing characters and have been employed to obtain valuable insights into vertical excitation energies from the ground state.[80,75,78,60,96,79,44] To further describe their electronic spectra and gain deeper insight into their spectroscopic behavior, it is necessary to locate the minima of the excited-state potential energy surfaces. This enables the calculation of adiabatic excitation energies as well as vertical emission energies from the excited-state minima. However, computing energy gradients based on a multireference wavefunction remains a challenging and computationally demanding task.

Due to the lack of analytic energy gradients in many MR methods, excited-state geometry optimizations are often performed only at the CASSCF level, followed by single-point calculations at a higher level of theory. This approach has been used in several studies. Serrano-Andrés and coauthors,[80] as well as Angeli and Pastore,[75] studied octatetraene using CASPT2 based on CASSCF-optimized geometries. This same approach was also applied by Nakayama et al.,[78] who studied polyenes ranging from ethylene to octatetraene. Recently, Guareschi and Angeli21 successfully obtained the optimized geometries of the ground and excited $2^1A_g^-$ state of hexatriene via numerical gradients based on an N-electron valence perturbation theory (NEVPT2) wavefunction. An important finding from these studies is that upon geometry relaxation, the covalent $2^1A_g^-$ state, which lies very close to the ionic state at the Franck–Condon geometry, is highly stabilized with

respect to the $1^1B_u^+$ state.

In recent work, uncontracted MR-CISD and MR-AQCC methods have been employed to accurately compute the vertical excitation energies of all-trans polyenes, from hexatriene up to dodecahexaene.[96] The variational character of the MR-CISD method enables efficient analytic energy gradients for any selection of electronic states.[97,98,83] The computational cost of gradient evaluation is only a fraction of that required for a single-point energy calculation. In this work, the minima of the ground $1^1A_g^-$ and the excited $2^1A_g^-$ and $1^1B_u^+$ states have been calculated for hexatriene, octatetraene, and decapentaene using analytic energy gradients based on the MR-CISD wavefunction, enabling the description of adiabatic electronic transitions and vertical emission energies of these compounds.

Bibliography

1 KIM, Heechan et al. Relief of excited-state antiaromaticity enables the smallest red emitter. **Nature Communications**, Springer US, v. 12, n. 1, p. 5409, Dec. 2021.

2 EL BAKOURI, Ouissam; SMITH, Joshua R.; OTTOSSON, Henrik. Strategies for Design of Potential Singlet Fission Chromophores Utilizing a Combination of Ground-State and Excited-State Aromaticity Rules. **Journal of the American Chemical Society**, v. 142, n. 12, p. 5602–5617, Mar. 2020.

3 ULLRICH, Tobias; MUNZ, Dominik; GULDI, Dirk M. Unconventional singlet fission materials. **Chemical Society Reviews**, v. 50, n. 5, p. 3485–3518, 2021.

4 ANTHONY, John E. Functionalized Acenes and Heteroacenes for Organic Electronics. **Chemical Reviews**, v. 106, n. 12, p. 5028–5048, Dec. 2006.

5 _____. The Larger Acenes: Versatile Organic Semiconductors. **Angewandte Chemie International Edition**, v. 47, n. 3, p. 452–483, Jan. 2008.

6 WEIL, Tanja et al. The Rylene Colorant Family-Tailored Nanoemitters for Photonics Research and Applications. **Angewandte Chemie International Edition**, v. 49, n. 48, p. 9068–9093, Nov. 2010.

7 DAS, Anita et al. Local Electron Correlation Treatment in Extended Multireference Calculations: Effect of Acceptor–Donor Substituents on the Biradical Character of the Polycyclic Aromatic Hydrocarbon Heptazethrene. **Journal of Chemical Theory and Computation**, v. 13, n. 6, p. 2612–2622, June 2017.

8 KRYGOWSKI, Tadeusz M. et al. Aromaticity from the Viewpoint of Molecular Geometry: Application to Planar Systems. **Chemical Reviews**, v. 114, n. 12, p. 6383–6422, June 2014.

9 KRYGOWSKI, Tadeusz M. et al. Relation between the Substituent Effect and Aromaticity. **The Journal of Organic Chemistry**, v. 69, n. 20, p. 6634–6640, Oct. 2004.

10 KRYGOWSKI, Tadeusz Marek; STEPIEŃ, Beata Tamara. Sigma- and Pi-Electron Delocalization: Focus on Substituent Effects. **Chemical Reviews**, v. 105, n. 10, p. 3482–3512, Oct. 2005.

11 KRYGOWSKI, Tadeusz M. et al. Relation between the substituent effect and aromaticity. Part II. The case ofmeta- andpara-homodisubstituted benzene derivatives. **Journal of Physical Organic Chemistry**, v. 19, n. 12, p. 889–895, Dec. 2006.

12 SIODLA, T. et al. Difference in pi-electron delocalization for monosubstituted olefinic and aromatic systems. **RSC Advances**, v. 6, n. 99, p. 96527–96530, 2016.

13 SZATYLOWICZ, Halina; JEZUITA, Anna; KRYGOWSKI, Tadeusz M. On the relations between aromaticity and substituent effect. **Structural Chemistry**, v. 30, n. 5, p. 1529–1548, Oct. 2019.

14 BÁEZ-GREZ, Rodrigo; PINO-RIOS, Ricardo. Evaluation of Slight Changes in Aromaticity through Electronic and Density Functional Reactivity Theory-Based Descriptors. **ACS Omega**, American Chemical Society, v. 7, n. 25, p. 21939–21945, June 2022.

15 DOBROWOLSKI, Jan Cz; LIPIŃSKI, Piotr F. J.; KARPIŃSKA, Grażyna. Substituent Effect in the First Excited Singlet State of Monosubstituted Benzenes. **The Journal of Physical Chemistry A**, v. 122, n. 19, p. 4609–4621, May 2018.

16 DOBROWOLSKI, Jan Cz; KARPIŃSKA, Grażyna. Substituent Effect in the First Excited Triplet State of Monosubstituted Benzenes. **ACS Omega**, v. 5, n. 16, p. 9477–9490, Apr. 2020.

17 BARANAC-STOJANOVIĆ, Marija. Substituent Effect on Triplet State Aromaticity of Benzene. **The Journal of Organic Chemistry**, v. 85, n. 6, p. 4289–4297, Mar. 2020.

18 MINKIN, Vladimir I.; GLUKHOVTSEV, Mikhail N.; SIMKIN, Boris Ya. **Aromaticity and Antiaromaticity: Electronic and Structural Aspects**. New York: John Wiley & Sons, Inc., 1994.

19 SCHLEYER, P. Rague von; JIAO, Haijun. What is aromaticity? **Pure and Applied Chemistry**, v. 68, n. 2, p. 209–218, Jan. 1996.

20 CYRAŃSKI, Michal K. et al. To What Extent Can Aromaticity Be Defined Uniquely? **The Journal of Organic Chemistry**, v. 67, n. 4, p. 1333–1338, Feb. 2002.

21 CYRAŃSKI, Michal K. et al. Facts and artifacts about aromatic stability estimation. **Tetrahedron**, v. 59, n. 10, p. 1657–1665, Mar. 2003.

22 CYRAŃSKI, Michał Ksawery. Energetic Aspects of Cyclic Pi-Electron Delocalization: Evaluation of the Methods of Estimating Aromatic Stabilization Energies. **Chemical Reviews**, v. 105, n. 10, p. 3773–3811, Oct. 2005.

23 POATER, Jordi et al. The Delocalization Index as an Electronic Aromaticity Criterion: Application to a Series of Planar Polycyclic Aromatic Hydrocarbons. **Chemistry - A European Journal**, v. 9, n. 2, p. 400–406, Jan. 2003.

24 KRUSZEWSKI, J.; KRYGOWSKI, T.M. Definition of aromaticity basing on the harmonic oscillator model. **Tetrahedron Letters**, v. 13, n. 36, p. 3839–3842, 1972.

25 KRYGOWSKI, Tadeusz Marek. Crystallographic studies of inter- and intramolecular interactions reflected in aromatic character of π-electron systems. **Journal of Chemical Information and Computer Sciences**, v. 33, n. 1, p. 70–78, Jan. 1993.

26 KRYGOWSKI, Tadeusz Marek; CYRAŃSKI, Michal. Separation of the energetic and geometric contributions to the aromaticity. Part IV. A general model for the π-electron systems. **Tetrahedron**, v. 52, n. 30, p. 10255–10264, July 1996.

27 KRYGOWSKI, Tadeusz Marek; CYRAŃSKI, Michał Ksawery. Structural Aspects of Aromaticity. **Chemical Reviews**, v. 101, n. 5, p. 1385–1420, May 2001.

28 SCHLEYER, Paul Von Ragué et al. Nucleus-Independent Chemical Shifts: A Simple and Efficient Aromaticity Probe. **Journal of the American Chemical Society**, American Chemical Society, v. 118, n. 26, p. 6317–6318, Jan. 1996.

29 CORMINBOEUF, Clémence; HEINE, Thomas; WEBER, Jacques. Evaluation of aromaticity: A new dissected NICS model based on canonical orbitals. **Physical Chemistry Chemical Physics**, v. 5, n. 2, p. 246–251, Jan. 2003.

30 HEINE, Thomas et al. Analysis of Aromatic Delocalization: Individual Molecular Orbital Contributions to Nucleus-Independent Chemical Shifts. **The Journal of Physical Chemistry A**, v. 107, n. 33, p. 6470–6475, Aug. 2003.

31 CORMINBOEUF, Clémence et al. Induced magnetic fields in aromatic [n]-annulenes—interpretation of NICS tensor components. **Physical Chemistry Chemical Physics**, v. 6, n. 2, p. 273–276, 2004.

32 CHEN, Zhongfang et al. Nucleus-Independent Chemical Shifts (NICS) as an Aromaticity Criterion. **Chemical Reviews**, v. 105, n. 10, p. 3842–3888, Sept. 2005.

33 KRYGOWSKI, T M; STEPIEŃ, B T. Changes in aromaticity in the ring of monosubstituted benzene derivatives. **Polish Journal of Chemistry**, v. 78, p. 2213–2217, 2004.

34 CAMPANELLI, Anna Rita; DOMENICANO, Aldo; RAMONDO, Fabio. Electronegativity, Resonance, and Steric Effects and the Structure of Monosubstituted Benzene Rings: An ab Initio MO Study. **The Journal of Physical Chemistry A**, v. 107, n. 33, p. 6429–6440, Aug. 2003.

35 GRONDELLE, Rienk van et al. Energy transfer and trapping in photosynthesis. **Biochimica et Biophysica Acta (BBA) - Bioenergetics**, v. 1187, n. 1, p. 1–65, Aug. 1994.

36 AMERONGEN, Herbert van; GRONDELLE, Rienk van. Understanding the Energy Transfer Function of LHCII, the Major Light-Harvesting Complex of Green Plants. **The Journal of Physical Chemistry B**, v. 105, n. 3, p. 604–617, Jan. 2001.

37 HORTON, P.; RUBAN, A. V.; WALTERS, R. G. REGULATION OF LIGHT HARVESTING IN GREEN PLANTS. **Annual Review of Plant Physiology and Plant Molecular Biology**, v. 47, n. 1, p. 655–684, June 1996.

38 NIYOGI, Krishna K. PHOTOPROTECTION REVISITED: Genetic and Molecular Approaches. **Annual Review of Plant Physiology and Plant Molecular Biology**, v. 50, n. 1, p. 333–359, June 1999.

39 RUBAN, Alexander V. et al. Identification of a mechanism of photoprotective energy dissipation in higher plants. **Nature**, v. 450, n. 7169, p. 575–578, Nov. 2007.

40 YANAI, Takeshi et al. Multireference quantum chemistry through a joint density matrix renormalization group and canonical transformation theory. **The Journal of Chemical Physics**, v. 132, n. 2, Jan. 2010.

41 SAURI, Vicenta et al. Multiconfigurational Second-Order Perturbation Theory Restricted Active Space (RASPT2) Method for Electronic Excited States: A Benchmark Study. **Journal of Chemical Theory and Computation**, v. 7, n. 1, p. 153–168, Jan. 2011.

42 SCHRIBER, Jeffrey B.; EVANGELISTA, Francesco A. Adaptive Configuration Interaction for Computing Challenging Electronic Excited States with Tunable Accuracy. **Journal of Chemical Theory and Computation**, v. 13, n. 11, p. 5354–5366, Nov. 2017.

43 MÜLLER, Thomas; DALLOS, Michal; LISCHKA, Hans. The ethylene 1^1B_{1u} V state revisited. **The Journal of Chemical Physics**, v. 110, n. 15, p. 7176–7184, Apr. 1999.

44 DALLOS, Michal; LISCHKA, Hans. A systematic theoretical investigation of the lowest valence- and Rydberg-excited singlet states of trans-butadiene. The character of the 1^1B_u (V) state revisited. **Theoretical Chemistry Accounts: Theory, Computation, and Modeling (Theoretica Chimica Acta)**, v. 112, n. 1, p. 16–26, Apr. 2004.

45 SOKOLOV, Alexander Yu. et al. Time-dependent N-electron valence perturbation theory with matrix product state reference wavefunctions for large active spaces and basis sets: Applications to the chromium dimer and all-trans polyenes. **The Journal of Chemical Physics**, v. 146, n. 24, June 2017.

46 SAMANTA, Pradipta Kumar et al. Excited states with internally contracted multireference coupled-cluster linear response theory. **The Journal of Chemical Physics**, v. 140, n. 13, Apr. 2014.

47 GU, Junjing et al. Valence Bond Theory Reveals Hidden Delocalized Diradical Character of Polyenes. **Journal of the American Chemical Society**, American Chemical Society, v. 139, n. 27, p. 9302–9316, July 2017.

48 MARIAN, Christel M.; GILKA, Natalie. Performance of the Density Functional Theory/Multireference Configuration Interaction Method on Electronic Excitation of Extended π-Systems. **Journal of Chemical Theory and Computation**, v. 4, n. 9, p. 1501–1515, Sept. 2008.

49 KHOKHLOV, Daniil; BELOV, Aleksandr. Toward an Accurate Ab Initio Description of Low-Lying Singlet Excited States of Polyenes. **Journal of Chemical Theory and Computation**, American Chemical Society, v. 17, n. 7, p. 4301–4315, July 2021.

50 LU, Tian; CHEN, Feiwu. Multiwfn: A multifunctional wavefunction analyzer. **Journal of Computational Chemistry**, v. 33, n. 5, p. 580–592, Feb. 2012.

51 CASAL, Mariana T. do et al. Using diketopyrrolopyrroles to stabilize double excitation and control internal conversion. **Physical Chemistry Chemical Physics**, v. 24, n. 38, p. 23279–23288, 2022.

52 GIRIJA, Aswathy V. et al. Singlet Fission in Pechmann Dyes: Planar Chromophore Design and Understanding. **Journal of the American Chemical Society**, v. 146, n. 27, p. 18253–18261, July 2024.

53 WANG, Peng et al. Low-lying singlet states of carotenoids having 8–13 conjugated double bonds as determined by electronic absorption spectroscopy. **Chemical Physics Letters**, v. 410, n. 1-3, p. 108–114, July 2005.

54 CHRISTENSEN, Ronald L. et al. Energies of Low-Lying Excited States of Linear Polyenes. **The Journal of Physical Chemistry A**, v. 112, n. 49, p. 12629–12636, Dec. 2008.

55 GAVIN, R. M.; RISEMBERG, Salomon; RICE, Stuart A. Spectroscopic properties of polyenes. I. The lowest energy allowed singlet-singlet transition for cis- and trans-1,3,5-hexatriene. **The Journal of Chemical Physics**, v. 58, n. 8, p. 3160–3165, Apr. 1973.

56 GAVIN, R. M. et al. Spectroscopic properties of polyenes. III. 1,3,5,7-Octatetraene. **The Journal of Chemical Physics**, v. 68, n. 2, p. 522–529, Jan. 1978.

57 D'AMICO, Kevin L.; MANOS, Christopher; CHRISTENSEN, Ronald L. Electronic energy levels in a homologous series of unsubstituted linear polyenes. **Journal of the American Chemical Society**, v. 102, n. 6, p. 1777–1782, Mar. 1980.

58 SCHMIDT, Maximilian; TAVAN, Paul. Electronic excitations in long polyenes revisited. **The Journal of Chemical Physics**, v. 136, n. 12, Mar. 2012.

59 KHOKHLOV, Daniil; BELOV, Aleksandr. Ab Initio Study of Low-Lying Excited States of Carotenoid-Derived Polyenes. **The Journal of Physical Chemistry A**, American Chemical Society, v. 124, n. 28, p. 5790–5803, July 2020.

60 GUARESCHI, Riccardo; ANGELI, Celestino. The lowest singlet states of hexatriene revisited. **Theoretical Chemistry Accounts**, Springer Science and Business Media Deutschland GmbH, v. 142, n. 12, p. 127, Dec. 2023.

61 PARISER, Rudolph; PARR, Robert G. A Semi-Empirical Theory of the Electronic Spectra and Electronic Structure of Complex Unsaturated Molecules. I. **The Journal of Chemical Physics**, v. 21, n. 3, p. 466–471, Mar. 1953.

62 _____. A Semi-Empirical Theory of the Electronic Spectra and Electronic Structure of Complex Unsaturated Molecules. II. **The Journal of Chemical Physics**, v. 21, n. 5, p. 767–776, May 1953.

63 POPLE, J. A. Electron interaction in unsaturated hydrocarbons. **Transactions of the Faraday Society**, v. 49, p. 1375, 1953.

64 SCHULTEN, K.; OHMINE, I.; KARPLUS, M. Correlation effects in the spectra of polyenes. **The Journal of Chemical Physics**, v. 64, n. 11, p. 4422–4441, June 1976.

65 KIMBER, Patrick; PLASSER, Felix. Classification and Analysis of Molecular Excited States. In: [s.l.]: Elsevier, 2024. p. 55–83.

66 CASAL, Mariana T. do et al. Classification of doubly excited molecular electronic states. **Chemical Science**, v. 14, n. 15, p. 4012–4026, 2023.

67 SILVA-JUNIOR, Mario R. et al. Benchmarks for electronically excited states: Time-dependent density functional theory and density functional theory based multireference configuration interaction. **The Journal of Chemical Physics**, v. 129, n. 10, Sept. 2008.

68 HSU, Chao-Ping; HIRATA, So; HEAD-GORDON, Martin. Excitation Energies from Time-Dependent Density Functional Theory for Linear Polyene Oligomers: Butadiene to Decapentaene. **The Journal of Physical Chemistry A**, v. 105, n. 2, p. 451–458, Jan. 2001.

69 PEACH, Michael J. G. et al. Structural and Electronic Properties of Polyacetylene and Polyyne from Hybrid and Coulomb-Attenuated Density Functionals. **The Journal of Physical Chemistry A**, v. 111, n. 46, p. 11930–11935, Nov. 2007.

70 STARCKE, Jan Hendrik et al. How much double excitation character do the lowest excited states of linear polyenes have? **Chemical Physics**, v. 329, n. 1-3, p. 39–49, Oct. 2006.

71 BOGUSLAWSKI, Katharina. Targeting excited states in all-trans polyenes with electron-pair states. **The Journal of Chemical Physics**, v. 145, n. 23, Dec. 2016.

72 MONTE, Silmar A. do et al. Quantification of the Ionic Character of Multiconfigurational Wave Functions: The Q a t Diagnostic. **The Journal of Physical Chemistry A**, American Chemical Society (ACS), v. 127, n. 46, p. 9842–9852, Nov. 2023.

73 BOGGIO-PASQUA, Martial et al. A computational strategy for geometry optimization of ionic and covalent excited states, applied to butadiene and hexatriene. **The Journal of Chemical Physics**, v. 120, n. 17, p. 7849–7860, May 2004.

74 ANGELI, Celestino. On the nature of the $\pi \rightarrow \pi^*$ ionic excited states: The V state of ethene as a prototype. **Journal of Computational Chemistry**, v. 30, n. 8, p. 1319–1333, June 2009.

75 ANGELI, Celestino; PASTORE, Mariachiara. The lowest singlet states of octatetraene revisited. **The Journal of Chemical Physics**, v. 134, n. 18, May 2011.

76 TRAN, Thierry et al. Molecular Vertical Excitation Energies Studied with First-Order RASSCF (RAS[1,1]): Balancing Covalent and Ionic Excited States. **The Journal of Physical Chemistry A**, v. 123, n. 25, p. 5223–5230, June 2019.

77 LISCHKA, Hans et al. Multireference Approaches for Excited States of Molecules. **Chemical Reviews**, v. 118, n. 15, p. 7293–7361, Aug. 2018.

78 NAKAYAMA, Kenichi; NAKANO, Haruyuki; HIRAO, Kimihiko. Theoretical study of the $\pi\pi^*$ excited states of linear polyenes: The energy gap between 11Bu+ and 21Ag states and their character. **International Journal of Quantum Chemistry**, John Wiley & Sons, Inc, v. 66, n. 2, p. 157–175, 1998.

79 SERRANO-ANDRÉS, Luis et al. Towards an accurate molecular orbital theory for excited states: Ethene, butadiene, and hexatriene. **The Journal of Chemical Physics**, v. 98, n. 4, p. 3151–3162, Feb. 1993.

80 SERRANO-ANDRES, Luis et al. Theoretical study of the electronic spectrum of all-trans-1,3,5,7-octatetraene. **The Journal of Physical Chemistry**, v. 97, n. 37, p. 9360–9368, Sept. 1993.

81 SCHREIBER, Marko et al. Benchmarks for electronically excited states: CASPT2, CC2, CCSD, and CC3. **The Journal of Chemical Physics**, v. 128, n. 13, Apr. 2008.

82 VÉRIL, Mickaël et al. QUESTDB : A database of highly accurate excitation energies for the electronic structure community. **WIREs Computational Molecular Science**, John Wiley and Sons Inc, v. 11, n. 5, Sept. 2021.

83 SZALAY, Péter G. et al. Multiconfiguration Self-Consistent Field and Multireference Configuration Interaction Methods and Applications. **Chemical Reviews**, v. 112, n. 1, p. 108–181, Jan. 2012.

84 SZALAY, Péter G.; BARTLETT, Rodney J. Multi-reference averaged quadratic coupled-cluster method: a size-extensive modification of multi-reference CI. **Chemical Physics Letters**, v. 214, n. 5, p. 481–488, Nov. 1993.

85 _____. Approximately extensive modifications of the multireference configuration interaction method: A theoretical and practical analysis. **The Journal of Chemical Physics**, v. 103, n. 9, p. 3600–3612, Sept. 1995.

86 LISCHKA, Hans et al. High-level multireference methods in the quantum-chemistry program system COLUMBUS: Analytic MR-CISD and MR-AQCC gradients and MR-AQCC-LRT for excited states, GUGA spin–orbit CI and parallel CI density. **Physical Chemistry Chemical Physics**, v. 3, n. 5, p. 664–673, 2001.

87 SZALAY, P'eter G.; MÜLLER, Thomas; LISCHKA, Hans. Excitation energies and transition moments by the multireference averaged quadratic coupled cluster (MR-AQCC) method. **Physical Chemistry Chemical Physics**, v. 2, n. 10, p. 2067–2073, 2000.

88 BUMA, Wybren Jan; KOHLER, Bryan E.; SONG, Kyuseok. Location of the 21 A g state in hexatriene. **The Journal of Chemical Physics**, v. 92, n. 7, p. 4622–4623, Apr. 1990.

89 GAVIN, R. M.; RICE, Stuart A. Spectroscopic properties of polyenes. II. The vacuum ultraviolet spectra of cis- and trans-1,3,5-hexatriene. **The Journal of Chemical Physics**, v. 60, n. 8, p. 3231–3237, Apr. 1974.

90 LEOPOLD, D. G. et al. Direct absorption spectroscopy of jet-cooled polyenes. II. The $1^1B_u^+ \leftarrow 1^1A_g^-$ transitions of butadienes and hexatrienes. **The Journal of Chemical Physics**, v. 81, n. 10, p. 4218–4229, Nov. 1984.

91 PETEK, Hrvoje et al. The 2^1A_g state of trans,trans-1,3,5,7-octatetraene in free jet expansions. **The Journal of Chemical Physics**, v. 98, n. 5, p. 3777–3794, Mar. 1993.

92 LEOPOLD, D. G.; VAIDA, V.; GRANVILLE, Mark F. Direct absorption spectroscopy of jet-cooled polyenes. I. The $1^1B_u^+ \leftarrow 1^1A_g^-$ transition of trans,trans-1,3,5,7-octatetraene. **The Journal of Chemical Physics**, v. 81, n. 10, p. 4210–4217, Nov. 1984.

93 HEIMBROOK, Lou Ann et al. Free-jet fluorescence excitation spectrum of trans,trans-1,3,5,7-octatetraene. **The Journal of Chemical Physics**, v. 75, n. 9, p. 4338–4342, Nov. 1981.

94 HEIMBROOK, Lou Ann; KOHLER, Bryan E.; LEVY, Irvin J. Fluorescence from the 1^1B_u state of trans,trans-1,3,5,7-octatetraene in a free jet. **The Journal of Chemical Physics**, v. 81, n. 4, p. 1592–1597, Aug. 1984.

95 BOUWMAN, Wim G. et al. Fluorescence of gaseous tetraenes and pentaenes. **The Journal of Physical Chemistry**, v. 94, n. 19, p. 7429–7434, Sept. 1990.

96 CHAGAS, Julio C. V. et al. Low-lying excited states of linear all-trans polyenes: the σ–π electron correlation and the description of ionic states. **Physical Chemistry Chemical Physics**, v. 27, n. 15, p. 7916–7928, 2025.

97 SHEPARD, R. et al. A general multireference configuration interaction gradient program. **The Journal of Chemical Physics**, v. 96, n. 3, p. 2085–2098, Feb. 1992.

98 LISCHKA, H.; DALLOS, M.; SHEPARD, R. Analytic MRCI gradient for excited states: formalism and application to the $n - \pi$ valence- and n-(3s,3p)* Rydberg states of formaldehyde. **Molecular Physics**, v. 100, n. 11, p. 1647–1658, June 2002.

3 Theory

In this chapter, the theoretical background used to obtain the results presented in the following chapters is outlined. Unless otherwise specified, the derivations and discussions presented here are adapted from the seminal textbooks by George Schatz and Mark Ratner,[1] Ira Levine,[2] Frank Jensen,[3] and Donald McQuarrie.

3.1 The Molecular Schrödinger Equation

At the heart of quantum chemistry lies the time-independent Schrödinger equation, which governs the behavior of electrons and nuclei in a molecular system. The central goal in any quantum chemistry problem is finding its solution, which allows for the determination of the molecular properties of a system. The state of a system of n particles is described by its wavefunction $\Psi(\mathbf{x}_1, ..., \mathbf{x}_n)$, where each $\mathbf{x}_i$ denotes the spatial and spin coordinates of particle i. The wavefunction is obtained as an eigenfunction of the Hamiltonian operator H, and the corresponding energy E is given by the eigenvalue in the solution of the time-independent Schrödinger equation:

$$H\Psi = E\Psi \tag{3.1}$$

The complete non-relativistic Hamiltonian of an arbitrary free molecule is:

$$H = T_N + T_e + V_{eN} + V_{ee} + V_{NN} \tag{3.2}$$

where:

- $\hat{T}_N$ = kinetic energy of the nuclei
- $\hat{T}_e$ = kinetic energy of the electrons
- $\hat{V}_{eN}$ = electron-nuclear attractive Coulomb potential,
- $\hat{V}_{ee}$ = electron-electron repulsive Coulomb potential,

- $\hat{V}_{NN}$ = nuclear-nuclear repulsive Coulomb potential

Using the index α to label the N nuclei and i to label the n electrons, the explicit form of each term in equation 3.2 is (in atomic units)

$$T_N = \sum_{\alpha}^{N} \frac{P_\alpha^2}{2M_\alpha} \tag{3.3a}$$

$$T_e = \sum_{i}^{n} \frac{P_i^2}{2} \tag{3.3b}$$

$$V_{eN} = -\sum_{\alpha}^{N}\sum_{i}^{n} \frac{Z_\alpha}{R_{i\alpha}} \tag{3.3c}$$

$$V_{ee} = \sum_{i}^{n}\sum_{j<i}^{n} \frac{1}{r_{ij}} \tag{3.3d}$$

$$V_{NN} = \sum_{\alpha}^{N}\sum_{\beta<\alpha}^{N} \frac{Z_\alpha Z_\beta}{R_{\alpha\beta}} \tag{3.3e}$$

This Hamiltonian cannot be solved exactly for any system more complicated than the hydrogen atom. Consequently, a series of accurate and simplifying approximations and computational methods have been developed to obtain practical solutions.

3.1.1 The Born-Oppenheimer Approximation

Nuclei are much heavier than electrons, *i.e.*, $m_\alpha \gg m_e$, thus, the electrons move much faster than the nuclei, so it can be approximated that electrons instantaneously adjust to any change in nuclear coordinates. Hence, for most os chemical applications, it is a good approximation to assume that the Schrödinger equation can be parametrically separated into a product of electronic and nuclear parts (Equation 3.4). This accurate and simplifying procedure is the remarkable adiabatic approximation due to Born and Oppenheimer,[4,5] which leads to factorization of the wavefunction as follow:

$$\Psi(\mathbf{r}, \mathbf{R}) = \psi(\mathbf{r}; \mathbf{R})\chi(\mathbf{R}) \tag{3.4}$$

where:

- $\psi(\mathbf{r}; \mathbf{R})$ is the electronic wavefunction depending explicitly on the electronic coordinates $\mathbf{r}$ and parametrically on the nuclear coordinates $\mathbf{R}$,
- $\chi(\mathbf{R})$ is the nuclear wavefunction depending only on the nuclear coordinates.

The electronic Schrödinger equation includes all the terms in Equation 3.2 that depend on electronic coordinates and is given by

$$(T_e + V_{eN} + V_{ee})\psi = E_{\text{el}}\psi \tag{3.5}$$

where the energy E_{el} is also a parametric function of the nuclear coordinates $\mathbf{R}$. If Equation 3.4 is substituted into Equation 3.1 and Equation 3.5 is applied, it follows that:

$$(T_N + V_{NN} + E_{\text{el}})\psi\chi = E\psi\chi \tag{3.6}$$

where E is the total electron-nuclear energy. The Born-Oppenheimer approximation now consists of neglecting the $\mathbf{R}$ dependence of ψ, so that $T_N\psi\chi = \psi T_N\chi$. This allows us to cancel ψ from both sides of Equation 3.6, giving us

$$(T_N + V)\chi = E\chi \tag{3.7}$$

where

$$V = V_{NN} + E_{\text{el}} \tag{3.8}$$

is the electronic potential energy surface that governs nuclear motion.

3.1.2 The Pauli Principle

A physically valid electronic wavefunction must not only satisfy the Schrödinger equation (Equation 3.1), but also comply with the Pauli exclusion principle. For electrons—and all other fermions—this implies that the total wavefunction ψ must be antisymmetric with respect to the exchange of any two electrons:

$$\psi(\ldots, \mathbf{x}_i, \ldots, \mathbf{x}_j, \ldots) = -\psi(\ldots, \mathbf{x}_j, \ldots, \mathbf{x}_i, \ldots) \tag{3.9}$$

A general way to enforce antisymmetry is to express the wavefunction as a determinant of molecular spin orbitals χ, known as a Slater determinant. Each spin orbital is a product of a spatial molecular orbital $\phi(\mathbf{r})$ and a spin function, either $\alpha(s)$ or $\beta(s)$:

$$\chi(\mathbf{x}) = \phi(\mathbf{r})\,\alpha(s)$$
$$\chi(\mathbf{x}) = \phi(\mathbf{r})\,\beta(s)$$

where $\mathbf{x} = (\mathbf{r}, s)$ denotes both the spatial coordinates and the spin variable of a single electron. The general form of the Slater determinant for a system of n electrons is:

$$\psi(\mathbf{x}_1, \ldots, \mathbf{x}_n) = \frac{1}{\sqrt{n!}} \begin{vmatrix} \chi_1(\mathbf{x}_1) & \chi_2(\mathbf{x}_1) & \cdots & \chi_n(\mathbf{x}_1) \\ \chi_1(\mathbf{x}_2) & \chi_2(\mathbf{x}_2) & \cdots & \chi_n(\mathbf{x}_2) \\ \vdots & \vdots & \ddots & \vdots \\ \chi_1(\mathbf{x}_n) & \chi_2(\mathbf{x}_n) & \cdots & \chi_n(\mathbf{x}_n) \end{vmatrix} \tag{3.10}$$

This determinant automatically satisfies the Pauli principle: interchanging the coordinates of any two electrons (i.e., swapping two rows of the determinant) changes the sign of the wavefunction. In addition, no two electrons can occupy the same spin orbital, as this would make two columns in the determinant equal, rendering the wavefunction identically zero.

3.2 Electronic Structure Methods

3.2.1 The Hartree-Fock Method

Hartree–Fock (HF) theory is the foundation of the methods that will be used in this work. It approximates the many-electron wavefunction as a single Slater determinant and solves the resulting equations self-consistently.

The HF method is grounded in the variational principle, which states that the expectation value of the Hamiltonian over any normalized trial wavefunction ϕ provides an upper bound to the true ground state energy E_0: $E_0 \leq \langle\phi|\hat{H}|\phi\rangle$. If we apply variational theory to the determination of the optimum spatial orbitals ϕ_i, the following one-electron Schrödinger equation may be derived:

$$f_i\phi_i = \varepsilon_i\phi_i \tag{3.11}$$

where operator f_i is

$$f_i = -\frac{1}{2}\nabla_i^2 - \sum_{\alpha=1}^{N} \frac{Z_\alpha}{R_{i\alpha}} + \sum_{j=1}^{n/2} [2J_j(i) - K_j(i)] \tag{3.12}$$

and ε_i is the one-electron energy eigenvalue.

Equation 3.11 is the Hartree-Fock or self-consistent field (SCF) equation, and f_i is the Fock operator. The Fock operator (Equation 3.12) includes exact kinetic energy and electron-nuclear attraction terms plus two approximate electron–electron repulsion terms,

the Coulomb J and exchange K operators. These are defined in terms of their action on the orbital ϕ_i as follows:

$$J_j(i)\phi_i = \langle\phi_j|\frac{1}{r_{ij}}|\phi_j\rangle\phi_i \tag{3.13}$$

$$K_j(i)\phi_i = \langle\phi_j|\frac{1}{r_{ij}}|\phi_i\rangle\phi_j \tag{3.14}$$

where the integration variable is the coordinate r_j associated with electron j.

The total electronic energy E_{el} associated with the Slater determinant (Equation 3.10) using orbitals that satisfy Equation 3.11 is given by:

$$E_{\text{el}} = \sum_{i=1}^{n/2}\varepsilon_i - \sum_{i}^{n/2}\sum_{j}^{n/2}(2J_{ij} - K_{ij}) \tag{3.15}$$

A standard method for solving the Hartree–Fock (SCF) equation for molecules involves expanding each molecular orbital ϕ_i as a linear combination of atomic orbitals:

$$\phi_i = \sum_{\mu} c_{i\mu}\varphi_\mu \tag{3.16}$$

where φ_μ is an atomic orbital. In most molecular electronic structure calculations, the φ_μ's are chosen to be gaussian functions (or sums of gaussians), as this facilitates multicenter two-electron integral evaluation.

Because the Coulomb (Equation 3.13) and exchange (Equation 3.14) operators in f_i (Equation 3.12) depend on the orbitals of interest, the solution to Equation 3.11 must be accomplished self-consistently, where c_{pi} (Equatio 3.16) are the variational coefficients. A typical procedure follows as:

1. Make an initial guess for the orbital coefficients c_{pi}.
2. Compute J_{ij} and K_{ij}.
3. Solve the secular equations to obtain new c_{pi} and orbital energies ε_i.
4. Repeat steps 2–3 until energy and orbitals converge (self-consistent field, SCF).

A secular equation to determine the optimized energies. In the present case this secular equation is

$$|\mathbf{f} - \epsilon\mathbf{s}| = 0 \tag{3.17}$$

Here $\mathbf{s}$ is an overlap matrix involving the AO basis functions and $\mathbf{f}$ is the matrix representation of the Fock operator.

By minimizing this energy with respect to the spin orbitals in the Slater determinant, Hartree–Fock finds the best possible approximation within the space of single-determinant wavefunctions. However, in this case, electrons are statistically independent and have no effect on each other, in such a way that it neglects dynamic electron correlation because each electron moves in an average field created by others. To overcome this, the methods that are discussed bellow were developed, and, based on the HF wave function, they follow an hyherarchi, reaching, to this day, the state of art of computational chemistry, in accuracy competitive with experimental results.

3.2.2 Multireference methods

As discussed previously, within the Hartree–Fock (HF) approximation, each electron moves independently in the average electrostatic field generated by all other electrons, resulting in a set of coupled one-electron equations. While this mean-field approach captures the antisymmetry of the wavefunction through a single Slater determinant, it inherently neglects explicit electron–electron correlation. In other words, the instantaneous repulsion between electrons is not properly accounted for in the HF wavefunction.

Electron correlation can be broadly classified into two categories: (i) static (or nondynamic) correlation and (ii) dynamic correlation. Although this distinction is not always sharply defined, it provides a useful conceptual framework. Static correlation arises in situations where a single electronic configuration is insufficient to qualitatively describe the electronic structure of the system. Dynamic correlation, on the other hand, refers to the short-range, instantaneous interactions between electrons and is typically treated as a correction to a qualitatively correct zeroth-order description.

To address these deficiencies, multireference methods have been developed that extend beyond the single-reference framework. The first method discussed here, the Multiconfigurational Self-Consistent Field (MCSCF), is primarily designed to recover static correlation by allowing multiple electron configurations and optimizing both the orbital and configuration interaction parameters. Subsequent post-MCSCF treatments, such as Multireference Configuration Interaction with Single and Double excitations (MR-CISD) and the Multireference Averaged Quadratic Coupled-Cluster (MR-AQCC) method, aim to recover dynamic correlation.

3.2.2.1 Multiconfigurational Self-Consistent Field

The Multiconfigurational Self-Consistent Field (MCSCF) method constitutes the foundation of multireference electronic structure theory. It represents a critical improvement over the Hartree–Fock model in situations where a single Slater determinant fails to cap-

ture the essential features of the electronic wavefunction. This typically occurs in systems characterized by near-degeneracies, such as bond dissociation processes, open-shell singlets, transition states, or excited electronic states with significant multiconfigurational character.

The MCSCF wavefunction is constructed as a linear combination of configuration state functions (CSFs), which are spin-adapted functions that ensure the wavefunction is an eigenfunction of the total spin operator, and often also of the spatial symmetry operators of the molecule. Each CSF is itself a linear combination of Slater determinants. Formally, the MCSCF wavefunction is expressed as:

$$|\Psi_{\mathrm{MCSCF}}\rangle = \sum_n b_n |\Phi_n\rangle, \tag{3.18}$$

where $\{|\Phi_n\rangle\}$ are CSFs constructed from a set of molecular orbitals (MOs), and b_n are variational coefficients. A central feature of MCSCF is that both the CI coefficients $\{b_n\}$ and the MOs themselves are variationally optimized, the latter expanded in terms of atomic basis functions (Equation 3.16).

The most widely used MCSCF variant is the Complete Active Space Self-Consistent Field (CASSCF) method.[6] In CASSCF, orbitals are divided into inactive (always doubly occupied or unoccupied) and active subspaces. All possible occupations of the active orbitals by the active electrons, consistent with spin and spatial symmetry, are included in the expansion of the wavefunction. The notation CAS(n_e, n_o) indicates that n_e electrons are distributed among n_o active orbitals. Due to the factorial growth of the complete active space (CAS) with the number of active orbitals, occupation restrictions have been introduced through the concept of restricted active spaces (RAS),[7] which partition the active space into three subspaces: the restricted (RAS), complete (CAS), and auxiliary (AUX) subspaces (Figure 3.1). In the RAS subspace, a specified maximum number of holes is allowed; in the CAS subspace, all possible occupations are permitted; and in the AUX subspace, electrons may be placed up to a predefined maximum.

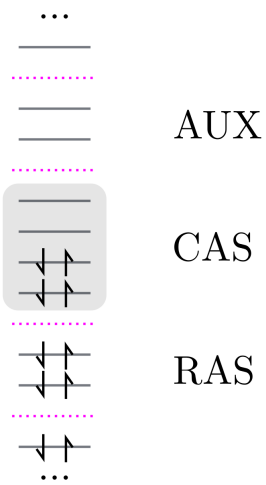

FIGURE 3.1 – Schematic representation of the active spaces (RAS, CAS, and AUX) when restricted active subspaces are employed

A balanced description of both ground and excited states usually requires a state-averaged (SA-MCSCF)[8] variant of MCSCF, in which the average energy of several states is optimized to obtain a balanced description of these states. State-averaging allows one to get a single set of optimized orbitals, which are, in principle, equally good for all electronic states considered.

CASSCF provides an accurate treatment of static correlation and serves as the reference for subsequent dynamic correlation treatments (Sections 3.2.2.2 and 3.2.2.3). However, the method's accuracy and, crucially, the qualitatively correct wave function, hinge critically on the adequate choice of the active space.

3.2.2.2 Multireference Configuration Interaction

Once a qualitatively correct wavefunction is obtained, it is often necessary to recover dynamic correlation, which accounts for the finer details of electron–electron interactions beyond the static correlation already included. MRCI operates by initially constructing a space of reference configurations, exciting electrons out of these configurations, and solving the electronic Schrödinger equation by variationally minimizing the energy in the resulting configuration space. In its uncontracted variant (which is the focus of this work), excitations are performed with respect to each individual reference configuration.

The union of all such excited configurations, up to a given excitation level, forms the full MRCI configuration space. For practical reasons, only single and double excitations are typically included, leading to the widely used MR-CISD (Multireference Configuration Interaction with Single and Double excitations) approximation. The MR-CISD wavefunc-

tion takes the form:[9]

$$|\Psi_{\text{MR-CISD}}\rangle = \sum_r b_r|\Phi_r\rangle + \sum_{r,i,a} b_i^a|\Phi_i^a(r)\rangle + \sum_{r,i<j,a<b} b_{ij}^{ab}|\Phi_{ij}^{ab}(r)\rangle, \tag{3.19}$$

where $|\Phi_r\rangle$ are the reference CSFs, $|\Phi_i^a(r)\rangle$ are single excitations, and $|\Phi_{ij}^{ab}(r)\rangle$ are double excitations from the reference CSFs. Each excitation is spin-adapted and consistent with the desired total spin and spatial symmetry. Here, only the CI coefficients $\{b_r, b_i^a, b_{ij}^{ab}\}$ are optimized variationally to minimize the total electronic energy. The variationality of MRCI also leads to the fact that wave function properties, such as dipole moments and energy gradients, can be easily computed.

Although MR-CISD significantly improves upon the static correlation described at the CASSCF level, it is not size-extensive. Size-extensivity refers to the property of a method whereby the total energy scales correctly with the number of electrons or the system size.[10] A related but distinct concept is size-consistency, which requires that the energy of two non-interacting subsystems computed together equals the sum of their individual energies computed separately.[11] Truncated CI methods, including MR-CISD, violate both properties due to the exclusion of disconnected higher-order excitations.

To partially correct for this deficiency, several *a posteriori* corrections have been developed. Two commonly used classes are the Davidson[12,13] and Pople[11] corrections, which aim to approximate the missing contribution of unlinked higher excitations.

A key advantage of *a posteriori* size-extensivity corrections lies in their low computational cost and numerical stability. However, these benefits come at the expense of a fundamental drawback: such corrections break the variational nature of the underlying method. This has two major implications. First, the extensivity corrected energy is no longer an upper bound to the true energy. Second, it is not readily possible to compute the gradient of the extensivity corrected energy or to compute extensivity corrections to other wave function properties. An alternative to *a posteriori* corrections is to employ multireference methods that intrinsically incorporate size-extensivity. Among these, the multireference averaged quadratic coupled-cluster (MR-AQCC)[14] method stands out as a particularly effective approach.

3.2.2.3 Multireference Averaged Quadratic Coupled-Cluster (MR-AQCC)

A more rigorous way to address the lack of size-extensivity in truncated CI-based methods, such as MR-CISD, is to modify the underlying energy functional itself. The Multireference Averaged Quadratic Coupled-Cluster (MR-AQCC) method achieves this by introducing an intrinsic size-extensivity correction that is incorporated directly into the iterative solution procedure.[14] In this approach, the correlation energy is expressed as

a functional of the CI coefficient vector $\mathbf{b}$, defined as:

$$F(\mathbf{b}) = \frac{\left\langle \sum_{m=1}^{N_{\mathrm{CI}}} b_m \Phi_m \middle| \hat{H} - E_{\mathrm{ref}} \middle| \sum_{m=1}^{N_{\mathrm{CI}}} b_m \Phi_m \right\rangle}{\sum_k (b_k^{\mathrm{int}})^2 + G \sum_l (b_l^{\mathrm{ext}})^2}, \tag{3.20}$$

where E_{ref} is the energy of the multireference reference function. The set $\{\Phi_m\}$ includes both internal (reference) and external (singly and doubly excited) configurations. The summations in the denominator run over the internal (b_k^{int}) and external (b_l^{ext}) components of the CI vector, respectively. The factor G controls the relative weighting of the external configurations in the denominator and effectively distinguishes between different methods: $G = 1$ corresponds to standard MRCI, while $G < 1$ yields size-extensive variants.

For MR-AQCC, the value of G is chosen as:

$$G = 1 - \frac{(n_e - 3)(n_e - 2)}{n_e(n_e - 1)}, \tag{3.21}$$

where n_e is the number of correlated electrons. This choice results in a reduction of the energetic contribution of external configurations, mimicking the effect of including higher-order disconnected excitations absent in MR-CISD.

Minimizing the functional $F(\mathbf{c})$ yields the MR-AQCC energy, and the procedure can be interpreted as solving a shifted eigenvalue problem where the Hamiltonian matrix elements involving external configurations are scaled by $(1 - G)\Delta E$, with ΔE being the correlation energy. In practice, this leads to a renormalization of the CI coefficients, which are optimized variationally during the MR-AQCC procedure. As a result, gradients and other wavefunction-dependent properties can be evaluated consistently.

These multireference methods—CASSCF, MR-CISD, and MR-AQCC—form the theoretical backbone for the accurate description of complex electronic structures in this work. Each method addresses different facets of the electron correlation problem, and their combination provides a powerful toolkit for the investigation of excited states.

3.2.3 Density Functional Theory

Although not central to this work, Density Functional Theory (DFT) was employed for ground-state geometry optimizations and harmonic vibrational frequency calculations, owing to its favorable balance between computational cost and chemical accuracy. DFT reformulates the many-body Schrödinger equation in terms of the electron density $\rho(\mathbf{r})$ rather than the many-electron wavefunction, resulting in a substantial computational advantage: while the electronic wavefunction depends on three spatial coordinates (plus spin) for each electron, the electron density depends only on three spatial (and spin)

coordinates in total.

The foundation of DFT lies in the Hohenberg–Kohn theorems,[15] which establish that the ground-state properties of a many-electron system are uniquely determined by its electron density, and that a variational principle applies to the total energy as a functional of $\rho(\mathbf{r})$.

In practice, the Kohn–Sham approach[16] is employed, wherein the interacting system is mapped onto a fictitious system of noninteracting electrons subject to an effective potential. This potential includes the external potential, the Coulomb repulsion, and the exchange–correlation potential $V_{\mathrm{xc}}[\rho]$, which is not known exactly and must be approximated. The accuracy of DFT, therefore, depends on the quality of the exchange–correlation functional used.

Excited electronic states are often accessed within the DFT framework using time-dependent density functional theory (TDDFT), which calculates poles in the response of the ground-state density to a time-varying applied electric field. These poles correspond to Bohr frequencies, or excitation energies.[17] However, TDDFT often does not yield a potential with the correct long-range Coulomb tail. As a result, excitation energies corresponding to states that sample this tail—such as diffuse Rydberg states and certain charge-transfer excited states—are not accurately predicted. The method also fails to describe static correlation effects well, as it is based on a single-reference configuration of Kohn–Sham orbitals. These limitations restrict the applicability of TDDFT in cases where strong or static correlation plays a central role.

Bibliography

1 SCHATZ, George C; RATNER, Mark A. **Quantum mechanics in chemistry**. Mineola, NY: Dover Publications, 2002.

2 LEVINE; N, Ira. **Quantum Chemistry**. 7. ed. [S.l.]: Pearson Prentice Hall, 2014.

3 JENSEN, Frank. **Introduction to Computational Chemistry**. 3. ed. [S.l.]: Wiley, 2017.

4 BORN, M.; OPPENHEIMER, R. Zur Quantentheorie der Molekeln. **Annalen der Physik**, v. 389, n. 20, p. 457–484, 1927.

5 BORN, M.; HUANG, K. **Dynamical theory of crystal lattices**. Oxford: Oxford University Press, 1954.

6 ROOS, Björn O.; TAYLOR, Peter R.; SIGBAHN, Per E.M. A complete active space SCF method (CASSCF) using a density matrix formulated super-CI approach. **Chemical Physics**, North-Holland, v. 48, n. 2, p. 157–173, May 1980.

7 MALMQVIST, Per Aake.; RENDELL, Alistair.; ROOS, Bjoern O. The restricted active space self-consistent-field method, implemented with a split graph unitary group approach. **The Journal of Physical Chemistry**, v. 94, n. 14, p. 5477–5482, July 1990.

8 WERNER, Hans-Joachim; MEYER, Wilfried. A quadratically convergent MCSCF method for the simultaneous optimization of several states. **The Journal of Chemical Physics**, v. 74, n. 10, p. 5794–5801, May 1981.

9 SHAMASUNDAR, K. R.; KNIZIA, Gerald; WERNER, Hans-Joachim. A new internally contracted multi-reference configuration interaction method. **The Journal of Chemical Physics**, v. 135, n. 5, Aug. 2011.

10 BARTLETT, R J. Many-Body Perturbation Theory and Coupled Cluster Theory for Electron Correlation in Molecules. **Annual Review of Physical Chemistry**, v. 32, n. 1, p. 359–401, Oct. 1981.

11 POPLE, J. A.; SEEGER, R.; KRISHNAN, R. Variational configuration interaction methods and comparison with perturbation theory. **International Journal of Quantum Chemistry**, v. 12, S11, p. 149–163, June 2009.

12 LANGHOFF, Stephen R.; DAVIDSON, Ernest R. Configuration interaction calculations on the nitrogen molecule. **International Journal of Quantum Chemistry**, v. 8, n. 1, p. 61–72, Jan. 1974.

13 DAVIDSON, Ernest R.; SILVER, Donald W. Size consistency in the dilute helium gas electronic structure. **Chemical Physics Letters**, v. 52, n. 3, p. 403–406, Dec. 1977.

14 SZALAY, Péter G.; BARTLETT, Rodney J. Multi-reference averaged quadratic coupled-cluster method: a size-extensive modification of multi-reference CI. **Chemical Physics Letters**, v. 214, n. 5, p. 481–488, Nov. 1993.

15 HOHENBERG, P.; KOHN, W. Inhomogeneous Electron Gas. **Physical Review**, v. 136, 3B, b864–b871, Nov. 1964.

16 KOHN, W.; SHAM, L. J. Self-Consistent Equations Including Exchange and Correlation Effects. **Physical Review**, v. 140, 4A, a1133–a1138, Nov. 1965.

17 CASIDA, Mark E. Time-Dependent Density Functional Response Theory for Molecules. In: [s.l.: s.n.], Nov. 1995. p. 155–192.

4 A Multi-Descriptor Analysis of Substituent Effects on the Structure and Aromaticity of Benzene Derivatives: π-Conjugation vs. Charge Effects

4.1 Computational details

Geometry optimizations and analytical vibrational frequency calculations for the monosubstituted (X = CH_3, CH_2^-, CH_2^+, NH_2, NH^-, NH^+, OH, O^-, and O^+) and *para*-homodisubstituted (X = CH_3, CH_2, NH_2, NH, OH, and O) benzene derivatives (Figure 4.1) were performed using the hybrid functional B3LYP[1,2] with the def2-TZVP basis set.[3,4] An ultrafine integration grid and tight convergence criteria (10^{-8} for the SCF calculations and 10^{-8} atomic units for the geometry optimizations) were used. The equilibrium geometries and analytical harmonic frequencies were also obtained using the ωB97X-D[5] with the def2-TZVPD[3,4] basis set. Upon comparing the geometries obtained at both levels of theory, no root mean square deviation (RMSD) values larger than 0.008 Åwere observed for the superposition between the respective geometries, with an average value of 0.006 Å. A few aromaticity descriptors (specifically HOMA, AI(vib), and NICS) were computed at both levels of theory, showing no discrepancies in the results (see Table A.21 in the Supplementary Information for this chapter in Appendix A). Herein, all presented results are based on the geometries and analytical harmonic frequencies obtained at the B3LYP/def2-TZVP level of theory.

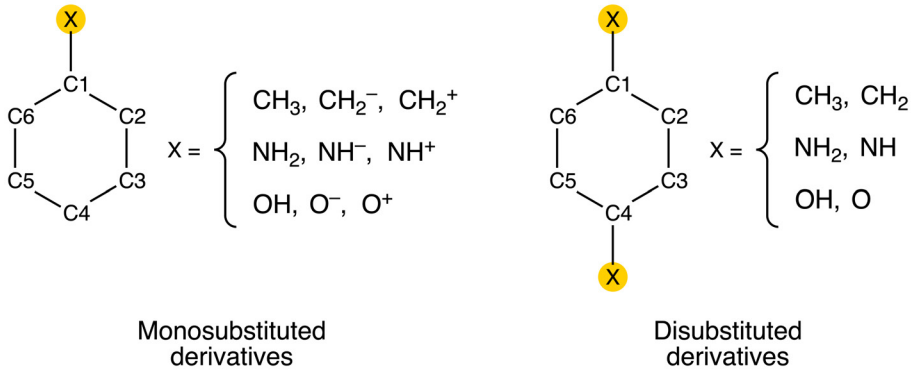

FIGURE 4.1 – Scheme of monosubstituted and disubstituted benzene derivatives investigated in this study. The carbon numbering presented is used throughout the work.

The equilibrium geometries were used to investigate the geometry-based aromatic character according to the harmonic oscillator model of aromaticity (HOMA).[6–10] This model utilizes the Kekulé benzene alternated single and double bonds as a reference of a non-aromatic system to set Equation 4.1.

$$\begin{aligned} \mathrm{HOMA} &= 1 - \frac{\alpha}{\mathrm{NB}} \sum \left(R_{\mathrm{opt}} - R_{\mathrm{i}}\right)^2 \\ &= 1 - \alpha \left[\left(R_{\mathrm{opt}} - R_{\mathrm{av}}\right)^2 + \frac{1}{\mathrm{NB}} \sum \left(R_{\mathrm{av}} - R_{\mathrm{i}}\right)^2 \right] \\ &= 1 - \mathrm{EN} - \mathrm{GEO} \end{aligned} \tag{4.1}$$

where R_{opt} (1.394 Å) is determined by averaging the single- and double-bond lengths of Kekulé benzene, modeled by the CC bonds of trans-1,3-butadiene (B3LYP/def2-TZVP level of theory). NB is equal to six, the total number of CC bonds of the aromatic system; $\alpha = 285.34$ Å^{-2} is set to enforce HOMA = 0 for the Kekulé benzene; R_{i} is the CC bond distances of the molecule considered, and Rav is the average value of CC bond lengths. Positive values indicate a decrease in bond alternation, thus an increase in aromaticity, whereas negative values indicate antiaromaticity. The components EN (the second term in Equation 4.1b) and GEO (the third term in Equation 4.1b) quantitatively describe the decrease of the π-electron delocalization due to the elongation of the mean bond length and the increase of the bond length alternation, respectively.

An alternative approach to HOMA based on vibrational spectroscopy is provided by the aromaticity index AI(vib). The AI(vib) is based on local stretching force constants (k^a), a more sensitive and reliable bond strength parameter,[11,12] capable of probing the strength of a bond for an infinitesimal change in the bond length. Local vibrational modes and associated local force constants are obtained by solving a local equivalent of the Wilson equation of vibrational spectroscopy through a procedure detailed in a recent review article.[13]

To simplify the analysis of the bond strength, k^a values are converted into Relative

Bond Strength Orders RBSO (n) through the power relationship $n = a(k^a)^b$, according to the generalized Badger rule.[14] The a and b constants are defined by two reference values and assuming that for $k^a = 0$, $n = 0$. In this work, ethane and ethene were used to obtain the constants a and b. Setting $n = 1$ for ethane CC single bond (k^a(CC) = 4.247 mdyn Å^{-1}) and $n = 2$ for ethene CC double bond (k^a(CC) = 10.001 mdyn Å^{-1}), one can find a and b to be 0.310 and 0.809, respectively.

Analogously to the HOMA equation, AI(vib) is given by Equation 4.2

$$\begin{aligned} \mathrm{AI(vib)} &= 1 - \frac{\gamma}{\mathrm{NB}} \sum \left(n_{\mathrm{opt}} - n_{\mathrm{i}}\right)^2 \\ &= 1 - \gamma \left[\left(n_{\mathrm{opt}} - n_{\mathrm{av}}\right)^2 + \frac{1}{\mathrm{NB}} \sum \left(n_{\mathrm{av}} - n_{\mathrm{i}}\right)^2 \right] \\ &= 1 - \mathrm{WS} - \mathrm{ALT} \end{aligned} \tag{4.2}$$

where n_{opt} (1.546 unitless) is the optimal RBSO, determined by averaging the single- and double-bond strength orders of Kekulé benzene, modeled by the CC bonds of trans-1,3-butadiene; n_{av} is the averaged RBSO of the target molecule, and $\gamma = 6.839$ (unitless) is chosen to make AI(vib) = 0 for Kekulé benzene. WS (the second term in Equation 4.2b) is the weakening-strengthening index of all bonds compared to the average RBSO, and ALT (the third term in Equation 4.2b) is the degree of bond strength alternation. The Cartesian coordinates and harmonic frequencies of ethane, ethene, and 1-3-butadiene are presented in Section A.1, and their RBSO values are shown in Figures A.1 and A.2 in the Supplementary Information for this chapter in Appendix A. For derivatives containing the methyl group, the force constant of the first normal mode, which is related to the rotation of the substituent, is small but non-zero (0.0003 and 0.0001 mdyn/Åfor methylbenzene and p-dimethylbenzene, respectively). This small value reflects the low internal rotation potential barrier of the methyl group (within 0.03 kcal mol^{-1}), indicating a nearly free rotor system.[15] However, this leads to numerical instability when calculating local CC stretching frequencies and force constants, resulting in an unreliable value of AI(vib). To overcome this issue, the first normal mode was projected out from the calculation of the local modes of methylbenzene and p-dimethylbenzene. Local mode analysis was performed using the LModeA-nano package.[16] A complementary analysis in the context of the quantum theory of atoms in molecules (QTAIM)[17] was performed to probe the nature of the bonds of interest. The electron density ρ, its Laplacian $\nabla^2\rho$, and the energy density H were calculated at the path critical points using the Multiwfn software.[18]

Topological analysis of the aromaticity based on the Electron Localization Function (ELF)[19,20] was also performed. The ELF is originally derived from the spherically averaged conditional pair probability density within the Hartree-Fock approximation.[19] In the context of the density functional theory, it was later interpreted as the excess of local

kinetic energy density, which arises from Pauli repulsion[20]

$$\mathrm{ELF}(\mathbf{r}) = \frac{1}{1 + [D(\mathbf{r})/D_0(\mathbf{r})]^2} \tag{4.3}$$

where $D(\mathbf{r})$ can be seen as the exact kinetic energy density of the non-interacting electrons system and reveals the excess of local kinetic energy density caused by Pauli repulsion. On the other hand, $D_0(\mathbf{r})$ can be interpreted as the Thomas-Fermi kinetic energy density, which is the exact kinetic energy density of a non-interacting, uniform electron gas.[21] Formally, for a closed shell system

$$\begin{aligned} D(\mathbf{r}) &= \frac{1}{2}\sum_i \eta_i |\nabla\phi_i(\mathbf{r})|^2 - \frac{1}{8}\frac{|\nabla\rho(\mathbf{r})|^2}{\rho(\mathbf{r})} \\ D_0(\mathbf{r}) &= \frac{3}{10}\left(3\pi^2\right)^{2/3}\rho(\mathbf{r})^{5/3} \\ \rho &= \sum_i \eta_i |\phi_i(\mathbf{r})|^2 \end{aligned} \tag{4.4}$$

where ϕ is the orbital wave function and η the occupation number of the ith orbital. Since $D(\mathbf{r})$ is weighted by the corresponding quantity for a uniform electron gas reference, $D_0(\mathbf{r})$, the ELF reveals the degree of relative localization and is constrained to vary in the interval [0,1]. The Pauli principle has little effect on the behavior of electrons when they are alone or in pairs of antiparallel spins; as a result, the excess local kinetic energy is low, and ELF is close to 1. In contrast, at the boundaries between these regions, there is a higher probability of finding parallel spin electrons close to one another; as a result, the excess local kinetic energy is high, and ELF is low. A rational quantitative description of the aromaticity was achieved by determining the bifurcation value for ring closure of the π-basin.[22] The π-densities derived from the density functional theory (DFT) and multireference configuration interaction (MRCI) were analyzed using the Multiwfn software.[18] Natural orbitals were used in the case of the MRCI density analysis.

The electronic aspect of aromaticity was assessed through a multicenter analysis that characterizes the extent of delocalized cyclic bonding in individual benzenoid rings. For a restricted single-determinant wavefunction, utilizing the AIM atomic partition, the I_{ring} index[23] is determined by

$$I_{\mathrm{ring}}(\mathcal{A}) = 2^n \sum_{i_1,i_2,\ldots,i_n}^{N_{occ}} S_{i_1 i_2}(A_1)\cdots S_{i_n i_1}(A_n), \tag{4.5}$$

where the n atoms in the string $\mathcal{A} = A_1, A_2, \cdots, A_n$ are ordered according to their connectivity in the ring, and $S_{ij}(A_1)$ represents the matrix element corresponding to the overlap integral between occupied molecular orbitals i and j computed over the basin

of atom A. The I_{ring} index considers only the term with the numbering of the atoms that reflects the bonding interactions typical for Kekulé structures. Summing up all the possible I_{ring} contributions resulting from the permutations of atomic labels $A_1, \ldots, A_n$, one obtains the multicenter index (MCI),[24,25] whose formula is given by

$$\text{MCI}(\mathcal{A}) = \frac{1}{2n} \sum_{P(\mathcal{A})} I_{\text{ring}}(\mathcal{A}), \tag{4.6}$$

where $P(\mathcal{A})$ represents a permutation operator that interchanges the atomic labels $A_1, \cdots, A_n$ to generate $n!$ permutations of the elements in the string $\mathcal{A}$. By doing this, one considers not only the term referring to the Kekulé structure but also all valence bond structures corresponding to different permutations of the atomic labels. The atomic overlap matrices, calculated using the AIM partition, were computed using the AIMAll software.[26] Both I_{ring} and MCI were calculated using the ESI-3D program.[27]

The nucleus-independent chemical shift (NICS)[28] was used to depict the magnetic aspect of the aromaticity; it is defined as the negative of the spherically averaged magnetic shielding computed at chosen points of interest:

$$\text{NICS}\left(\mathbf{R}\right) = -\frac{1}{3}\text{tr}\left[\underline{\sigma}(\mathbf{R})\right] = -\frac{1}{3}\left(\sigma_{xx}\left(\mathbf{R}\right) + \sigma_{yy}\left(\mathbf{R}\right) + \sigma_{zz}\left(\mathbf{R}\right)\right) \tag{4.7}$$

in which the chemical shielding tensor $\underline{\sigma}\left(\mathbf{R}\right)$ at point $\mathbf{R}$ describes the relation between applied ($\mathbf{B}_{\text{ext}}$) and induced ($\mathbf{B}_{\text{ind}}$) magnetic field.[29] Such relation is defined as $\mathbf{B}_{\text{ind}}\left(\mathbf{R}\right) = -\underline{\sigma}\left(\mathbf{R}\right)\mathbf{B}_{\text{ext}}$ where the tensor $\underline{\sigma}\left(\mathbf{R}\right)$ is given as a non-symmetric 3×3 matrix containing nine independent values. A detailed analysis of the shielding tensors was accomplished through visualization of the chemical shielding tensors (VIST) method[30] implemented in TheoDORE.[31] VIST proceeds by computing the principal axes $\mathbf{q}^{(1)}$, $\mathbf{q}^{(2)}$, $\mathbf{q}^{(3)}$ of the shielding tensor via an eigenvalue decomposition: $\underline{\sigma}\mathbf{q}^{(i)} = t^{(i)}\mathbf{q}^{(i)}$. Subsequently, a local coordinate system oriented according to the eigenvectors $\mathbf{q}^{(i)}$ is constructed. It is worth noting that in analogy to Equation (4.7), the NICS value is one-third of the sum of the three eigenvalues $t^{(i)}$:

$$\text{NICS} = -\frac{1}{3}\text{tr}\left[\underline{\sigma}\right] = -\frac{1}{3}\left(t^{(1)} + t^{(2)} + t^{(3)}\right). \tag{4.8}$$

This method provides graphical information about the chemical shielding tensor and allows the visualization of local variations in aromaticity and antiaromaticity.[30] The chemical shielding tensors were calculated employing the gauge-independent atomic orbital (GIAO) method[32] utilizing the B3LYP functional with the basis set pcS-3[33] downloaded from the Basis Set Exchange software,[34] which was previously found to result in good accuracy.[35]

The strength of the π-electron accepting/donating character was estimated in terms of the pEDA (π-electron donor-acceptor) and sEDA (σ-electron donor-acceptor) descriptors,[36] constructed in the context of the natural population analysis based on natural bond orbital theory[37]:

$$\text{pEDA} = \sum_{j=1}^{6} \pi^{j}_{\text{C}_6\text{H}_5\text{X}} - \sum_{j=1}^{6} \pi^{j}_{\text{C}_6\text{H}_6}, \tag{4.9}$$

$$\text{sEDA} = \sum_{j=1}^{6} \sigma^{j}_{\text{C}_6\text{H}_5\text{X}} - \sum_{j=1}^{6} \sigma^{j}_{\text{C}_6\text{H}_6}, \tag{4.10}$$

where $\pi^{j}_{\text{C}_6\text{H}_5\text{X}}/\pi^{j}_{\text{C}_6\text{H}_6}$ denotes the occupancy of the respective p_z orbital, and $\sigma^{j}_{\text{C}_6\text{H}_5\text{X}}/\sigma^{j}_{\text{C}_6\text{H}_6}$ denotes the occupancy of the respective s, p_x, and p_y valence orbitals of the jth benzene ring C-atom of the benzene (C_6H_6) or benzene derivative molecule ($\text{C}_6\text{H}_5\text{X}$). In a concise manner, the pEDA and sEDA descriptors provide insight into the direction of π-electron and σ-electron shifts, whether they occur towards or away from the substituent.

Static and dynamic electronic correlation effects were incorporated using the MRCI method.[38,39] Using the B3LYP/def2-TZVP equilibrium geometries, the complete active space self-consistent field (CASSCF) approach[40,41] with full valence π-electrons and π-orbitals was employed to compute the molecular orbitals and the set of reference configuration state functions (CSFs). The MRCI wave functions were constructed using the CSFs generated by CASSCF and allowing all single and double excitations. In the MRCI calculations, size-extensivity contributions were included with the Davidson-Silver method.[42,43] The corrected value is denoted by MRCI+Q. The MRCI calculations were performed for the lowest singlet S_0 and the lowest triplet T_1 state using the def2-TZVP[3,4] basis set. The vertical singlet-triplet splitting ($\text{S}_0 - \text{T}_1$ splitting), calculated as $E(\text{T}_1) - E(\text{S}_0)$, where E denotes the energy, was also estimated.

The multireference calculations were performed using the COLUMBUS program package.[44–46] For DFT calculations, Gaussian 09[47] was used.

4.2 Results and Discussion

The results for HOMA and AI(vib) indices of monosubstituted benzene derivatives are presented in Figure 4.2. The numerical values of all indices reported are available in the Supplementary Information for this chapter in Appendix A (Tables A.1 to A.14).

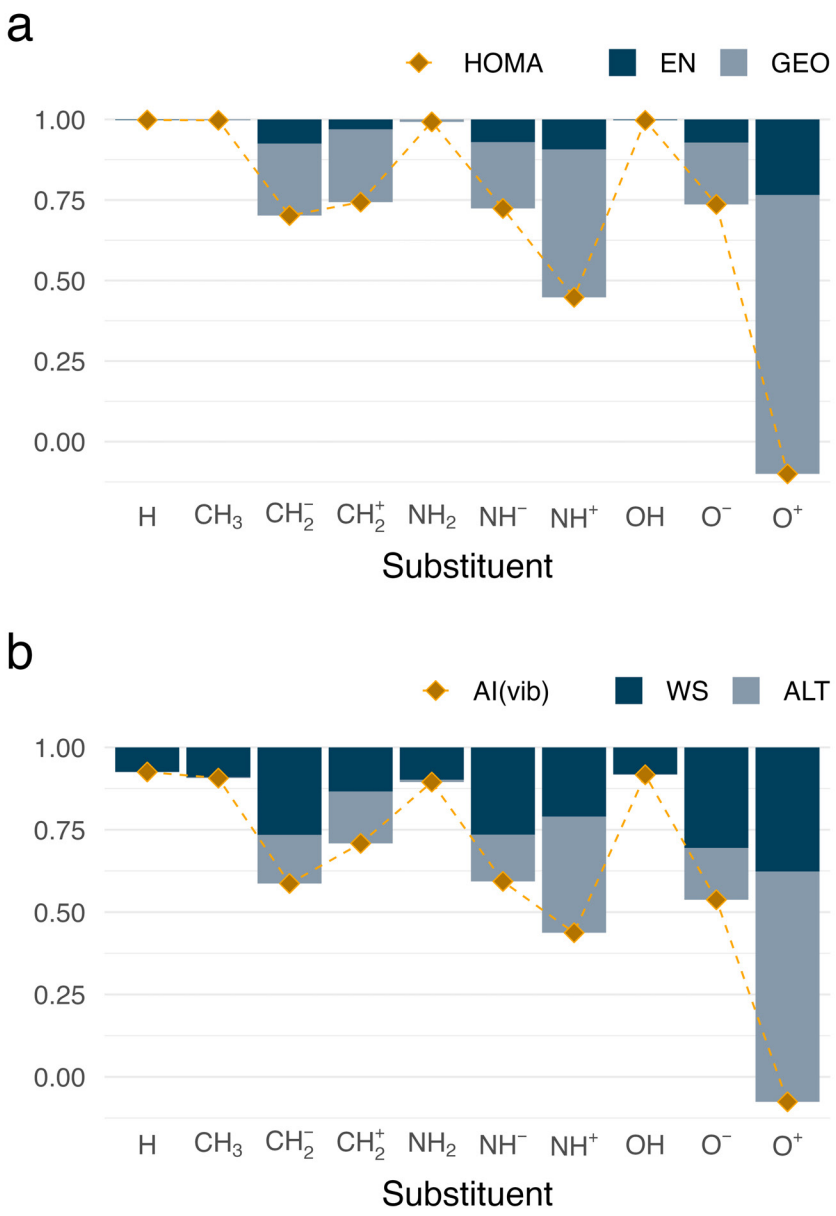

FIGURE 4.2 – Aromaticity indices (a) HOMA and (b) AI(vib) of benzene and monosubstituted benzene derivatives (yellow dashed line). The components EN (bond length elongation) and GEO (bond length alternation) of HOMA, and the components WS (bond strength weakening-strengthening) and ALT (bond strength alternation) of AI(vib) are shown in bars. The HOMA and AI(vib) indices were calculated using the geometry and frequencies obtained at the B3LYP/def2-TZVP level of theory.

As expected from previous works,[48,49] systems modified with the substituents CH_3, NH_2, and OH, have values of the structural indices HOMA and AI(vib) close to 1. On the other hand, the other substituents were found to significantly affect π-electron delocalization and reduce the index to values below 0.8. The main difference between the two groups is the availability of a p orbital on the heavy atom of the substituent. Substituents that have filled, i.e., π-electron donating (CH_2^-, NH^-, and O^-) or unfilled, i.e., π-electron accepting (CH_2^+, NH^+, and O^+) orbitals of suitable size and symmetry can interact with

the π-density of the ring and reduce the π-electron delocalization to the corresponding extent as the strength of the interaction.

The chemical bonds of interest were thoroughly studied through the charge density ρ (e Å^{-3}), its Laplacian $\nabla^2\rho$ (e Å^{-5}), and energy density H (h Å^{-3}) computed at the path critical point $\mathbf{r}_c$, which corresponds to a saddle point of the charge density ρ, i.e., $\rho(\mathbf{r}_c)$ is a minimum of $\rho(\mathbf{r})$ in the direction along the internuclear axis, but it is a maximum in the direction perpendicular to it. Essentially, the Laplacian of the charge density at the critical point $\rho(\mathbf{r}_c)$, $\nabla^2\rho(\mathbf{r}_c)$, gives evidence of the charge concentration or depletion in the bounding region, and $H(\mathbf{r}_c)$, given as a sum of the kinetic and potential energies ($H(\mathbf{r}_c) = T(\mathbf{r}_c) + V(\mathbf{r}_c)$), reveals whether the charge concentration in the internuclear region is stabilizing or destabilizing.[50]

In terms of valence bond formalism, the reduction of the π-electron delocalization can be explained by the increase in the contributions from polar canonical forms to the molecule's electronic structure.[51] Data presented in Table 4.1 reflect a strong interaction between the ring and such substituents: while the C1-C2 bond tends to get weaker and the C2-C3 bond tends to get stronger in comparison to benzene.

TABLE 4.1 – Bond Length r (Å), Local Mode Force Constants k^a (mdyn Å^{-1}), Relative Bond Strength Order Values (n), Electron Density ρ (e Å^{-3}) and its Gradient $\nabla^2\rho$ (e Å^{-5}), and Energy Density H (E_h Å^{-3}) at the Path Critical Points for benzene and monosubstituted benzene derivatives. Carbons are Numbered in Accordance with Figure 4.1.

substituent	symmetry	bond	r	k^a	n	ρ_c	$\nabla^2\rho$	H_c
H	D_{6h}	C1-C2	1.387	6.629	1.434	0.321	-0.951	-0.345
CH_3	Cs	X-C1	1.504	4.544	1.056	0.258	-0.674	-0.230
		C1-C2	1.392	6.111	1.342	0.319	-0.938	-0.341
		C2-C3	1.387	6.289	1.374	0.321	-0.952	-0.345
		C3-C4	1.387	6.359	1.386	0.321	-0.953	-0.345
CH_2^-	C_{2v}	X-C1	1.380	6.916	1.484	0.318	-0.909	-0.347
		C1-C2	1.443	5.248	1.187	0.289	-0.806	-0.284
		C2-C3	1.375	7.075	1.511	0.325	-0.954	-0.356
		C3-C4	1.400	6.188	1.356	0.310	-0.891	-0.326
CH_2^+	C_{2v}	X-C1	1.359	8.127	1.691	0.343	-1.081	-0.391
		C1-C2	1.434	5.661	1.262	0.298	-0.864	-0.298
		C2-C3	1.365	7.533	1.590	0.337	-1.036	-0.377
		C3-C4	1.401	6.254	1.368	0.316	-0.945	-0.335
NH_2	C_s	X-C1	1.391	5.280	1.193	0.307	-0.966	-0.409
		C1-C2	1.395	6.351	1.385	0.317	-0.935	-0.339

		C2-C3	1.384	6.708	1.448	0.321	-0.947	-0.346
		C3-C4	1.387	6.613	1.431	0.320	-0.947	-0.344
NH^-	C_s	X-C1	1.324	7.575	1.597	0.362	-1.229	-0.525
		C1-C2	1.440	5.303	1.197	0.294	-0.838	-0.292
		C2-C3	1.376	7.078	1.512	0.325	-0.955	-0.355
		C3-C4	1.400	6.236	1.365	0.311	-0.895	-0.326
		C4-C5	1.396	6.381	1.390	0.313	-0.905	-0.331
		C5-C6	1.379	6.908	1.482	0.323	-0.943	-0.350
		C6-C1	1.441	5.191	1.176	0.292	-0.817	-0.289
NH^+	C_s	X-C1	1.281	9.826	1.972	0.392	-1.129	-0.693
		C1-C2	1.459	5.056	1.152	0.290	-0.843	-0.282
		C2-C3	1.360	7.792	1.634	0.341	-1.059	-0.386
		C3-C4	1.404	6.165	1.352	0.314	-0.943	-0.333
		C4-C5	1.413	5.903	1.305	0.309	-0.921	-0.323
		C5-C6	1.355	8.022	1.673	0.343	-1.065	-0.391
		C6-C1	1.460	4.917	1.126	0.287	-0.822	-0.278
OH	C_s	X-C1	1.359	6.088	1.338	0.295	-0.565	-0.463
		C1-C2	1.389	6.530	1.416	0.323	-0.974	-0.351
		C2-C3	1.384	6.740	1.453	0.321	-0.949	-0.346
		C3-C4	1.389	6.580	1.425	0.320	-0.945	-0.343
		C4-C5	1.386	6.679	1.443	0.321	-0.951	-0.346
		C5-C6	1.387	6.626	1.433	0.319	-0.938	-0.342
		C6-C1	1.389	6.493	1.410	0.322	-0.956	-0.347
O^-	C_{2v}	X-C1	1.261	9.031	1.841	0.380	-0.612	-0.665
		C1-C2	1.440	5.080	1.156	0.295	-0.839	-0.294
		C2-C3	1.380	6.873	1.476	0.322	-0.943	-0.350
		C3-C4	1.396	6.387	1.391	0.313	-0.908	-0.332
O^+	C_{2v}	X-C1	1.203	12.636	2.417	0.427	0.070	-0.771
		C1-C2	1.491	4.107	0.973	0.274	-0.771	-0.255
		C2-C3	1.351	8.223	1.707	0.346	-1.083	-0.397
		C3-C4	1.416	5.737	1.276	0.308	-0.918	-0.322

The electron density in the interatomic surface is proportional to the forces exerted on the bonding electrons by the nuclei;[50] hence all the parameters shown in Table 4.1 give an outright overview of the chemical bonds. We use benzene as our baseline for all the observations that follow. Values of $\nabla^2\rho(\mathbf{r}_c)$ indicate a high concentration of charge density in the bond path C1-X and C2-C3. Values $H(\mathbf{r}_c)$ indicate a clear dominance of $V(\mathbf{r}_c)$, which suggests that accumulation of electronic charge in the internuclear region is

stabilizing ($V(\mathbf{r}_c) < 0$) and nuclei are strongly bonded, as evidenced by bond lengths r and local mode force constants k_a for C1-X and C2-C3 bonds.

All the bonds presented in Table 4.1 are classified as covalent (shared shell interactions) based on the Bader-Shaik criterion ($\rho(\mathbf{r}_c) > 0.10$ and $\nabla^2\rho(\mathbf{r}_c) < 0$).[52] However, it is observed that the O^+ substituent results in a significantly smaller value of $\nabla^2\rho(\mathbf{r}_c)$compared to other substituents in the bounding region with the ring. This reduced value, combined with the proximity of the critical point to the less electronegative atom, indicates a charge-shift interaction. In the context of valence bond theory, this interaction is characterized by considerable resonance energies associated with the mixing of covalent and ionic components.[53]

All parameters indicate a substantial quinoid character for systems modified with CH_2^-, CH_2^+, NH^-, NH^+, O^-, and O^+; the bond lengths and the local mode force constants changes are reflected by the indices HOMA and AI(vib), respectively. Of course, the high contribution of the GEO and ALT components (which measures the bond length and strength alternation) to HOMA and AI(vib) values, respectively, is also a response to the structural changes caused by the substituents. On the other hand, systems modified with CH_3, NH_2, and OH have the structural parameters preserved in comparison to benzene; the data shown in Table 4.1 suggest that the ring retains the π-electron delocalization and C1-X is characterized by a single bond, although it gets stronger proportionally to the polarity of the bond (see below).

Although the AI(vib) index is more sensitive to changes in the electronic structure, the results follow roughly the same tendency obtained using HOMA. However, AI(vib) predicts slightly lower aromaticity for toluene compared to benzene due to the weakening of C2−C3 and C3−C4 bonds in toluene, which is not captured by bond distances (Table 4.1). Since magnetic and topological indices showed similar π-electron delocalization for toluene and benzene, the weakening of those bonds might be attributed to subtle electronic effects unrelated to the π-electron delocalization.

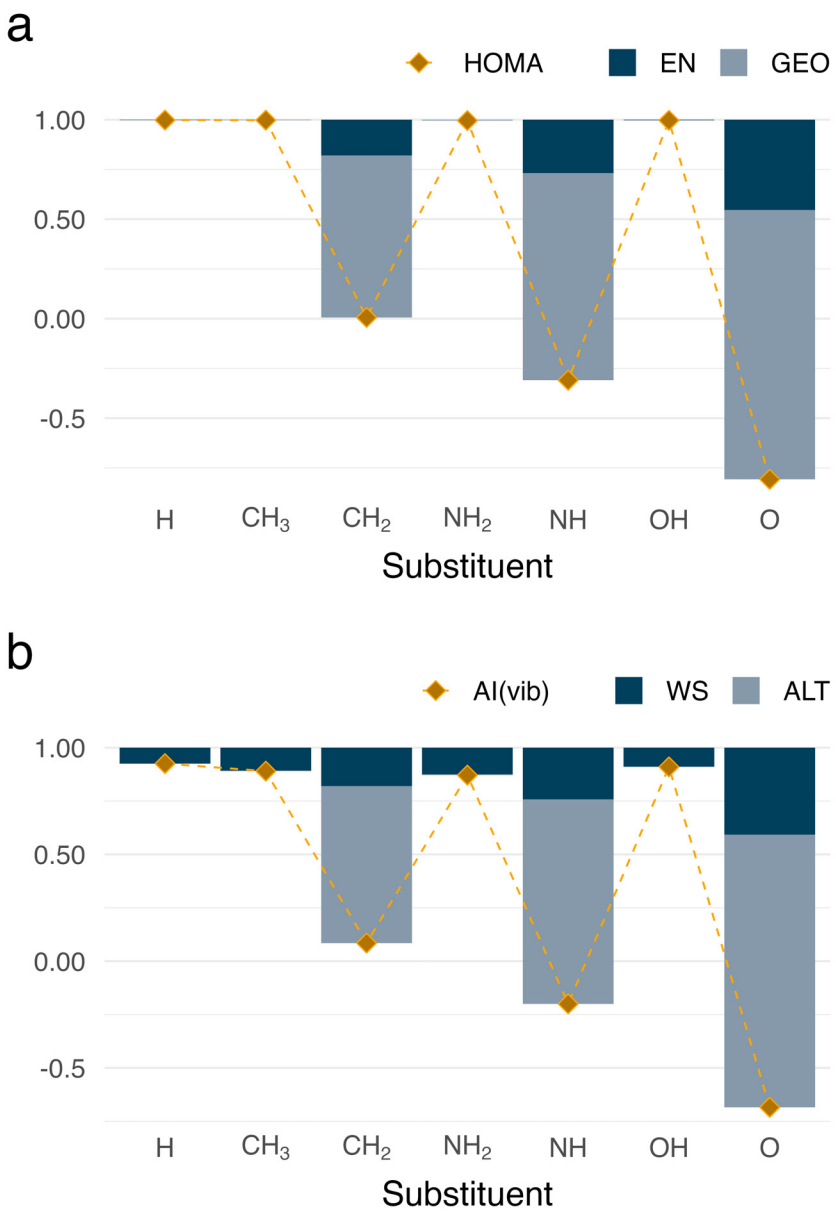

FIGURE 4.3 – Aromaticity indices (a) HOMA and (b) AI(vib) of benzene and disubstituted benzene derivatives (yellow dashed line). The components EN (bond length elongation) and GEO (bond length alternation) of HOMA, and the components WS (bond strength weakening-strengthening) and ALT (bond strength alternation) of AI(vib) are shown in bars. The HOMA and AI(vib) indices were calculated using the geometry and frequencies obtained at the B3LYP/def2-TZVP level of theory.

For disubstituted benzene derivatives, we have a more straightforward case. Substituents that have filled or unfilled p orbitals available can strongly interact with the π-electron density of the ring, resulting in a high-character quinoid structure. The data presented in Table 4.2 show that the bonds C1-X and C3-C4 (as well as the symmetry-equivalent bonds) have a high double bond character. Consequently, the aromaticity indices (Figure 4.3) are substantially reduced.

TABLE 4.2 – Bond Length r (Å), Local Mode Force Constants k^a (mdyn Å^{-1}), Relative Bond Strength Order Values (n), Electron Density ρ (e Å^{-3}) and its Gradient $\nabla^2\rho$ (e Å^{-5}), and Energy Density H (E_h Å^{-3}) at the Path Critical Points for disubstituted benzene derivatives. Carbons are Numbered in Accordance with Figure 4.1.

substituent	symmetry	bond	r	k^a	RBSO	ρ_c	$\nabla^2\rho$	H_c
CH_3	C_{2v}	X-C1	1.504	4.552	1.058	0.258	-0.673	-0.230
		C1-C2	1.387	6.592	1.427	0.321	-0.948	-0.345
		C2-C3	1.389	6.543	1.419	0.319	-0.945	-0.342
		C4-C5	1.394	6.370	1.388	0.318	-0.933	-0.338
		C5-C6	1.383	6.774	1.459	0.323	-0.959	-0.349
CH_2	D_{2h}	X-C1	1.339	8.998	1.836	0.350	-1.074	-0.406
		C1-C2	1.460	5.084	1.157	0.282	-0.792	-0.271
		C2-C3	1.336	9.208	1.871	0.352	-1.086	-0.412
NH_2	C_{2h}	X-C1	1.402	5.201	1.178	0.300	-0.918	-0.383
		C1-C2	1.392	6.408	1.395	0.319	-0.941	-0.341
		C2-C3	1.384	6.624	1.433	0.320	-0.937	-0.344
NH	C_{2h}	X-C1	1.276	10.268	2.043	0.397	-1.236	-0.697
		C1-C2	1.469	4.875	1.118	0.282	-0.803	-0.269
		C2-C3	1.332	9.389	1.900	0.355	-1.103	-0.417
		C3-C4	1.470	4.756	1.096	0.280	-0.784	-0.266
OH	C_{2h}	X-C1	1.364	6.006	1.324	0.292	-0.571	-0.454
		C1-C2	1.386	6.601	1.429	0.325	-0.977	-0.352
		C2-C3	1.385	6.651	1.438	0.319	-0.932	-0.342
		C3-C4	1.389	6.480	1.408	0.322	-0.955	-0.347
O	D_{2h}	X-C1	1.210	12.488	2.394	0.421	-0.072	-0.760
		C1-C2	1.484	4.360	1.021	0.276	-0.773	-0.259
		C2-C3	1.330	9.497	1.918	0.357	-1.113	-0.421

It is noteworthy that for mono and disubstituted benzene derivatives, the C1-X bond gets stronger as the polarity of the bond increases. As pointed out previously, the strength of a bond depends on the degree of overlap between the interacting atomic orbitals, and the bond polarity is reflected by the difference in the energies of the atomic orbitals involved in bonding.[54]

Aromaticity can be closely related to electron delocalization from an electron density viewpoint. In this sense, a topological analysis based on the Electron Localization Function, particularly its π component (ELF$_\pi$), provides both a meaningful measure of the aromaticity and an assessment of the degree to which the substituent affects the

π-electron delocalization.

In the context of multireference methods, an accurate evaluation of ELF can be achieved by adequate reformulations.[55] However, the extent of ELF to multiconfigurational wave functions is fairly complicated and challenging to implement. The densities involved in the expression of ELF (Equations (4.3) and (4.4)) can be calculated based on natural orbitals derived from multireference methods. Although the result of this implementation is not identical to the one mentioned above, it is also strict and physically meaningful, providing valuable insights into the π-electron delocalization and aromaticity trends.

For benzene, our reference system, the π component of the electron localization function (ELF_π) derived from natural orbitals of the multireference wave function is slightly more localized than ELF_π obtained at DFT/B3LYP level (Figure A.3). However, it has been shown that for polycyclic aromatic compounds for which correlation effects are more pronounced, the ELF_π obtained at multireference methods is more uniformly distributed along the whole molecule.[56] In fact, dynamical correlation allows us to capture the effect of instantaneous mutual repulsion between electrons of antiparallel spins, thus reducing the Pauli repulsion effect, which results in larger ELF values; on the other hand, the inclusion of static correlation at the CASSCF level leads to only slight changes in the ELF_π properties in comparison to DFT results.[56,57] Despite numerical differences, there is a good agreement between ELF_π isosurfaces calculated with DFT/B3LYP and MRCI methods, as discussed below.

The monosubstituted benzene derivatives modified with the substituents CH_3, NH_2, and OH, which have the central atom sp^3 hybridized, have their electron delocalization somewhat preserved in comparison to benzene (Figure 4.4). Although the π-density around C6−C1−C2 is mainly affected, no bifurcation is observed in the ring's density domain (basin). On the other hand, groups with filled (CH_2^-, NH^-, and O^-) or unfilled (CH_2^+, NH^+, and O^+) p orbitals have the π-electron localization strongly affected by the substituent. It is noteworthy that the unfilled p orbital favors a quinoid structure; the π-density around C1−X, C2−C3, and C5−C6 is more appreciable than the corresponding bonds in negatively charged systems, which is also evidenced by the relative bond strength orders (Table 4.1).

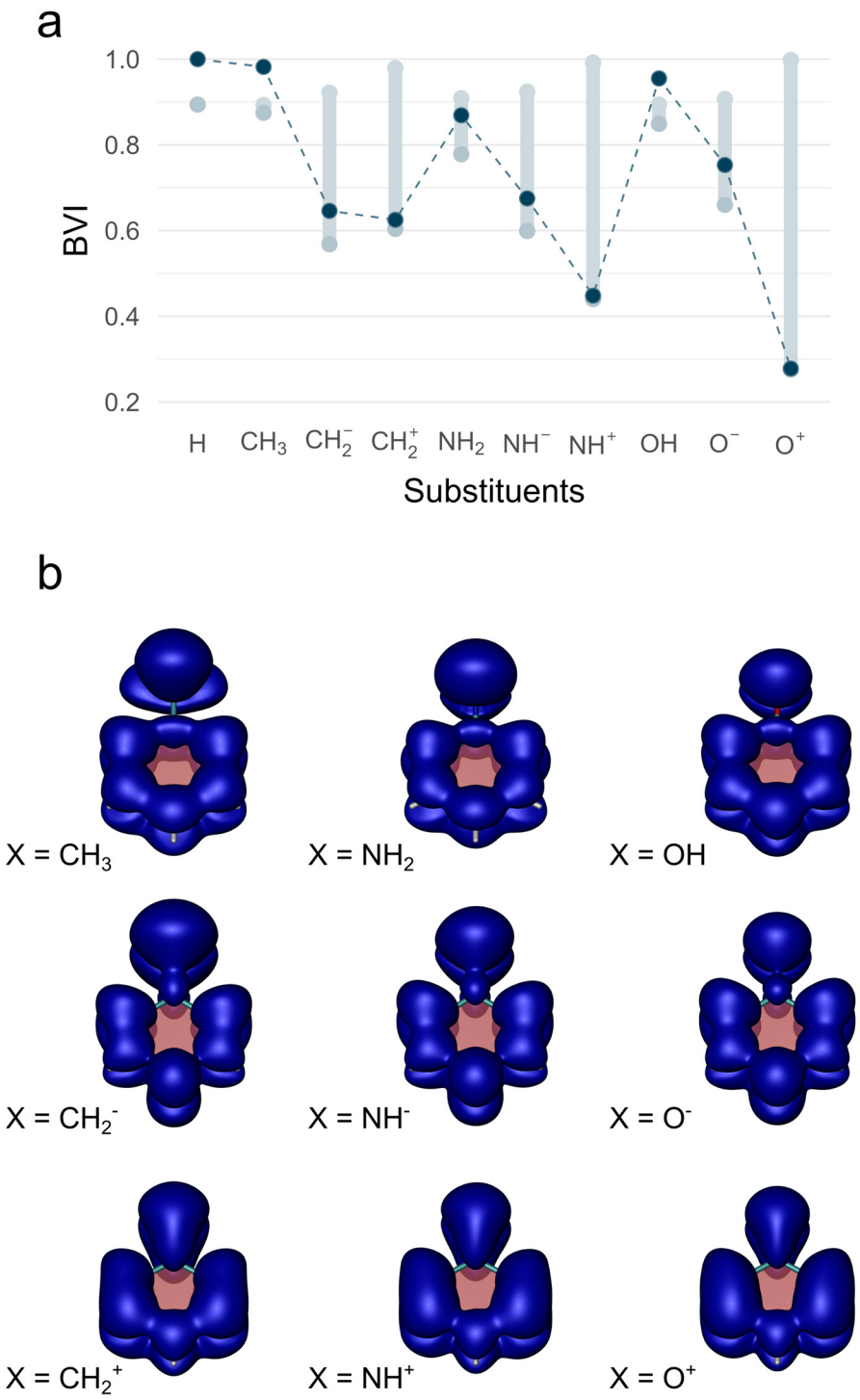

FIGURE 4.4 – (a) ELF_π-based indices for benzene and monosubstituted benzene derivatives. The vertical dumbbells show the range between BV_{max} (upper side) and BV_{min} (bottom side). The quantity $1-\Delta BV$ (where ΔBV is the span in bifurcation values ($\Delta BV = BV_{max} - BV_{min}$), defined as BVI, is represented by the dashed line. (b) Isosurface plots of the π-contribution to the electron localization function (ELF_π = 0.75) for monosubstituted benzene derivatives. The results were obtained at the B3LYP/def2-TZVP level of theory.

A rational description of the π-electron delocalization based on the ELF_π topology of

benzene derivatives can be achieved by determining the ring's bifurcation values (BV), which allows us to measure the degree to which the substituent affects the π-electron delocalization. The bifurcation values are obtained by gradually varying the isovalues of the ELF_π isosurface until merging or splitting the molecular space into different nonoverlapping regions enclosing a single electron or a lone pair. The first bifurcation value, BV_{min}, denotes the first split in the π-density of the ring; in contrast, BV_{max} is defined at the point where there are six density domains along the ring. Generally, the more uniform the electron density distribution in the π-system (characterized by larger values of BV_{min} in the ELF_π isosurface), the more aromatic the compound is expected to be. Therefore, the difference between BV_{max} and BV_{min} within a cyclic structure (ΔBV) should be ideally zero for a perfect aromatic system.

To facilitate the comparison to the other indices, here we propose the bifurcation value index (BVI), calculated as $1 - \Delta BV(ELF_\pi)$. Only the BVs of the ring are considered, i.e., the BV of the π-density between the ring and substituent is not taken into account. Since a fully aromatic compound should have $BV_{max} = BV_{min}$, BVI is expected to be 1. In contrast, BVI below 0.7 reveals a non-uniform π-delocalization, indicating that the disturbance caused by the substituent is substantial. That is the case of π-electron donating and π-electron accepting substituents (Figure 4.4). On the other hand, systems substituted with the CH_3, NH_2, and OH groups, which do not have orbitals available for mixing with the π orbitals of the ring, have indices comparable to those of benzene, and the π-electron system of the ring preserved for the most part.

For disubstituted benzene derivatives modified with π-electron donating or π-electron accepting substituents, it is possible to observe a low excess of local kinetic energy around the bonds C1-X, C2-C3, and their respective symmetry-equivalents, which causes the ELF to have high values in such regions, indicating, in this case, the presence of pairs of electrons with antiparallel spins. From the valence bond theory viewpoint, this can be understood as a dominant character of quinoid structures. In contrast, molecules modified with CH_3, NH_2, and OH present a high degree of π-delocalization around the ring, which is reflected in the BVI values (Figure 4.5).

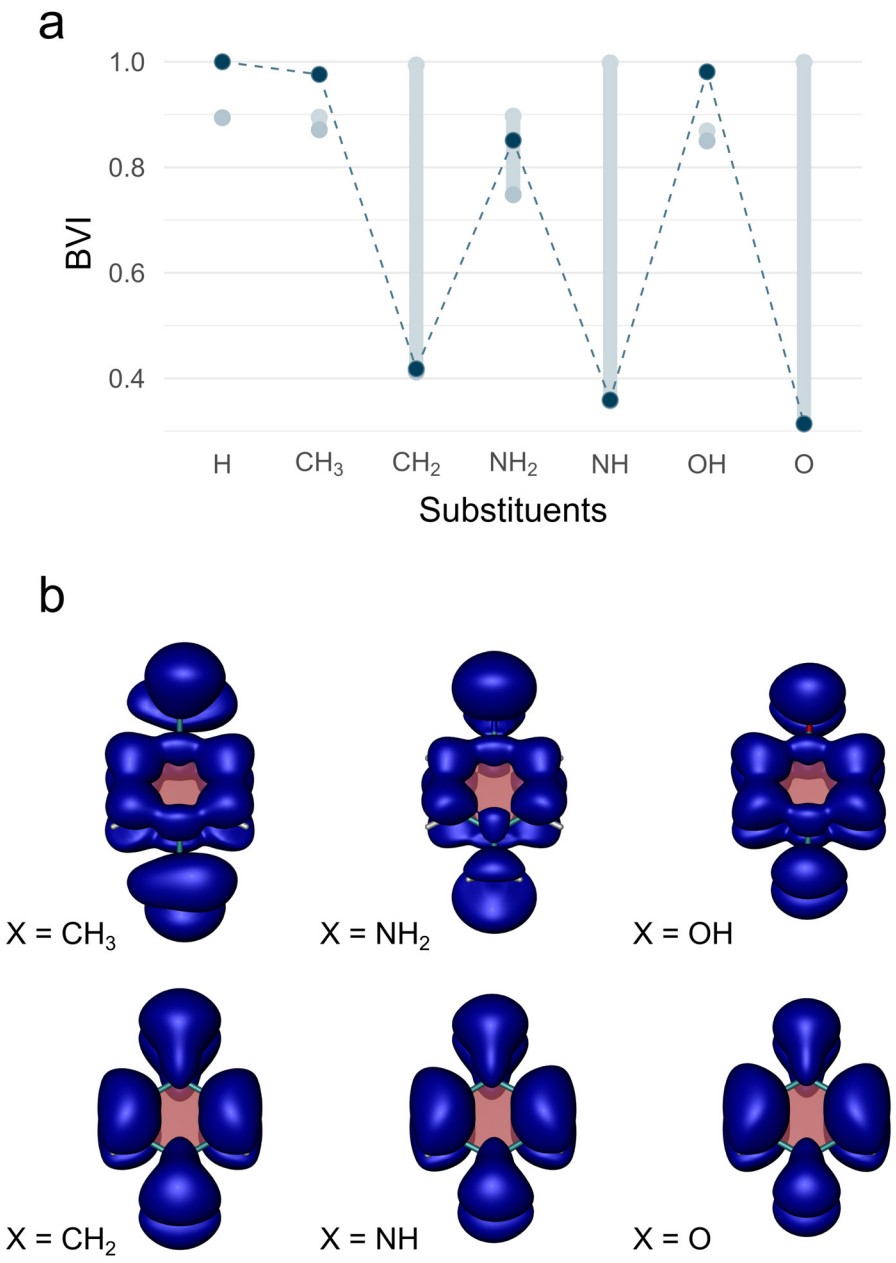

FIGURE 4.5 – (a) ELF_π-based indices for benzene and disubstituted benzene derivatives. The vertical dumbbells show the range between BV_{max} (upper side) and BV_{min} (bottom side). The quantity $1-\Delta BV$ (where ΔBV is the span in bifurcation values ($\Delta BV = BV_{max} - BV_{min}$), defined as BVI, is represented by the dashed line. (b) Isosurface plots of the π-contribution to the electron localization function (ELF_π = 0.75) for monosubstituted benzene derivatives. The results were obtained at the B3LYP/def2-TZVP level of theory.

The only notable deviation between the DFT and MRCI densities is observed for the derivative disubstituted with NH_2 (Figure A.5). Although the formulation of the ELF used in this work is initially formulated for single reference densities rather than multireference densities, and hence the ELF calculated using natural orbitals derived from MRCI calculations are only approximate, a better agreement between ΔBVI and other

indices is observed in this case. Furthermore, the first bifurcation value (BV_{min}) also provides a meaningful measure of the π-electron delocalization and follows approximately the same trend as ΔBV. A higher BV_{min} indicates a more substantial resistance of the π-density against changes caused by the substituent.

From the electronic point of view, the multicenter indices characterize the degree of cyclic delocalized conjugation within a benzenoid ring. Both evaluated indices, namely I_{ring} and MCI, provide insights into the extent of cyclic delocalized conjugation. In practical terms, I_{ring} gauges the delocalization along the ring, whereas MCI also considers the delocalization across the ring. A greater numerical value indicates a more notable simultaneous sharing of electrons among the atoms in the ring, suggesting an increased aromatic character.

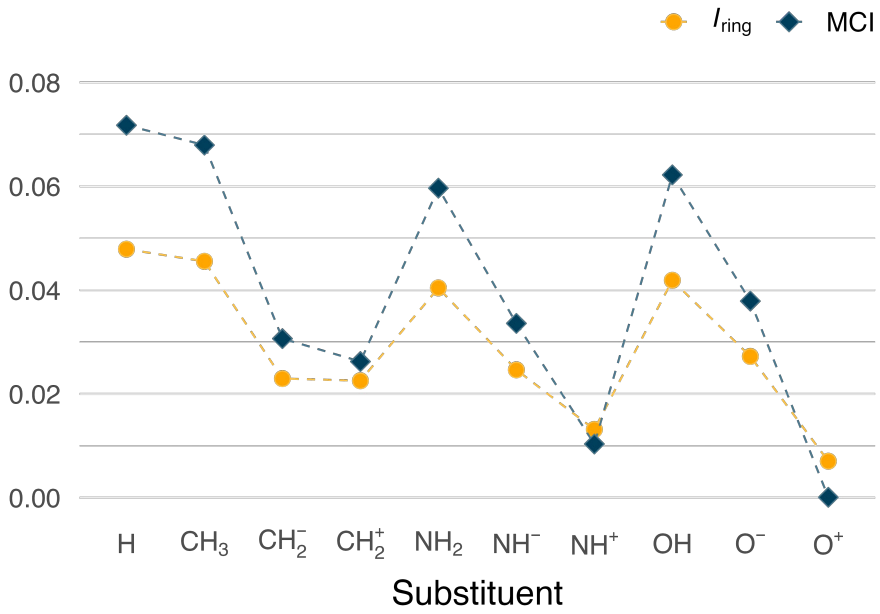

FIGURE 4.6 – Multicenter descriptors I_{ring} and MCI of benzene and monosubstituted benzene derivatives. The results were obtained at the B3LYP/def2-TZVP level of theory using the AIM atomic partitioning.

As observed, the electronic descriptors reflect the general aromatic character trend indicated by other descriptors (see Table 4.3). This trend holds for both monosubstituted (Figure 4.6) and disubstituted (Figure 4.7) benzene derivatives. For conjugated structures, the term corresponding to bonding interactions reflected in the Kekulé structures - the only one that I_{ring} considers - has a dominant contribution, and both indices give quantitatively similar results. However, for structures with a high degree of π-electron delocalization, there is an evident difference between I_{ring} and MCI. This difference arises from the fact that the contributions of other terms added by the permutation of atomic labels (Equation 4.6) play a relevant role. This agrees with the intuitive idea that a higher degree of electron delocalization across the ring leads to a more pronounced aromatic character.

It is worth noting that this quantitative discrepancy should not be interpreted as an underestimation of the aromatic character by the I_{ring} index. The qualitative result remains consistent, and the benzene molecule serves as our reference for a fully aromatic system (refer to Table 4.3 for the correlation between descriptors).

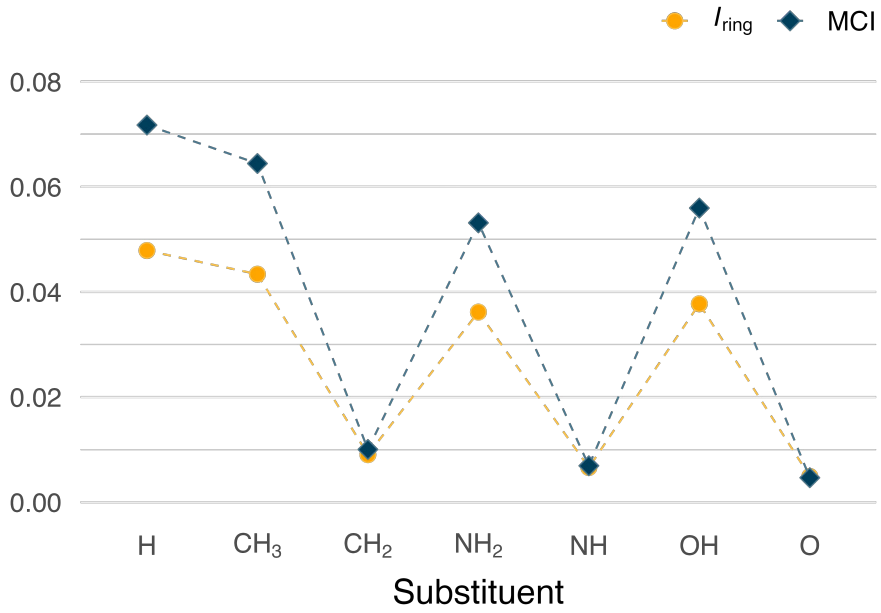

FIGURE 4.7 – Multicenter descriptors I_{ring} and MCI of benzene and monosubstituted benzene derivatives. The results were obtained at the B3LYP/def2-TZVP level of theory using the AIM atomic partitioning.

From the magnetic point of view, a quantitative measure of aromaticity can be provided by the nucleus-independent chemical shifts (NICS). Significantly negative (i.e., magnetically shielded) NICS values indicate the presence of induced diatropic ring currents or high aromatic character. In contrast, significantly positive values (i.e., deshielded) denote paratropic ring currents and high antiaromatic character.[58] The visualization of the chemical shielding tensors (VIST) method enables a thorough investigation of the shielding tensors. The three components (see Equation (4.8)) are visualized as dumbbells, the size and length of which depend on the absolute value of the associated eigenvalue $|t^{(i)}|$, and the color of which depends on the sign (blue for shielded, i.e., aromatic, and red for deshielded, i.e., antiaromatic).

For our reference system (Figure A.6), the shielding tensor computed at the center of the ring, NICS(0), clearly shows that benzene has appreciable shielding along all three coordinate axes, which is interpreted in the sense that the electron density surrounds the center of the ring on all sides; the tensor representation shows a dominant out-of-plane component (-16.3 ppm) along with two smaller in-plane components (both -3.7 ppm), which average an overall isotropic value of -7.9 ppm (see Equation (4.8)). In turn, the corresponding shielding tensor computed 1 Å above the center of the ring, denoted

NICS(1), has a dominant out-of-plane component, whereas the in-plane components vanish. The contribution of the bulk of the σ-electrons decreases for larger distances from the center of the ring; thus, NICS(1) is expected to reflect the π-electron structure details better since it has considerably less influence of the σ-system than NICS(0). In particular, the out-of-plane component of NICS(1) corresponds more directly to the induced current densities in the molecular ring system when a magnetic field is applied perpendicularly to the ring, thus, providing a suitable measure for aromaticity.[29]

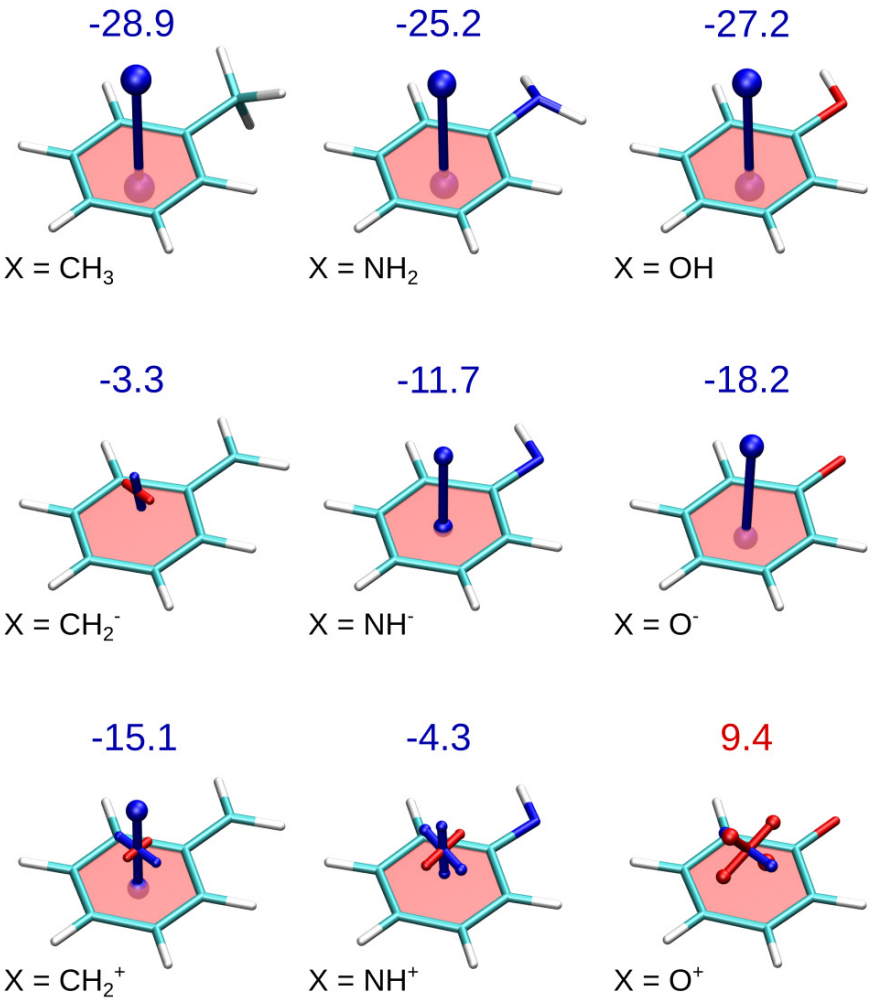

FIGURE 4.8 – Visualization of the chemical shielding tensors (VIST) in monosubstituted benzene derivatives computed 1 Å above the geometric center of the ring. Negative (shielded/aromatic) contributions are shown in blue, and positive (deshielded/antiaromatic) in red. Above the pictures, isotropic $NICS(1)_{zz}$ values are given in ppm. Results obtained at the GIAO-B3LYP/pcS-3//B3LYP/def2-TZVP level of theory.

The tensor representation for monosubstituted benzene derivatives and the numerical value of the out-of-plane component, ascribed to the π-electrons, are shown in Figure 4.8. Complementary data of NICS(0) and NICS(1) are available in the Supplementary Information for this chapter in Appendix A (Tables A.19 and A.20). Molecules modified with CH_3, NH_2, and OH exhibit a dominant out-of-plane component (-28.9, -25.2, and

-27.2 ppm, respectively) comparable to benzene (-30.0 ppm), with almost negligible in-plane components. In other words, molecules expected to have a high degree of π-electron delocalization demonstrate a dominant contribution of a shielded out-of-plane component. In contrast, molecules containing π-electron donating or π-electron accepting substituents exhibit considerably smaller shielded components and, eventually, the contribution of deshielded components.

The highest dominance of deshielded components is observed for cation $C_6H_5O^+$, which is expected to have the highest antiaromatic character according to the analysis based on structural and topological aspects of aromaticity reported. The structural tilt with respect to the plane of the molecule observed for this system represents a non-trivial combination of the tensor components. The values of NICS(0), NICS(1), and its out-of-plane component roughly follow the same trend of aromaticity as the structure-based and topology-based descriptors presented, with no significant deviation observed (see Table 4.3 Figure A.7).

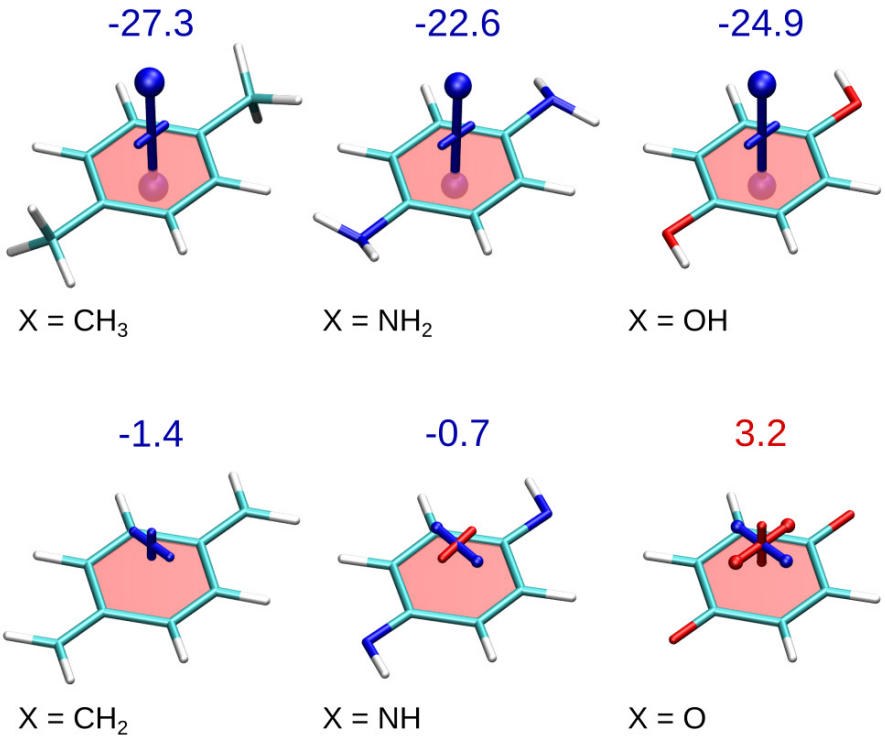

FIGURE 4.9 – Visualization of the chemical shielding tensors (VIST) in disubstituted benzene derivatives computed 1 Å above the geometric center of the ring. Negative (shielded/aromatic) contributions are shown in blue, and positive (deshielded/antiaromatic) in red. Above the pictures, isotropic $NICS(1)_{zz}$ values are given in ppm. Results obtained at the GIAO-B3LYP/pcS-3//B3LYP/def2-TZVP level of theory.

For disubstituted benzene derivatives (Figure 4.9), it is shown that systems modified with substituents containing the central atom sp^3 hybridized exhibit significantly enhanced shielding when compared to benzene derivatives having groups with filled (CH_2^-,

NH^-, and O^-) or unfilled (CH_2^+, NH^+, and O^+) p orbitals, which have a high degree of quinoid character. Interestingly, the disubstituted derivatives modified with CH_3, NH_2, and OH have a slightly small dominance of the out-of-plane component compared to monosubstituted analogous. However, with a higher contribution of in-plane components, disubstituted derivatives average an overall isotropic NICS(1) value equivalent to monosubstituted benzene derivatives (Figures A.7 and A.8).

Estimating the degree of aromaticity using descriptors based on chemical reactivity is not straightforward. However, the energy difference between the ground state S_0 and the first excited triplet state T_1, $S_0 - T_1$ splitting (ΔE_{ST}) can provide valuable insights into the electronic structure regarding the chemical stability of the systems.

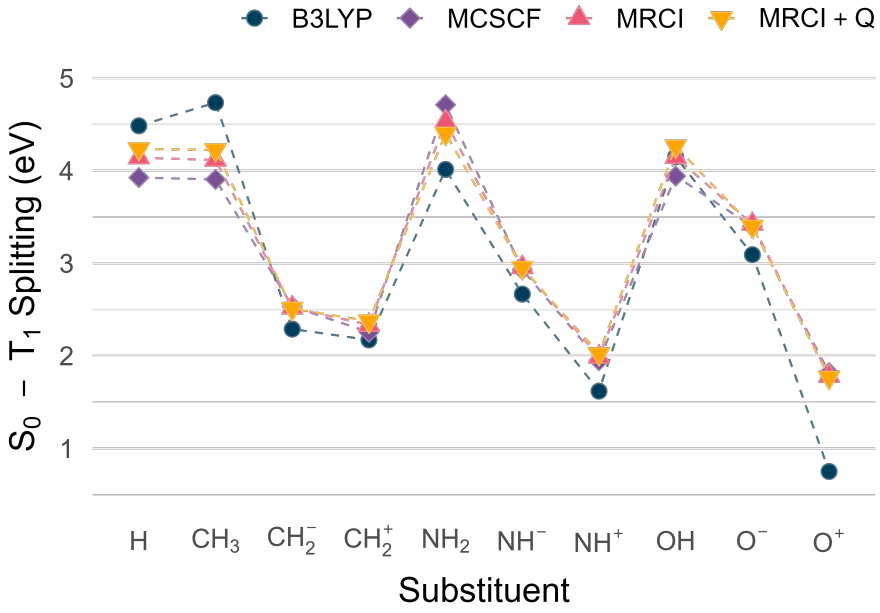

FIGURE 4.10 – Vertical singlet-triplet splitting in eV of benzene and monosubstituted benzene derivatives. The results are presented at the MCSCF, MRCI, and MRCI+Q levels of theory, using the the B3LYP/def2-TZVP equilibrium geometry. Full valence π-electrons and π-orbitals were considered in the CASSCF. MRCI wave functions, incorporating all single and double excitations (MR-CISD), were constructed based on CSFs generated by CASSCF. Size-extensivity contributions were incorporated using the Davidson-Silver method (MRCI+Q).

Figure 4.10 presents the singlet-triplet splitting for monosubstituted benzene derivatives. One can see a direct correlation by comparing singlet-triplet splitting results with the abovementioned indices. Higher ΔE_{ST} is obtained for systems with a high degree of π-electron delocalization. In contrast, a decrease in ΔE_{ST} is observed as the disturbance caused by the substituent to the π-electron delocalization increases. In other words, singlet-triplet splitting and aromaticity indices follow roughly the same trend for the monosubstituted benzene derivatives studied.

Notably, the inclusion of dynamical correlation does not play a central role; the results obtained using MCSCF, and MRCI are similar. Although there are numerical differences,

the obtained values of ΔE_{ST} follow roughly the same trend. In most cases, the DFT result underestimates the values compared to the wave function methods used.

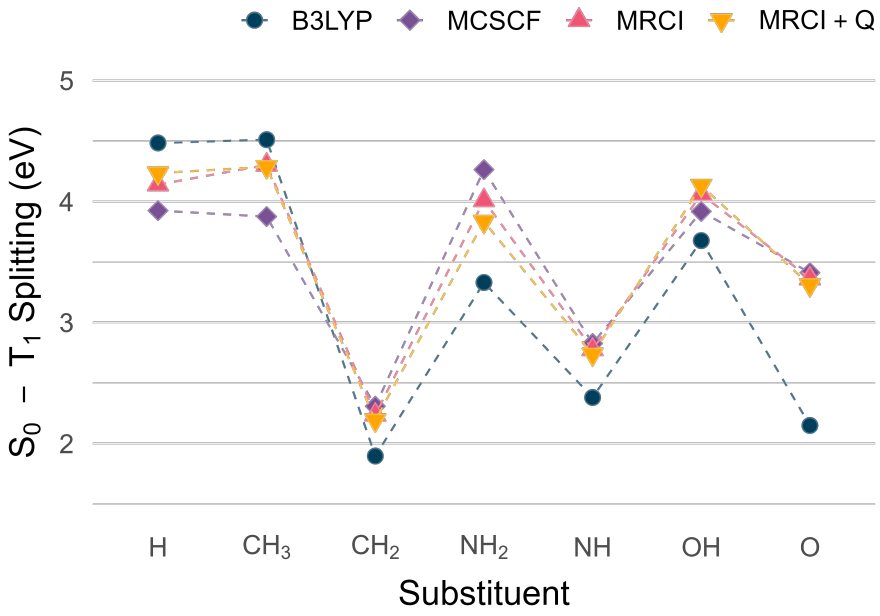

FIGURE 4.11 – Vertical singlet-triplet splitting in eV of benzene and disubstituted benzene derivatives. The results are presented at the MCSCF, MRCI, and MRCI+Q levels of theory, using the the B3LYP/def2-TZVP equilibrium geometry. Full valence π-electrons and π-orbitals were considered in the CASSCF. MRCI wave functions, incorporating all single and double excitations (MR-CISD), were constructed based on CSFs generated by CASSCF. Size-extensivity contributions were incorporated using the Davidson-Silver method (MRCI+Q).

Concerning disubstituted benzene derivatives (Figure 4.11), systems expected to have a high degree of π-electron delocalization, i.e., systems modified with CH_3, NH_2, or OH, have the singlet-triplet splitting comparable to benzene. However, ΔE_{ST} and aromaticity indices follow opposite trends for systems substituted with CH_2, NH, and O, i.e., the lower the π-electron delocalization pointed by the indices, the higher the ΔE_{ST}. In fact, the quinoid character plays a key role in the stability of the systems. A close inspection (Table 4.2) reveals that the quinoid character (enhanced double-bond character of C1-X, C2-C3, and symmetry-equivalent bonds) of those systems follows the same trend as ΔE_{ST}. This interpretation is further supported by the total number of effectively unpaired electrons N_U,[59,60] estimated by analyzing the deviations of individual natural orbitals occupation numbers (derived from MRCI calculations) from zero (unoccupied) and two (doubly occupied) following the nonlinear Head-Gordon's approach[61] (Equation S1). N_U values of 0.306 e, 0.282 e, and 0.240 e, respectively, were found for the structures containing CH_2, NH, and O (Table A.24). According to this finding, $C_6H_4(CH_2)_2$ has the highest radicaloid character, followed by $C_6H_4(NH)_2$ and $C_6H_4O_2$, which has the highest quinoid character.

In summary, the discussion above highlights that in monosubstituted benzene deriva-

tives, the substituent strongly influences the π-electron delocalization of the ring, and the aromaticity indices, as well as the ΔE_{ST} follow the same trend. However, when considering highly quinoidal structures, i.e., disubstituted systems modified with CH_2, NH, and O, π-electron delocalization and chemical stability follow the opposite trend. As the quinoid character increases (indicating a decrease in biradicaloid character), the chemical stability increases.

In the context of natural population analysis, we investigate the correlation between the strength of the π-electron accepting/donating character and the extent to which each substituent influences the stability and π-electron delocalization of the systems. Additionally, we examine the impact of other charged substituents on the ring's π-electron delocalization. To achieve this, we incorporate other charged non-π-electron donor/acceptor substituents: OH_2^+, NH_3^+, BH_3^-, Be^+, as well as orthogonally positioned CH_2^+ and CH_2^- substituents relative to the plane of the ring (although this geometry configuration does not represent the minimum energy conformation, it allows us to eliminate the π-resonance effects and independently analyze the σ-field-inductive effects).

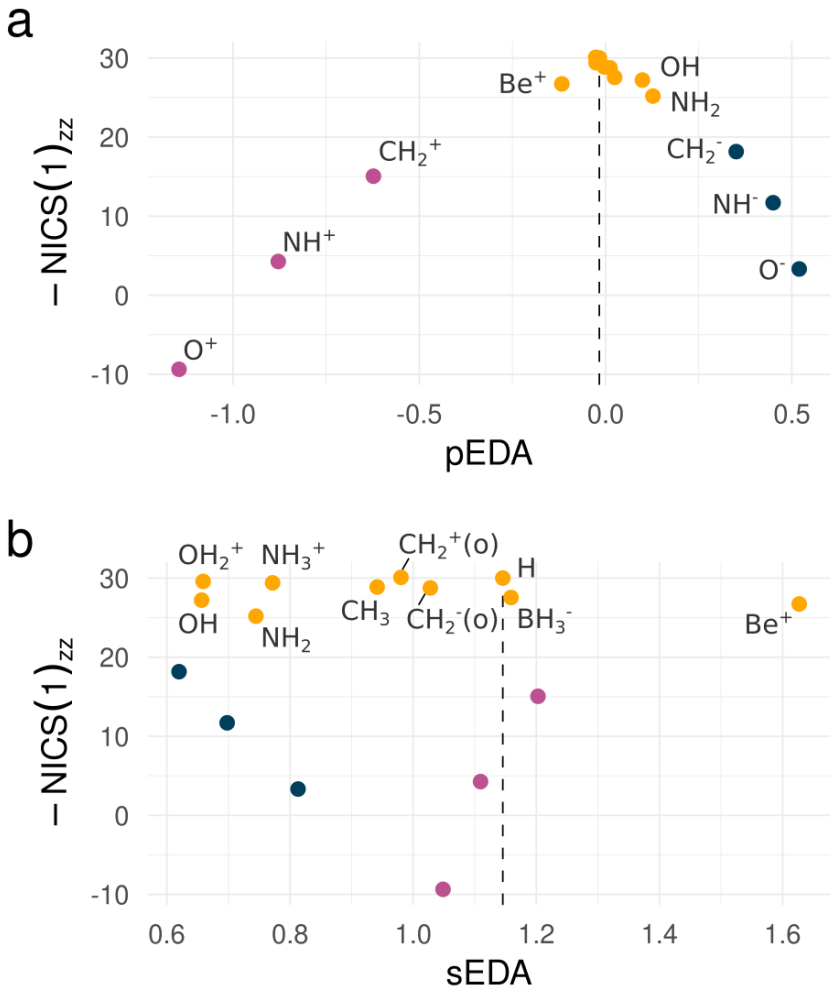

FIGURE 4.12 – Relationship between (a) pEDA - π-electron donor-acceptor and (b) sEDA - σ-electron donor-acceptor descriptor (B3LYP/def2-TZVP level of theory) and NICS(1)$_{zz}$ (GIAO-B3LYP/pcS-3//B3LYP/def2-TZVP) for monosubstituted benzene derivatives. In addition to the substituents analyzed in this paper, the derivatives encompass the charged substituents OH_2^+, NH_3^+, BH_3^-, Be^+, as well as CH_2^+ and CH_2^- substituents positioned orthogonally (o). The dashed line in the figure represents the reference value for benzene. The π-electron donors are depicted in dark blue, π-electron acceptors in magenta, and non-π donors or acceptors in yellow.

The estimated π-electron shift from or toward the substituent (evaluated using the pEDA descriptor, as shown in Equation 4.9) indicates that positively charged groups induce a higher degree of π-electron shift toward the substituents compared to the extent of π-electron shift toward the ring caused by negatively charged substituents (Figure 4.12a). These findings align with the previously reported descriptors, which demonstrate that positively charged substituents have a more pronounced effect on the π-electron delocalization and stability in comparison to negatively charged substituents.

Another important observation arising from the analysis of charged non-π-electron donor/acceptor substituents relates to the role played by the charge of the substituent as a potential factor responsible for influencing the π-electron domain. The results suggest

that the charge factor plays a minor role in influencing π-electron delocalization. This is particularly evident in the case of orthogonally positioned CH_2^+ and CH_2^- substituents, where the p_z orbital of the carbon atom of the substituent is oriented perpendicular to the p_z orbitals of the carbon atoms of the ring. In this conformation, the absence of p_z orbital interactions prevents π-resonance effects from occurring, which allows a high degree of π-electron delocalization compared to the respective minimum energy coplanar derivatives.

Furthermore, the π-electron shift from or toward the substituents is directly proportional to the extent of disturbance caused by the substituent in terms of aromaticity and system stability indicated by other descriptors such as HOMA and singlet-triplet splitting (see Figure A.9). It is worth noting that the non-bonding orbitals in phenol and aniline molecules induce a slight π-electron shift toward the ring, resulting in a slight disturbance to π-electron delocalization. This subtle effect is not captured by the geometrically-based descriptor HOMA; however, more sensitive descriptors indicate a slight reduction in π-electron delocalization.

In contrast, the σ-electron shift from or toward the substituent (evaluated using the sEDA descriptor, see Equation (4.10)) reveals that the strength of the σ-electron donor/acceptor character does not significantly disrupt the π-electron delocalization. This is evident from the nearly unchanged aromaticity index $NICS(1)_{zz}$, despite a significant variation in the σ-electron donor/acceptor character. However, the atom directly bonded to the ring plays a significant role in determining the σ-electron donor/acceptor character. This is evidenced by observing that non-π-electron donor/acceptor substituents with the same heaviest atoms are roughly grouped into different ranges in terms of their σ-electron donor/acceptor character.

It is noteworthy that the number of non-bonding σ orbitals of the π-electron donor/acceptor substituents plays a central role in determining the extent to which the π or σ domain of the ring is affected. Based on our results, a higher number of non-bonding molecular orbitals has a greater impact on the π domain, whereas the presence of bonding orbitals tends to disturb the σ domain.

As a final remark, it should be mentioned that aromaticity descriptors exhibit limitations. Predictions relying on a specific aspect of aromaticity might diverge from those based on other aspects.[62,63] Contradictions arising from diverse indices are frequently reconciled by acknowledging the multidimensional nature of aromaticity.[64] Moreover, divergent orderings among various indices are understandable, as the phenomenon may have one of its dimensions less pronounced than the others.[65] Therefore, it is recommended to use descriptors based on different aspects of aromaticity for a reasonable understanding of its nature.

TABLE 4.3 – Coefficient of determination (R^2) for the relationship between all pairs of aromaticity descriptors. The analysis includes benzene and all the derivatives studied in this work.

	HOMA	AI(vib)	BVI	I_{ring}	MCI	NICS(0)	NICS(1)	$\text{NICS(1)}_{\text{zz}}$
HOMA	1.00	0.99	0.81	0.80	0.75	0.75	0.73	0.75
AI(vib)		1.00	0.82	0.81	0.76	0.76	0.75	0.76
BVI			1.00	0.97	0.98	0.92	0.92	0.95
I_{ring}				1.00	0.99	0.86	0.89	0.93
MCI					1.00	0.88	0.90	0.94
NICS(0)						1.00	0.95	0.94
NICS(1)							1.00	0.99
$\text{NICS(1)}_{\text{zz}}$								1.00

However, for the set of derivatives analyzed in this work, the descriptors provide an overview of several aspects of aromaticity and are complementary to each other. No significant discrepancies were found among the different descriptors (Table 4.3). The linear correlation coefficients (R^2) for all pairs of aromaticity descriptors were satisfactory, with no R^2 value smaller than 0.73. Notably, the correlation between individual indices based on the same aspect of aromaticity—structural, electronic, or magnetic—tends to be more substantial, with R^2 approaching 1.

Bibliography

1 BECKE, Axel D. Density-functional thermochemistry. III. The role of exact exchange. **The Journal of Chemical Physics**, American Institute of PhysicsAIP, v. 98, n. 7, p. 5648–5652, Apr. 1993.

2 LEE, Chengteh; YANG, Weitao; PARR, Robert G. Development of the Colle-Salvetti correlation-energy formula into a functional of the electron density. **Physical Review B**, American Physical Society, v. 37, n. 2, p. 785–789, Jan. 1988.

3 WEIGEND, Florian; AHLRICHS, Reinhart. Balanced basis sets of split valence, triple zeta valence and quadruple zeta valence quality for H to Rn: Design and assessment of accuracy. **Physical Chemistry Chemical Physics**, The Royal Society of Chemistry, v. 7, n. 18, p. 3297, Aug. 2005.

4 WEIGEND, Florian. Accurate Coulomb-fitting basis sets for H to Rn. **Physical Chemistry Chemical Physics**, v. 8, n. 9, p. 1057, 2006.

5 CHAI, Jeng-Da; HEAD-GORDON, Martin. Long-range corrected hybrid density functionals with damped atom–atom dispersion corrections. **Physical Chemistry Chemical Physics**, The Royal Society of Chemistry, v. 10, n. 44, p. 6615–6620, 2008.

6 KRUSZEWSKI, J.; KRYGOWSKI, T.M. Definition of aromaticity basing on the harmonic oscillator model. **Tetrahedron Letters**, v. 13, n. 36, p. 3839–3842, 1972.

7 KRYGOWSKI, Tadeusz Marek. Crystallographic studies of inter- and intramolecular interactions reflected in aromatic character of π-electron systems. **Journal of Chemical Information and Computer Sciences**, v. 33, n. 1, p. 70–78, Jan. 1993.

8 KRYGOWSKI, Tadeusz Marek; CYRAŃSKI, Michal. Separation of the energetic and geometric contributions to the aromaticity. Part IV. A general model for the π-electron systems. **Tetrahedron**, v. 52, n. 30, p. 10255–10264, July 1996.

9 KRYGOWSKI, Tadeusz Marek; CYRAŃSKI, Michał Ksawery. Structural Aspects of Aromaticity. **Chemical Reviews**, v. 101, n. 5, p. 1385–1420, May 2001.

10 DOBROWOLSKI, Jan Cz. Three Queries about the HOMA Index. **ACS Omega**, American Chemical Society, v. 4, n. 20, p. 18699–18710, Nov. 2019.

11 KRAKA, Elfi; SETIAWAN, Dani; CREMER, Dieter. Re-evaluation of the bond length–bond strength rule: The stronger bond is not always the shorter bond. **Journal of Computational Chemistry**, v. 37, n. 1, p. 130–142, Jan. 2016.

12 ZHAO, Lili; ZHI, Minna; FRENKING, Gernot. The strength of a chemical bond. **International Journal of Quantum Chemistry**, v. 122, n. 8, Apr. 2022.

13 KRAKA, Elfi; ZOU, Wenli; TAO, Yunwen. Decoding chemical information from vibrational spectroscopy data: Local vibrational mode theory. **WIREs Computational Molecular Science**, v. 10, n. 5, Sept. 2020.

14 KRAKA, Elfi; LARSSON, John Andreas; CREMER, Dieter. Generalization of the Badger Rule Based on the Use of Adiabatic Vibrational Modes. In: COMPUTATIONAL Spectroscopy: Methods, Experiments and Applications. Weinheim: Wiley, Oct. 2010. p. 105–149.

15 BREEN, P. J. et al. A study of nonrigid aromatic molecules by supersonic molecular jet spectroscopy. I. Toluene and the xylenes. **The Journal of Chemical Physics**, v. 87, n. 4, p. 1917–1926, Aug. 1987.

16 TAO, Yunwen et al. LModeA-nano: A PyMOL Plugin for Calculating Bond Strength in Solids, Surfaces, and Molecules via Local Vibrational Mode Analysis. **Journal of Chemical Theory and Computation**, v. 18, n. 3, p. 1821–1837, Mar. 2022.

17 BADER, R.F.W.; BADER, R.F. **Atoms in Molecules: A Quantum Theory**. Oxford: Clarendon Press, 1990. (International series of monographs on chemistry).

18 LU, Tian; CHEN, Feiwu. Multiwfn: A multifunctional wavefunction analyzer. **Journal of Computational Chemistry**, v. 33, n. 5, p. 580–592, Feb. 2012.

19 BECKE, A. D.; EDGECOMBE, K. E. A simple measure of electron localization in atomic and molecular systems. **The Journal of Chemical Physics**, American Institute of PhysicsAIP, v. 92, n. 9, p. 5397–5403, May 1990.

20 SAVIN, Andreas et al. Electron Localization in Solid-State Structures of the Elements: the Diamond Structure. **Angewandte Chemie International Edition in English**, John Wiley & Sons, Ltd, v. 31, n. 2, p. 187–188, Feb. 1992.

21 TIAN, LU; FEI-WU, CHEN. Meaning and Functional Form of the Electron Localization Function. **Acta Physico-Chimica Sinica**, v. 27, n. 12, p. 2786–2792, 2011.

22 SANTOS, J. C. et al. *Sigma–pi* separation of the electron localization function and aromaticity. **The Journal of Chemical Physics**, v. 120, n. 4, p. 1670–1673, Jan. 2004.

23 GIAMBIAGI, Mario et al. Multicenter bond indices as a measure of aromaticity. **Physical Chemistry Chemical Physics**, v. 2, n. 15, p. 3381–3392, Aug. 2000.

24 BULTINCK, Patrick; PONEC, Robert; DAMME, Sofie Van. Multicenter bond indices as a new measure of aromaticity in polycyclic aromatic hydrocarbons. **Journal of Physical Organic Chemistry**, v. 18, n. 8, p. 706–718, Aug. 2005.

25 BULTINCK, Patrick et al. Electron Delocalization and Aromaticity in Linear Polyacenes: Atoms in Molecules Multicenter Delocalization Index. **The Journal of Physical Chemistry A**, v. 110, n. 24, p. 7642–7648, June 2006.

26 KEITH, Todd A. **AIMAll**. [S.l.]: TK Gristmill Software, 2019.

27 MATITO, E. **ESI-3D: Electron Sharing Indices Program for 3D Molecular Space Partitioning**. [S.l.: s.n.], 2006.

28 SCHLEYER, Paul Von Ragué et al. Nucleus-Independent Chemical Shifts: A Simple and Efficient Aromaticity Probe. **Journal of the American Chemical Society**, American Chemical Society, v. 118, n. 26, p. 6317–6318, Jan. 1996.

29 CORMINBOEUF, Clémence et al. Induced magnetic fields in aromatic [n]-annulenes—interpretation of NICS tensor components. **Physical Chemistry Chemical Physics**, v. 6, n. 2, p. 273–276, 2004.

30 PLASSER, Felix; GLÖCKLHOFER, Florian. Visualisation of Chemical Shielding Tensors (VIST) to Elucidate Aromaticity and Antiaromaticity. **European Journal of Organic Chemistry**, v. 2021, n. 17, p. 2529–2539, May 2021.

31 PLASSER, F. TheoDORE: A toolbox for a detailed and automated analysis of electronic excited state computations. **The Journal of Chemical Physics**, AIP Publishing LLCAIP Publishing, v. 152, n. 8, p. 084108, Feb. 2020.

32 WOLINSKI, Krzysztof; HINTON, James F.; PULAY, Peter. Efficient implementation of the gauge-independent atomic orbital method for NMR chemical shift calculations. **Journal of the American Chemical Society**, American Chemical Society, v. 112, n. 23, p. 8251–8260, Nov. 1990.

33 JENSEN, Frank. Basis Set Convergence of Nuclear Magnetic Shielding Constants Calculated by Density Functional Methods. **Journal of Chemical Theory and Computation**, American Chemical Society, v. 4, n. 5, p. 719–727, May 2008.

34 PRITCHARD, Benjamin P. et al. New Basis Set Exchange: An Open, Up-to-Date Resource for the Molecular Sciences Community. **Journal of Chemical Information and Modeling**, American Chemical Society, v. 59, n. 11, p. 4814–4820, Nov. 2019.

35 GAJDA, Łukasz et al. Method and basis set dependence of the NICS indexes of aromaticity for benzene. **Magnetic Resonance in Chemistry**, v. 56, n. 4, p. 265–275, Apr. 2018.

36 OZIMIŃSKI, Wojciech P.; DOBROWOLSKI, Jan C. σ- and π-electron contributions to the substituent effect: natural population analysis. **Journal of Physical Organic Chemistry**, v. 22, n. 8, p. 769–778, Aug. 2009.

37 REED, Alan E.; CURTISS, Larry A.; WEINHOLD, Frank. Intermolecular interactions from a natural bond orbital, donor-acceptor viewpoint. **Chemical Reviews**, v. 88, n. 6, p. 899–926, Sept. 1988.

38 SZALAY, Péter G. et al. Multiconfiguration Self-Consistent Field and Multireference Configuration Interaction Methods and Applications. **Chemical Reviews**, v. 112, n. 1, p. 108–181, Jan. 2012.

39 LISCHKA, Hans et al. Multireference Approaches for Excited States of Molecules. **Chemical Reviews**, v. 118, n. 15, p. 7293–7361, Aug. 2018.

40 RUEDENBERG, K.; CHEUNG, L. M.; ELBERT, S. T. MCSCF optimization through combined use of natural orbitals and the brillouin-levy-berthier theorem. **International Journal of Quantum Chemistry**, John Wiley & Sons, Ltd, v. 16, n. 5, p. 1069–1101, Nov. 1979.

41 ROOS, Björn O.; TAYLOR, Peter R.; SIGBAHN, Per E.M. A complete active space SCF method (CASSCF) using a density matrix formulated super-CI approach. **Chemical Physics**, North-Holland, v. 48, n. 2, p. 157–173, May 1980.

42 LANGHOFF, Stephen R.; DAVIDSON, Ernest R. Configuration interaction calculations on the nitrogen molecule. **International Journal of Quantum Chemistry**, v. 8, n. 1, p. 61–72, Jan. 1974.

43 DAVIDSON, Ernest R.; SILVER, Donald W. Size consistency in the dilute helium gas electronic structure. **Chemical Physics Letters**, v. 52, n. 3, p. 403–406, Dec. 1977.

44 LISCHKA, Hans et al. Columbus—a program system for advanced multireference theory calculations. **WIREs Computational Molecular Science**, John Wiley & Sons, v. 1, n. 2, p. 191–199, Mar. 2011.

45 LISCHKA, Hans et al. High-level multireference methods in the quantum-chemistry program system COLUMBUS: Analytic MR-CISD and MR-AQCC gradients and MR-AQCC-LRT for excited states, GUGA spin–orbit CI and parallel CI density. **Physical Chemistry Chemical Physics**, v. 3, n. 5, p. 664–673, 2001.

46 LISCHKA, Hans et al. The generality of the GUGA MRCI approach in COLUMBUS for treating complex quantum chemistry. **The Journal of Chemical Physics**, AIP Publishing, LLC, v. 152, n. 13, p. 134110, Apr. 2020.

47 FRISCH, M. J. et al. **Gaussian 09, Revision B.01**. Wallingford CT: Gaussian, Inc., 2010.

48 KRYGOWSKI, Tadeusz M. et al. Relation between the Substituent Effect and Aromaticity. **The Journal of Organic Chemistry**, v. 69, n. 20, p. 6634–6640, Oct. 2004.

49 KRYGOWSKI, Tadeusz Marek; STEPIEŃ, Beata Tamara. Sigma- and Pi-Electron Delocalization: Focus on Substituent Effects. **Chemical Reviews**, v. 105, n. 10, p. 3482–3512, Oct. 2005.

50 CREMER, Dieter; KRAKA, Elfi. A Description of the Chemical Bond in Terms of Local Properties of Electron Density and Energy. **Croatica Chemica Acta**, v. 57, p. 1259–1281, 1984.

51 CAMPANELLI, Anna Rita; DOMENICANO, Aldo; RAMONDO, Fabio. Electronegativity, Resonance, and Steric Effects and the Structure of Monosubstituted Benzene Rings: An ab Initio MO Study. **The Journal of Physical Chemistry A**, v. 107, n. 33, p. 6429–6440, Aug. 2003.

52 BADER, R. F. W.; ESSÉN, H. The characterization of atomic interactions. **The Journal of Chemical Physics**, v. 80, n. 5, p. 1943–1960, Mar. 1984.

53 ZHANG, Lixian et al. Topology of Electron Charge Density for Chemical Bonds from Valence Bond Theory: A Probe of Bonding Types. **Chemistry - A European Journal**, v. 15, n. 12, p. 2979–2989, Mar. 2009.

54 KALESCKY, Robert; KRAKA, Elfi; CREMER, Dieter. Identification of the Strongest Bonds in Chemistry. **The Journal of Physical Chemistry A**, v. 117, n. 36, p. 8981–8995, Sept. 2013.

55 MATITO, Eduard et al. Electron localization function at the correlated level. **The Journal of Chemical Physics**, v. 125, n. 2, p. 024301, July 2006.

56 PINHEIRO JR, Max et al. Interplay between Aromaticity and Radicaloid Character in Nitrogen-Doped Oligoacenes Revealed by High-Level Multireference Methods. **The Journal of Physical Chemistry A**, v. 122, n. 49, p. 9464–9473, Dec. 2018.

57 VILLAUME, Sebastien; FOGARTY, Heather A.; OTTOSSON, Henrik. Triplet-State Aromaticity of 4nπ-Electron Monocycles: Analysis of Bifurcation in the π Contribution to the Electron Localization Function. **ChemPhysChem**, v. 9, n. 2, p. 257–264, Feb. 2008.

58 CHEN, Zhongfang et al. Nucleus-Independent Chemical Shifts (NICS) as an Aromaticity Criterion. **Chemical Reviews**, v. 105, n. 10, p. 3842–3888, Sept. 2005.

59 TAKATSUKA, Kazuo; FUENO, Takayuki; YAMAGUCHI, Kizashi. Distribution of odd electrons in ground-state molecules. **Theoretica Chimica Acta**, v. 48, n. 3, p. 175–183, 1978.

60 STAROVEROV, Viktor N.; DAVIDSON, Ernest R. Distribution of effectively unpaired electrons. **Chemical Physics Letters**, North-Holland, v. 330, n. 1-2, p. 161–168, Nov. 2000.

61 HEAD-GORDON, Martin. Characterizing unpaired electrons from the one-particle density matrix. **Chemical Physics Letters**, North-Holland, v. 372, n. 3-4, p. 508–511, Apr. 2003.

62 FEIXAS, Ferran et al. On the performance of some aromaticity indices: A critical assessment using a test set. **Journal of Computational Chemistry**, v. 29, n. 10, p. 1543–1554, July 2008.

63 SOLÀ, Miquel et al. A Critical Assessment of the Performance of Magnetic and Electronic Indices of Aromaticity. **Symmetry**, v. 2, n. 2, p. 1156–1179, June 2010.

64 CYRAŃSKI, Michal K. et al. To What Extent Can Aromaticity Be Defined Uniquely? **The Journal of Organic Chemistry**, v. 67, n. 4, p. 1333–1338, Feb. 2002.

65 KRYGOWSKI, T.M. et al. Aromaticity: a Theoretical Concept of Immense Practical Importance. **Tetrahedron**, v. 56, n. 13, p. 1783–1796, Mar. 2000.

5 Low-lying excited states of linear all-*trans* polyenes: the σ-π electron correlation and the description of ionic states

5.1 Computational details

The equilibrium geometry of the ground state of linear all *trans*-polyenes containing $N = 6$, 8, 10, and 12 π-electrons (*trans*,*trans*-1,3,5-hexatriene, all-*trans*-1,3,5,7-octatetraene, all-*trans*-1,3,5,7,9-decapentaene, and all-*trans*-1,3,5,7,9,11-dodecahexaene, herein called hexatriene, octatetraene, decapentaene, and dodecahexaene, respectively) was obtained using the long-range corrected hybrid functional ωB97X-D[1] with the cc-pVTZ[2] basis set. Optimized geometries and analytical harmonic frequencies are available in the supplementary information for this chapter in Appendix B. Based on the optimized geometries, the singlet states $1^1A_g^-$, $2^1A_g^-$, $1^1B_u^+$, and $2^1B_u^-$, as well as the triplet excited states $1^3A_g^-$ and $1^3B_u^-$, were calculated at the multireference levels described below. Vertical excitation energies and oscillator strengths were computed for transitions between the ground state and the aforementioned states of interest. All calculations were performed strictly under C_{2h} symmetry constraints.

The ground and excited states were investigated using a range of computational methods, including state-averaged complete active space self-consistent field (SA-CASSCF) method,[3] MR-CISD,[4,5] and MR-AQCC[6,7] approaches. Where specified, the Pople (+P) correction,[8] extended to the MR-CISD case, was applied to account for size-extensivity errors. MR-AQCC calculations on excited states were conducted utilizing the vector-following approach in which convergence to a selected eigenvector was achieved using the criterion of maximal overlap with a specific root of the eigenvector of the reference space.

At the SA-CASSCF level, six states–namely $1^1A_g^-$, $2^1A_g^-$, $1^1B_u^+$, $2^1B_u^-$, $1^3A_g^-$, and $1^3B_u^-$–were averaged with equal weights. The resulting set of molecular orbitals was then

used for subsequent MR-CISD and MR-AQCC calculations. SA-CASSCF computations were carried out with a standard valence active space, encompassing all valence π-electrons and valence π-orbitals of each molecule. To reduce the computational effort in the subsequent MR-CISD and MR-AQCC calculations, the reference space was constructed by splitting the π-valence space into three parts: a CAS(6,6), a complementary restrictive active space (RAS) for the remaining strongly occupied orbitals, and a corresponding auxiliary (AUX) space for weakly occupied orbitals of the π-valence space. Single excitations were used from RAS into CAS and AUX orbitals and from CAS into AUX orbitals. The specific choices used in our calculations are presented in Table 5.1. The restrictions imposed on the active space underwent extensive testing for decapentaene (Table B.1). The RAS(2)CAS(6,6)AUX(2) scheme, which contains ten π-orbitals, closely reproduces the results obtained with the complete π-valence CAS(10,10). At both the MR-CISD and MR-AQCC levels, generalized interacting space restrictions[9] were applied.

TABLE 5.1 – Active reference space scheme utilized at the MR-CISD and MR-AQCC levels for polyenes with N π-electrons.

N	Active space scheme
6	CAS(6,6)
8	RAS(1)CAS(6,6) AUX(1)
10	RAS(2)CAS(6,6) AUX(2)
12	RAS(3)CAS(6,6) AUX(3)

For computational economy, a freezing scheme of σ-orbitals was employed at both the MR-CISD and MR-AQCC levels. After testing several freezing options for hexatriene (Table S2), a scheme was adopted in which 50% of the reference doubly occupied σ-orbitals¯including the core orbitals on each carbon atom, which constitute approximately 30% of the total reference doubly occupied σ-orbitals¯and 50% of the reference virtual σ-orbitals were frozen. This freezing approach had no significant impact on excitation energies compared to the reference calculation, where only core orbitals were frozen (Table B.2).

The cc-pVnZ (n = D, T, Q) basis sets[2] were used with the outer shell of polarization functions excluded from the triple- and quadruple-ζ basis sets, as detailed below. Extrapolation to the complete basis set (CBS) limit was carried out using the two-point fit approach,[10] as shown in Equation 5.1 for the excitation energies obtained with the MR-CISD+P and MR-AQCC methods.

$$\mathrm{E}_{\mathrm{YX}}^{\infty} = \frac{\mathrm{E_X X^3} - \mathrm{E_Y Y^3}}{\mathrm{X^3} - \mathrm{Y^3}} \tag{5.1}$$

In Equation 5.1, E_{YX}^{∞} represents the CBS limit excitation energy, X and Y are the cardinal numbers for the respective basis sets, and E_X and E_Y denote the excitation energies obtained for those individual basis sets. The cc-pVTZ basis set without the f-function, i.e., with contraction $(10s, 5p, 2d)/[4s, 3p, 2d]$ (cc-pVTZ'), and the cc-pVQZ basis set without g-function, i.e., with contraction $(12s, 6p, 3d, 2f)/[5s, 4p, 3d, 2f]$ (cc-pVQZ') were used on carbon atoms for the basis set extrapolation to the CBS limit. The cc-pVDZ basis set was used on hydrogen in all cases.

Based on the optimized geometries, vertical excitation energies were also computed using second-order complete active space perturbation theory (CASPT2)[11] with the cc-pVDZ basis set. At the CASSCF level, singlet states of the same spatial symmetry were averaged with equal weights. The resulting set of molecular orbitals was used for subsequent CASPT2 computations, performed with IP-EA denominator shift 0.25. The SA-CASSCF and CASPT2 computations were performed with a standard valence CAS, including all valence π-electrons and π-orbitals of each molecule.

Geometry optimizations were carried out using the Gaussian 16 software package.[12] MR-CISD and MR-AQCC calculations were performed with the Columbus program system,[13–15] with integrals calculated by the Dalton program.[16] CASPT2 calculations were conducted using the OpenMolcas software package.[17]

5.1.1 Wavefunction descriptors

Based on the MR-CISD wavefunction, the ionic character of the excited states, the single-excitation character, and the participation ratio of natural transition orbitals (NTOs) were evaluated. To assess the ionic character of each state, the $Q_{\mathrm{a}}^{\mathrm{t}}$ diagnostic[18] was employed, as defined in Equation 5.2,

$$Q_{\mathrm{a}}^{\mathrm{t}} = \sum_{M} |q_M^{\mathrm{t}}| \tag{5.2}$$

where the transition charge q_M^{t} on atom M is calculated as the sum over the diagonal elements of the one-electron transition density matrix (1TDM) between the states of interest and the ground state. Large transition charges centered on individual atoms are associated with ionic states. The $Q_{\mathrm{a}}^{\mathrm{t}}$ values were computed based on the Löwdin-style population analysis.[19]

The participation ratio of natural transition orbitals ($\mathrm{PR_{NTO}}$)[20,21] was used as a measure of the multiconfigurational character of the excited states. The $\mathrm{PR_{NTO}}$ is computed as

$$\mathrm{PR_{NTO}} = \frac{\left[\mathrm{tr}(\gamma_{0I}\gamma_{0I}^{\mathrm{T}})\right]^2}{\mathrm{tr}(\gamma_{0I}\gamma_{0I}^{\mathrm{T}})^2} \tag{5.3}$$

where γ_{0I} is the 1TDM. $\mathrm{PR_{NTO}}$ counts how many different natural transition orbitals (NTOs) are participating and, thus, how many configurations are necessary to describe the excited state.

Finally, the single-excitation character, Ω, defined as $\Omega = \mathrm{tr}(\gamma_{0I}\gamma_{0I}^{\mathrm{T}})$,[22,23] was calculated. Values above 0.8 computed based on correlated *ab initio* methods are indicative of singly excited states.[24,25] The three mentioned wavefunction descriptors were computed using the TheoDORE 3.1.1 program package.[26]

5.2 Results and discussion

5.2.1 Singlet states

We begin our discussion by presenting the vertical singlet excitation energy results. As previously mentioned, while covalent states are well-described by the CASSCF method, significant issues arise for the excitation energy from the ground state to the ionic $1^1\mathrm{B_u^+}$ state. Using the cc-pVDZ basis set, CASSCF overestimates these excitation energies by 1.78 eV for hexatriene when compared to MR-CISD+P and MR-AQCC results (Table 5.2). This observation holds for the larger systems, with MR-AQCC tending to stabilize the ionic state slightly more than MR-CISD+P as the chain length increases. Overall, CASSCF overestimates the excitation energies by an average of 1.81 eV, ranging from 1.78 eV for hexatriene to 1.84 eV for dodecahexaene compared to MR-CISD+P results.

TABLE 5.2 – Vertical singlet excitation energies of polyenes computed using the CASSCF, MR-CISD, MR-CISD+P, MR-AQCC, and CASPT2 methods and the cc-pVDZ basis set.

N	State	Method				
		CASSCF[a]	MR-CISD	MR-CISD+P	MR-AQCC	CASPT2
6	$2^1A_g^-$	5.799	5.856	5.819	5.818	5.761
	$1^1B_u^+$	7.609	6.412	5.827	5.833	5.564
	$2^1B_u^-$	6.983	7.044	6.976	6.964	6.941
8	$2^1A_g^-$	5.080	5.144	5.002	5.065	4.956
	$1^1B_u^+$	6.916	5.743	5.138	5.102	4.924
	$2^1B_u^-$	6.276	6.347	6.197	6.236	6.157
10	$2^1A_g^-$	4.598	4.648	4.448	4.505	4.431
	$1^1B_u^+$	6.448	5.311	4.622	4.536	4.482
	$2^1B_u^-$	5.673	5.838	5.498	5.636	5.540
12	$2^1A_g^-$	4.268	4.323	4.093	4.153	4.069
	$1^1B_u^+$	6.123	4.978	4.282	4.160	4.167
	$2^1B_u^-$	5.216	5.377	5.030	5.157	5.052

[a] The B_u states are numbered according to wave function character, not by energetic order.

At the CASSCF level, the excitation energy to the ionic $1^1B_u^+$ state is not only higher than that of the $2^1A_g^-$ state but also exceeds that of the $2^1A_g^-$ state, causing the $1^1B_u^+$ state to become the second excited state of Bu symmetry. Notably, this inversion in the ordering of Bu symmetry states introduces additional challenges since, as discussed below, the ionic state in the systems studied here should be one of the two lowest-lying excited states when appropriate dynamic correlation is considered (Figure 5.1). These artifacts of the CASSCF state ordering are significantly corrected at the MR-AQCC and MR-CISD+P levels, as Table 5.2 shows. The ionic $1^1B_u^+$ state is substantially stabilized compared to the CASSCF results. However, the use of a larger basis set appears to be particularly important for the ionic state. Therefore, a more detailed discussion of the state ordering is postponed to the respective discussion below.

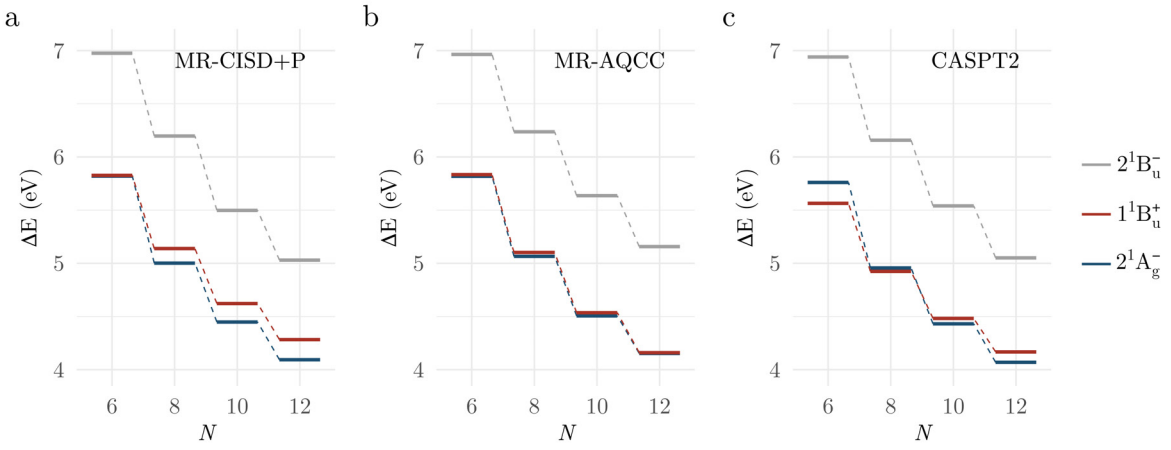

FIGURE 5.1 – Vertical singlet excitation energies of polyenes with N π-electrons computed using (a) MR-CISD+P, (b) MR-AQCC, and (c) CASPT2. Calculations were performed with the cc-pVDZ basis set. Numerical data are available in Table 2.

Size-extensivity corrections play a significant role in describing the low-lying excited-state manifold in these systems. A closer inspection of Table 5.2, comparing uncorrected MR-CISD with MR-CISD+P values, reveals that the size-extensivity correction is more pronounced for the ionic state. This state is stabilized by values ranging from 0.58 eV for hexatriene to 0.70 eV for dodecahexaene, with stabilization consistently increasing as the system size grows (Table 5.2). Covalent states, on the other hand, are less affected by this correction. Specifically, the $2^1A_g^-$ state is stabilized by 0.04 eV in hexatriene and 0.23 eV in dodecahexaene. For the $2^1B_u^-$ state, the stabilization ranges from 0.07 eV for hexatriene to 0.35 eV for dodecahexaene (Table 5.2). These results are depicted graphically in Figure B.1.

To assess the influence of the basis set on the excitation energies and to discuss the relative ordering of the two low-lying excited states across the series, extrapolation to the complete basis set (CBS) limit was performed using the two-point fit approach (Equation 5.1) based on MR-CISD+P and MR-AQCC calculations. The results obtained with the cc-pVDZ, cc-pVTZ', and cc-pVQZ' basis sets are presented in Table 5.3 for MR-CISD+P and MR-AQCC. The extrapolated values, derived from the double- to triple-ζ basis set (ΔE_{DT}^{∞}) and the triple- to quadruple-ζ basis set (ΔE_{TQ}^{∞}) extrapolation, are summarized in Table 5.4.

TABLE 5.3 – Singlet excitation energies (eV) of polyenes with N π-electrons, calculated at the MR-CISD+P and MR-AQCC levels using the cc-pVDZ ($\Delta E_{\text{cc-pVDZ}}$), cc-pVTZ' ($\Delta E_{\text{cc-pVTZ'}}$), and cc-pVQZ' ($\Delta E_{\text{cc-pVQZ'}}$) basis sets.

N	State	MR-CISD+P			MR-AQCC		
		$\Delta E_{\text{cc-pVDZ}}$	$\Delta E_{\text{cc-pVTZ'}}$	$\Delta E_{\text{cc-pVQZ'}}$	$\Delta E_{\text{cc-pVDZ}}$	$\Delta E_{\text{cc-pVTZ'}}$	$\Delta E_{\text{cc-pVQZ'}}$
6	$2^1A_g^-$	5.819	5.793	5.776	5.818	5.783	5.755
	$1^1B_u^+$	5.827	5.638	5.584	5.833	5.620	5.504
	$2^1B_u^-$	6.976	6.907	6.895	6.964	6.813	6.648
8	$2^1A_g^-$	5.002	4.984	4.988	5.065	5.036	5.025
	$1^1B_u^+$	5.138	4.975	4.941	5.102	4.904	4.804
	$2^1B_u^-$	6.197	6.168	6.180	6.236	6.152	6.079
10	$2^1A_g^-$	4.448	4.427	–	4.505	4.465	–
	$1^1B_u^+$	4.622	4.480	–	4.536	4.332	–
	$2^1B_u^-$	5.498	5.479	–	5.636	5.549	–
12	$2^1A_g^-$	4.093	4.026[a]	–	4.153	4.084[a]	–
	$1^1B_u^+$	4.282	4.139[a]	–	4.160	3.962[a]	–
	$2^1B_u^-$	5.030	5.075[a]	–	5.157	5.189[a]	–

[a] Estimated result based on a fit of excitation energies across the series (Figure B.4).

The first major observation is that the two low-lying excited states are affected differently when additional polarization functions are added to the basis set (Table 5.3). Let us first consider expanding the basis set from double- to triple-ζ. For hexatriene, the $2^1A_g^-$ state is stabilized by 0.03 eV, whereas the ionic state is stabilized by approximately 0.2 eV based on MR-AQCC results⁻a similar trend is observed with MR-CISD+P results. For octatetraene and decapentaene, at the MR-AQCC level, a similar trend is seen: the covalent state is stabilized by about 0.03–0.04 eV, while the ionic state is stabilized by about 0.2 eV. On the other hand, for the results obtained at the MR-CISD+P level, the behavior changes slightly as the chain length increases. While the covalent state is still stabilized by 0.02–0.03 eV, in agreement with MR-AQCC results, the stabilization of the ionic state decreases slightly with chain length, specifically, by 0.19 eV, 0.16 eV, and 0.14 eV in hexatriene, octatetraene, and decapentaene, respectively.

For dodecahexaene, computational cost constraints prevented the use of basis sets larger than the double-ζ cc-pVDZ. However, a crude estimate for the excitation energies using the cc-pVTZ' basis set was made for $N = 12$ using a power function fit (see Section B.2.1 of the SI for this chapter in Appendix B). This estimate suggests that these trends hold for dodecahexaene. While the covalent state is stabilized by 0.07 eV at both the MR-AQCC and MR-CISD+P levels, the ionic state is stabilized by 0.2 eV at the MR-

AQCC level and by 0.14 eV at the MR-CISD+P level. It is worth noting that, while the stabilization of the ionic state is consistent with what is observed for the smaller members of the series at both levels, the stabilization predicted for the covalent state is larger than the 0.02-0.03 eV observed for the smaller members of the series when expanding the basis set from double- to triple-ζ.

Using the cc-pVTZ basis set, our MR-AQCC results indicate that the ionic state is the first vertically excited state in hexatriene, octatetraene, decapentaene, and dodecahexaene, lying 0.16 eV, 0.13 eV, 0.13 eV, and 0.12 eV below the covalent $2^1A_g^-$ state, respectively. In contrast, MR-CISD+P results suggest that the ionic state is the first vertically excited state in hexatriene, that the two low-lying excited states are nearly degenerate in octatetraene, and that the covalent $2^1A_g^-$ state lies below the ionic state by 0.05 eV in decapentaene and by 0.11 eV in dodecahexaene.

When comparing triple-ζ and quadruple-ζ basis set results, as expected, the stabilization effect is smaller than when expanding from the double- to triple-ζ basis set. For hexatriene, at the MR-AQCC level, the covalent state is stabilized by about 0.03 eV, while the ionic state is stabilized by approximately 0.12 eV. At the MR-CISD+P level, the covalent state is stabilized by 0.02 eV and the ionic state by 0.05 eV. For octatetraene, the covalent state shows a negligible effect from basis set expansion at both the MR-AQCC and MR-CISD+P levels. The ionic state, on the other hand, is further stabilized: by 0.10 eV at the MR-AQCC level, and by 0.03 eV at the MR-CISD+P level.

Using the cc-pVQZ basis set, MR-AQCC results show that the ionic state is the first vertically excited state in hexatriene and octatetraene, lying 0.25 eV and 0.22 eV below the covalent $2^1A_g^-$ state, respectively. MR-CISD+P results indicate the same ordering, with a splitting between the two low-lying excited states of 0.19 eV and 0.05 eV in hexatriene and octatetraene, respectively. The results obtained for the different basis sets are shown graphically in Figure 5.2 for MR-AQCC and in Figure B.2 for MR-CISD+P.

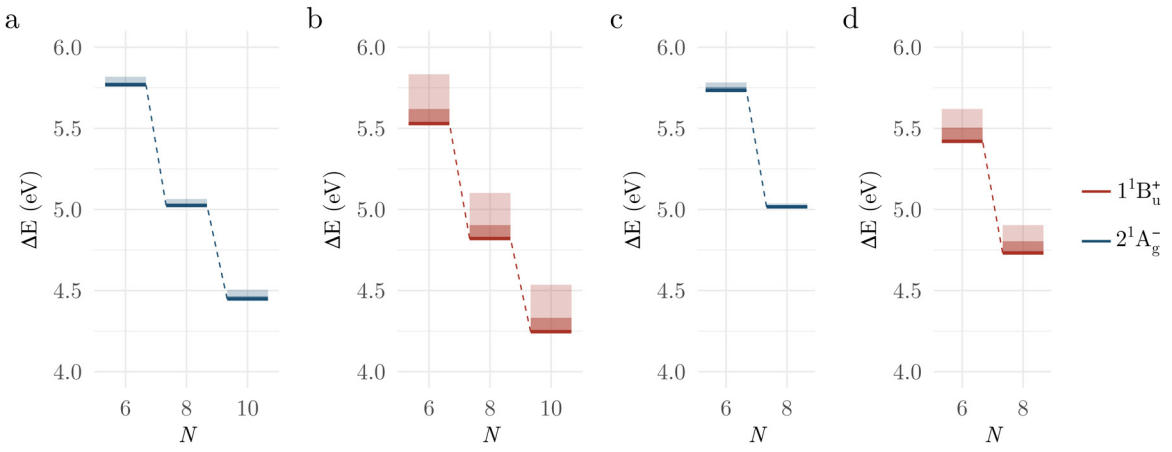

FIGURE 5.2 – Vertical singlet excitation energies of polyenes with N π-electrons, obtained by extrapolating MR-AQCC results to the complete basis set limit using (a, b) DT and (c, d) TQ extrapolations. The height of the lighter shaded bar indicates the difference between excitation energies obtained with the smaller and larger basis sets. The height of the darker shaded bar represents the difference between the larger basis set result and the extrapolated CBS value (represented by the marker).

Benchmark theoretical vertical excitation energy values are available for hexatriene and octatetraene (Table 5.4). In addition to data from the QUESTDB database of highly accurate excitation energies,[27] reference CASPT2 results for the ionic state were collected from the benchmark for electronically excited states in Reference (28), whereas CASPT2 results for the covalent state were taken from the reference energies for double excitations collection in Reference (29). All collected reference values were computed using triple-ζ basis sets.

TABLE 5.4 – MR-CISD+P and MR-AQCC vertical singlet excitation energies (in eV) of polyenes with N π-electrons at the CBS limit. Values were computed by extrapolating from the double-ζ cc-pVDZ to the triple-ζ cc-pVTZ' (DT) and from the triple-ζ cc-pVTZ' to the quadruple-ζ cc-pVQZ' (TQ). Reference theoretical values are provided for comparison.

N	State	MR-CISD+P		MR-AQCC		TBE[b]	CASPT2
		ΔE^{∞}_{DT}	ΔE^{∞}_{TQ}	ΔE^{∞}_{DT}	ΔE^{∞}_{TQ}		
6	$2^1A_g^-$	5.781	5.765	5.768	5.734	5.62[c]	5.57[e]
	$1^1B_u^+$	5.559	5.543	5.530	5.420	5.37[c]	5.31[f]
	$2^1B_u^-$	6.879	6.886	6.749	6.528	–	–
8	$2^1A_g^-$	4.977	4.991	5.025	5.016	4.90[d]	4.74[e]
	$1^1B_u^+$	4.906	4.917	4.820	4.731	4.78[d]	4.70[f]
	$2^1B_u^-$	6.156	6.188	6.117	6.026	–	–
10	$2^1A_g^-$	4.418	–	4.449	–	–	–
	$1^1B_u^+$	4.420	–	4.246	–	–	–
	$2^1B_u^-$	5.471	–	5.513	–	–	–
12	$2^1A_g^-$	4.019[a]	–	4.070[a]	–	–	–
	$1^1B_u^+$	4.080[a]	–	3.883[a]	–	–	–
	$2^1B_u^-$	5.082[a]	–	5.166[a]	–	–	–

[a] Estimated result based on a fit of excitation energies across the series (Figure B.5).
[b] Theoretical best estimates (TBE) collected from reference 48, computed as "A/SB + [B/TB - B/SB]," where A/SB is the excitation energy computed with a method A in a smaller basis (SB), and B/SB and B/TB are excitation energies computed with a method B in the small basis and target basis TB, respectively.
[c] CCSDT/AVDZ + [CC3/AVTZ − CC3/AVDZ].
[d] CCSDT/6-31+G(d) + [CC3/AVTZ − CC3/6-31+G(d)].
[e] Collected from Reference (29), aug-cc-pVTZ basis set.
[f] Collected from Reference (28), TZVP basis set.

For hexatriene, the theoretical best estimates (TBE) from the QUESTDB database[27] predict the ionic state to lie 0.25 eV below the covalent $2^1A_g^-$ state (Table 5.4). This aligns with the reference CASPT2 values, which predict the ionic state to lie 0.26 eV below the covalent state. The ΔE^{∞}_{DT} extrapolated excitation energies based on MR-AQCC results suggest the ionic state lies 0.24 eV below the covalent state, while the equivalent value based on MR-CISD+P computation is 0.22 eV. For the ΔE^{∞}_{TQ} extrapolated values, the relative differences between the two low-lying states are 0.31 eV at the MR-AQCC level and 0.22 eV at the MR-CISD+P level, with the ionic state being the first vertically excited state. The agreement between the reference theoretical values and our extrapolated results provides strong evidence that the ionic state is the first vertically excited state in hexatriene.

For octatetraene, data from the QUESTDB database indicate that the ionic state lies 0.12 eV below the covalent $2^1A_g^-$ state (Table 5.4). The reference CASPT2 results suggest that these states are nearly degenerate, with the ionic state lying only 0.04 eV below the covalent state, a difference within chemical accuracy. The ΔE_{DT}^{∞} extrapolated excitation energies based on MR-AQCC and MR-CISD+P results suggest that the ionic state lies below the covalent state by 0.21 eV and 0.07 eV, respectively. The ΔE_{TQ}^{∞} extrapolated values show the same trend as the ΔE_{DT}^{∞} extrapolated values, with relative differences between the two states of 0.29 eV at the MR-AQCC level and 0.07 eV at the MR-CISD+P level. Our MR-AQCC results suggest that the $1^1B_u^+$ state is the first vertically excited state in octatetraene, whereas MR-CISD+P, while suggesting the same ordering, shows a splitting of only 0.07 eV between the two low-lying excited states.

For decapentaene, excitation energies were obtained using double- and triple-ζ basis sets. Calculations with a quadruple-ζ basis set were not feasible, precluding a more reliable ΔE_{TQ}^{∞} extrapolation. Based on ΔE_{DT}^{∞} values, MR-AQCC results indicate that the ionic state remains lower than the covalent $2^1A_g^-$ state by approximately 0.20 eV (Table 5.4). MR-CISD+P results predict that the $2^1A_g^-$ and $1^1B_u^+$ states are virtually degenerate, with the splitting between the two states within chemical accuracy.

For dodecahexaene, the computational cost associated with using basis sets larger than the double-ζ cc-pVDZ prevented an accurate assignment of the relative ordering of the two low-lying excited states. However, a crude estimate for the ΔE_{DT}^{∞} extrapolated results made for $N = 12$ using a power function fit (Figure B.5) indicates that, at the MR-AQCC level, the ionic state is the first vertically excited state, lying 0.19 eV below the covalent $2^1A_g^-$ state. The MR-CISD+P estimates suggest that the covalent $2^1A_g^-$ state is the first vertically excited state, lying 0.06 eV below the ionic state.

The results in Table 5.4 incorporate all relevant effects necessary for accurately describing both the ionic and covalent states, including σ-electron correlation, size-extensivity correction, and basis set effects. Thus, these results represent a comprehensive and well-balanced description of vertical excitation energies. In summary, compared to excitation energies obtained at the MR-AQCC and MR-CISD+P levels using the cc-pVDZ basis set (Table 5.2), the significant stabilization of the ionic state relative to the covalent $2^1A_g^-$ state—caused by including larger shells of polarization functions—leads to the $1^1B_u^+$ state becoming the first vertically excited state in hexatriene and octatetraene. This state ordering, obtained at both the MR-AQCC and MR-CISD+P levels, agrees well with the reference TBE and CASPT2 values (Table 4). Extrapolated MR-AQCC results show somewhat better numerical agreement with the aforementioned reference data. Beyond octatetraene (Table 5.4), MR-AQCC consistently stabilizes the ionic state further, which remains slightly lower in energy than the covalent state for the polyene sizes investigated here. Extrapolated MR-CISD+P results (Table 5.4) suggest a slightly different picture, as

they stabilize the ionic state less. The two lowest excited states are virtually degenerate in decapentaene, with the covalent $2^1A_g^-$ state being the first vertically excited state in longer polyenes. The extrapolated results are shown graphically in Figure 5.2 for MR-AQCC calculations and B.2 for MR-CISD+P calculations.

The accuracy of experimental estimates for vertical excitation energies varies significantly between the $1^1B_u^+$ and $2^1A_g^-$ states due to their differing accessibility in one-photon processes. The $1^1B_u^+$ state is easily observed in one-photon absorption experiments, whereas the $2^1A_g^-$ state is optically dark, requiring more sophisticated detection techniques. Experimental estimates for the excitation energies for the $2^1A_g^-$ state have been extensively debated in the literature.[30–32] These estimates are made using the mirror-image symmetry rule, which assumes that the energy difference between the (0-0) and vertical excitation energies is equal to the difference between the (0-0) and fluorescence intensity maximum–i.e., vertical excitation energies are estimated as (0-0) + [(0-0) – fluorescence intensity maximum]. However, this approximation is valid only under the assumption that the potential energy surfaces of the $1^1A_g^-$ and $2^1A_g^-$ states are sufficiently similar–a condition that is not necessarily true for polyenes. Indeed, theoretical studies show that this approach can significantly underestimate the excitation energy due to substantial differences in the potential energy surfaces of the electronic states involved.[33,34]

On the other hand, the experimental vertical excitation energy to the ionic $1^1B_u^+$ state is typically estimated from the absorption spectrum, where the maximum of the absorption band associated with the $1^1B_u^+ \leftarrow 1^1A_g^-$ excitation—which, in this case, also represents the origin peak—is often compared with theoretical vertical excitation energies. However, it has been previously demonstrated that vertical excitation energies at the ground-state minimum are blue-shifted relative to the band maximum by about 0.2 eV.[35] For hexatriene and octatetraene, gas-phase spectra or high-resolution spectra of the jet-cooled compound are available,[36–42] whereas for decapentaene and dodecahexaene fewer experimental data are available. An extrapolation to the gas phase from the origins of the two lowest-lying excited states measured in the condensed phase was carried out by D'Amico and coworkers for decapentaene and dodecahexaene.[43] This extrapolation has been shown to be in good agreement with gas-phase data for decapentaene.[43]

TABLE 5.5 – Experimental estimates for gas-phase vertical excitation energies (eV) for the two lowest excited singlet states of polyenes with N π-electrons.

N	State	Experimental data
6	$2^1A_g^-$	-
	$1^1B_u^+$	4.93[a]; 4.93[b]
8	$2^1A_g^-$	4.08[c]
	$1^1B_u^+$	4.41[d]; 4.41[e]
10	$2^1A_g^-$	3.48[f]
	$1^1B_u^+$	3.98[g]
12	$2^1A_g^-$	2.91[f]
	$1^1B_u^+$	3.65[g]

[a] Absorption band maximum.[36]

[b] Absorption band maximum of the jet-cooled compound.[40]

[c] Estimated assuming mirror symmetry between absorption and emission.[42]

[d] Absorption band maximum of the jet-cooled compound.[39]

[e] Absorption band maximum of the jet-cooled compound.[41]

[f] Estimated assuming mirror symmetry between absorption and emission. Vibronic patterns for the gas and condensed phases are assumed to be similar.[43]

[g] Absorption band maximum in the condensed phase. Extrapolated to gas phase using solvent shift theory.[43]

Experimental gas-phase estimates for vertical singlet excitation energies of linear all-trans polyenes are presented in Table 5.5. For hexatriene, when comparing the experimental estimates for the $1^1B_u^+$ state with the ΔE_{TQ}^{∞} extrapolated results obtained at the MR-AQCC level (Table 5.4)–which best match the reference theoretical values–our calculated vertical excitation energy for the ionic state in hexatriene is 0.49 eV higher than the experimental estimate. The reference TBE from QUESTDB is 0.44 eV higher, while the reference CASPT2 result is 0.38 eV higher than the experimental estimate. These reference theoretical values are in good agreement with our findings. Taking into account that vertical excitation energies are estimated to be around 0.2 eV higher than the experimental band maximum,[35] our calculated values also show good agreement with the experimental estimate.

In octatetraene, our ΔE_{TQ}^{∞} extrapolated MR-AQCC results for the $1^1B_u^+$ state suggest a vertical excitation energy that is 0.32 eV higher than the experimental band maximum (Table 5.4, Table 5.5). The reference TBE from QUESTDB is 0.37 eV higher, while the CASPT2 result is 0.29 eV higher than the experimental estimate. Again, these findings are consistent with our results and are in good agreement with the experimental estimate,

assuming, as before, that vertical excitation energies are blue-shifted relative to the band maximum by about 0.2 eV.[35] For the vertical excitation energy to the covalent $2^1A_g^-$ state, the ΔE_{TQ}^{∞} extrapolated results indicate that the experimental estimate based on the mirror-image symmetry rule underestimates the vertical excitation energy by 0.94 eV. This underestimation is 0.82 eV based on the QUESTDB reference, and 0.66 eV based on the CASPT2 reference result.

In decapentaene, ΔE_{DT}^{∞} extrapolated MR-AQCC results predict that the vertical excitation energy for the $1^1B_u^+$ state is 0.27 eV higher than the band maximum (Tables 5.4 and 5.5). For the $2^1A_g^-$ state, the extrapolated result suggests that the experimental estimate based on the mirror-image symmetry rule underestimates the vertical excitation energy by 0.97 eV, consistent with what was observed for octatetraene.

In dodecahexaene, based on our estimate for the ΔE_{DT}^{∞} extrapolated MR-AQCC results (Table 4), the vertical excitation energy for the $1^1B_u^+$ state is predicted to be 0.23 eV higher than the band maximum (Tables 5.4 and 5.5). Our results for the covalent $2^1A_g^-$ state suggest that the experimental estimate based on the mirror-image symmetry rule underestimates the vertical excitation energy by 1.16 eV, in agreement with what was observed for the smaller members of the series.

5.2.2 Triplet states

The two lowest triplet states–$1^3A_g^-$ and $1^3B_u^-$–are covalent states. Similar to the singlet covalent states, these triplet states are well-described without the need for extensive dynamic correlation treatments. Considering all the polyenes studied, SA-CASSCF results exhibit an average difference of 0.08 eV for the $1^3A_g^-$ state and 0.04 eV for the $1^3B_u^-$ state compared to MR-CISD+P values (Table 5.6). When compared to MR-AQCC results, the average differences are 0.08 eV and 0.05 eV for the $1^3A_g^-$ and $1^3B_u^-$ states, respectively.

TABLE 5.6 – Vertical triplet excitation energies of polyenes with N π-electrons computed using CASSCF, MR-CISD, MR-CISD+P, MR-AQCC, and CASPT2 methods. Calculations were performed with the cc-pVDZ basis set.

N	State	Method				
		CASSCF	MR-CISD	MR-CISD+P	MR-AQCC	CASPT2
6	$1^3A_g^-$	2.860	2.940	2.948	2.945	2.941
	$1^3B_u^-$	4.421	4.574	4.608	4.598	4.553
8	$1^3A_g^-$	2.539	2.563	2.581	2.562	2.569
	$1^3B_u^-$	3.845	3.931	3.933	3.928	3.925
10	$1^3A_g^-$	2.330	2.321	2.330	2.294	2.335
	$1^3B_u^-$	3.429	3.502	3.465	3.466	3.466
12	$1^3A_g^-$	2.193	2.169	2.182	2.137	2.178
	$1^3B_u^-$	3.121	3.182	3.116	3.121	3.140

The differences between MR-CISD+P, MR-AQCC, and CASPT2 results for both the $1^3A_g^-$ and $1^3B_u^-$ states do not exceed 0.05 eV (Table 5.6). This indicates that these triplet states are reliably calculated using these methods. The CASSCF results are in close agreement with those obtained using MR-CISD+P, MR-AQCC, and CASPT2 (Table 5.6), suggesting that σ-π electron correlation does not significantly impact the description of these states. The primary exception is the excitation energy to the $1^3A_g^-$ state of hexatriene, where the CASSCF result underestimates the energy by approximately 0.18 eV compared to MR-CISD+P and MR-AQCC.

Size-extensivity corrections also have no significant effect on the vertical excitation energies of the $1^3A_g^-$ and $1^3B_u^-$ states for the systems studied. The MR-CISD results are not significantly different from the size-extensivity-corrected MR-CISD+P values (Table 5.6). Likewise, the addition of polarization functions to the basis set does not substantially change the vertical excitation energies for these states when using either the MR-CISD+P (Table B.3) or MR-AQCC (Table B.3) methods.

Experimental data for hexatriene and octatetraene are available from low-energy electron impact spectra and electron energy loss spectra, respectively (Table 5.7). In comparison with MR-AQCC results for hexatriene (Table 5.6), the calculated results predict excitation energies that are 0.34 eV and 0.49 eV higher than the band maximum for the $1^3B_u^-$ and $1^3A_g^-$ states, respectively. For octatetraene, the MR-AQCC results suggest that the excitation energies are 0.46 eV and 0.38 eV higher than the band maximum of the electron energy loss spectrum for the $1^3B_u^-$ and $1^3A_g^-$ states, respectively.

TABLE 5.7 – Experimental estimates for gas-phase vertical excitation energies (eV) for the two lowest triplet states of polyenes with N π-electrons.

N	State	Experimental data
6	$1^3A_g^-$	2.61[a]
	$1^3B_u^-$	4.11[a]
8	$1^3A_g^-$	2.10[b]
	$1^3B_u^-$	3.55[b]

[a] Band maximum of low-energy electron impact spectrum.[44]

[b] Band maximum of electron energy-loss spectrum.[45]

5.2.3 Wavefunction analysis

We now shift our focus to analyzing the wave functions of the polyenes, with particular emphasis on the singlet states. Figures B.6 to B.9 illustrate the hole and electron natural transition orbitals (NTOs) computed at the MR-CISD level for each system. The transition densities for the excited states $2^1A_g^-$, $1^1B_u^+$, and $2^1B_u^-$ of hexatriene, calculated with respect to the ground state, are shown in Figure 5.3. Transition densities for all the systems are depicted in Figure B.10.

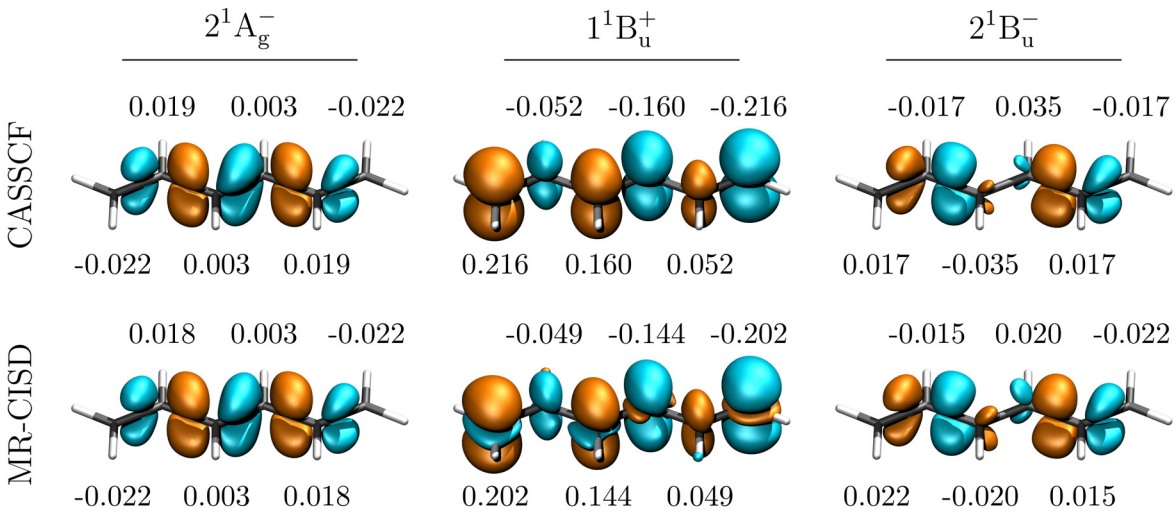

FIGURE 5.3 – Transition densities (isovalue: $\pm$0.002 a.u.) between the ground state and the excited states $2^1A_g^-$, $1^1B_u^+$, and $2^1B_u^-$ of hexatriene, computed at the CASSCF and MR-CISD levels of theory. Transition charges on carbon atoms are displayed.

Examination of the transition density (Figure 5.3) shows that for covalent states, the transition densities are centered along the bonds, while for the ionic state, they are localized on the atoms. In covalent states, transition density contributions from either side of an atom tend to cancel out, resulting in a net zero transition charge q_M^t (transition

charge values are available in Section B.5). In contrast, ionic states exhibit non-vanishing transition charges on individual atoms. Moreover, the importance of σ-π electron correlation is evident not only in the excitation energies but also in the transition densities. The transition density of the ionic state at the MR-CISD level shows distinct σ-contributions that are absent in the CASSCF transition density. This observation holds consistently across all polyenes investigated.

These σ-contributions are associated with the reduction of transition density self-repulsion. Self-repulsion is generally large when there is significant spatial overlap between the involved orbitals and becomes smaller when the orbitals are spatially separated.[46,25,47–49] The role of transition density self-repulsion has been investigated by Kimber and Plasser.[46,25,49] Their works demonstrate that, while the self-repulsion term raises the excitation energy, it can be compensated by $\sigma\sigma^*$ excitations. Consequently, the inclusion of σ-contributions in the wavefunction reduces the energetic penalty of the pure HOMO-LUMO transition,[18] lowering the excitation energy and resulting in reduced oscillator strengths, as observed in MR-CISD calculations compared to CASSCF results (Table B.5).

As anticipated, progressively reducing the degree of σ-π electron correlation by freezing σ-orbitals at the CI step has noticeable effects on transition densities (Figure 5.4a) and excitation energies (Figure 5.4b). Freezing 50% of reference doubly occupied σ-orbitals and 50% of reference virtual σ-orbitals has minimal impact on the excitation energies or transition densities. However, as the percentage of frozen σ-orbitals increases, the σ-contributions in the transition densities vanish, the excitation energies increase, and size-extensivity corrections become less effective.

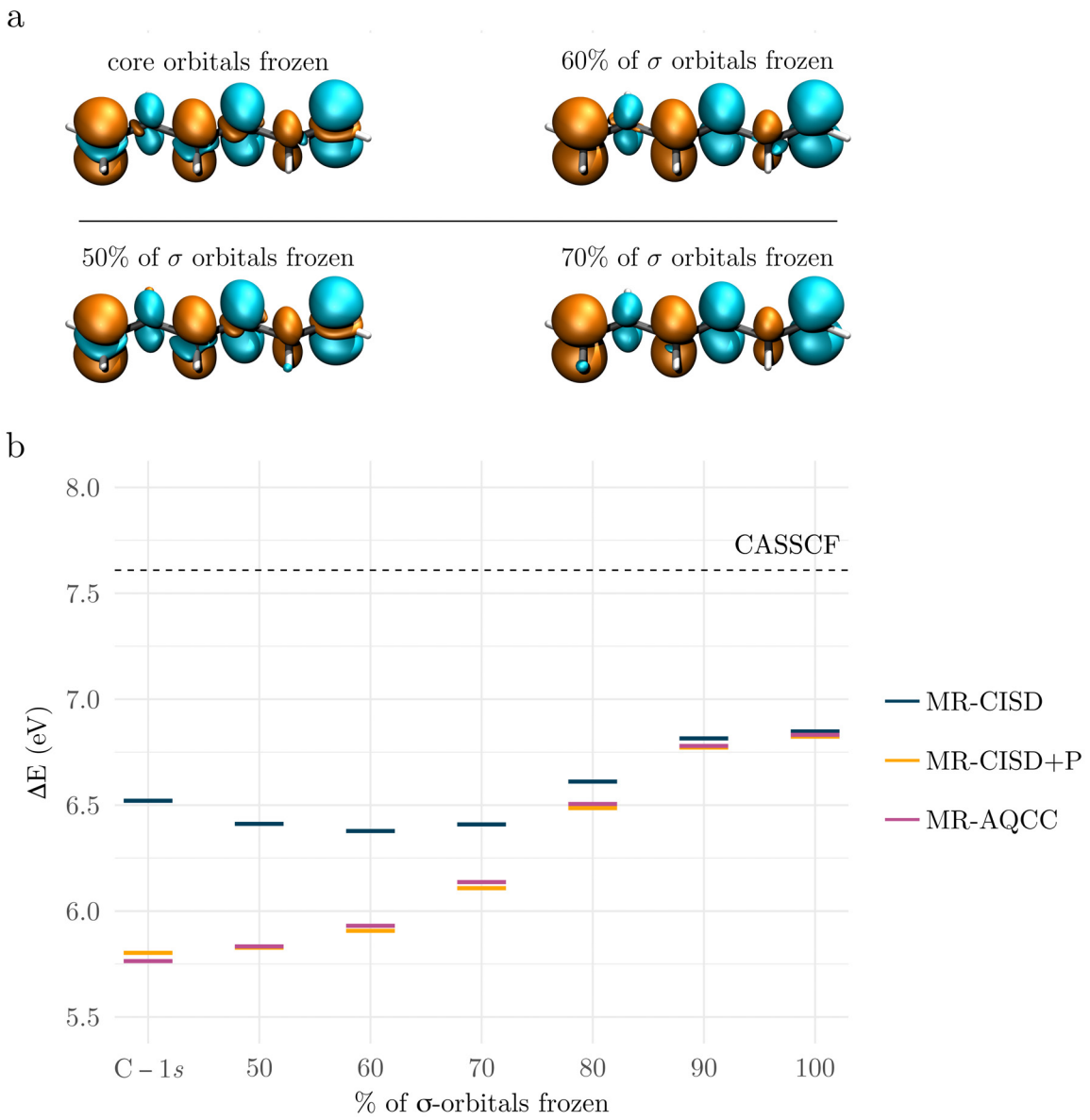

FIGURE 5.4 – Influence of freezing σ-orbitals in hexatriene on (a) transition densities (isovalue: ± 0.002 a.u.) between the ground state and the $1^1B_u^+$ state, and (b) excitation energies computed at the MR-CISD level with the cc-pVDZ basis set. The percentage of σ-orbitals refers to the percentage of reference doubly occupied σ-orbitals and the corresponding percentage of reference virtual σ-orbitals frozen. C-1s indicates that only carbon core orbitals were frozen.

Lastly, we examine the evolution of the wavefunction across the polyene series in terms of ionic character (Q_a^t), multiconfigurational character (PRNTO), and single-excitation character (Ω). The results for these descriptors are summarized in Table 5.8.

TABLE 5.8 – Characterization of excited states based on ionic character Q_a^t, single-excitation character Ω, and NTO participation ratio PR_{NTO} calculated from the MR-CISD wave function.

N	State	Q_a^t	PR_{NTO}	Ω
6	$2^1A_g^-$	0.089	1.994	0.404
	$1^1B_u^+$	0.872	1.087	0.871
	$2^1B_u^-$	0.117	1.994	0.468
8	$2^1A_g^-$	0.090	2.029	0.368
	$1^1B_u^+$	0.879	1.101	0.854
	$2^1B_u^-$	0.148	2.158	0.402
10	$2^1A_g^-$	0.078	2.062	0.344
	$1^1B_u^+$	0.889	1.119	0.839
	$2^1B_u^-$	0.120	2.176	0.366
12	$2^1A_g^-$	0.071	2.094	0.324
	$1^1B_u^+$	0.914	1.137	0.829
	$2^1B_u^-$	0.129	2.247	0.350

The results in Table 8 suggest that the descriptors for excitation to the ionic state change only slightly across the polyene series. The Q_a^t values effectively distinguish the ionic state from the covalent states by indicating significant transition charges localized on individual atoms, as has been observed in other systems.[18] Additionally, the NTO participation ratio (PRNTO) shows that the ionic state is predominantly described by a single pair of hole and electron NTOs, which is consistent with the fact that these are predominant HOMO-LUMO transitions. The single-excitation character (Ω), with values higher than 0.8, emphasizes its singly-excited nature with only minor correlation contributions.

In contrast, the covalent states exhibit more pronounced changes in their wavefunction descriptors throughout the series. The multiconfigurational character of the $2^1A_g^-$ state remains nearly constant, while for the $2^1B_u^-$ state it increases slightly as the chain lengthens. Regarding the single-excitation character Ω, we note that this value is below 0.5 for both covalent states of all molecules investigated, highlighting that these states possess more than 50% double excitation character. In addition, we note that the single-excitation character slightly decreases suggesting that the contribution of doubly excited configurations grows with the length of the chain for both the $2^1A_g^-$ and $2^1B_u^-$ states.

Bibliography

1 CHAI, Jeng-Da; HEAD-GORDON, Martin. Long-range corrected hybrid density functionals with damped atom–atom dispersion corrections. **Physical Chemistry Chemical Physics**, v. 10, n. 44, p. 6615, 2008.

2 DUNNING, Thom H. Gaussian basis sets for use in correlated molecular calculations. I. The atoms boron through neon and hydrogen. **The Journal of Chemical Physics**, v. 90, n. 2, p. 1007–1023, Jan. 1989.

3 ROOS, Björn O.; TAYLOR, Peter R.; SIGBAHN, Per E.M. A complete active space SCF method (CASSCF) using a density matrix formulated super-CI approach. **Chemical Physics**, North-Holland, v. 48, n. 2, p. 157–173, May 1980.

4 LISCHKA, Hans et al. Multireference Approaches for Excited States of Molecules. **Chemical Reviews**, v. 118, n. 15, p. 7293–7361, Aug. 2018.

5 SZALAY, Péter G. et al. Multiconfiguration Self-Consistent Field and Multireference Configuration Interaction Methods and Applications. **Chemical Reviews**, v. 112, n. 1, p. 108–181, Jan. 2012.

6 SZALAY, Péter G.; BARTLETT, Rodney J. Multi-reference averaged quadratic coupled-cluster method: a size-extensive modification of multi-reference CI. **Chemical Physics Letters**, v. 214, n. 5, p. 481–488, Nov. 1993.

7 _____. Approximately extensive modifications of the multireference configuration interaction method: A theoretical and practical analysis. **The Journal of Chemical Physics**, v. 103, n. 9, p. 3600–3612, Sept. 1995.

8 POPLE, J. A.; SEEGER, R.; KRISHNAN, R. Variational configuration interaction methods and comparison with perturbation theory. **International Journal of Quantum Chemistry**, v. 12, S11, p. 149–163, June 2009.

9 BUNGE, Annik. Electronic Wavefunctions for Atoms. III. Partition of Degenerate Spaces and Ground State of C. **The Journal of Chemical Physics**, v. 53, n. 1, p. 20–28, July 1970.

10 HALKIER, Asger et al. Basis-set convergence in correlated calculations on Ne, N2, and H2O. **Chemical Physics Letters**, v. 286, n. 3-4, p. 243–252, Apr. 1998.

11 ANDERSSON, Kerstin. et al. Second-order perturbation theory with a CASSCF reference function. **The Journal of Physical Chemistry**, v. 94, n. 14, p. 5483–5488, July 1990.

12 FRISCH, M J et al. **Gaussian 16 Revision C.01**. [S.l.: s.n.], 2016. Gaussian Inc. Wallingford CT.

13 LISCHKA, Hans et al. High-level multireference methods in the quantum-chemistry program system COLUMBUS: Analytic MR-CISD and MR-AQCC gradients and MR-AQCC-LRT for excited states, GUGA spin–orbit CI and parallel CI density. **Physical Chemistry Chemical Physics**, v. 3, n. 5, p. 664–673, 2001.

14 LISCHKA, Hans et al. Columbus—a program system for advanced multireference theory calculations. **WIREs Computational Molecular Science**, John Wiley & Sons, v. 1, n. 2, p. 191–199, Mar. 2011.

15 LISCHKA, Hans et al. The generality of the GUGA MRCI approach in COLUMBUS for treating complex quantum chemistry. **The Journal of Chemical Physics**, AIP Publishing, LLC, v. 152, n. 13, p. 134110, Apr. 2020.

16 HELGAKER, T et al. **DALTON, an ab initio electronic structure program, Release 1.0**. [S.l.: s.n.], 1997.

17 MANNI, Giovanni Li et al. The OpenMolcas Web : A Community-Driven Approach to Advancing Computational Chemistry. **Journal of Chemical Theory and Computation**, v. 19, n. 20, p. 6933–6991, Oct. 2023.

18 MONTE, Silmar A. do et al. Quantification of the Ionic Character of Multiconfigurational Wave Functions: The Q a t Diagnostic. **The Journal of Physical Chemistry A**, American Chemical Society (ACS), v. 127, n. 46, p. 9842–9852, Nov. 2023.

19 LÖWDIN, Per-Olov. On the Non-Orthogonality Problem Connected with the Use of Atomic Wave Functions in the Theory of Molecules and Crystals. **The Journal of Chemical Physics**, v. 18, n. 3, p. 365–375, Mar. 1950.

20 PLASSER, Felix; LISCHKA, Hans. Analysis of Excitonic and Charge Transfer Interactions from Quantum Chemical Calculations. **Journal of Chemical Theory and Computation**, v. 8, n. 8, p. 2777–2789, Aug. 2012.

21 PLASSER, Felix. Entanglement entropy of electronic excitations. **The Journal of Chemical Physics**, v. 144, n. 19, May 2016.

22 PLASSER, Felix; WORMIT, Michael; DREUW, Andreas. New tools for the systematic analysis and visualization of electronic excitations. I. Formalism. **The Journal of Chemical Physics**, v. 141, n. 2, July 2014.

23 MATSIKA, Spiridoula et al. What We Can Learn from the Norms of One-Particle Density Matrices, and What We Can't: Some Results for Interstate Properties in Model Singlet Fission Systems. **The Journal of Physical Chemistry A**, v. 118, n. 51, p. 11943–11955, Dec. 2014.

24 CASAL, Mariana T. do et al. Classification of doubly excited molecular electronic states. **Chemical Science**, v. 14, n. 15, p. 4012–4026, 2023.

25 KIMBER, Patrick; PLASSER, Felix. Toward an understanding of electronic excitation energies beyond the molecular orbital picture. **Physical Chemistry Chemical Physics**, Royal Society of Chemistry, v. 22, n. 11, p. 6058–6080, Mar. 2020.

26 PLASSER, F. TheoDORE: A toolbox for a detailed and automated analysis of electronic excited state computations. **The Journal of Chemical Physics**, AIP Publishing LLCAIP Publishing, v. 152, n. 8, p. 084108, Feb. 2020.

27 VÉRIL, Mickaël et al. QUESTDB : A database of highly accurate excitation energies for the electronic structure community. **WIREs Computational Molecular Science**, John Wiley and Sons Inc, v. 11, n. 5, Sept. 2021.

28 SCHREIBER, Marko et al. Benchmarks for electronically excited states: CASPT2, CC2, CCSD, and CC3. **The Journal of Chemical Physics**, v. 128, n. 13, Apr. 2008.

29 KOSSOSKI, Fábris et al. Reference Energies for Double Excitations: Improvement and Extension. **Journal of Chemical Theory and Computation**, v. 20, n. 13, p. 5655–5678, July 2024.

30 GUARESCHI, Riccardo; ANGELI, Celestino. The lowest singlet states of hexatriene revisited. **Theoretical Chemistry Accounts**, Springer Science and Business Media Deutschland GmbH, v. 142, n. 12, p. 127, Dec. 2023.

31 ANGELI, Celestino; PASTORE, Mariachiara. The lowest singlet states of octatetraene revisited. **The Journal of Chemical Physics**, v. 134, n. 18, May 2011.

32 SERRANO-ANDRES, Luis et al. Theoretical study of the electronic spectrum of all-trans-1,3,5,7-octatetraene. **The Journal of Physical Chemistry**, v. 97, n. 37, p. 9360–9368, Sept. 1993.

33 NAKAYAMA, Kenichi; NAKANO, Haruyuki; HIRAO, Kimihiko. Theoretical study of the $\pi\pi^*$ excited states of linear polyenes: The energy gap between 11Bu+ and 21Ag states and their character. **International Journal of Quantum Chemistry**, John Wiley & Sons, Inc, v. 66, n. 2, p. 157–175, 1998.

34 MENGER, Maximilian F. S. J.; KÖPPEL, Horst. On the Fluorescence Properties and Nonradiative Transitions in Medium-Sized All-Trans Polyenes. **The Journal of Physical Chemistry A**, American Chemical Society, v. 127, n. 41, p. 8501–8507, Oct. 2023.

35 BARBATTI, Mario; AQUINO, Adelia J. A.; LISCHKA, Hans. The UV absorption of nucleobases: semi-classical ab initio spectra simulations. **Physical Chemistry Chemical Physics**, v. 12, n. 19, p. 4959, 2010.

36 GAVIN, R. M.; RISEMBERG, Salomon; RICE, Stuart A. Spectroscopic properties of polyenes. I. The lowest energy allowed singlet-singlet transition for cis- and trans-1,3,5-hexatriene. **The Journal of Chemical Physics**, v. 58, n. 8, p. 3160–3165, Apr. 1973.

37 GAVIN, R. M. et al. Spectroscopic properties of polyenes. III. 1,3,5,7-Octatetraene. **The Journal of Chemical Physics**, v. 68, n. 2, p. 522–529, Jan. 1978.

38 GAVIN, R. M.; RICE, Stuart A. Spectroscopic properties of polyenes. II. The vacuum ultraviolet spectra of cis- and trans-1,3,5-hexatriene. **The Journal of Chemical Physics**, v. 60, n. 8, p. 3231–3237, Apr. 1974.

39 LEOPOLD, D. G.; VAIDA, V.; GRANVILLE, Mark F. Direct absorption spectroscopy of jet-cooled polyenes. I. The $1^1B_u^+ \leftarrow 1^1A_g^-$ transition of trans,trans-1,3,5,7-octatetraene. **The Journal of Chemical Physics**, v. 81, n. 10, p. 4210–4217, Nov. 1984.

40 LEOPOLD, D. G. et al. Direct absorption spectroscopy of jet-cooled polyenes. II. The $1^1B_u^+ \leftarrow 1^1A_g^-$ transitions of butadienes and hexatrienes. **The Journal of Chemical Physics**, v. 81, n. 10, p. 4218–4229, Nov. 1984.

41 HEIMBROOK, Lou Ann; KOHLER, Bryan E.; LEVY, Irvin J. Fluorescence from the 1^1B_u state of trans,trans-1,3,5,7-octatetraene in a free jet. **The Journal of Chemical Physics**, v. 81, n. 4, p. 1592–1597, Aug. 1984.

42 PETEK, Hrvoje et al. The 2^1A_g state of trans,trans-1,3,5,7-octatetraene in free jet expansions. **The Journal of Chemical Physics**, v. 98, n. 5, p. 3777–3794, Mar. 1993.

43 D'AMICO, Kevin L.; MANOS, Christopher; CHRISTENSEN, Ronald L. Electronic energy levels in a homologous series of unsubstituted linear polyenes. **Journal of the American Chemical Society**, v. 102, n. 6, p. 1777–1782, Mar. 1980.

44 FLICKER, Wayne M.; MOSHER, Oren A.; KUPPERMANN, Aron. Low energy, variable angle electron-impact excitation of 1,3,5-hexatriene. **Chemical Physics Letters**, v. 45, n. 3, p. 492–497, Feb. 1977.

45 ALLAN, Michael; NEUHAUS, Louis; HASELBACH, Edwin. all-E-1,3,5,7-Octatetraene: Electron-Energy-Loss and Electron-Transmission Spectra. **Helvetica Chimica Acta**, v. 67, n. 7, p. 1776–1782, Nov. 1984.

46 KIMBER, Patrick; PLASSER, Felix. Classification and Analysis of Molecular Excited States. In: [s.l.]: Elsevier, 2024. p. 55–83.

47 YANG, Zhiyong et al. Recent advances in organic thermally activated delayed fluorescence materials. **Chemical Society Reviews**, Royal Society of Chemistry, v. 46, n. 3, p. 915–1016, Feb. 2017.

48 DIAS, Fernando B; PENFOLD, Thomas J; MONKMAN, Andrew P. Photophysics of thermally activated delayed fluorescence molecules. **Methods and Applications in Fluorescence**, v. 5, n. 1, p. 012001, Mar. 2017.

49 KIMBER, Patrick; PLASSER, Felix. Energy Component Analysis for Electronically Excited States of Molecules: Why the Lowest Excited State Is Not Always the HOMO/LUMO Transition. **Journal of Chemical Theory and Computation**, American Chemical Society, v. 19, n. 8, p. 2340–2352, Apr. 2023.

6 Low-lying excited states of linear All-*trans* polyenes: insights from analytical gradient calculations based on a multireference Wavefunction

6.1 Computational details

The equilibrium geometries of the ground ($1^1A_g^-$) and the singlet excited states $2^1A_g^-$, and $1^1B_u^+$ of hexatriene, octatetraene, and decapentaene were obtained via analytic energy gradient based on the MR-CISD wavefunction. All geometry optimizations were performed under C_{2h} symmetry constraints. All the geometries are provided in the Supplementary Information (SI). To account for size-extensivity errors inherent to MR-CISD, the Pople (+P) correction,[1] extended to the MR-CISD case, was considered in all single-point calculations presented throughout this work.

At the CASSCF level, an equal-weight state averaging was performed over six electronic states: $1^1A_g^-$, $2^1A_g^-$, $1^1B_u^+$, $2^1B_u^-$, $1^3A_g^-$, and $1^3B_u^-$. The CASSCF computations were carried out using a standard valence active space, encompassing all valence π-electrons and valence π-orbitals of each molecule. The molecular orbitals obtained from this state-averaged procedure were subsequently employed in the MR-CISD calculations. To reduce the computational demands of the MR-CISD steps, the reference space was constructed by splitting the π-valence space into three subsets: a CAS(6,6), a complementary restricted active space (RAS) for the remaining strongly occupied orbitals, and a corresponding auxiliary (AUX) space for weakly occupied orbitals. Single excitations were permitted from the RAS into the CAS and AUX spaces, as well as from the CAS into AUX orbitals. The specific schemes adopted in our calculations are listed in Table 6.1. Based on this reference space, single and double excitations into all virtual orbitals were generated, forming the expansion space of the MR-CISD wavefunction. Generalized interacting space restrictions[2] were applied at the MR-CISD level.

TABLE 6.1 – Active reference space scheme utilized at the MR-CISD level for polyenes with N π-electrons.

N	Active space scheme
6	CAS(6,6)
8	RAS(1)CAS(6,6) AUX(1)
10	RAS(2)CAS(6,6) AUX(2)
12	RAS(3)CAS(6,6) AUX(3)

Based on the optimized geometries of the ground and excited states obtained using the double-zeta cc-pVDZ basis set, single point calculations using the triple-zeta cc-pVTZ basis sets[3] were carried out. Extrapolation to the complete basis set (CBS) limit was performed using the two-point fit approach[4] (Eq. 6.1) for energies splitting obtained at the MR-CISD+P level.

$$\mathrm{E}_{\mathrm{YX}}^{\infty} = \frac{\mathrm{E_X X^3 - E_Y Y^3}}{\mathrm{X^3 - Y^3}} \tag{6.1}$$

Here, $\mathrm{E}_{\mathrm{YX}}^{\infty}$ represents the CBS limit excitation energy, X and Y are the cardinal numbers for the respective basis sets, and $\mathrm{E_X}$ and $\mathrm{E_Y}$ denote the excitation energies obtained for those individual basis sets. The cc-pVTZ basis set without the f-function, i.e., with contraction $(10s, 5p, 2d)/[4s, 3p, 2d]$ (cc-pVTZ') was used on carbon atoms for the basis set extrapolation to the CBS limit. The cc-pVDZ basis set was used on hydrogen in all cases.

All calculations were performed using the described formalism implemented in the COLUMBUS program system,[5–7] with integrals calculated by the Dalton program.[8]

6.2 Results and discussion

6.2.1 Adiabatic excitation energies

We begin our discussion by presenting results for adiabatic excitation energies, calculated as the difference between the ground and excited states at their respective relaxed geometries. From the experimental point of view, this is comparable to the energy of the 0-0 excitation band, although only the electronic contribution is considered here. Vibrational corrections typically reduce excitation energies by 0.1–0.2 eV.[9] The adiabatic excitation energies to the two lowest singlet excited states of hexatriene, octatetraene, and decapentaene are presented in Table 6.2.

TABLE 6.2 – Adiabatic excitation energies (eV) of singlet states in polyenes with N π-electrons computed at the MR-CISD+P level based on geometries obtained via analytic energy gradients using the MR-CISD wavefunction and the cc-pVDZ basis set. Reference theoretical values and experimental data are provided for comparison.

N	State	MR-CISD+P	CASPT2	Exp. 0-0
6	$2^1A_g^-$	4.365	4.195[a]; 4.17[b]	$\leq$4.22[e]
	$1^1B_u^+$	5.335	5.177[c]; 4.84[b]	4.93[f]; 4.93[g]
8	$2^1A_g^-$	3.645	3.30 [d]; 3.50[b]	3.59[h]; 3.59[i];
	$1^1B_u^+$	4.698	4.46 [d]; 4.34[b]	4.40[j]; 4.41[k]; 4.41[l]
10	$2^1A_g^-$	3.122	2.99 [b]	3.10[m]
	$1^1B_u^+$	4.236	3.88 [b]	4.02[n]

[a] Geometry optimized at CASSCF/NEVPT2 level; single-point energy at CASPT2 level.[9]

[b] Geometry optimized at CASSCF level; single-point energy at CASPT2 level.[10]

[c] Geometry optimized at RASSCF level; single-point energy at CASPT2 level.[9]

[d] Geometry optimized at CASSCF level; single-point energy at CASPT2 level.[11]

[e] Estimate origin of absorption of the multiphoton ionization spectrum.[12]

[f] Origin of absorption for the isolated compound.[13]

[g] Origin of absorption for the jet-cooled compound.[14]

[h] Origin of absorption extrapolated to the gas phase using solvent shift theory.[15]

[i] Origin of absorption of the two-photon excitation spectrum.[16]

[j] Origin of absorption for the isolated compound.[15]

[k] Origin of absorption for the jet-cooled compound.[17]

[l] Origin of absorption for the jet-cooled compound.[18]

[m] Origin of absorption extrapolated to the gas phase using solvent shift theory.[19]

[n] Origin of absorption for the isolated compound.[19]

The origin of the ionic state is observed experimentally in the gas phase and is located at 4.93 eV.[14,13] Our results overestimate the adiabatic excitation energy by 0.41 eV. At the CBS limit, this agreement is improved by 0.14 eV (Table C.1). The selected CASPT2 results provide good agreement with the experimental observation, with one of the values overestimating the excitation energy by 0.25 eV and the other matching it to within just under 0.1 eV (Table 6.2). On the other hand, the origin of the $2^1A_g^-$ state in hexatriene has not been unambiguously defined for the trans isomer. Buma and coauthors[12] estimated the origin of the $2^1A_g^-$ state to have an energy $\leq$4.22 eV. Corroborating this result, it is generally assumed[20] that the origin of this state lies within a few hundred wavenumbers of the corresponding state in the *cis* isomer of hexatriene, which can be obtained from the experimental spectrum and is unambiguously defined at 4.26 eV.[12,21] The MR-CISD+P results estimate an energy splitting of 4.365 eV, which is 0.15 eV higher than the minimum value of the origin estimated experimentally. Both CASPT2 results provide accurate predictions (Table 6.2).

As for hexatriene, the origin of the $1^1B_u^+ \leftarrow 1^1A_g^-$ transition in octatetraene is observed in gas-phase one-photon absorption experiments.[15,17,18] Recent experiments yield a value of 4.41 eV.[17,18] Our calculated adiabatic excitation energy is 4.698 eV, representing an overestimation of 0.29 eV with respect to the experimental result. The CASPT2 results also give accurate predictions in comparison with the experimental value (Table 6.2). The origin of the $2^1A_g^- \leftarrow 1^1A_g^-$ transition has also been precisely observed in the gas phase by means of two-photon absorption experiments.[16] Additionally, the origin of this transition has been measured in the condensed phase and extrapolated to the gas phase.[15] Both experimental results suggest that the minimum of the $2^1A_g^-$ state lies 3.59 eV above the minimum of the ground state. Our results yield 3.645 eV–an excellent agreement, matching the experimental results remarkably well. The selected CASPT2 results reproduce the experimental value within a deviation of approximately 0.1–0.3eV (Table 6.2).

Experimental and theoretical data for decapentaene are less abundant. The origin of the $1^1B_u^+ \leftarrow 1^1A_g^-$ transition is directly observable in the gas phase and is also shown to coincide with the absorption maximum of the spectrum at 4.02 eV.[19] The MR-CISD+P value lies 0.22 eV above this, at 4.236 eV, showing acceptable accuracy. The CASPT2 results underestimate the excitation energy by just over 0.1 eV (Table 6.2). The $2^1A_g^- \leftarrow 1^1A_g^-$ transition energy has only been measured in the condensed phase and extrapolated to the gas phase.[19] This approach applied to the ionic state–both in octatetraene[15] and decapentaene[19]–is shown to be reliable, yielding results in good accuracy with respect to gas-phase data. The accepted extrapolated experimental value is 3.10 eV. The adiabatic excitation energy calculated at the MR-CISD+P level is 3.122 eV, in excellent agreement with the experimental data. CASPT2 also performs well, underestimating this value by just above 0.1 eV (Table 6.2).

In summary, the MR-CISD+P adiabatic excitation energies (Table 6.2) agree closely with experimental and other theoretical benchmarks. Better agreement with experimental results is observed for the $2^1A_g^- \leftarrow 1^1A_g^-$ transition than for the $1^1B_u^+ \leftarrow 1^1A_g^-$ transition. This stems from the high demands placed by the ionic state in terms of σ-π electron correlation and high-order excitations needed to accurately describe the $1^1B_u^+$ state.[22,23]3 Performing single-point calculations using the triple-zeta basis set cc-pVTZ' on the relaxed geometries obtained with the double-zeta basis set—except for hexatriene, where slightly better agreement with experiment is observed at the CBS limit—has no significant impact on adiabatic excitation energies (Table C.1).

6.2.2 Vertical excitation and emission energies

In this section, we present and discuss the vertical excitations to the bright state, as well as the vertical emission energies from the two lowest singlet excited states of the

polyenes, estimating the fluorescence intensity maximum based on a vertical transition from the excited-state minimum to the ground state. Vertical excitation energies are obtained by calculating the energies of the excited states at the equilibrium geometry of the ground state. These values are generally compared to the absorption band maximum ($\lambda_{\mathrm{abs}}^{\mathrm{max}}$) under the assumption of classical vibrations.[24] Note that, for theses systems, the $\lambda_{\mathrm{abs}}^{\mathrm{max}}$ also corresponds to the 0-0 excitation band. Vertical excitation energies to the two lowest singlet excited states are presented in Table S3. For a more detailed discussion of vertical excitation energies, see Reference (22). Conversely, vertical emission energies can be estimated by calculating the ground-state energy at the minimum of the excited state. An experimental estimate of the vertical emission energy is the wavelength corresponding to the maximum of the emission spectrum ($\lambda_{\mathrm{emi}}^{\mathrm{max}}$). In Table 6.3, we present the absorption, and the emission energies obtained at the MR-CISD+P level.

TABLE 6.3 – Absorption (ΔE_{abs}) and emission (ΔE_{emi}) energies (eV) for polyenes with N π-electrons computed at the MR-CISD+P level based on geometries obtained via analytic energy gradients using the MR-CISD wavefunction. Experimental values for the band maxima of absorption ($\lambda_{\mathrm{abs}}^{\mathrm{max}}$) and emission ($\lambda_{\mathrm{emi}}^{\mathrm{max}}$) spectra are provided for comparison.

N	MR-CISD+P			Exp.	
	ΔE_{abs} [a]	ΔE_{emi}		$\lambda_{\mathrm{abs}}^{\mathrm{max}}$	$\lambda_{\mathrm{emi}}^{\mathrm{max}}$
	$1^1B_u^+ \leftarrow 1^1A_g^-$	$1^1A_g^- \leftarrow 2^1A_g^-$	$1^1A_g^- \leftarrow 1^1B_u^+$	$1^1B_u^+ \leftarrow 1^1A_g^-$	$1^1A_g^- \leftarrow 2^1A_g^-$
6	5.442	3.630	5.140	4.93[b]	–
8	4.825	2.963	4.522	4.40[c]	3.1[d]
10	4.364	2.500	4.072	4.02[e]	2.7[f]

[a] Values computed at the basis set limit. See Table C.2.

[b] Origin of absorption for the isolated compound.[13]

[c] Origin of absorption for the isolated compound.[15,19]

[d] Vibronic patterns assumed similar in gas and condensed phases.[19]

[e] Origin of absorption for the isolated compound.[19]

[f] Vibronic patterns assumed similar in gas and condensed phases.[19]

For vertical excitation, we compare our results with the experimental estimates using values extrapolated to the basis set limit ($\Delta E_{\mathrm{DT}}^{\infty}$), as the basis set can significantly influence the $1^1B_u^+ \leftarrow 1^1A_g^-$ vertical excitation energy due to the sensitive nature of the $1^1B_u^+$ state with respect to electron correlation and orbital relaxation effects.[22,23] The results obtained for each basis set are presented in Table C.2. For the studied compounds, the MR-CISD+P results extrapolated to the basis set limit predict vertical excitation energies higher than the absorption band maxima: they exceed the experimental estimates by 0.51 eV in hexatriene, 0.43 eV in octatetraene, and 0.34 eV in decapentaene. The larger deviation observed for the smaller systems is attributed to the more significant role of extensive dynamic *sigma*-π electron correlation and the higher-order excitations

required to properly describe the exchange interaction arising from the HOMO→LUMO excitation in systems with fewer electrons.[25] Previous studies have shown that vertical excitation energies from the ground-state minimum are typically blue-shifted relative to the absorption band maximum by approximately 0.2 eV,[24,26] and, as will be discussed in the next section, this trend is consistent with our findings. Taking this into account, the MR-CISD+P values show good agreement with the experimental estimates. Similar CASPT2 results (Table C.2) were obtained by Nakayama and co-workers[10] and by Angeli et al.[11,9]

Regarding vertical emission energies, it is known that octatetraene is the smallest unsubstituted polyene with detectable fluorescence. The trans isomer of hexatriene exhibits no detectable fluorescence. For octatetraene, the photophysical behavior differs between condensed-phase and gas-phase environments. In the condensed phase, upon excitation into the bright $1^1B_u^+$ state, the system undergoes rapid internal conversion to the $2^1A_g^-$ state, occurring on sub-picosecond timescales. This indicates the presence of a conical intersection near the Franck–Condon region, which provides an efficient pathway for population of the $2^1A_g^-$ state.[16] From there, the system decays radiatively to the ground state.[19] In contrast, in the gas phase, no Stokes shift is observed between absorption and emission, which supports a $1^1A_g^- \leftarrow 1^1B_u^+$ assignment for the fluorescence.[15,27]

For the $1^1A_g^- \leftarrow 2^1A_g^-$vertical emission, in both cases where experimental data are available, the MR-CISD+P results indicate that the vertical emission energy is 0.14 eV and 0.20 eV lower than the emission band maximum for octatetraene and decapentaene, respectively. These results suggest that the vertical emission is red-shifted relative to the maximum of the emission spectrum. For hexatriene, which shows no detectable fluorescence, the MR-CISD+P results predict a vertical emission energy of 3.63 eV for the $1^1A_g^- \leftarrow 2^1A_g^-$ transition, corresponding to approximately 342 nm. Considering the $1^1A_g^- \leftarrow 1^1B_u^+$ vertical emission energies (Table 6.3), the difference between absorption and emission is approximately 0.30 eV for all studied compounds. This small difference is consistent with experimental findings in the gas phase, where little to no Stokes shift is observed.

6.2.3 Relaxation energies and equilibrium geometries

Having analyzed both adiabatic (Table 6.2) and vertical excitation energies (Tables 6.3, C.2), the first striking observation when comparing these values is the notable stabilization experienced by the covalent state relative to the ground-state minimum. Figure 6.1 illustrates the stabilization energy for each state. For the purpose of discussing relaxation energy, we consider our calculations employing the cc-pVDZ basis set for vertical excitations (Table C.2) alongside the adiabatic excitation energies obtained using the same

basis set (Table 6.2).

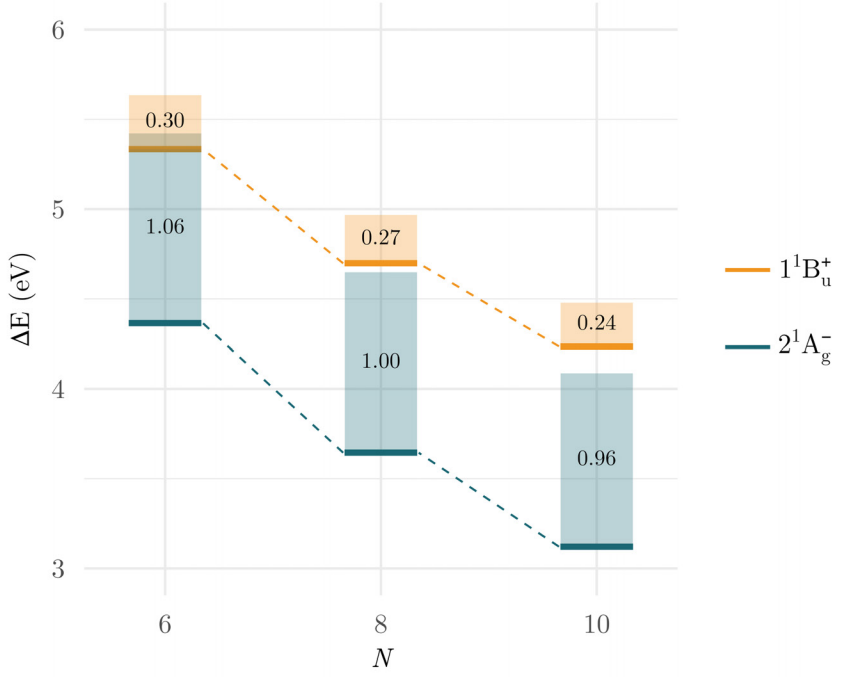

FIGURE 6.1 – Relaxation energy (eV) in polyenes with N π-electrons computed at the MR-CISD+P level using the cc-pVDZ basis set. Relaxation energy–represented by the bar size and numeric values–is defined as the energy difference between vertical excitation energies (top of the bar; numerical data from Table 6.2) and adiabatic excitation energies (bottom of the bar; numerical data from Table 6.2).

The relaxation energy observed for the covalent $2^1A_g^-$ state ranges from 1.06 eV for hexatriene to 0.96 eV for decapentaene (Figure 6.1). This substantial relaxation energy highlights a significant difference in the nuclear equilibrium geometries of the states involved. Indeed, upon closer inspection of their optimized structures, we find that the geometry of the $2^1A_g^-$ state exhibits an alternating single-double bond pattern opposite to that observed in the ground state (Figure 6.2, Table C.3). Specifically, whereas the ground state features a C-C double bond in the terminal pair of carbon atoms (Figure Figure 6.2a), the $2^1A_g^-$ state displays a characteristic C-C single bond at the same position (Figure Figure 6.2b).

In contrast, the ionic $1^1B_u^+$ state is only slightly stabilized at its minimum relative to its energy at the Franck-Condon geometry. The relaxation energy for this state ranges from 0.30 eV for hexatriene to 0.24 eV for decapentaene (Figure 6.1). Unlike the covalent state, which shows a distinct single-double bond alternation, the ionic state exhibits a more uniform bond-length distribution (Figure 6.2c, Table C.3). Notably, the geometries obtained at the CASSCF level by Nakayama et al.[10] are in good agreement with those obtained via analytical gradients based on the MR-CISD wavefunction (Table C.3). This agreement holds across all three states and all studied polyenes, with no differences larger

than 0.051 Åobserved for CC bond lengths between the respective geometries obtained at both levels.

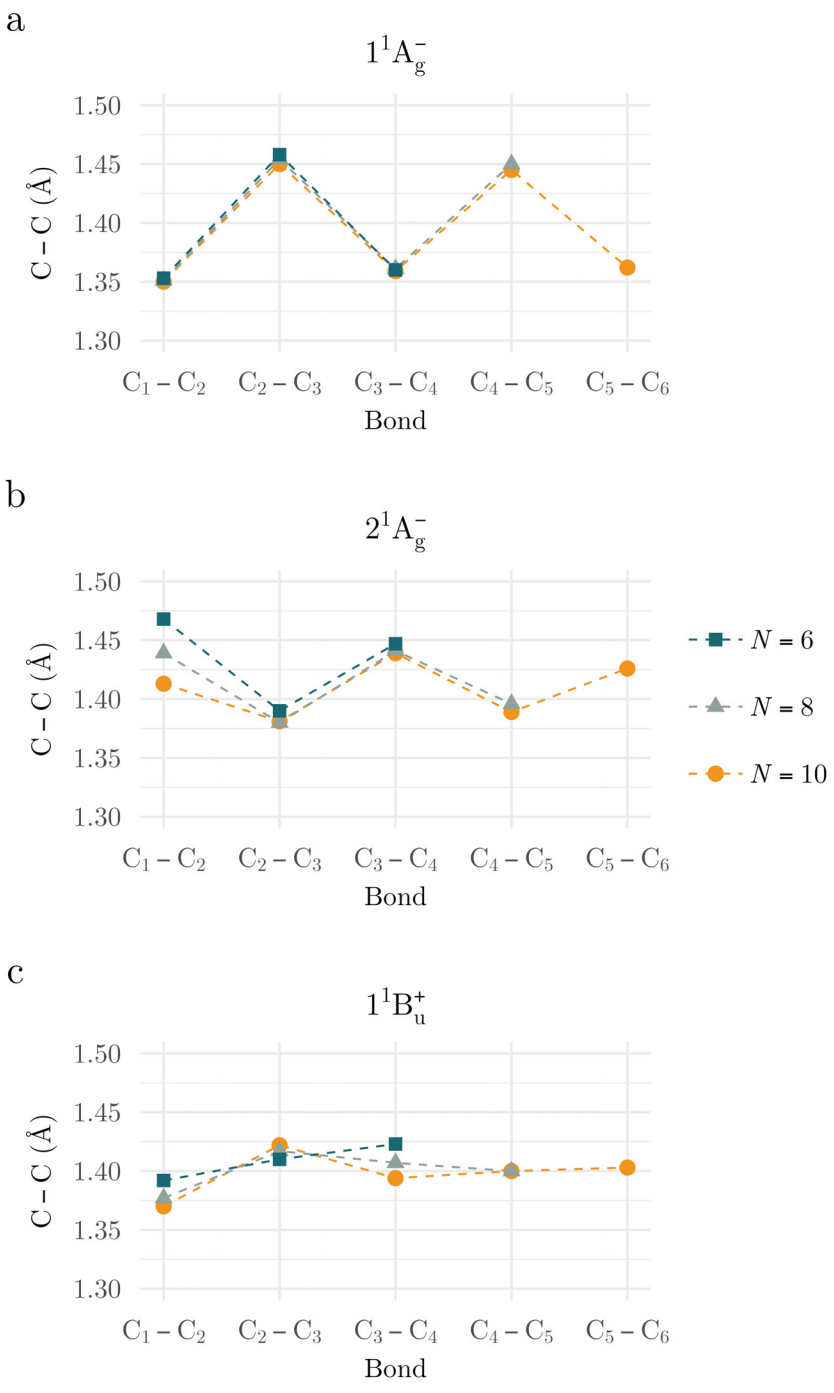

FIGURE 6.2 – CC bond lengths of the optimized geometries obtained via analytic energy gradients based on the MR-CISD wavefunction for the states: (a) $1^1A_g^-$, (b) $2^1A_g^-$, and (c) $1^1B_u^+$ of polyenes with N π-electrons. Numeral data from Table C.1.

The results obtained here show that excitation into the bright state is followed by a structural relaxation of approximately 0.2-0.3 eV (Figure 6.1). Experimentally, the ab-

sorption band maximum is known to correspond to the 0–0 transition.[14,15,19] Although vertical excitation energies are often compared directly with this band maximum, such comparisons implicitly assume that vibrational effects are negligible or treated classically. The observed relaxation implies that vertical excitation energies from the ground-state equilibrium geometry are systematically blue-shifted by 0.2-0.3 eV relative to the absorption band maximum. This shift is consistent with previous high-level theoretical studies.[24,26]

Bibliography

1 POPLE, J. A.; SEEGER, R.; KRISHNAN, R. Variational configuration interaction methods and comparison with perturbation theory. **International Journal of Quantum Chemistry**, v. 12, S11, p. 149–163, June 2009.

2 BUNGE, Annik. Electronic Wavefunctions for Atoms. III. Partition of Degenerate Spaces and Ground State of C. **The Journal of Chemical Physics**, v. 53, n. 1, p. 20–28, July 1970.

3 DUNNING, Thom H. Gaussian basis sets for use in correlated molecular calculations. I. The atoms boron through neon and hydrogen. **The Journal of Chemical Physics**, v. 90, n. 2, p. 1007–1023, Jan. 1989.

4 HALKIER, Asger et al. Basis-set convergence in correlated calculations on Ne, N2, and H2O. **Chemical Physics Letters**, v. 286, n. 3-4, p. 243–252, Apr. 1998.

5 LISCHKA, Hans et al. Columbus—a program system for advanced multireference theory calculations. **WIREs Computational Molecular Science**, John Wiley & Sons, v. 1, n. 2, p. 191–199, Mar. 2011.

6 LISCHKA, Hans et al. High-level multireference methods in the quantum-chemistry program system COLUMBUS: Analytic MR-CISD and MR-AQCC gradients and MR-AQCC-LRT for excited states, GUGA spin–orbit CI and parallel CI density. **Physical Chemistry Chemical Physics**, v. 3, n. 5, p. 664–673, 2001.

7 LISCHKA, Hans et al. The generality of the GUGA MRCI approach in COLUMBUS for treating complex quantum chemistry. **The Journal of Chemical Physics**, AIP Publishing, LLC, v. 152, n. 13, p. 134110, Apr. 2020.

8 HELGAKER, T et al. **DALTON, an ab initio electronic structure program, Release 1.0**. [S.l.: s.n.], 1997.

9 GUARESCHI, Riccardo; ANGELI, Celestino. The lowest singlet states of hexatriene revisited. **Theoretical Chemistry Accounts**, Springer Science and Business Media Deutschland GmbH, v. 142, n. 12, p. 127, Dec. 2023.

10 NAKAYAMA, Kenichi; NAKANO, Haruyuki; HIRAO, Kimihiko. Theoretical study of the $\pi\pi^*$ excited states of linear polyenes: The energy gap between 11Bu+ and 21Ag states and their character. **International Journal of Quantum Chemistry**, John Wiley & Sons, Inc, v. 66, n. 2, p. 157–175, 1998.

11 ANGELI, Celestino; PASTORE, Mariachiara. The lowest singlet states of octatetraene revisited. **The Journal of Chemical Physics**, v. 134, n. 18, May 2011.

12 BUMA, Wybren Jan; KOHLER, Bryan E.; SONG, Kyuseok. Location of the 21 A g state in hexatriene. **The Journal of Chemical Physics**, v. 92, n. 7, p. 4622–4623, Apr. 1990.

13 GAVIN, R. M.; RISEMBERG, Salomon; RICE, Stuart A. Spectroscopic properties of polyenes. I. The lowest energy allowed singlet-singlet transition for cis- and trans-1,3,5-hexatriene. **The Journal of Chemical Physics**, v. 58, n. 8, p. 3160–3165, Apr. 1973.

14 LEOPOLD, D. G. et al. Direct absorption spectroscopy of jet-cooled polyenes. II. The $1^1B_u^+ \leftarrow 1^1A_g^-$ transitions of butadienes and hexatrienes. **The Journal of Chemical Physics**, v. 81, n. 10, p. 4218–4229, Nov. 1984.

15 GAVIN, R. M. et al. Spectroscopic properties of polyenes. III. 1,3,5,7-Octatetraene. **The Journal of Chemical Physics**, v. 68, n. 2, p. 522–529, Jan. 1978.

16 PETEK, Hrvoje et al. The 2^1A_g state of trans,trans-1,3,5,7-octatetraene in free jet expansions. **The Journal of Chemical Physics**, v. 98, n. 5, p. 3777–3794, Mar. 1993.

17 LEOPOLD, D. G.; VAIDA, V.; GRANVILLE, Mark F. Direct absorption spectroscopy of jet-cooled polyenes. I. The $1^1B_u^+ \leftarrow 1^1A_g^-$ transition of trans,trans-1,3,5,7-octatetraene. **The Journal of Chemical Physics**, v. 81, n. 10, p. 4210–4217, Nov. 1984.

18 HEIMBROOK, Lou Ann et al. Free-jet fluorescence excitation spectrum of trans,trans-1,3,5,7-octatetraene. **The Journal of Chemical Physics**, v. 75, n. 9, p. 4338–4342, Nov. 1981.

19 D'AMICO, Kevin L.; MANOS, Christopher; CHRISTENSEN, Ronald L. Electronic energy levels in a homologous series of unsubstituted linear polyenes. **Journal of the American Chemical Society**, v. 102, n. 6, p. 1777–1782, Mar. 1980.

20 MARIAN, Christel M.; GILKA, Natalie. Performance of the Density Functional Theory/Multireference Configuration Interaction Method on Electronic Excitation of Extended π-Systems. **Journal of Chemical Theory and Computation**, v. 4, n. 9, p. 1501–1515, Sept. 2008.

21 BUMA, Wybren Jan; KOHLER, Bryan E.; SONG, Kyuseok. Lowest energy excited singlet state of isolated *cis*-hexatriene. **The Journal of Chemical Physics**, v. 94, n. 10, p. 6367–6376, May 1991.

22 CHAGAS, Julio C. V. et al. Low-lying excited states of linear all-trans polyenes: the σ–π electron correlation and the description of ionic states. **Physical Chemistry Chemical Physics**, v. 27, n. 15, p. 7916–7928, 2025.

23 ANGELI, Celestino. On the nature of the $\pi \rightarrow \pi^*$ ionic excited states: The V state of ethene as a prototype. **Journal of Computational Chemistry**, v. 30, n. 8, p. 1319–1333, June 2009.

24 DAVIDSON, Ernest R.; JARZECKI, Andrzej A. Zero point corrections to vertical excitation energies. **Chemical Physics Letters**, v. 285, n. 3-4, p. 155–159, Mar. 1998.

25 ZENG, Weixuan et al. Understanding and Tuning Singlet–Triplet (S 1 –T 1) Energy Gaps in Planar Organic Chromophores. **Angewandte Chemie International Edition**, Apr. 2025.

26 BARBATTI, Mario; AQUINO, Adelia J. A.; LISCHKA, Hans. The UV absorption of nucleobases: semi-classical ab initio spectra simulations. **Physical Chemistry Chemical Physics**, v. 12, n. 19, p. 4959, 2010.

27 HEIMBROOK, Lou Ann; KOHLER, Bryan E.; LEVY, Irvin J. Fluorescence from the 1^1B_u state of trans,trans-1,3,5,7-octatetraene in a free jet. **The Journal of Chemical Physics**, v. 81, n. 4, p. 1592–1597, Aug. 1984.

7 Concluding Remarks

In Chapter 4, a detailed multi-component analysis of aromaticity in mono- and disubstituted benzene derivatives strongly affected by the substituent effects. We demonstrate that π-electron-donating and π-electron-accepting substituents of suitable size and symmetry can interact with the π-system of the ring and substantially impact π-electron delocalization. We also investigated the influence of charged non-π-electron donor/acceptor substituents. Our findings indicate that the charges play a minor role in influencing π-electron delocalization. The crucial factor that influences the aromatic character is the availability of a p_z orbital capable of interacting with the delocalized π-electron system of benzene.

Due to the various aspects of aromaticity, a single descriptor is not flexible enough to provide a comprehensive overview of π-electron delocalization unambiguously. In this sense, the multiple indices presented offer complementary information on the electronic structure and reactivity of the substituted benzene compounds. The perturbation caused by π-electron-donating and π-electron-accepting substituents impacts the geometry, vibrational properties, π-topology, electronic structure, magnetic susceptibility, and chemical stability of the system. The findings of this study can contribute to applied research aimed at modulating the electronic structure of organic compounds, such as polycyclic aromatic compounds, to achieve desired properties.

In Chapter 5, we show that the relative position of the ionic $1^1B_u^+$ excited state in polyenes is strongly influenced by the level of theory employed due to the more sensitive nature of this state with respect to electron correlation and orbital relaxation effects. Thus, a proper description of ionic states requires a combination of factors at the variational MR-CISD and MR-AQCC levels. Polarization through enhanced σ-π electron correlation significantly stabilizes the ionic state, whereas covalent states are already well described with an adequate treatment of non-dynamic correlation involving valence π-orbitals. Expanding the basis set to include larger polarization shells further stabilizes the ionic state but has minimal effect on covalent states. Additionally, size-extensivity corrections play a crucial role in stabilizing the ionic state. Therefore, an accurate description of the ionic state requires extensive treatment of σ-π electron correlation, a sufficiently large basis set, and the inclusion of size-extensivity corrections.

Based on these considerations, MR-CISD+P and MR-AQCC provide mutually consistent predictions that the $1^1B_u^+$ state is the first excited state in hexatriene and octatetraene. These findings align with theoretical reference benchmark values. For decapentaene, extrapolated MR-CISD+P results suggest that the $2^1A_g^-$ and $1^1B_u^+$ states are nearly degenerate, while MR-AQCC indicates that the ionic state lies approximately 0.2 eV below the covalent state. For dodecahexaene, the high computational cost associated with using an appropriate basis set precluded an accurate assignment of the ordering of the two low-lying states. However, our findings using the cc-pVDZ basis set suggest that the covalent $2^1A_g^-$ state is the lowest excited state, lying 0.2 eV below the ionic state at the MR-CISD+P level, while MR-AQCC results suggest that these states are virtually degenerate. The triplet states $1^3A_g^-$ and $1^3B_u^-$ are already well-described at the CASSCF level and can be reliably calculated using MR-CISD, MR-AQCC, or CASPT2.

Wavefunction analysis further revealed how the character of the wavefunctions evolves across the series in terms of ionic character, multiconfigurational character, and single-excitation character. The ionic state remains consistently well-represented by a single HOMO-LUMO excitation, whereas the contribution of doubly excited configurations increases with chain length for both covalent states. Notably, the $2^1B_u^-$ state exhibits an increasingly multiconfigurational character as the chain lengthens.

In Chapter 6, an accurate and balanced description of the ground and two lowest-lying excited states ($2^1A_g^-$ and $1^1B_u^+$) in hexatriene, octatetraene, and decapentaene is achieved at the multireference level, providing valuable insights into the spectroscopic behavior of polyenes and bridging theoretical predictions with experimental spectroscopy. The adiabatic excitation energy for the $2^1A_g^-$ state is estimated with excellent accuracy (within 0.1-0.02 eV) relative to the experimental values, where available. Slightly larger, though still reasonable, deviations (0.2-0.4 eV) are observed for the ionic $1^1B_u^+$ state, reflecting the complexity of describing this state at the multireference level due to the intricate interplay of σ-π electron correlation and high-order excitations. Nonetheless, the high accuracy achieved for adiabatic excitation energies highlights the robustness of the MR-CISD wavefunction in providing reliable energy gradients.

Our findings suggest that vertical excitation energies from the ground state to the $1^1B_u^+$ state are blue-shifted by 0.2–0.3 eV relative to the absorption spectrum's band maximum. Vertical emission energies corresponding to radiative decay to the ground state were also computed. These results indicate that vertical emission from the $2^1A_g^-$ state is red-shifted by approximately 0.2 eV relative to the experimental emission maximum, while the small or absent Stokes shift observed experimentally in the gas phase is consistent with a $1^1A_g^- \leftarrow 1^1B_u^+$ radiative decay.

Our results for the studied systems show that, upon geometry relaxation from the Franck-Condon structure, the $2^1A_g^-$ state is stabilized by approximately 1 eV, whereas

the bright $1^1B_u^+$ state is stabilized by 0.2-0.3 eV. This difference in relaxation energy is closely related to the distinct nuclear equilibrium geometries of the states involved. While the $2^1A_g^-$ state exhibits an alternating single-double bond pattern opposite to that of the ground state, the $1^1B_u^+$ state features a more equalized bond-length distribution along the polyene chain.

Taken together, the studies presented in this thesis offer a comprehensive view of the electronic structure of conjugated organic molecules, ranging from the modulation of aromaticity in the benzenoid ring to the complex excited-state behavior of linear polyenes. By critically employing state-of-the-art multireference methods, we have gained detailed insight into both ground- and excited-state properties across these systems, highlighting the importance of orbital interaction, electron correlation, and state-specific geometry effects. These findings not only enhance our understanding of electronic features such as aromaticity but also elucidate dynamic phenomena such as excited-state ordering and radiative decay pathways. In this way, the thesis fulfills its aim of exploring the *Electronic Structure of Conjugated Organic Molecules: From Aromaticity to Excited-State Dynamics*, bridging fundamental electronic structure theory with spectroscopic observables and contributing to the broader understanding of conjugated systems in theoretical chemistry.

Appendix A - Supplementary Information for Chapter 4

A.1 Reference Molecules - HOMA and AI(vib) descriptors

Equilibrium geometry, analytical harmonic frequencies, and local mode force constants of the reference molecules used in the determination of relative bond strength order, n_{opt}, γ (AI(vib)), r_{opt}, and α (HOMA).

B3LYP/def2-TZVP

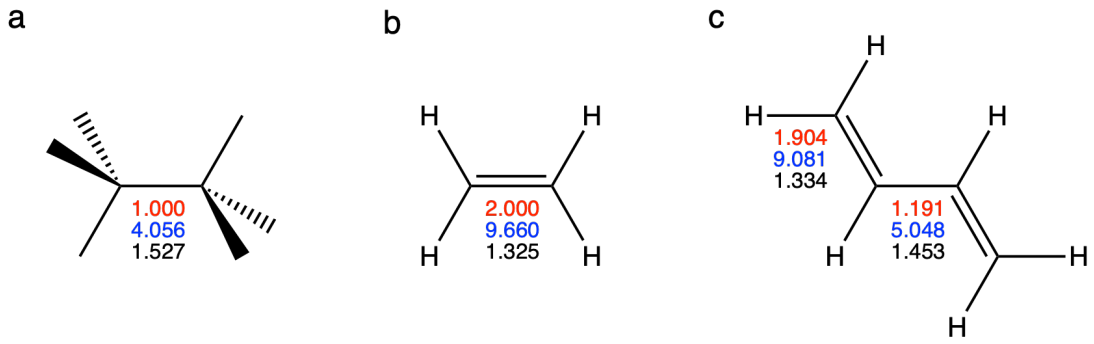

FIGURE A.1 – Reference molecules (a) ethane and (b) ethene were employed to establish the relative bond strength order. Buta-1,3-diene (c) was utilized for determining n_{opt} and γ values in AI(vib) calculations, as well as r_{opt} and α values in HOMA calculations. Red numbers represent the relative bond strength order, blue numbers denote local mode force constants (mdyn Å^{-1}), and black numbers indicate interatomic distances (Å). All values were obtained at the B3LYP/def2-TZVP level of theory.

Equilibrium geometries

C_2H_6 (S_0, D_{3d})			
Atom	x	y	z
C	0.000000	0.000000	0.763372
C	0.000000	0.000000	-0.763372
H	0.000000	1.017065	1.160943
H	-0.880804	-0.508532	1.160943
H	0.880804	-0.508532	1.160943
H	0.880804	0.508532	-1.160943
H	0.000000	-1.017065	-1.160943
H	-0.880804	0.508532	-1.160943

C_2H_4 (S_0, D_{2h})			
Atom	x	y	z
C	0.000000	0.000000	0.662376
C	0.000000	0.000000	-0.662376
H	0.000000	0.921381	1.232419
H	0.000000	-0.921381	1.232419
H	0.000000	-0.921381	-1.232419
H	0.000000	0.921381	-1.232419

C_4H_6 (S_0, C_{2h})			
Atom	x	y	z
C	0.599706	1.744284	0.000000
C	0.599706	0.409847	0.000000
C	-0.599706	-0.409847	0.000000
C	-0.599706	-1.744284	0.000000
H	1.520252	2.312490	0.000000
H	-0.325310	2.309580	0.000000
H	1.547033	-0.122846	0.000000
H	-1.547033	0.122846	0.000000
H	0.325310	-2.309580	0.000000
H	-1.520252	-2.312490	0.000000

Analytical harmonic frequencies

C_2H_6 (S_0, D_{3d})		
306.7265	827.9056	827.9056
998.0252	1223.0953	1223.0955
1412.4088	1423.1222	1502.2944
1502.2945	1505.7710	1505.7713
3029.7967	3030.8738	3073.8742
3073.8742	3099.2559	3099.2560

C_2H_4 (S_0, D_{2h})		
837.2152	978.7098	983.2476
1062.9807	1246.4293	1382.9622
1479.2742	1692.5248	3130.1379
3143.1520	3199.1444	3227.3639

C_4H_6 (S_0, C_{2h})		
174.7359	298.3523	519.4948
540.0030	782.5650	901.9208
942.9602	943.2290	1001.7873
1008.1646	1055.5497	1230.6022
1319.1759	1325.1317	1420.5846
1479.7137	1653.7660	1704.6984
3127.8470	3138.5175	3140.9526
3141.0108	3224.9418	3225.3140

ωB97X-D/def2-TZVPD

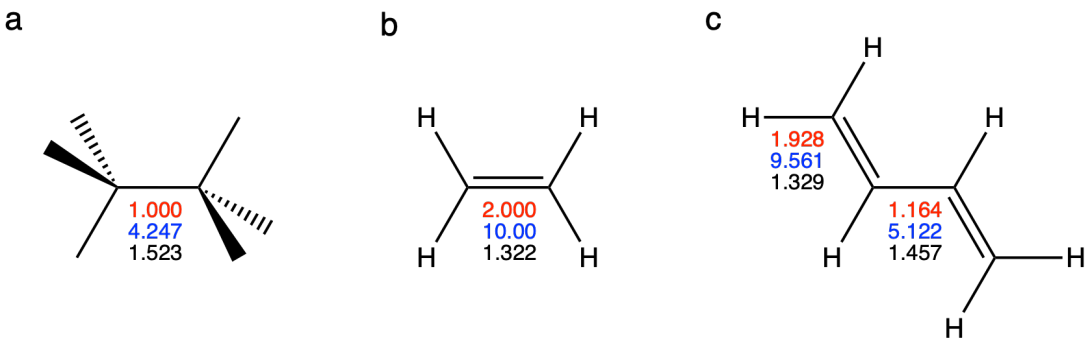

FIGURE A.2 – Reference molecules (a) ethane and (b) ethene were employed to establish the relative bond strength order. Buta-1,3-diene (c) was utilized for determining n_{opt} and γ values in AI(vib) calculations, as well as r_{opt} and α values in HOMA calculations. Red numbers represent the relative bond strength order, blue numbers denote local mode force constants (mdyn Å^{-1}), and black numbers indicate interatomic distances (Å). All values were obtained at the ωB97X-D/def2-TZVPD level of theory.

Equilibrium geometries

C_2H_6 (S_0, D_{3d})			
Atom	x	y	z
C	0.00000000	0.00000000	0.76138861
C	0.00000000	0.00000000	-0.76138861
H	0.00000000	1.01703852	1.15745108
H	-0.88078120	-0.50851926	1.15745108
H	0.88078120	-0.50851926	1.15745108
H	0.88078120	0.50851926	-1.15745108
H	0.00000000	-1.01703852	-1.15745108
H	-0.88078120	0.50851926	-1.15745108

C_2H_4 (S_0, D_{2h})			
Atom	x	y	z
C	0.00000000	0.00000000	0.66092924
C	0.00000000	0.00000000	-0.66092924
H	0.00000000	0.92270534	1.22919880
H	0.00000000	-0.92270534	1.22919880
H	0.00000000	-0.92270534	-1.22919880
H	0.00000000	0.92270534	-1.22919880

C_4H_6 (S_0, C_{2h})			
Atom	x	y	z
C	0.60379698	1.73649241	0.00000000
C	0.60379698	0.40747954	0.00000000
C	-0.60379698	-0.40747954	0.00000000
C	-0.60379698	-1.73649241	0.00000000
H	1.52548876	2.30352042	0.00000000
H	-0.32300215	2.29974212	0.00000000
H	1.54876697	-0.12909026	0.00000000
H	-1.54876697	0.12909026	0.00000000
H	0.32300215	-2.29974212	0.00000000
H	-1.52548876	-2.30352042	0.00000000

Analytical harmonic frequencies

C_2H_6 (S_0, D_{3d})		
310.2848	833.8049	833.8193
1017.7210	1226.0732	1226.0806
1412.1971	1432.9030	1507.6199
1507.6214	1508.0296	1508.0312
3053.0851	3054.1185	3111.4476
3111.4549	3135.3404	3135.3455

C_2H_4 (S_0, D_{2h})		
841.5026	987.7744	1000.3653
1071.1467	1247.7254	1390.3166
1476.1581	1714.2330	3148.5381
3166.5817	3227.1925	3253.7526

C_4H_6 (S_0, C_{2h})		
164.7367	302.7216	525.2373
542.3878	790.9244	906.0479
960.9435	962.4648	1011.8799
1018.3208	1065.5867	1235.8851
1326.5167	1329.4543	1425.0963
1480.7523	1682.1240	1746.0978
3153.7316	3156.8739	3164.5906
3169.8008	3249.5926	3249.7766

A.2 Numerical Values of Descriptors

B3LYP/def2-TZVP

Tables A.1 to A.14 present the numerical data for the descriptors HOMA, AI(vib), BVI, I_{ring}, MCI, NICS, and S_0-T_1 splitting. The results are based on the geometries and analytical harmonic frequencies obtained at the B3LYP/def2-TZVP level of theory.

TABLE A.1 – HOMA, EN, and GEO of benzene and monosubstituted benzene derivatives.

X	HOMA	EN	GEO
H	0.998	0.002	0.000
CH_3	0.997	0.001	0.002
CH_2^-	0.702	0.075	0.223
CH_2^+	0.743	0.031	0.226
NH_2	0.992	0.000	0.008
NH_2^-	0.724	0.071	0.206
NH_2^+	0.448	0.093	0.459
OH	0.997	0.002	0.001
O^-	0.736	0.072	0.192
O^+	-0.100	0.234	0.865

TABLE A.2 – HOMA, EN, and GEO of disubstituted benzene derivatives.

X	HOMA	EN	GEO
CH_3	0.997	0.000	0.003
CH_2	0.006	0.180	0.814
NH_2	0.995	0.000	0.005
NH	-0.309	0.269	1.041
OH	0.997	0.003	0.001
O	-0.808	0.454	1.353

TABLE A.3 – AI(vib), WS, and ALT of benzene and monosubstituted benzene derivatives.

X	AI(vib)	WS	ALT
H	0.925	0.075	0.000
CH_3	0.907	0.090	0.003
CH_2^-	0.587	0.266	0.148
CH_2^+	0.709	0.134	0.157
NH_2	0.895	0.098	0.007
NH_2^-	0.593	0.265	0.142
NH_2^+	0.437	0.210	0.353
OH	0.917	0.081	0.002
O^-	0.537	0.305	0.157
O^+	-0.076	0.377	0.699

TABLE A.4 – AI(vib), WS, and ALT of disubstituted benzene derivatives.

X	AI(vib)	WS	ALT
CH_3	0.890	0.107	0.003
CH_2	0.085	0.180	0.735
NH_2	0.871	0.125	0.004
NH	-0.200	0.242	0.958
OH	0.910	0.089	0.001
O	-0.684	0.408	1.277

TABLE A.5 – Topological analysis of ELF_π of benzene and monosubstituted benzene derivatives. B3LYP/def2-TZVP level of theory.

X	BV_{max}	BV_{min}	ΔBV	BVI
H	0.894	0.894	0.000	1.000
CH_3	0.893	0.875	0.018	0.982
CH_2^-	0.922	0.568	0.354	0.646
CH_2^+	0.979	0.604	0.375	0.625
NH_2	0.909	0.778	0.131	0.869
NH_2^-	0.924	0.599	0.325	0.675
NH_2^+	0.992	0.440	0.552	0.448
OH	0.894	0.849	0.045	0.955
O^-	0.907	0.660	0.247	0.753
O^+	0.998	0.276	0.722	0.278

TABLE A.6 – Topological analysis of ELF_π of benzene and monosubstituted benzene derivatives. MRCI/def2-TZVP//B3LYP/def2-TZVP level of theory. Natural orbitals were used to construct the π-density.

X	BV_{max}	BV_{min}	ΔBV	BVI
H	0.840	0.837	0.003	0.997
CH_3	0.837	0.818	0.019	0.981
CH_2^-	0.896	0.505	0.391	0.609
CH_2^+	0.954	0.538	0.416	0.584
NH_2	0.835	0.685	0.150	0.850
NH_2^-	0.893	0.518	0.375	0.625
NH_2^+	0.972	0.360	0.612	0.388
OH	0.838	0.791	0.047	0.953
O^-	0.876	0.609	0.267	0.733
O^+	0.982	0.230	0.752	0.248

TABLE A.7 – Topological analysis of ELF_π of disubstituted benzene derivatives. B3LYP/def2-TZVP level of theory.

X	BV_{max}	BV_{min}	ΔBV	BVI
CH_3	0.895	0.871	0.024	0.976
CH_2	0.994	0.412	0.582	0.418
NH_2	0.897	0.748	0.149	0.851
NH	0.998	0.357	0.641	0.359
OH	0.869	0.850	0.019	0.981
O	0.999	0.313	0.686	0.314

TABLE A.8 – Topological analysis of ELF_π of disubstituted benzene derivatives. MRCI/def2-TZVP//B3LYP/def2-TZVP level of theory. Natural orbitals were used to construct the π-density.

X	BV_{max}	BV_{min}	ΔBV	BVI
CH_3	0.835	0.801	0.034	0.966
CH_2	0.976	0.323	0.653	0.347
NH_2	0.789	0.749	0.040	0.960
NH	0.982	0.262	0.720	0.280
OH	0.811	0.803	0.008	0.992
O	0.987	0.229	0.758	0.242

TABLE A.9 – Multicenter descriptors I_{ring} and MCI of benzene ans monosubstituted benzene derivatives. The results were obtained at the B3LYP/def2-TZVP level of theory using the AIM atomic partitioning.

X	I_{ring}	MCI
H	0.0479	0.0717
CH_3	0.0455	0.0679
CH_2^-	0.0230	0.0306
CH_2^+	0.0225	0.0262
NH_2	0.0404	0.0596
NH_2^-	0.0246	0.0336
NH_2^+	0.0132	0.0103
OH	0.0419	0.0622
O^-	0.0272	0.0379
O^+	0.0070	0.0001

TABLE A.10 – Multicenter descriptors I_{ring} and MCI of disubstituted benzene derivatives. The results were obtained at the B3LYP/def2-TZVP level of theory using the AIM atomic partitioning.

X	I_{ring}	MCI
CH_3	0.0434	0.0644
CH_2	0.0090	0.0100
NH_2	0.0362	0.0531
NH	0.0066	0.0069
OH	0.0377	0.0560
O	0.0049	0.0047

TABLE A.11 – NICS(0), NICS(1), and NICS(1)_{zz} of benzene and monosubstituted benzene derivatives. GIAO-B3LYP/pcS-3//B3LYP/def2-TZVP level of theory.

X	NICS(0)	NICS(1)	NICS(1)_{zz}
H	-7.90	-9.99	-30.00
CH_3	-7.84	-9.84	-28.87
CH_2^-	1.75	-0.74	-3.32
CH_2^+	-1.28	-5.80	-15.05
NH_2	-7.65	-8.68	-25.18
NH_2^-	-1.73	-3.59	-11.70
NH_2^+	4.67	-1.79	-4.27
OH	-8.81	-9.44	-27.21
O^-	-3.93	-5.65	-18.17
O^+	13.86	3.91	9.36

TABLE A.12 – NICS(0), NICS(1), and $NICS(1)_{zz}$ of disubstituted benzene derivatives. GIAO-B3LYP/pcS-3//B3LYP/def2-TZVP level of theory.

X	NICS(0)	NICS(1)	$NICS(1)_{zz}$
CH_3	-7.80	-9.55	-27.33
CH_2	2.62	-1.37	-1.36
NH_2	-8.12	-8.24	-22.64
NH	4.17	-0.89	-0.73
OH	-9.83	-9.11	-24.94
O	8.86	1.37	3.20

TABLE A.13 – S_0-T_1 splitting of benzene and monosubstituted benzene derivatives. Full valence π-electrons and π-orbitals were considered in the complete active space self-consistent field (CASSCF). MRCI wave functions, including all single and double excitations (MR-CISD), were constructed based on CSFs generated by CASSCF. Size-extensivity contributions were incorporated using the Davidson-Silver method (MRCI+Q). The def2-TZVP basis set was employed at both steps.

X	B3LYP	CASSCF	MRCI	MRCI+Q
H	4.484	3.926	4.140	4.235
CH_3	4.735	3.906	4.115	4.224
CH_2^-	2.289	2.534	2.521	2.512
CH_2^+	2.172	2.255	2.333	2.374
NH_2	4.014	4.712	4.531	4.402
NH_2^-	2.667	2.933	2.956	2.952
NH_2^+	1.619	1.948	1.989	2.022
OH	4.150	3.941	4.146	4.264
O^-	3.092	3.398	3.422	3.398
O^+	0.751	1.817	1.781	1.768

TABLE A.14 – S_0-T_1 splitting of disubstituted benzene derivatives. Full valence π-electrons and π-orbitals were considered in the complete active space self-consistent field (CASSCF). MRCI wave functions, including all single and double excitations (MR-CISD), were constructed based on CSFs generated by CASSCF. Size-extensivity contributions were incorporated using the Davidson-Silver method (MRCI+Q). The def2-TZVP basis set was employed at both steps.

X	B3LYP	CASSCF	MRCI	MRCI+Q
CH_3	4.511	3.876	4.303	4.287
CH_2	1.898	2.309	2.239	2.193
NH_2	3.332	4.264	4.010	3.835
NH	2.382	2.827	2.778	2.738
OH	3.678	3.918	4.062	4.132
O	2.150	3.413	3.365	3.311

ωB97X-D/def2-TZVPD

Tables A.15 to A.21 present the numerical data of the descriptors HOMA, AI(vib), and NICS. The results are based on the geometries and analytical harmonic frequencies obtained at the ωB97X-D/def2-TZVPD level of theory.

TABLE A.15 – HOMA, EN, and GEO of benzene and monosubstituted benzene derivatives.

X	HOMA	EN	GEO
H	0.992	0.008	0.000
CH_3	0.993	0.005	0.001
CH_2^-	0.766	0.042	0.191
CH_2^+	0.794	0.013	0.194
NH_2	0.991	0.004	0.005
NH_2^-	0.796	0.036	0.167
NH_2^+	0.520	0.060	0.420
OH	0.991	0.008	0.001
O^-	0.809	0.037	0.154
O^+	0.027	0.174	0.799

TABLE A.16 – HOMA, EN, and GEO of disubstituted benzene derivatives.

X	HOMA	EN	GEO
CH_3	0.992	0.004	0.004
CH_2	0.000	0.160	0.840
NH_2	0.994	0.003	0.003
NH	-0.256	0.232	1.024
OH	0.990	0.010	0.000
O	-0.663	0.383	1.280

TABLE A.17 – AI(vib), WS, and ALT of benzene and monosubstituted benzene derivatives.

X	AI(vib)	WS	ALT
H	0.914	0.086	0.000
CH_3	0.900	0.099	0.002
CH_2^-	0.621	0.259	0.120
CH_2^+	0.739	0.133	0.128
NH_2	0.889	0.107	0.005
NH_2^-	0.634	0.253	0.113
NH_2^+	0.485	0.203	0.312
OH	0.907	0.092	0.001
O^-	0.587	0.287	0.126
O^+	0.026	0.354	0.620

TABLE A.18 – AI(vib), WS, and ALT of disubstituted benzene derivatives.

X	AI(vib)	WS	ALT
CH_3	0.884	0.112	0.004
CH_2	0.069	0.157	0.775
NH_2	0.867	0.131	0.002
NH	-0.166	0.209	0.957
OH	0.898	0.101	0.001
O	-0.570	0.349	1.222

TABLE A.19 – NICS(0), NICS(1), and $NICS(1)_{zz}$ of benzene and monosubstituted benzene derivatives. GIAO-B3LYP/pcS-3//ωB97XD/def2-TZVPD level of theory.

X	NICS(0)	NICS(1)	$NICS(1)_{zz}$
H	-7.903	-10.005	-30.115
CH_3	-7.845	-9.855	-28.970
CH_2^-	1.818	-0.692	-3.260
CH_2^+	-1.287	-5.843	-15.209
NH_2	-7.641	-8.678	-25.259
NH_2^-	-1.681	-3.555	-11.702
NH_2^+	4.688	-1.821	-4.386
OH	-8.789	-9.427	-27.256
O^-	-3.897	-5.629	-18.192
O^+	13.726	3.788	9.098

TABLE A.20 – NICS(0), NICS(1), and $NICS(1)_{zz}$ of disubstituted benzene derivatives. GIAO-B3LYP/pcS-3//ωB97XD/def2-TZVPD level of theory.

X	NICS(0)	NICS(1)	$NICS(1)_{zz}$
CH_3	-7.766	-9.543	-27.361
CH_2	2.685	-1.293	-1.126
NH_2	-8.103	-8.234	-22.684
NH	4.217	-0.830	-0.597
OH	-9.807	-9.093	-24.965
O	8.827	1.357	3.193

Statistical data

TABLE A.21 – Coefficient of determination (R^2) for the relationship between aromaticity descriptors values obtained at both levels of theory (B3LYP/def2-TZVP and ωB97X-D/def2-TZVPD). The analysis includes benzene and all the derivatives studied in this work.

Descriptor	R^2
HOMA	0.9956
AI(vib)	0.9968
NICS(0)	1.0000
NICS(1)	0.9999
$NICS(1)_{zz}$	0.9999

A.3 Bonding Analysis

TABLE A.22 – Bond Length r (Å), Local Mode Force Constants k^a (mdyn Å^{-1}), Relative Bond Strength Order Values (n), Electron Density ρ (e Å^{-3}) and its Gradient $\nabla^2\rho$ (e Å^{-5}), and Energy Density H (E_h Å^{-3}) at the Path Critical Points for benzene and monosubstituted benzene derivatives. Carbons are Numbered in Accordance with Figure 1. Results obtained at the ωB97X-D/def2-TZVPD.

substituent	symmetry	bond	r	k^a	n	ρ_c	$\nabla^2\rho$	H_c
H	D_{6h}	C1-C2	1.387	6.629	1.434	0.321	-0.951	-0.345
CH_3	Cs	X-C1	1.504	4.544	1.056	0.258	-0.674	-0.230
		C1-C2	1.392	6.111	1.342	0.319	-0.938	-0.341
		C2-C3	1.387	6.289	1.374	0.321	-0.952	-0.345
		C3-C4	1.387	6.359	1.386	0.321	-0.953	-0.345
CH_2^-	C_{2v}	X-C1	1.380	6.916	1.484	0.318	-0.909	-0.347
		C1-C2	1.443	5.248	1.187	0.289	-0.806	-0.284
		C2-C3	1.375	7.075	1.511	0.325	-0.954	-0.356
		C3-C4	1.400	6.188	1.356	0.310	-0.891	-0.326
CH_2^+	C_{2v}	X-C1	1.359	8.127	1.691	0.343	-1.081	-0.391
		C1-C2	1.434	5.661	1.262	0.298	-0.864	-0.298
		C2-C3	1.365	7.533	1.590	0.337	-1.036	-0.377
		C3-C4	1.401	6.254	1.368	0.316	-0.945	-0.335
NH_2	C_s	X-C1	1.391	5.280	1.193	0.307	-0.966	-0.409
		C1-C2	1.395	6.351	1.385	0.317	-0.935	-0.339
		C2-C3	1.384	6.708	1.448	0.321	-0.947	-0.346
		C3-C4	1.387	6.613	1.431	0.320	-0.947	-0.344
NH^-	C_s	X-C1	1.324	7.575	1.597	0.362	-1.229	-0.525
		C1-C2	1.440	5.303	1.197	0.294	-0.838	-0.292
		C2-C3	1.376	7.078	1.512	0.325	-0.955	-0.355
		C3-C4	1.400	6.236	1.365	0.311	-0.895	-0.326
		C4-C5	1.396	6.381	1.390	0.313	-0.905	-0.331
		C5-C6	1.379	6.908	1.482	0.323	-0.943	-0.350
		C6-C1	1.441	5.191	1.176	0.292	-0.817	-0.289
NH^+	C_s	X-C1	1.281	9.826	1.972	0.392	-1.129	-0.693
		C1-C2	1.459	5.056	1.152	0.290	-0.843	-0.282
		C2-C3	1.360	7.792	1.634	0.341	-1.059	-0.386
		C3-C4	1.404	6.165	1.352	0.314	-0.943	-0.333
		C4-C5	1.413	5.903	1.305	0.309	-0.921	-0.323
		C5-C6	1.355	8.022	1.673	0.343	-1.065	-0.391
		C6-C1	1.460	4.917	1.126	0.287	-0.822	-0.278
OH	C_s	X-C1	1.359	6.088	1.338	0.295	-0.565	-0.463

		C1-C2	1.389	6.530	1.416	0.323	-0.974	-0.351
		C2-C3	1.384	6.740	1.453	0.321	-0.949	-0.346
		C3-C4	1.389	6.580	1.425	0.320	-0.945	-0.343
		C4-C5	1.386	6.679	1.443	0.321	-0.951	-0.346
		C5-C6	1.387	6.626	1.433	0.319	-0.938	-0.342
		C6-C1	1.389	6.493	1.410	0.322	-0.956	-0.347
O^-	C_{2v}	X-C1	1.261	9.031	1.841	0.380	-0.612	-0.665
		C1-C2	1.440	5.080	1.156	0.295	-0.839	-0.294
		C2-C3	1.380	6.873	1.476	0.322	-0.943	-0.350
		C3-C4	1.396	6.387	1.391	0.313	-0.908	-0.332
O^+	C_{2v}	X-C1	1.203	12.636	2.417	0.427	0.070	-0.771
		C1-C2	1.491	4.107	0.973	0.274	-0.771	-0.255
		C2-C3	1.351	8.223	1.707	0.346	-1.083	-0.397
		C3-C4	1.416	5.737	1.276	0.308	-0.918	-0.322

TABLE A.23 – Bond Length r (Å), Local Mode Force Constants k^a (mdyn Å^{-1}), Relative Bond Strength Order Values (n), Electron Density ρ (e Å^{-3}) and its Gradient $\nabla^2\rho$ (e Å^{-5}), and Energy Density H (E_h Å^{-3}) at the Path Critical Points for disubstituted benzene derivatives. Carbons are Numbered in Accordance with Figure 1. Results obtained at the ωB97X-D/def2-TZVPD.

substituent	symmetry	bond	r	k^a	RBSO	ρ_c	$\nabla^2\rho$	H_c
CH_3	C_{2v}	X-C1	1.504	4.552	1.058	0.258	-0.673	-0.230
		C1-C2	1.387	6.592	1.427	0.321	-0.948	-0.345
		C2-C3	1.389	6.543	1.419	0.319	-0.945	-0.342
		C4-C5	1.394	6.370	1.388	0.318	-0.933	-0.338
		C5-C6	1.383	6.774	1.459	0.323	-0.959	-0.349
CH_2	D_{2h}	X-C1	1.339	8.998	1.836	0.350	-1.074	-0.406
		C1-C2	1.460	5.084	1.157	0.282	-0.792	-0.271
		C2-C3	1.336	9.208	1.871	0.352	-1.086	-0.412
NH_2	C_{2h}	X-C1	1.402	5.201	1.178	0.300	-0.918	-0.383
		C1-C2	1.392	6.408	1.395	0.319	-0.941	-0.341
		C2-C3	1.384	6.624	1.433	0.320	-0.937	-0.344
NH	C_{2h}	X-C1	1.276	10.268	2.043	0.397	-1.236	-0.697
		C1-C2	1.469	4.875	1.118	0.282	-0.803	-0.269
		C2-C3	1.332	9.389	1.900	0.355	-1.103	-0.417
		C3-C4	1.470	4.756	1.096	0.280	-0.784	-0.266
OH	C_{2h}	X-C1	1.364	6.006	1.324	0.292	-0.571	-0.454
		C1-C2	1.386	6.601	1.429	0.325	-0.977	-0.352
		C2-C3	1.385	6.651	1.438	0.319	-0.932	-0.342
		C3-C4	1.389	6.480	1.408	0.322	-0.955	-0.347
O	D_{2h}	X-C1	1.210	12.488	2.394	0.421	-0.072	-0.760
		C1-C2	1.484	4.360	1.021	0.276	-0.773	-0.259
		C2-C3	1.330	9.497	1.918	0.357	-1.113	-0.421

A.4 Electron Localization Function

Isosurface plots of the π-contribution to the electron localization function of benzene (Figure A.3). The ELF_π-based indices of benzene and its derivatives, obtained from B3LYP and MRCI densities, are also presented (Figures A.4 and A.5).

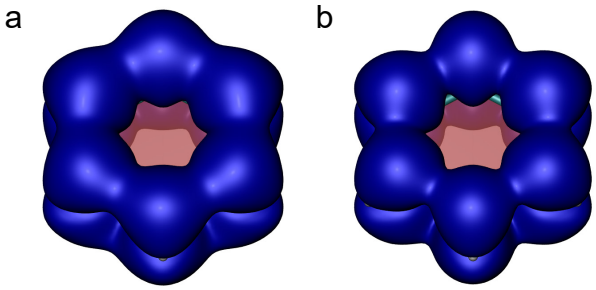

FIGURE A.3 – Isosurface plots of the π-contribution to the electron localisation function ($ELF_\pi = 0.75$) of the benzene using (a) B3LYP and (b) MRCI methods. The MR π-density was constructed using natural orbitals.

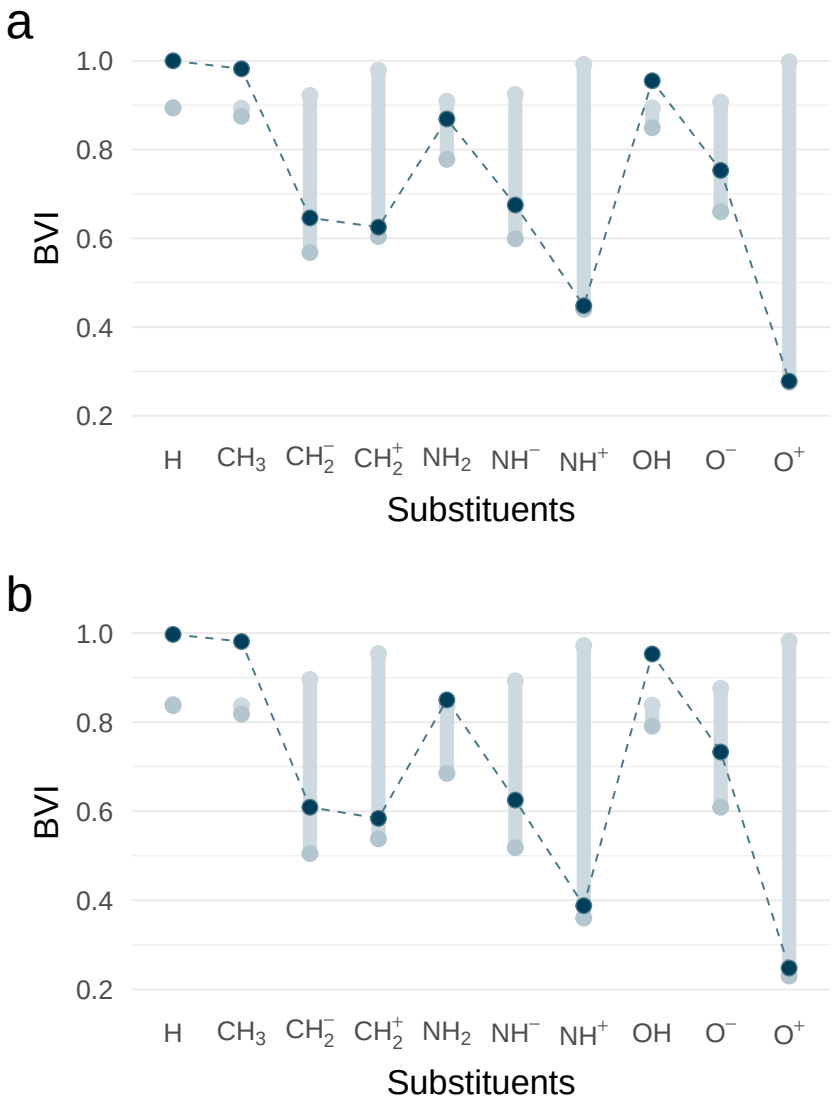

FIGURE A.4 – ELF_π-based indices of benzene and monosubstituted benzene derivatives. The span in bifurcation values ($\Delta BV = BV_{max} - BV_{min}$) has been calculated for both (a) B3LYP and (b) MRCI π-densities. The vertical dumbbells show the range between BV_{max} (upper side) and BV_{min} (bottom side). The quantity $1 - \Delta BV$, defined as BVI, is represented by the dashed line. The MR π-density was constructed using natural orbitals.

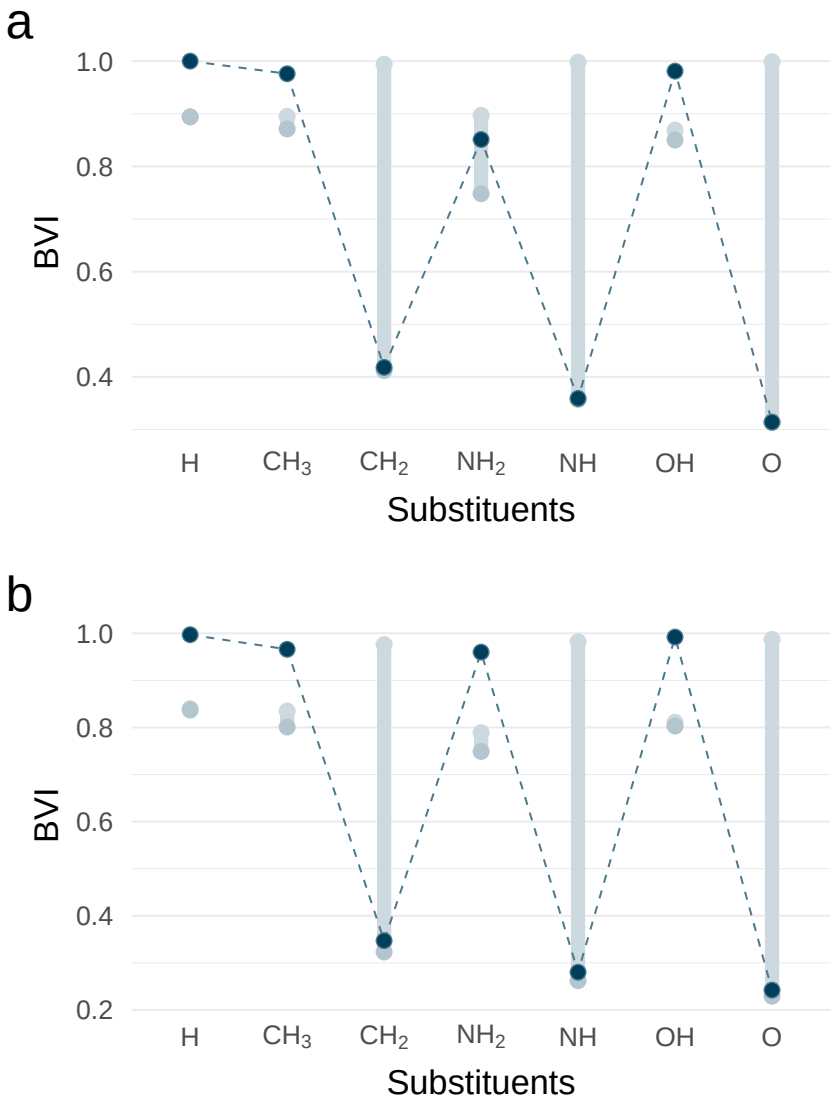

FIGURE A.5 – ELF_{π}-based indices of benzene and disubstituted benzene derivatives. The span in bifurcation values ($\Delta BV = BV_{max} - BV_{min}$) has been calculated for both (a) B3LYP and (b) MRCI π-densities. The vertical dumbbells shows the range between BV_{max} (upper side) and BV_{min} (bottom side). The quantity $1 - \Delta BV$, defined as BVI, is represented by the dashed line. The MR π-density was constructed using natural orbitals.

A.5 Nucleus-Independent Chemical Shifts

Visualization of the chemical shielding tensors of benzene (Figure A.6) and NICS plots of benzene and its derivatives (Figure A.7 and A.8).

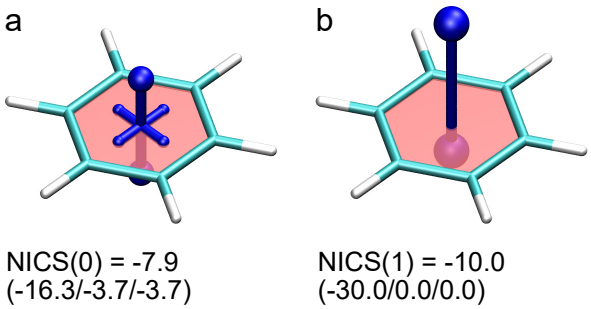

FIGURE A.6 – Visualization of benzene's chemical shielding tensors (VIST). Shielding tensors were computed at (a) the center of the ring and (b) 1 Å above the plane. GIAO-B3LYP/pcS-3//B3LYP/def2-TZVP level of theory.

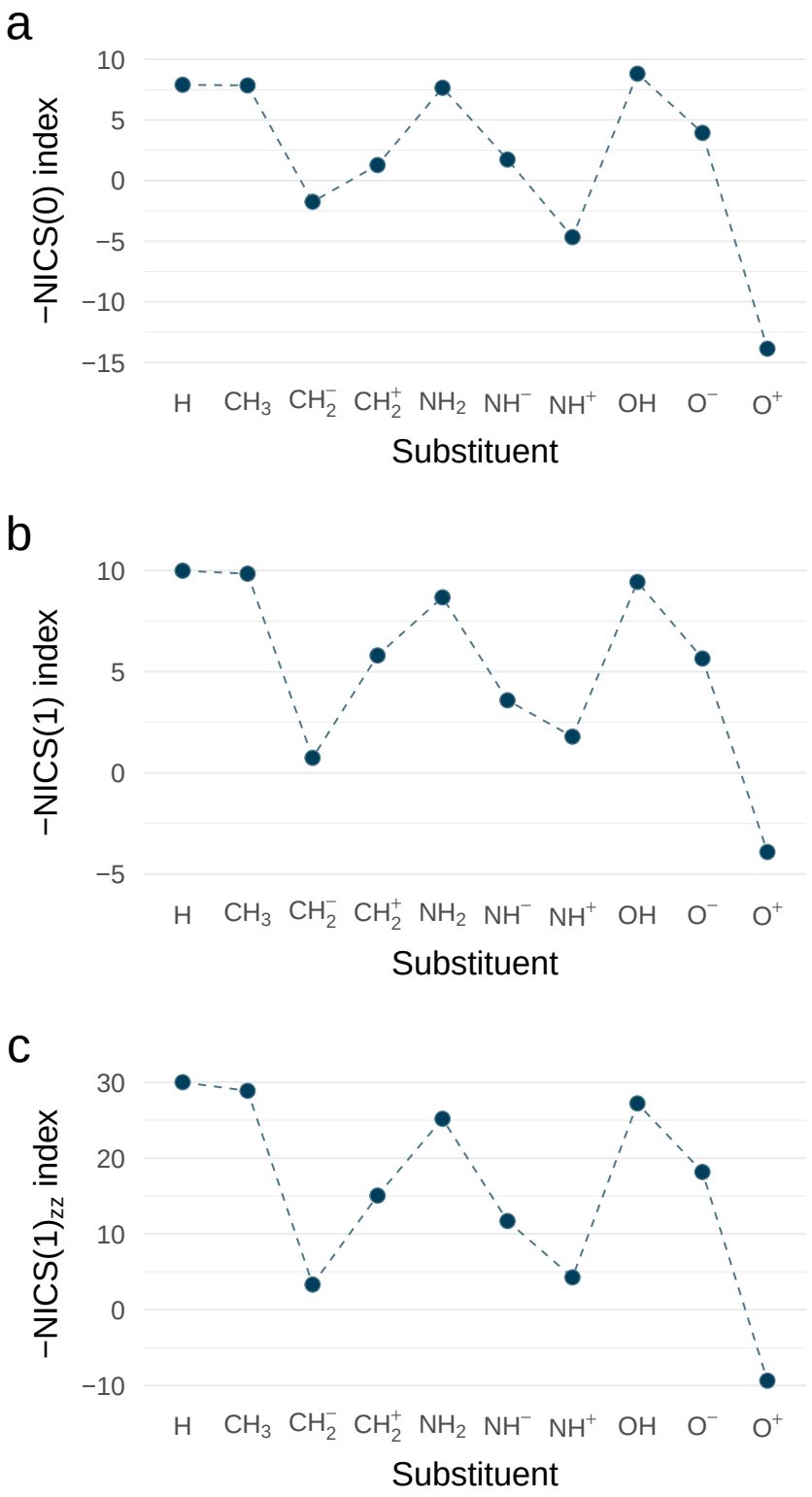

FIGURE A.7 – Relation between nuclear independent chemical shift computed at the center of the ring NICS(0), 1Å above the plane NICS(1), and its zz-component NICS(1)$_{zz}$ of benzene and monosubstituted benzene derivatives. The magnetic properties were calculated using the Gauge-Independent Atomic Orbital method GIAO-B3LYP/pcS-3 at B3LYP/def2-TZVP equilibrium geometries.

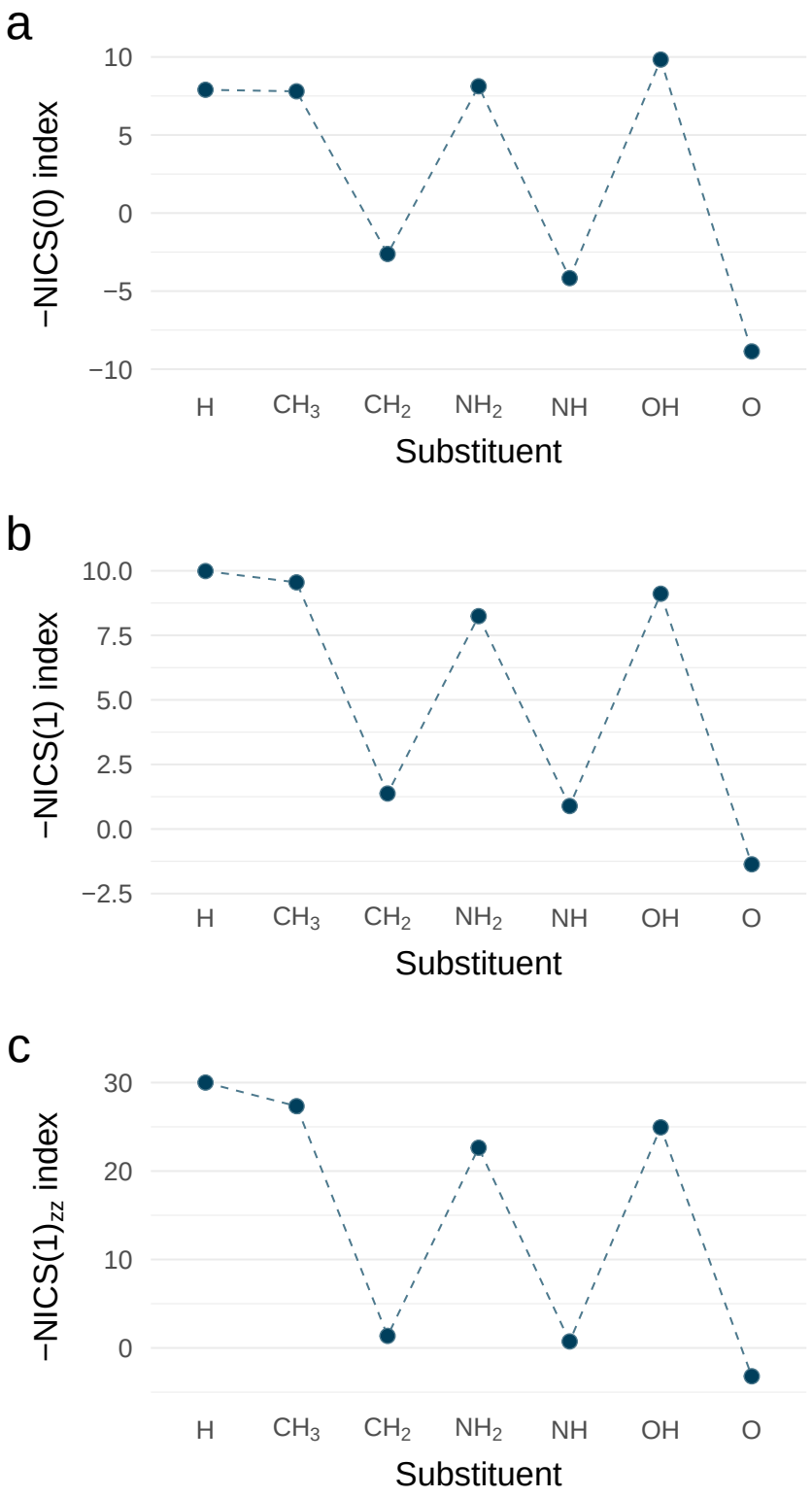

FIGURE A.8 – Relation between nuclear independent chemical shift computed at the center of the ring NICS(0), 1Å above the plane NICS(1), and its zz-component NICS(1)$_{zz}$ of benzene and disubstituted benzene derivatives. The magnetic properties were calculated using the Gauge-Independent Atomic Orbital method GIAO-B3LYP/pcS-3 at B3LYP/def2-TZVP equilibrium geometries.

A.6 Number of Effectively Unpaired Electrons

To evaluate the extent of the radical character of the structures, the total number of effectively unpaired electrons N_U[1,2] was estimated by analyzing the deviations of individual NO occupations n_i from zero (unoccupied), and two (doubly occupied) following Head-Gordon's approach.[3] Specifically, the non-linear expression

$$N_U = \sum_{i=1}^{M} n_i^2 \left(2 - n_i\right)^2 \tag{A.1}$$

where n_i is the occupation number of the i^{th} natural orbital derived from the MRCI calculations. The results are presented in Table A.24.

TABLE A.24 – Number of Effectively unpaired electrons of benzene, monosubstituted, and unsubstituted benzene derivatives.

Monosubstituted		Disubstituted	
X	N_U	X	N_U
H	0.163	CH_3	0.159
CH_3	0.160	CH_2	0.306
CH_2^-	0.144	NH_2	0.156
CH_2^+	0.193	NH	0.282
NH_2	0.155	OH	0.156
NH_2^-	0.140		
NH_2^+	0.234		
OH	0.155		
O^-	0.131		
O^+	0.229		

A.7 pEDA descriptor

Relation between pEDA (π-electron donor-acceptor descriptor) and S_0-T_1 splitting (Figure A.9).

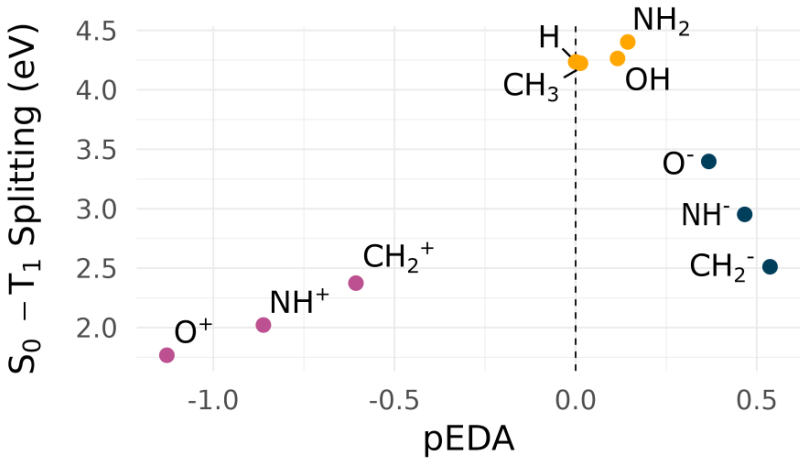

FIGURE A.9 – Relation between pEDA (π-electron donor-acceptor descriptor) and S_0-T_1 splitting (MRCI+Q at the B3LYP/def2-TZVP equilibrium geometries) of benzene and monosubstituted benzene derivatives.

A.8 Equilibrium Geometries

Equilibrium geometries (Å) obtained at the B3LYP/def-TZVP level of theory.

B3LYP/def-TZVP

C_6H_6 (S_0, D_{2h})			
Atom	x	y	z
C	0.00000000	1.20467177	0.69551377
C	0.00000000	0.00000000	1.39102632
C	0.00000000	-1.20467177	0.69551377
C	0.00000000	-1.20467177	-0.69551377
C	0.00000000	0.00000000	-1.39102632
C	0.00000000	1.20467177	-0.69551377
H	0.00000000	2.14253772	1.23699958
H	0.00000000	0.00000000	2.47398441
H	0.00000000	-2.14253772	1.23699958
H	0.00000000	-2.14253772	-1.23699958
H	0.00000000	0.00000000	-2.47398441
H	0.00000000	2.14253772	-1.23699958

$C_6H_5CH_3$ (S_0, C_s)			
Atom	x	y	z
C	0.00427725	0.91099631	0.00000000
C	0.00734300	0.19349167	1.19730125
C	0.00734300	-1.19662177	1.20029486
C	0.00631594	-1.89799658	-0.00000000
C	0.00734300	-1.19662177	-1.20029486
C	0.00734300	0.19349167	-1.19730125
C	-0.02810302	2.41726180	0.00000000
H	0.01224741	0.73041592	2.13919046
H	0.01200744	-1.73218916	2.14171530
H	0.00921256	-2.98067333	-0.00000000
H	0.01200744	-1.73218916	-2.14171530
H	0.01224741	0.73041592	-2.13919046
H	-1.05761813	2.78755937	0.00000000
H	0.46436137	2.82632628	0.88334269
H	0.46436137	2.82632628	-0.88334269

$C_6H_5CH_2^-$ (S_0, C_{2v})			
Atom	x	y	z
C	0.00000000	0.00000000	-1.87359840
C	0.00000000	1.19539407	-1.13609343
C	0.00000000	1.20828374	0.24234692
C	0.00000000	0.00000000	1.03742770
C	0.00000000	-1.20828374	0.24234692
C	0.00000000	-1.19539407	-1.13609343
H	0.00000000	0.00000000	-2.95686748
H	0.00000000	2.14678987	-1.66523341
H	0.00000000	2.16167914	0.76455731
H	0.00000000	-2.16167914	0.76455731
H	0.00000000	-2.14678987	-1.66523341
C	0.00000000	0.00000000	2.42187554
H	0.00000000	0.92653312	2.98447440
H	0.00000000	-0.92653312	2.98447440

$C_6H_5CH_2^+$ (S_0, C_{2v})			
Atom	x	y	z
C	0.00000000	0.00000000	-1.79437962
C	0.00000000	1.23044901	-1.11629352
C	0.00000000	1.24108004	0.25280749
C	0.00000000	0.00000000	0.97913438
C	0.00000000	-1.24108004	0.25280749
C	0.00000000	-1.23044901	-1.11629352
H	0.00000000	0.00000000	-2.87809572
H	0.00000000	2.15459644	-1.67761959
H	0.00000000	2.17268486	0.80452323
H	0.00000000	-2.17268486	0.80452323
H	0.00000000	-2.15459644	-1.67761959
C	0.00000000	0.00000000	2.34328792
H	0.00000000	0.92473686	2.90893239
H	0.00000000	-0.92473686	2.90893239

$C_6H_5NH_2$ (S_0, C_s)			
Atom	x	y	z
C	0.00238281	0.93537128	0.00000000
C	0.00308528	0.21991924	1.20312775
C	0.00308528	-1.16770899	1.19773958
C	0.00327083	-1.87500590	0.00000000
C	0.00308528	-1.16770899	-1.19773958
C	0.00308528	0.21991924	-1.20312775
N	0.06046324	2.32811227	0.00000000
H	0.00762686	0.75852110	2.14411494
H	0.00211452	-1.70017548	2.14104633
H	0.00254513	-2.95686736	0.00000000
H	0.00211452	-1.70017548	-2.14104633
H	0.00762686	0.75852110	-2.14411494
H	-0.27661955	2.77733747	-0.83661613
H	-0.27661955	2.77733747	0.83661613

$C_6H_5NH^-$ (S_0, C_s)			
Atom	x	y	z
C	0.02454445	-1.84506321	0.00000000
C	1.21425217	-1.09904300	0.00000000
C	1.21499143	0.27991286	0.00000000
C	-0.00000000	1.06113414	0.00000000
C	-1.20119584	0.25621411	0.00000000
C	-1.17653382	-1.12629806	0.00000000
H	0.03583178	-2.92853243	0.00000000
H	2.16878090	-1.62203177	0.00000000
H	2.15106255	0.82941632	0.00000000
N	0.05304504	2.38655437	0.00000000
H	-2.15798326	0.77452757	0.00000000
H	-2.12152737	-1.66680947	0.00000000
H	-0.90383029	2.74640814	0.00000000

$C_6H_5NH^+$ (S_0, C_s)			
Atom	x	y	z
C	0.01278430	-1.76304419	0.00000000
C	1.24999109	-1.09093007	0.00000000
C	1.25984754	0.27355027	0.00000000
C	0.00000000	1.01238425	0.00000000
C	-1.25711669	0.26870978	0.00000000
C	-1.23371473	-1.09154121	0.00000000
H	0.01200744	-2.84767578	0.00000000
H	2.17036087	-1.65871990	0.00000000
H	2.17194807	0.85682686	0.00000000
N	0.08831621	2.29682198	0.00000000
H	-2.18816867	0.82323111	0.00000000
H	-2.14890880	-1.66796387	0.00000000
H	-0.82620141	2.76177480	0.00000000

C_6H_5OH (S_0, C_s)			
Atom	x	y	z
C	0.02168082	-1.85087446	0.00000000
C	-1.18373444	-1.15997402	0.00000000
C	-1.20047910	0.23039486	0.00000000
C	0.00000000	0.93680239	0.00000000
C	1.21293860	0.25180476	0.00000000
C	1.21625605	-1.13581879	0.00000000
H	0.03157977	-2.93274138	0.00000000
H	-2.12123943	-1.70188591	0.00000000
H	-2.14414699	0.76573750	0.00000000
O	0.04801839	2.30273909	0.00000000
H	2.13521714	0.81760803	0.00000000
H	2.16214984	-1.66306458	0.00000000
H	-0.84767910	2.65842521	0.00000000

$C_6H_5O^-$ (S_0, C_{2v})			
Atom	x	y	z
C	0.00000000	0.00000000	-1.82338182
C	0.00000000	1.19678129	-1.09762593
C	0.00000000	1.20911977	0.28612463
C	0.00000000	0.00000000	1.07729702
C	0.00000000	-1.20911977	0.28612463
C	0.00000000	-1.19678129	-1.09762593
H	0.00000000	0.00000000	-2.90742241
H	0.00000000	2.14385394	-1.63452482
H	0.00000000	2.14975268	0.82930188
H	0.00000000	-2.14975268	0.82930188
H	0.00000000	-2.14385394	-1.63452482
O	0.00000000	0.00000000	2.34154909

$C_6H_5O^+$ (S_0, C_{2v})			
Atom	x	y	z
C	0.00000000	0.00000000	-1.73768605
C	0.00000000	1.25414149	-1.07344801
C	0.00000000	1.28098457	0.28272873
C	0.00000000	0.00000000	1.04611110
C	0.00000000	-1.28098457	0.28272873
C	0.00000000	-1.25414149	-1.07344801
H	0.00000000	0.00000000	-2.82329964
H	0.00000000	2.16384939	-1.65924881
H	0.00000000	2.19545929	0.86376005
H	0.00000000	-2.19545929	0.86376005
H	0.00000000	-2.16384939	-1.65924881
O	0.00000000	0.00000000	2.25654478

$C_6H_4(CH_3)_2$ (S_0, C_2)			
Atom	x	y	z
C	-0.01091327	1.41734015	0.00248065
C	-0.00620903	0.69389778	-1.19184232
C	0.00620903	-0.69389778	-1.19184232
C	0.01091327	-1.41734015	0.00248065
C	0.00616109	-0.69547983	1.19410760
C	-0.00616109	0.69547983	1.19410760
H	-0.01108426	1.22545047	-2.13709593
H	0.01108426	-1.22545047	-2.13709593
H	0.01086030	-1.22661867	2.13932447
H	-0.01086030	1.22661867	2.13932447
C	0.00616109	2.92373582	-0.00234330
C	-0.00616109	-2.92373582	-0.00234330
H	-0.64189072	3.32726420	-0.78269411
H	-0.32586034	3.32784847	0.95469869
H	1.01377060	3.30699773	-0.18864887
H	0.64189072	-3.32726420	-0.78269411
H	0.32586034	-3.32784847	0.95469869
H	-1.01377060	-3.30699773	-0.18864887

$C_6H_4(CH_2)_2$ (S_0, D_{2h})			
Atom	x	y	z
C	0.00000000	0.00000000	1.44255674
C	0.00000000	1.23576101	0.67162412
C	0.00000000	1.23576101	-0.67162412
C	0.00000000	0.00000000	-1.44255674
C	0.00000000	-1.23576101	-0.67162412
C	0.00000000	-1.23576101	0.67162412
C	0.00000000	0.00000000	2.79118410
H	0.00000000	2.17131457	1.21884313
H	0.00000000	2.17131457	-1.21884313
C	0.00000000	0.00000000	-2.79118410
H	0.00000000	-2.17131457	-1.21884313
H	0.00000000	-2.17131457	1.21884313
H	0.00000000	-0.92363598	-3.35516023
H	0.00000000	0.92363598	-3.35516023
H	0.00000000	0.92363598	3.35516023
H	0.00000000	-0.92363598	3.35516023

$C_6H_4(NH_2)_2$ (S_0, C_{2h})			
Atom	x	y	z
C	0.00068964	1.41618356	0.00000000
C	-0.00068964	0.69391873	1.19497899
C	0.00068964	-0.69391873	1.19497899
C	-0.00068964	-1.41618356	0.00000000
C	0.00068964	-0.69391873	-1.19497899
C	-0.00068964	0.69391873	-1.19497899
H	0.31054592	3.25185986	0.82986429
H	0.31054592	3.25185986	-0.82986429
H	-0.00752106	1.22419096	2.14078682
H	0.00752106	-1.22419096	2.14078682
N	0.06772003	-2.82022536	0.00000000
H	0.00752106	-1.22419096	-2.14078682
H	-0.00752106	1.22419096	-2.14078682
N	-0.06772003	2.82022536	-0.00000000
H	-0.31054592	-3.25185986	0.82986429
H	-0.31054592	-3.25185986	-0.82986429

$C_6H_4(NH)_2$ (S_0, C_{2h})			
Atom	x	y	z
C	1.22550535	-0.75565244	0.00000000
C	1.22550535	0.71083449	0.00000000
C	0.08607210	1.41388950	0.00000000
C	-1.22550535	0.75565244	0.00000000
C	-1.22550535	-0.71083449	0.00000000
C	-0.08607210	-1.41388950	0.00000000
N	2.35555472	-1.36523049	0.00000000
H	2.19682918	1.18866400	0.00000000
H	0.09918706	2.49836280	0.00000000
N	-2.35555472	1.36523049	0.00000000
H	-2.19682918	-1.18866400	0.00000000
H	-0.09918706	-2.49836280	0.00000000
H	-2.22336092	2.37838312	0.00000000
H	2.22336092	-2.37838312	0.00000000

$C_6H_4(OH)_2$ (S_0, C_{2h})			
Atom	x	y	z
C	1.20720217	-0.70065789	0.00000000
C	1.20720217	0.68947114	0.00000000
C	0.00509579	1.38532901	0.00000000
C	-1.20720217	0.70065789	0.00000000
C	-1.20720217	-0.68947114	0.00000000
C	-0.00509579	-1.38532901	0.00000000
O	2.42158347	-1.33812988	0.00000000
H	2.15154731	1.21736109	0.00000000
H	0.01538568	2.47005037	0.00000000
O	-2.42158347	1.33812988	0.00000000
H	-2.15154731	-1.21736109	0.00000000
H	-0.01538568	-2.47005037	0.00000000
H	-2.28522040	2.29168294	0.00000000
H	2.28522040	-2.29168294	0.00000000

$C_6H_4O_2$ (S_0, D_{2h})			
Atom	x	y	z
C	0.00000000	0.00000000	1.43899360
C	0.00000000	1.26587017	0.66802593
C	0.00000000	1.26587017	-0.66802593
C	0.00000000	0.00000000	-1.43899360
C	0.00000000	-1.26587017	-0.66802593
C	0.00000000	-1.26587017	0.66802593
H	0.00000000	2.17696713	1.25374060
H	0.00000000	2.17696713	-1.25374060
H	0.00000000	-2.17696713	-1.25374060
H	0.00000000	-2.17696713	1.25374060
O	0.00000000	0.00000000	-2.65666095
O	0.00000000	0.00000000	2.65666095

$C_6H_5Be^+$ (S_0, C_{2v})			
Atom	x	y	z
C	0.000000	0.000000	1.596758
C	0.000000	1.210910	0.908428
C	0.000000	1.221756	-0.476778
C	0.000000	0.000000	-1.184032
C	0.000000	-1.221756	-0.476778
C	0.000000	-1.210910	0.908428
H	0.000000	0.000000	2.679219
H	0.000000	2.147025	1.451250
H	0.000000	2.171840	-0.995567
H	0.000000	-2.171840	-0.995567
H	0.000000	-2.147025	1.451250
Be	0.000000	0.000000	-2.811684

$C_6H_5BH_3^-$ (S_0, C_s)			
Atom	x	y	z
C	0.008888	-1.891370	0.000000
C	0.010046	-1.178556	1.196707
C	0.010046	0.213762	1.186154
C	0.004252	0.971866	0.000000
C	0.010046	0.213762	-1.186154
C	0.010046	-1.178556	-1.196707
H	0.012741	-2.976484	0.000000
H	0.015098	-1.713310	2.142907
H	0.017815	0.745723	2.133212
H	0.017815	0.745723	-2.133212
H	0.015098	-1.713310	-2.142907
B	-0.038454	2.592641	0.000000
H	0.505481	3.041081	1.009317
H	0.505481	3.041081	-1.009317
H	-1.217213	2.960844	0.000000

$C_6H_5CH_2^-$(o) (S_0, C_{2v})			
Atom	x	y	z
C	0.000000	0.000000	-1.869617
C	0.000000	1.196338	-1.157448
C	0.000000	1.187286	0.236430
C	0.000000	0.000000	1.011928
C	0.000000	-1.187286	0.236430
C	0.000000	-1.196338	-1.157448
H	0.000000	0.000000	-2.955014
H	0.000000	2.142146	-1.693820
H	0.000000	2.121947	0.786942
H	0.000000	-2.121947	0.786942
H	0.000000	-2.142146	-1.693820
C	0.000000	0.000000	2.483490
H	0.932550	0.000000	3.033092
H	-0.932550	0.000000	3.033092

$C_6H_5CH_2^+$(o) (S_0, C_{2v})			
Atom	x	y	z
C	0.000000	0.000000	-1.822047
C	0.000000	1.199226	-1.123877
C	0.000000	1.229764	0.261309
C	0.000000	0.000000	0.960317
C	0.000000	-1.229764	0.261309
C	0.000000	-1.199226	-1.123877
H	0.000000	0.000000	-2.903121
H	0.000000	2.144382	-1.653448
H	0.000000	2.168900	0.794364
H	0.000000	-2.168900	0.794364
H	0.000000	-2.144382	-1.653448
C	0.000000	0.000000	2.372370
H	0.927061	0.000000	2.954138
H	-0.927061	0.000000	2.954138

$C_6H_5NH_3^+$ (S_0, C_1)			
Atom	x	y	z
C	1.912767	0.000000	0.005938
C	1.222940	1.207648	0.001503
C	-0.167303	1.217653	-0.005735
C	-0.824157	0.000000	-0.008932
C	-0.167303	-1.217653	-0.005735
C	1.222940	-1.207648	0.001503
H	2.994414	0.000000	0.009257
H	1.762052	2.145031	0.000424
H	-0.709566	2.155895	-0.009396
H	-0.709566	-2.155895	-0.009396
H	1.762052	-2.145031	0.000424
N	-2.317992	0.000000	0.007719
H	-2.690839	-0.825094	-0.469780
H	-2.691075	-0.000033	0.962902
H	-2.690837	0.825129	-0.469721

$C_6H_5OH_2^+$ (S_0, C_1)			
Atom	x	y	z
C	1.895461	0.021714	-0.000001
C	1.227220	-1.198379	0.000002
C	-0.165537	-1.236688	-0.000001
C	-0.799961	-0.018808	0.000000
C	-0.200860	1.219403	0.000002
C	1.191776	1.222650	-0.000001
H	2.976977	0.038191	-0.000003
H	1.781347	-2.126972	-0.000001
H	-0.715510	-2.167331	0.000000
H	-0.766594	2.142204	0.000006
H	1.718397	2.167080	0.000000
O	-2.303861	-0.082481	-0.000002
H	-2.726169	0.273654	0.804776
H	-2.726162	0.273680	-0.804773

ωB97X-D/def-TZVPD

Equilibrium geometries (Å) obtained at the ωB97X-D/def-TZVPD level of theory.

C_6H_6 (S_0, D_{2h})			
Atom	x	y	z
C	0.00000000	1.20157450	0.69368391
C	0.00000000	0.00000000	1.38734165
C	0.00000000	-1.20157450	0.69368391
C	0.00000000	-1.20157450	-0.69368391
C	0.00000000	0.00000000	-1.38734165
C	0.00000000	1.20157450	-0.69368391
H	0.00000000	2.13930947	1.23523271
H	0.00000000	0.00000000	2.47020715
H	0.00000000	-2.13930947	1.23523271
H	0.00000000	-2.13930947	-1.23523271
H	0.00000000	0.00000000	-2.47020715
H	0.00000000	2.13930947	-1.23523271

$C_6H_5CH_3$ (S_0, C_s)			
Atom	x	y	z
C	0.00472103	0.90749488	0.00000000
C	0.00725879	0.19330637	1.19435135
C	0.00725879	-1.19315768	1.19737201
C	0.00626995	-1.89241082	-0.00000000
C	0.00725879	-1.19315768	-1.19737201
C	0.00725879	0.19330637	-1.19435135
C	-0.02782367	2.41087091	0.00000000
H	0.01183184	0.73142430	2.13566292
H	0.01127369	-1.72894068	2.13856185
H	0.00892780	-2.97500065	-0.00000000
H	0.01127369	-1.72894068	-2.13856185
H	0.01183184	0.73142430	-2.13566292
H	-1.05815928	2.77565545	0.00000000
H	0.46490281	2.81843195	0.88340055
H	0.46490281	2.81843195	-0.88340055

$C_6H_5CH_2^-$ (S_0, C_{2v})			
Atom	x	y	z
C	0.00000000	0.00000000	-1.86784468
C	0.00000000	1.19203023	-1.13287501
C	0.00000000	1.20605172	0.24213176
C	0.00000000	0.00000000	1.03414264
C	0.00000000	-1.20605172	0.24213176
C	0.00000000	-1.19203023	-1.13287501
H	0.00000000	0.00000000	-2.95104259
H	0.00000000	2.14288596	-1.66206661
H	0.00000000	2.15918370	0.76429024
H	0.00000000	-2.15918370	0.76429024
H	0.00000000	-2.14288596	-1.66206661
C	0.00000000	0.00000000	2.41458952
H	0.00000000	0.92844110	2.97509472
H	0.00000000	-0.92844110	2.97509472

$C_6H_5CH_2^+$ (S_0, C_{2v})			
Atom	x	y	z
C	0.00000000	0.00000000	-1.78630374
C	0.00000000	1.22856853	-1.11306050
C	0.00000000	1.23871085	0.25232906
C	0.00000000	0.00000000	0.97547439
C	0.00000000	-1.23871085	0.25232906
C	0.00000000	-1.22856853	-1.11306050
H	0.00000000	0.00000000	-2.87029801
H	0.00000000	2.15193103	-1.67526085
H	0.00000000	2.17040094	0.80473504
H	0.00000000	-2.17040094	0.80473504
H	0.00000000	-2.15193103	-1.67526085
C	0.00000000	0.00000000	2.33435251
H	0.00000000	0.92592552	2.89949394
H	0.00000000	-0.92592552	2.89949394

$C_6H_5NH_2$ (S_0, C_s)			
Atom	x	y	z
C	0.00319794	0.93202730	0.00000000
C	0.00419134	0.21975526	1.19989606
C	0.00419134	-1.16442503	1.19454872
C	0.00403666	-1.86957973	0.00000000
C	0.00419134	-1.16442503	-1.19454872
C	0.00419134	0.21975526	-1.19989606
N	0.05573515	2.32194378	0.00000000
H	0.00978720	0.75845027	2.14077819
H	0.00397739	-1.69704542	2.13767406
H	0.00380945	-2.95136958	0.00000000
H	0.00397739	-1.69704542	-2.13767406
H	0.00978720	0.75845027	-2.14077819
H	-0.28274225	2.76815267	-0.83552156
H	-0.28274225	2.76815267	0.83552156

$C_6H_5NH^-$ (S_0, C_s)			
Atom	x	y	z
C	0.02513031	-1.83950845	0.00000000
C	1.21130833	-1.09569038	0.00000000
C	1.21200694	0.27989193	0.00000000
C	0.00000000	1.05661279	0.00000000
C	-1.19794186	0.25601810	0.00000000
C	-1.17250609	-1.12305116	0.00000000
H	0.03642532	-2.92284078	0.00000000
H	2.16561398	-1.61809171	0.00000000
H	2.14850957	0.82842211	0.00000000
N	0.05070317	2.37928668	0.00000000
H	-2.15472037	0.77373958	0.00000000
H	-2.11704618	-1.66319946	0.00000000
H	-0.90169031	2.74132647	0.00000000

$C_6H_5NH^+$ (S_0, C_s)			
Atom	x	y	z
C	0.01333071	-1.75456750	0.00000000
C	1.24921906	-1.08805216	0.00000000
C	1.25822252	0.27220824	0.00000000
C	0.00000000	1.01048347	0.00000000
C	-1.25607044	0.26722076	0.00000000
C	-1.23262916	-1.08800306	0.00000000
H	0.01244177	-2.83960671	0.00000000
H	2.16858528	-1.65692615	0.00000000
H	2.17034266	0.85637658	0.00000000
N	0.08781804	2.28799593	0.00000000
H	-2.18731815	0.82214507	0.00000000
H	-2.14655669	-1.66590209	0.00000000
H	-0.82465727	2.75220324	0.00000000

C_6H_5OH (S_0, C_s)			
Atom	x	y	z
C	0.02201139	-1.84538777	0.00000000
C	-1.18004103	-1.15623454	0.00000000
C	-1.19726688	0.23039211	0.00000000
C	0.00000000	0.93543450	0.00000000
C	1.20971194	0.25196298	0.00000000
C	1.21321132	-1.13195219	0.00000000
H	0.03200876	-2.92715922	0.00000000
H	-2.11741445	-1.69828385	0.00000000
H	-2.14151073	0.76463094	0.00000000
O	0.04668557	2.29350611	0.00000000
H	2.13239724	0.81716952	0.00000000
H	2.15912949	-1.65905984	0.00000000
H	-0.84385542	2.64936306	0.00000000

$C_6H_5O^-$ (S_0, C_{2v})			
Atom	x	y	z
C	0.00000000	0.00000000	-1.81812524
C	0.00000000	1.19320294	-1.09396106
C	0.00000000	1.20580766	0.28626143
C	0.00000000	0.00000000	1.07262911
C	0.00000000	-1.20580766	0.28626143
C	0.00000000	-1.19320294	-1.09396106
H	0.00000000	0.00000000	-2.90194824
H	0.00000000	2.14026629	-1.62972661
H	0.00000000	2.14702502	0.82793691
H	0.00000000	-2.14702502	0.82793691
H	0.00000000	-2.14026629	-1.62972661
O	0.00000000	0.00000000	2.33386249

$C_6H_5O^+$ (S_0, C_{2v})			
Atom	x	y	z
C	0.00000000	0.00000000	-1.72965487
C	0.00000000	1.25353732	-1.07040480
C	0.00000000	1.28000502	0.28065161
C	0.00000000	0.00000000	1.04574338
C	0.00000000	-1.28000502	0.28065161
C	0.00000000	-1.25353732	-1.07040480
H	0.00000000	0.00000000	-2.81573853
H	0.00000000	2.16205084	-1.65743828
H	0.00000000	2.19496773	0.86156920
H	0.00000000	-2.19496773	0.86156920
H	0.00000000	-2.16205084	-1.65743828
O	0.00000000	0.00000000	2.24849799

$C_6H_4(CH_3)_2$ (S_0, C_{2v})			
Atom	x	y	z
C	0.00000000	1.41197451	0.00607723
C	0.00000000	0.69456649	1.19350798
C	0.00000000	-0.69456649	1.19350798
C	0.00000000	-1.41197451	0.00607723
C	0.00000000	-0.69124393	-1.18687495
C	0.00000000	0.69124393	-1.18687495
H	0.00000000	1.22625307	2.13842898
H	0.00000000	-1.22625307	2.13842898
H	0.00000000	-1.22505799	-2.13104433
H	0.00000000	1.22505799	-2.13104433
C	0.00000000	2.91559523	-0.00672452
C	0.00000000	-2.91559523	-0.00672452
H	0.00000000	3.32084467	1.00519378
H	0.87980767	3.30413539	-0.52424644
H	-0.87980767	3.30413539	-0.52424644
H	0.00000000	-3.32084467	1.00519378
H	-0.87980767	-3.30413539	-0.52424644
H	0.87980767	-3.30413539	-0.52424644

$C_6H_4(CH_2)_2$ (S_0, D_{2h})			
Atom	x	y	z
C	0.00000000	0.00000000	1.43983571
C	0.00000000	1.23922296	0.66785793
C	0.00000000	1.23922296	-0.66785793
C	0.00000000	0.00000000	-1.43983571
C	0.00000000	-1.23922296	-0.66785793
C	0.00000000	-1.23922296	0.66785793
C	0.00000000	0.00000000	2.77915534
H	0.00000000	2.17387668	1.21672306
H	0.00000000	2.17387668	-1.21672306
C	0.00000000	0.00000000	-2.77915534
H	0.00000000	-2.17387668	-1.21672306
H	0.00000000	-2.17387668	1.21672306
H	0.00000000	-0.92510661	-3.34198957
H	0.00000000	0.92510661	-3.34198957
H	0.00000000	0.92510661	3.34198957
H	0.00000000	-0.92510661	3.34198957

$C_6H_4(NH_2)_2$ (S_0, C_{2h})			
Atom	x	y	z
C	0.00056917	1.41117216	0.00000000
C	-0.00056917	0.69218551	1.19155578
C	0.00056917	-0.69218551	1.19155578
C	-0.00056917	-1.41117216	0.00000000
C	0.00056917	-0.69218551	-1.19155578
C	-0.00056917	0.69218551	-1.19155578
H	0.31961827	3.24054680	0.82876598
H	0.31961827	3.24054680	-0.82876598
H	-0.00746519	1.22259122	2.13726259
H	0.00746519	-1.22259122	2.13726259
N	0.05973114	-2.81213554	0.00000000
H	0.00746519	-1.22259122	-2.13726259
H	-0.00746519	1.22259122	-2.13726259
N	-0.05973114	2.81213554	0.00000000
H	-0.31961827	-3.24054680	0.82876598
H	-0.31961827	-3.24054680	-0.82876598

$C_6H_4(NH)_2$ (S_0, C_{2h})			
Atom	x	y	z
C	1.22334428	0.75406198	0.00000000
C	-0.08880038	1.41432162	0.00000000
C	-1.22334428	0.71599538	0.00000000
C	-1.22334428	-0.75406198	0.00000000
C	0.08880038	-1.41432162	0.00000000
C	1.22334428	-0.71599538	0.00000000
N	2.26953419	1.48459231	0.00000000
H	-0.07872853	2.49683008	0.00000000
H	-2.18667770	1.21418852	0.00000000
N	-2.26953419	-1.48459231	0.00000000
H	0.07872853	-2.49683008	0.00000000
H	2.18667770	-1.21418852	0.00000000
H	-3.11356566	-0.91290166	0.00000000
H	3.11356566	0.91290166	0.00000000

$C_6H_4(OH)_2$ (S_0, C_{2h})			
Atom	x	y	z
C	1.20405615	-0.69984748	0.00000000
C	1.20405615	0.68639827	0.00000000
C	0.00574242	1.38133469	0.00000000
C	-1.20405615	0.69984748	0.00000000
C	-1.20405615	-0.68639827	0.00000000
C	-0.00574242	-1.38133469	0.00000000
O	2.41056995	-1.33533667	0.00000000
H	2.14818289	1.21483636	0.00000000
H	0.01796520	2.46603209	0.00000000
O	-2.41056995	1.33533667	0.00000000
H	-2.14818289	-1.21483636	0.00000000
H	-0.01796520	-2.46603209	0.00000000
H	-2.27647298	2.28446964	0.00000000
H	2.27647298	-2.28446964	0.00000000

$C_6H_4O_2$ (S_0, D_{2h})			
Atom	x	y	z
C	0.00000000	0.00000000	1.43661406
C	0.00000000	1.26739327	0.66510491
C	0.00000000	1.26739327	-0.66510491
C	0.00000000	0.00000000	-1.43661406
C	0.00000000	-1.26739327	-0.66510491
C	0.00000000	-1.26739327	0.66510491
H	0.00000000	2.17862605	1.25047480
H	0.00000000	2.17862605	-1.25047480
H	0.00000000	-2.17862605	-1.25047480
H	0.00000000	-2.17862605	1.25047480
O	0.00000000	0.00000000	-2.64660651
O	0.00000000	0.00000000	2.64660651

A.9 Analytical harmonic frequencies

B3LYP/def2-TZVP

Analytical harmonic frequencies (cm^{-1}) obtained at the B3LYP/def-TZVP level of theory.

C_6H_6 (S_0, D_{2h})		
412.4080	412.4508	623.7588
623.7800	688.9887	716.8786
862.5055	862.5273	963.0042
963.0268	992.1140	1015.3633
1028.8544	1061.5462	1061.5725
1176.5413	1199.7402	1199.7518
1336.1068	1388.4198	1517.9991
1518.0114	1636.9423	1636.9912
3160.4505	3169.9729	3170.0140
3185.4185	3185.4622	3195.3397

$C_6H_5CH_3$ (S_0, C_s)		
21.9825	208.5898	344.3435
415.1435	477.2406	529.8116
638.5697	710.1862	744.5306
800.7865	855.9649	907.4976
956.8441	974.3728	1002.5332
1021.5918	1053.5974	1064.9766
1113.6013	1183.0865	1205.7083
1231.3893	1329.2528	1362.0220
1415.8466	1472.5468	1489.7106
1504.5885	1534.1592	1626.6275
1648.4090	3025.2975	3077.4470
3104.2020	3156.6216	3158.1036
3171.0230	3179.2182	3191.6746

$C_6H_5CH_2^-$ (S_0, C_{2v})		
165.3772	355.9577	410.0837
418.8769	443.0686	528.5118
542.1521	547.2398	630.5278
664.3397	741.7399	768.4014
810.5388	859.6432	863.4038
950.5219	983.4222	1020.8231
1094.2680	1156.7149	1189.7026
1309.2220	1336.8822	1357.1143
1471.4394	1483.5357	1526.6144
1529.2331	1628.9009	3088.0650
3090.5182	3111.4353	3118.7587
3122.9075	3160.4159	3182.8477

$C_6H_5CH_2^+$ (S_0, C_{2v})		
167.7235	342.2093	360.7366
421.3185	537.3399	612.6948
632.7055	652.5747	811.9053
825.8603	854.3552	986.0371
1007.9038	1009.5956	1023.2891
1023.8661	1061.9238	1114.5069
1136.8401	1205.1189	1214.0198
1358.8828	1389.0085	1417.2171
1479.7613	1504.0966	1575.5242
1595.4478	1661.1254	3148.1833
3189.0942	3196.4049	3198.0521
3213.7407	3216.4586	3245.4326

$C_6H_5NH_2$ (S_0, C_s)		
220.9646	300.1306	383.7188
417.8573	504.7357	537.4653
576.9911	637.4021	702.3354
762.3303	824.7954	833.7786
882.3786	940.5150	952.6677
1014.7990	1050.1522	1065.2066
1136.6764	1181.0011	1202.2555
1303.6001	1347.5648	1373.4145
1505.6054	1535.7675	1628.4306
1647.0878	1662.5252	3155.5722
3156.5940	3172.6467	3178.0377
3195.7200	3556.8530	3652.6028

$C_6H_5NH^-$ (S_0, C_s)		
177.4557	421.4114	424.0139
442.2282	533.0050	572.4848
625.7139	671.2656	675.5300
785.9844	818.0010	823.0272
855.7748	893.2127	985.4172
1022.8553	1062.9422	1146.5028
1178.3469	1179.9312	1351.3200
1356.0077	1388.3240	1492.6474
1520.0641	1541.4046	1625.2591
3085.8573	3095.7957	3112.0733
3141.8158	3158.9650	3369.1335

$C_6H_5NH^+$ (S_0, C_s)		
155.8972	327.0075	401.9759
417.7469	531.7392	594.6475
623.1788	778.2731	800.8051
838.8062	928.7439	998.9319
1004.2062	1030.8131	1040.5269
1069.5109	1090.3690	1157.8362
1203.2566	1206.5507	1359.7875
1433.0345	1447.3585	1477.2565
1565.4040	1595.9250	1655.9837
3184.6859	3191.4242	3206.6363
3212.3043	3217.7880	3407.4748

C_6H_5OH (S_0, C_s)		
229.9515	340.7059	407.5459
421.5022	515.4509	537.2787
634.4466	696.2596	762.0132
824.0239	831.1573	890.5050
942.4128	962.1738	1017.8840
1046.1670	1095.8746	1178.4424
1193.0449	1193.4215	1283.3284
1350.3007	1374.9104	1506.6295
1534.0700	1638.5916	1649.5476
3151.7561	3171.2147	3179.4981
3193.2997	3199.7365	3800.6181

$C_6H_5O^-$ (S_0, C_{2v})		
191.3097	427.6764	448.0336
467.8332	534.2206	612.7764
616.8061	687.1835	792.5261
821.4771	848.7026	876.6250
892.6969	985.6616	1022.8681
1068.6367	1152.8228	1166.7587
1242.9735	1342.1960	1406.1180
1478.7038	1544.8969	1549.6219
1623.6197	3089.4770	3092.1970
3134.1900	3135.8185	3154.7744

$C_6H_5O^+$ (S_0, C_{2v})		
132.8162	307.8976	362.5880
437.0086	517.4368	560.8712
601.7106	753.2607	784.3340
857.3319	978.0969	990.2939
1031.2948	1049.6059	1074.8792
1099.7829	1166.8303	1192.6577
1263.0690	1399.8930	1435.0664
1485.2857	1567.7353	1647.8883
1724.4117	3178.4197	3200.2787
3201.1578	3211.1986	3213.0009

$C_6H_4(CH_3)_2$ (S_0, C_2)		
12.1187	35.6103	136.0575
287.0466	309.0540	388.0548
417.2380	465.1513	498.6748
660.7322	722.6808	730.4780
813.6195	839.0080	850.2442
947.9353	949.8974	990.3587
1026.3592	1042.5558	1061.8114
1066.9726	1143.8353	1210.9446
1224.7509	1241.2349	1323.9707
1346.9661	1416.0376	1416.3905
1440.4254	1487.5537	1488.3329
1490.0102	1501.7012	1552.9058
1615.2749	1659.1345	3024.3660
3024.5105	3074.2330	3074.3700
3102.4441	3102.4507	3150.1918
3152.7767	3167.1601	3171.1903

$C_6H_4(CH_2)_2$ (S_0, D_{2h})		
105.9231	275.3962	325.4320
378.3446	399.4151	469.1215
482.4421	629.4377	655.4346
707.0752	757.6536	786.0952
806.3664	833.9533	845.4413
901.5101	909.6178	954.5444
977.4309	981.0852	995.5706
998.5422	1161.9623	1207.3753
1323.9988	1363.8005	1375.3811
1425.3056	1461.4934	1487.5523
1604.4432	1622.2105	1660.8319
1696.1909	3146.9004	3147.0233
3158.2074	3159.3395	3176.1471
3179.3507	3231.6558	3231.7020

$C_6H_4(NH_2)_2$ (S_0, C_{2h})		
146.7013	228.0819	230.3581
317.0708	350.2151	418.4519
425.8085	475.5647	513.8473
630.8896	662.2455	663.1977
735.8125	778.6729	808.1921
839.5378	859.4021	908.6503
913.1430	1027.8966	1068.1438
1123.1889	1157.8259	1203.1027
1286.5731	1295.0261	1349.4953
1365.5654	1489.6840	1554.0651
1630.0835	1654.8260	1658.4493
1674.6633	3151.0076	3151.5746
3166.9682	3169.9629	3538.9210
3539.6280	3629.6516	3629.8326

$C_6H_4(NH)_2$ (S_0, C_{2h})		
100.9032	261.9683	365.7420
387.3430	456.7519	467.4067
502.6343	621.8261	738.7442
780.9190	787.2172	794.4506
875.1937	913.8379	939.8292
970.0084	1009.7334	1016.1323
1070.6168	1153.0122	1190.3482
1196.2486	1350.8641	1394.9834
1426.2018	1457.4518	1604.8084
1640.0430	1657.5923	1699.9796
3160.9024	3161.4531	3194.1692
3196.1167	3421.5545	3422.0498

$C_6H_4(OH)_2$ (S_0, C_{2h})		
154.2256	288.6878	290.7838
343.0755	365.7841	428.0271
449.7387	472.6274	519.9244
660.5597	715.7473	765.4556
804.1050	837.6576	864.6075
919.4579	925.7537	1026.8132
1116.5915	1180.0737	1185.3236
1195.9941	1267.3831	1288.6312
1359.0317	1366.0385	1489.9013
1551.2226	1646.0826	1668.0355
3155.0140	3156.6523	3195.9824
3197.6078	3806.8503	3808.0380

$C_6H_4O_2$ (S_0, D_{2h})		
93.2844	234.0432	340.7625
414.3547	456.3705	458.9275
517.3830	603.0938	754.8964
763.1464	771.5466	816.8840
917.0099	951.9110	1024.7587
1033.3653	1085.6449	1168.9754
1236.9230	1316.3911	1389.5880
1399.1502	1645.5441	1679.4770
1728.6876	1729.6579	3179.2873
3179.5212	3195.4945	3197.7894

ωB97X-D/def-TZVPD

Analytical harmonic frequencies (cm^{-1}) obtained at the ωB97X-D/def-TZVPD level of theory.

C_6H_6 (S_0, D_{2h})		
415.9246	416.0187	626.2035
626.3010	696.3469	732.0913
880.1509	880.2245	1012.9843
1013.0564	1029.3918	1029.8838
1039.6137	1072.4854	1072.5232
1177.6605	1206.8663	1207.2494
1339.1713	1366.6125	1527.2564
1527.3794	1668.0844	1668.2576
3186.9820	3196.3800	3197.2892
3212.5941	3213.4620	3223.4258

$C_6H_5CH_3$ (S_0, C_s)		
40.1583	211.4416	350.9860
419.7267	481.5639	534.3242
641.4236	724.1699	756.4553
809.8872	874.1709	932.1371
1008.9814	1010.3670	1027.5089
1028.8454	1065.3576	1072.3547
1122.7834	1186.9405	1214.8194
1246.8351	1331.8874	1365.4219
1420.9325	1478.9681	1494.0715
1512.9416	1548.2725	1659.3954
1682.7456	3051.5329	3116.0849
3138.6299	3182.9094	3184.3350
3197.5238	3207.0576	3219.3275

$C_6H_5CH_2^-$ (S_0, C_{2v})		
166.1952	362.6810	431.8835
433.3878	494.5014	531.9633
553.9972	633.8936	656.7850
690.6677	800.3916	802.5201
822.0517	956.4105	959.5644
962.4622	986.1820	1035.4380
1104.1121	1162.8064	1196.3023
1317.0541	1343.5419	1358.2172
1476.0299	1496.0658	1544.9992
1555.4047	1649.5018	3122.3498
3124.8862	3132.0077	3151.7910
3154.0945	3189.9727	3208.3329

$C_6H_5CH_2^+$ (S_0, C_{2v})		
163.4783	340.0939	366.7107
418.3829	541.0911	616.0623
642.1895	644.1550	810.2910
834.2696	862.0840	993.9762
1015.1032	1019.8440	1037.6495
1043.0038	1073.0783	1129.5140
1146.8873	1212.2193	1220.7750
1362.4622	1398.2065	1433.0129
1489.7251	1512.3284	1602.7898
1620.6293	1682.4291	3162.6825
3210.0006	3217.9616	3219.4227
3239.7187	3242.4269	3264.3814

$C_6H_5NH_2$ (S_0, C_s)		
223.4189	295.6102	391.1273
422.5547	507.2487	541.9589
574.8606	640.3954	715.0430
777.8092	844.3024	845.2509
909.7270	995.6334	1013.6448
1021.4795	1063.0386	1076.8952
1142.9044	1185.2710	1211.6311
1321.0661	1349.1080	1372.2388
1517.7362	1551.6500	1661.1435
1662.0407	1687.2715	3182.7906
3183.9811	3199.8351	3206.1431
3222.9901	3604.5445	3704.4684

$C_6H_5NH^-$ (S_0, C_s)		
178.1111	428.1271	435.8613
500.0493	536.7948	629.9868
673.8470	688.1154	713.8310
809.5585	831.1279	835.7040
959.6927	970.3880	988.6045
1037.3099	1076.7424	1155.7106
1181.6114	1187.9853	1351.9417
1361.4532	1401.5494	1505.3343
1538.7446	1572.7891	1648.4287
3121.2081	3130.5152	3146.5572
3172.3654	3189.3912	3448.4909

$C_6H_5NH^+$ (S_0, C_s)		
151.6109	323.6313	393.1240
422.2968	534.5014	596.5548
613.5116	788.1790	805.6718
840.3615	948.0797	1004.1012
1016.4089	1043.8688	1055.9647
1079.0480	1102.6124	1165.0099
1209.7221	1212.9898	1362.9647
1447.5363	1460.2545	1490.3646
1588.8218	1640.1218	1685.8501
3204.1765	3213.1622	3227.5591
3238.5172	3242.7045	3467.0220

C_6H_5OH (S_0, C_s)		
232.7421	355.4128	416.1613
426.5358	525.4470	542.1479
637.8458	715.8966	783.7596
843.0756	844.4051	918.4885
997.5273	1019.8523	1024.8440
1058.4451	1108.3696	1180.8915
1201.4001	1205.6657	1308.8948
1352.3374	1377.3449	1519.6030
1551.1689	1671.9909	1683.3019
3179.0214	3197.5072	3206.6297
3219.3884	3226.5181	3891.9619

$C_6H_5O^-$ (S_0, C_{2v})		
190.7608	436.1205	454.3745
513.9714	537.9005	622.2393
701.6218	739.1148	809.1945
835.3723	863.1070	968.1553
969.8097	990.7410	1037.1860
1081.5106	1159.6377	1175.8736
1255.2436	1345.5778	1419.0752
1491.7587	1571.4139	1575.7577
1647.8303	3125.7112	3129.2029
3166.2325	3167.3183	3186.0731

$C_6H_5O^+$ (S_0, C_{2v})		
128.8312	304.0431	354.0062
438.9368	519.3004	563.0228
598.3221	759.4562	791.2540
862.7118	985.9069	998.7239
1044.4101	1061.0009	1084.7597
1110.7480	1176.2223	1199.0753
1273.6457	1405.9980	1441.6331
1501.2079	1592.4370	1676.2802
1791.7842	3196.9999	3222.1465
3222.8756	3236.2674	3238.2088

$C_6H_4(CH_3)_2$ (S_0, C_{2v})		
11.5680	18.8707	139.5883
291.6063	315.1261	393.5147
422.5967	468.9448	501.8979
663.6219	734.6838	740.9701
826.1555	848.4986	868.3182
975.5797	996.7131	1006.7161
1029.7403	1051.7197	1071.6816
1074.2627	1149.8528	1219.9841
1243.6805	1252.4727	1328.6840
1350.6443	1420.9961	1421.2653
1452.7260	1489.6613	1490.4114
1493.7842	1508.8509	1571.0198
1650.2067	1696.0928	3051.4787
3051.6789	3113.4433	3113.5999
3136.2393	3136.2485	3175.3700
3179.5039	3193.4226	3198.2576

$C_6H_4(CH_2)_2$ (S_0, D_{2h})		
98.2712	262.9265	332.0418
381.8795	406.9179	470.0385
476.5473	629.5916	671.4430
733.4573	755.4570	790.1574
806.4522	844.7543	854.6955
929.9890	935.0376	962.8624
984.2343	1003.2110	1020.2809
1025.1451	1169.5912	1217.1732
1327.5773	1377.5875	1380.5664
1438.3939	1473.3263	1490.9210
1644.7659	1674.9303	1706.4646
1751.2614	3163.6111	3163.6580
3184.1315	3185.0293	3203.4940
3206.5897	3253.0246	3253.0647

$C_6H_4(NH_2)_2$ (S_0, C_{2h})		
148.5762	224.1767	225.4981
324.3307	356.8415	424.4985
434.3400	480.0367	517.0642
630.6889	657.1546	666.7792
743.2956	788.5590	828.7884
854.9548	871.2112	950.3196
969.7214	1037.2894	1080.7676
1130.9598	1160.9697	1213.5917
1300.3011	1320.6300	1347.7385
1370.4044	1505.1821	1573.9337
1661.1288	1664.6811	1665.4898
1710.8353	3178.0833	3178.6976
3194.7538	3197.7318	3589.6819
3590.3652	3684.2907	3684.4126

$C_6H_4(NH)_2$ (S_0, C_{2h})		
94.3374	254.6551	369.3665
393.6954	460.2815	468.4478
502.4922	623.2243	745.0951
784.5618	794.9099	797.0060
885.6520	933.8905	958.6843
974.2813	1035.4977	1039.7421
1082.0697	1156.5108	1198.4766
1198.4918	1354.5243	1399.4622
1438.2716	1469.9882	1658.7763
1688.9878	1712.8762	1755.0884
3186.8135	3187.1336	3218.9124
3220.9354	3482.5638	3483.1253

$C_6H_4(OH)_2$ (S_0, C_{2h})		
156.3953	301.9603	304.9037
350.7359	375.7548	433.7200
457.8297	477.9173	531.0101
665.6202	736.3131	778.8404
823.4136	858.0803	878.0331
954.6018	973.0767	1035.3047
1129.7533	1185.1232	1195.0559
1207.4605	1288.3059	1319.6050
1357.6624	1374.5111	1507.3564
1573.6318	1680.3104	1705.4746
3180.5401	3182.1876	3220.9685
3222.6850	3896.8919	3898.0885

$C_6H_4O_2$ (S_0, D_{2h})		
88.2595	231.2649	343.5049
420.2225	456.9388	459.6385
518.5308	607.3383	759.5345
767.0428	776.2600	829.3252
924.9736	957.5265	1045.5617
1052.1006	1095.2192	1176.3464
1246.4291	1331.1950	1393.4171
1410.2562	1691.6291	1720.3086
1792.7963	1799.0847	3205.0862
3205.1445	3222.3690	3224.6222

Bibliography

1 TAKATSUKA, Kazuo; FUENO, Takayuki; YAMAGUCHI, Kizashi. Distribution of odd electrons in ground-state molecules. **Theoretica Chimica Acta**, v. 48, n. 3, p. 175–183, 1978.

2 STAROVEROV, Viktor N.; DAVIDSON, Ernest R. Distribution of effectively unpaired electrons. **Chemical Physics Letters**, North-Holland, v. 330, n. 1-2, p. 161–168, Nov. 2000.

3 HEAD-GORDON, Martin. Characterizing unpaired electrons from the one-particle density matrix. **Chemical Physics Letters**, North-Holland, v. 372, n. 3-4, p. 508–511, Apr. 2003.

Appendix B - Supplementary Information for Chapter 5

B.1 Freezing schemes and reference active spaces selection

B.1.1 Active space

Tests on the active space were conducted on decapentaene. All tests were performed using the optimal freezing scheme adopted in this work (Table B.1). The relevant tests are presented in Table B.2. For all tests involving restricted active (RAS) and/or auxiliary (AUX) spaces, one hole was allowed in the RAS (single excitations from this space), and one electron was allowed in the AUX (single excitations to this space).

TABLE B.1 – Excitation energies (eV) of decapentaene calculated using a variety of reference spaces for the MR-CISD computation. Molecular orbitals were calculated at the SA6-CASSCF(10,10) level. All calculations were performed using the cc-pVDZ basis set.

Active Space	Excitation	ΔE_{CI}	ΔE_{CI+P}	ΔE_{AQCC}
MR-CISD(CAS(10,10))	$1^1A_g^- - 2^1A_g^-$	4.562	4.472	4.462
	$1^1A_g^- - 1^1B_u^+$	5.380	4.613	4.560
	$1^1A_g^- - 2^1B_u^-$	5.657	5.559	5.541
MR-CISD(RAS(1)CAS(8,8)AUX(1))	$1^1A_g^- - 2^1A_g^-$	4.599	4.453	4.477
	$1^1A_g^- - 1^1B_u^+$	5.350	4.618	4.547
	$1^1A_g^- - 2^1B_u^-$	5.691	5.537	5.547
MR-CISD(RAS(2)CAS(6,6)AUX(2))	$1^1A_g^- - 2^1A_g^-$	4.648	4.448	4.505
	$1^1A_g^- - 1^1B_u^+$	5.311	4.622	4.536
	$1^1A_g^- - 2^1B_u^-$	5.838	5.498	5.636
MR-CISD(CAS(8,8))[a]	$1^1A_g^- - 2^1A_g^-$	4.834	4.460	–
	$1^1A_g^- - 1^1B_u^+$	5.216	4.721	–
	$1^1A_g^- - 2^1B_u^-$	6.057	5.551	–
MR-CISD(CAS(6,6))[a]	$1^1A_g^- - 2^1A_g^-$	5.019	4.547	–
	$1^1A_g^- - 1^1B_u^+$	5.146	4.752	–
	$1^1A_g^- - 2^1B_u^-$	6.485	5.690	–

[a] Important configurations are not included in the active space, and hence, many intruder states appear at the MR-AQCC level.

B.1.2 Freezing scheme

Freezing scheme tests were conducted on hexatriene. Table B.2 present the relevant freezing schemes tested. Importantly, freezing schemes involving uneven percentage between reference doubly occupied (Docc) and virtual (Virt) orbitals were also tested, but no significant advantage was observed from using such freezing schemes, and hence, they were not listed below.

TABLE B.2 – Excitation energies (eV) of hexatriene calculated using a variety of freezing schemes of σ-orbitals at the CI/AQCC step. The frozen reference doubly occupied (Docc) and virtual (Virt) σ-orbitals were equally distributed over the irreps A_g and B_u. Molecular orbitals were calculated at the SA6-CASSCF(6,6) level. All calculations were performed using the cc-pVDZ basis set.

Freezing Scheme	Excitation	ΔE_{CI}	ΔE_{CI+P}	ΔE_{AQCC}
Docc: 30%[a]	$1^1A_g^- - 2^1A_g^-$	5.816	5.755	5.744
Virt: 0%	$1^1A_g^- - 1^1B_u^+$	6.521	5.803	5.764
	$1^1A_g^- - 2^1B_u^-$	7.005	6.915	6.880
Docc: 30%	$1^1A_g^- - 2^1A_g^-$	5.821	5.763	5.754
Virt: 30%	$1^1A_g^- - 1^1B_u^+$	6.487	5.785	5.757
	$1^1A_g^- - 2^1B_u^-$	7.008	6.918	6.888
Docc: 40%	$1^1A_g^- - 2^1A_g^-$	5.863	5.826	5.821
Virt: 40%	$1^1A_g^- - 1^1B_u^+$	6.434	5.797	5.791
	$1^1A_g^- - 2^1B_u^-$	7.057	6.989	6.969
Docc: 50%	$1^1A_g^- - 2^1A_g^-$	5.856	5.819	5.818
Virt: 50%	$1^1A_g^- - 1^1B_u^+$	6.412	5.827	5.833
	$1^1A_g^- - 2^1B_u^-$	7.044	6.976	6.964
Docc: 60%	$1^1A_g^- - 2^1A_g^-$	5.831	5.808	5.811
Virt: 60%	$1^1A_g^- - 1^1B_u^+$	6.362	5.941	5.971
	$1^1A_g^- - 2^1B_u^-$	6.997	6.942	6.944
Docc: 70%	$1^1A_g^- - 2^1A_g^-$	5.791	5.770	5.774
Virt: 70%	$1^1A_g^- - 1^1B_u^+$	6.409	6.108	6.137
	$1^1A_g^- - 2^1B_u^-$	6.945	6.896	6.902
Docc: 80%	$1^1A_g^- - 2^1A_g^-$	5.801	5.794	5.796
Virt: 80%	$1^1A_g^- - 1^1B_u^+$	6.612	6.486	6.505
	$1^1A_g^- - 2^1B_u^-$	6.918	6.894	6.899
Docc: 90%	$1^1A_g^- - 2^1A_g^-$	5.815	5.814	5.815
Virt: 90%	$1^1A_g^- - 1^1B_u^+$	6.813	6.770	6.777
	$1^1A_g^- - 2^1B_u^-$	6.926	6.915	6.919
Docc: 100%	$1^1A_g^- - 2^1A_g^-$	5.819	5.818	5.818
Virt: 100%	$1^1A_g^- - 1^1B_u^+$	6.848	6.824	6.832
	$1^1A_g^- - 2^1B_u^-$	6.933	6.924	6.930

[a] 30% of reference doubly occupied σ orbitals correspond to carbon $1s$ orbitals.

B.2 Singlet states

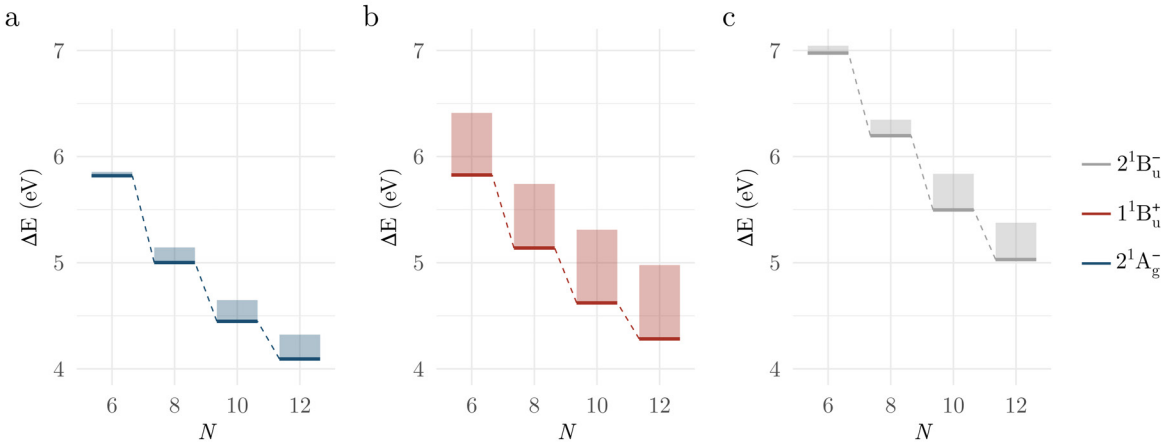

FIGURE B.1 – Vertical singlet excitation energies of polyenes with N π-electrons computed using MR-CISD and MR-CISD+P for the (a) $2A_g^-$, (b) $1B_u^+$, and (c) $2B_u^-$ states. The height of each bar indicates the difference between the MR-CISD result (top of the bar) and the MR-CISD+P result (denoted by the marker). Calculations were performed with the cc-pVDZ basis set.

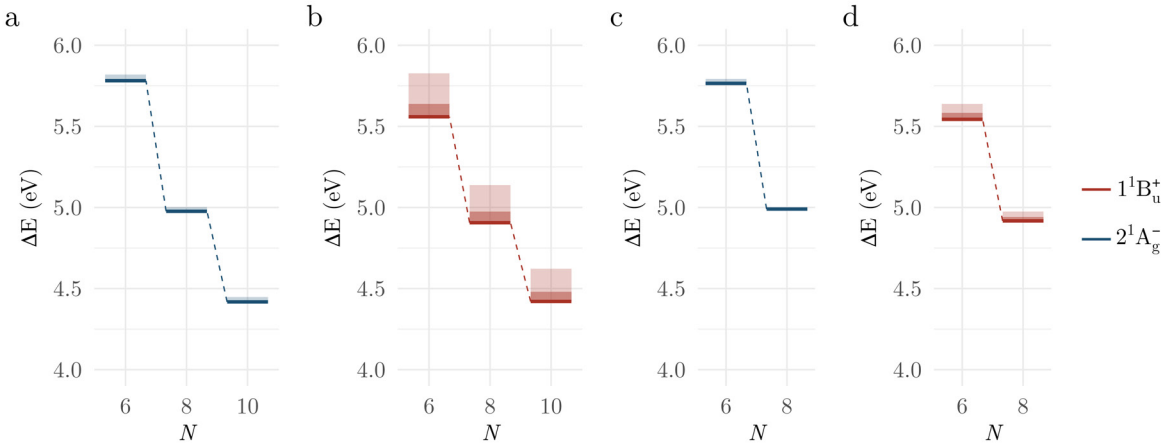

FIGURE B.2 – Vertical singlet excitation energies of polyenes with N π-electrons, obtained by extrapolating MR-CISD+P results to the complete basis set limit using (a, b) DT and (c, d) TQ extrapolations. The height of the lighter shaded bar indicates the difference between excitation energies obtained with the smaller and larger basis sets. The height of the darker shaded bar represents the difference between the larger basis set result and the extrapolated CBS value (represented by the marker).

B.2.1 An extrapolation for $N = 12$

An extrapolation for $N = 12$, both for the cc-pVTZ' basis set and for ΔE_{DT}^{∞} results, was performed using a 3-point power function fit. This fitting approach was chosen because it best predicts the excitation energy for dodecahexaene using the cc-pVDZ basis set, where the actual excitation energies are known (Figure B.3). Additionally, it aligns with the decrease in excitation energies observed for $N = 6 - 10$ when expanding from the double- to triple-ζ basis set.

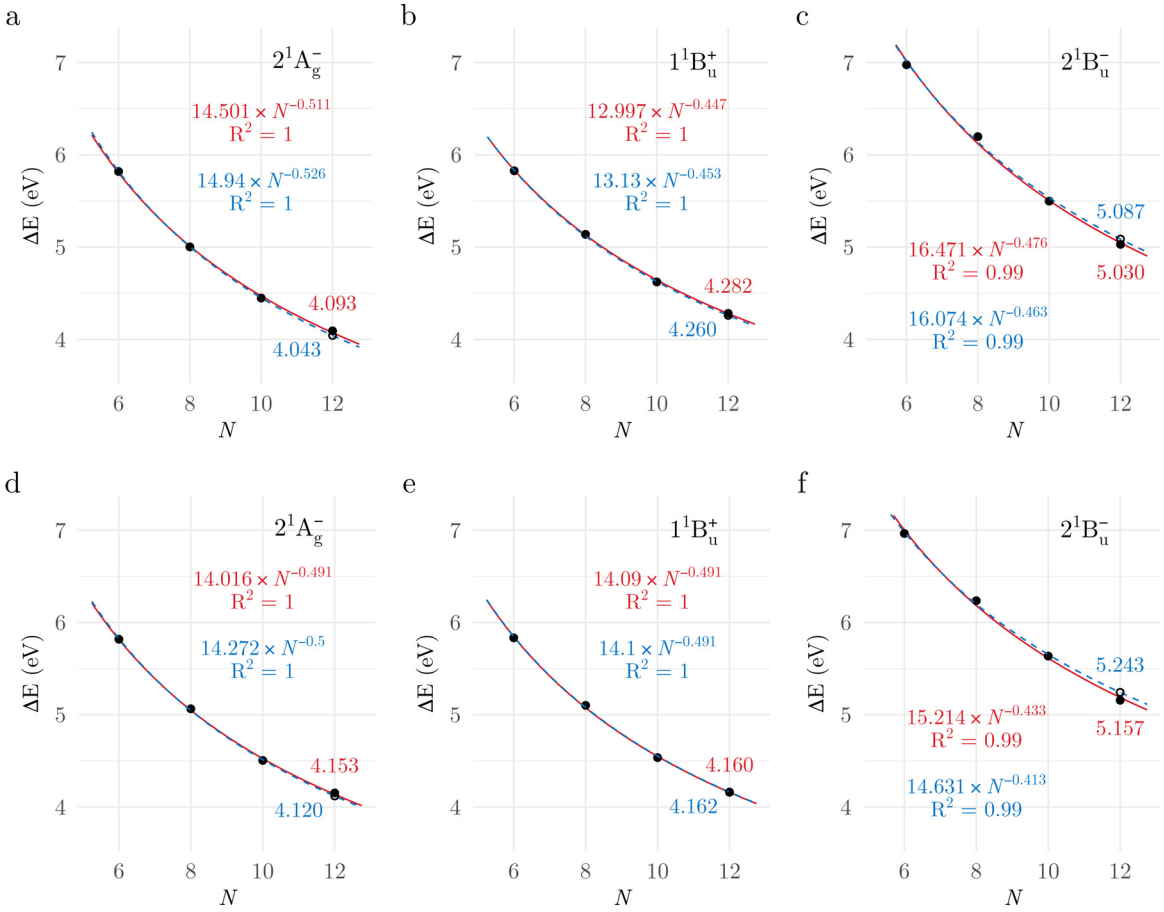

FIGURE B.3 – Vertical singlet excitation energies for the $2A_g^-$, $1B_u^+$, and $2B_u^-$ states of polyenes with N π-electrons calculated at the (a-c) MRCI+P and (d-f) MR-AQCC levels using the cc-pVDZ basis set. The dashed line represents the 3-point power function fit, while the solid line represents the 4-point power function fit. Numerical values for the actual (red) and estimated (blue) excitation energies are shown for $N = 12$. The equation and the coefficient of determination (R^2) for the 4-point (red) and 3-point (blue) power function fits are shown.

Based on the MR-CISD+P results using the cc-pVDZ basis set, this approach underestimates the excitation energy for the $2A_g^-$ and $1B_u^+$ states of dodecahexaene by 0.05 eV and 0.02 eV, respectively. For the $2B_u^-$ state, the excitation energy is overestimated by 0.06 eV. Slightly better results are also observed for the MR-AQCC estimates, where the excitation energy for the $2A_g^-$ state is underestimated by 0.03 eV, no difference between

the estimated and the actual excitation energy is observed for the $1B_u^+$ state, and the excitation energy for the $2B_u^-$ state is overestimated by 0.09 eV. The estimates for $N = 12$, both for the cc-pVTZ' basis set (Figure B.4) and for ΔE_{DT}^{∞} extrapolates values (Figure B.5), are presented below.

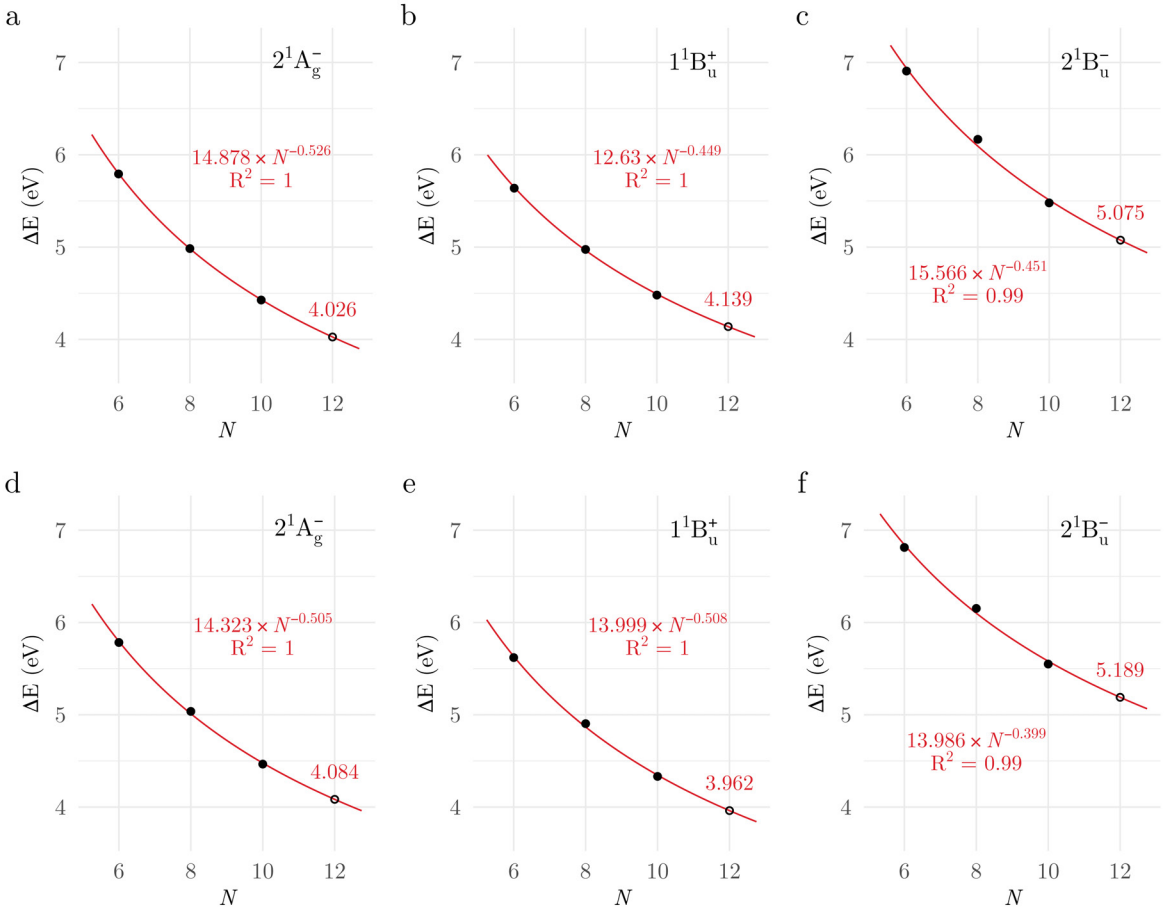

FIGURE B.4 – Vertical singlet excitation energies for the $2A_g^-$, $1B_u^+$, and $2B_u^-$ states of polyenes with N π-electrons calculated at the (a-c) MRCI+P and (d-f) MR-AQCC levels using the cc-pVTZ' basis set. The line indicates the 3-point power function fit. The estimated excitation energies for $N = 12$ are indicated. The equation and the coefficient of determination (R^2) for the 3-point power function fit are shown.

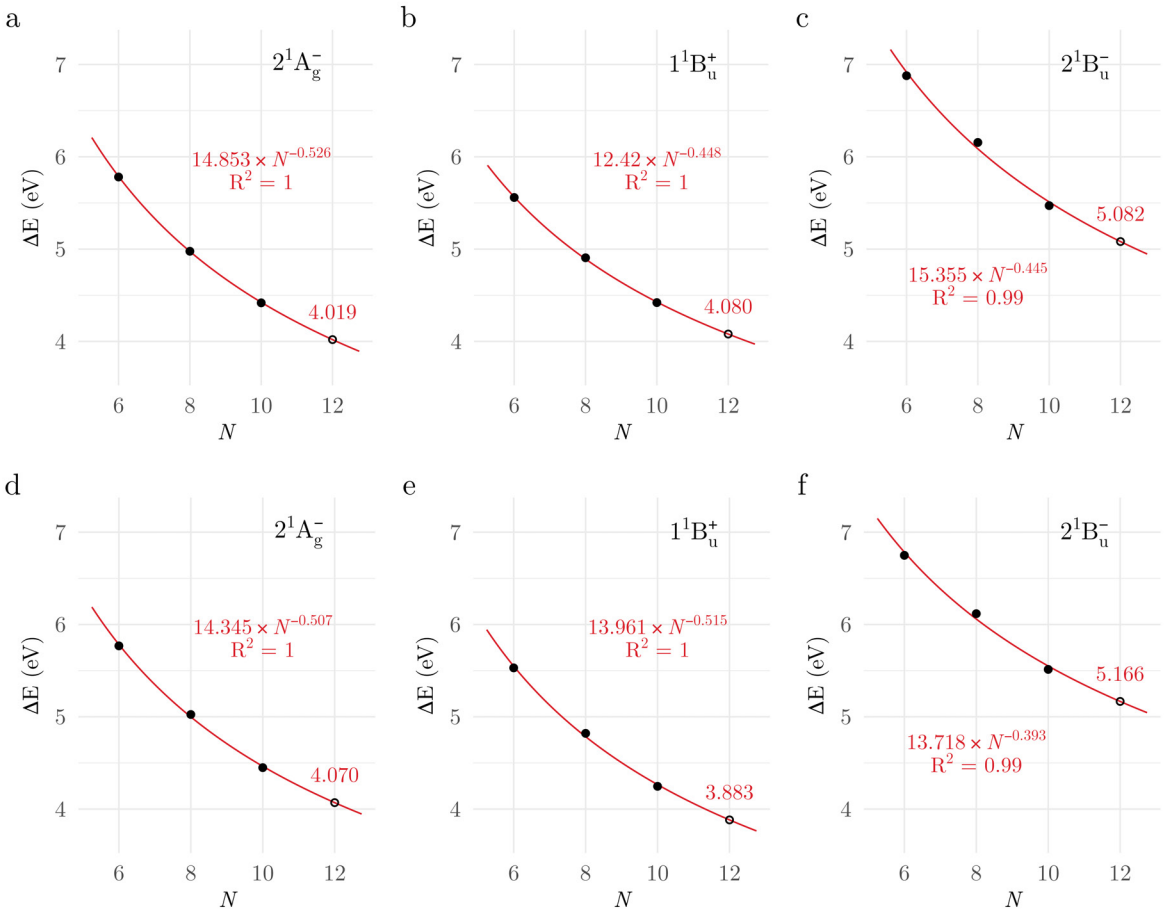

FIGURE B.5 – Vertical singlet excitation energies for the $2A_g^-$, $1B_u^+$, and $2B_u^-$ states of polyenes with N π-electrons calculated at the (a-c) MRCI+P and (d-f) MR-AQCC levels extrapolated from the double- to the triple-ζ basis set (ΔE_{DT}^{∞}). The line indicates the 3-point power function fit. The estimated excitation energies for $N = 12$ are indicated. The equation and the coefficient of determination (R^2) for the 3-point power function fit are shown.

B.3 Triplet states

TABLE B.3 – Triplet excitation energies (eV) of polyenes with N π-electrons calculated at the MR-CISD+P level using a variety of basis sets.

N	Excitation	$\Delta E_{\text{cc-pVDZ}}$[1]	$\Delta E_{\text{cc-pVTZ}}$[2]	$\Delta E_{\text{cc-pVQZ}}$[3]
6	$1^1A_g^- - 1^3A_g^-$	4.608	4.627	4.595
	$1^1A_g^- - 1^3B_u^-$	2.948	2.948	2.941
8	$1^1A_g^- - 1^3A_g^-$	3.933	3.928	3.934
	$1^1A_g^- - 1^3B_u^-$	2.581	2.578	2.581

[1] cc-pVDZ (H: $(4s,1p)/[2s,1p]$, C: $(9s,4p,1d)/[3s,2p,1d]$).
[2] cc-pVTZ (H: $(4s,1p)/[2s,1p]$, C: $(10s,5p,2d)/[4s,3p,2d]$).
[3] cc-pVQZ (H: $(4s,1p)/[2s,1p]$, C: $(12s,6p,3d,2f)/[5s,4p,3d,2f]$).

TABLE B.4 – Triplet excitation energies (eV) of polyenes with N π-electrons calculated at the MR-AQCC level using a variety of basis sets.

N	Excitation	$\Delta E_{\text{cc-pVDZ}}$[1]	$\Delta E_{\text{cc-pVTZ}}$[2]	$\Delta E_{\text{cc-pVQZ}}$[3]
6	$1^1A_g^- - 1^3A_g^-$	4.598	4.548	4.570
	$1^1A_g^- - 1^3B_u^-$	2.945	2.942	2.935
8	$1^1A_g^- - 1^3A_g^-$	3.928	3.913	3.908
	$1^1A_g^- - 1^3B_u^-$	2.562	2.557	2.557

[1] cc-pVDZ (H: $(4s,1p)/[2s,1p]$, C: $(9s,4p,1d)/[3s,2p,1d]$).
[2] cc-pVTZ (H: $(4s,1p)/[2s,1p]$, C: $(10s,5p,2d)/[4s,3p,2d]$).
[3] cc-pVQZ (H: $(4s,1p)/[2s,1p]$, C: $(12s,6p,3d,2f)/[5s,4p,3d,2f]$).

B.4 Natural transition orbitals and transition densities

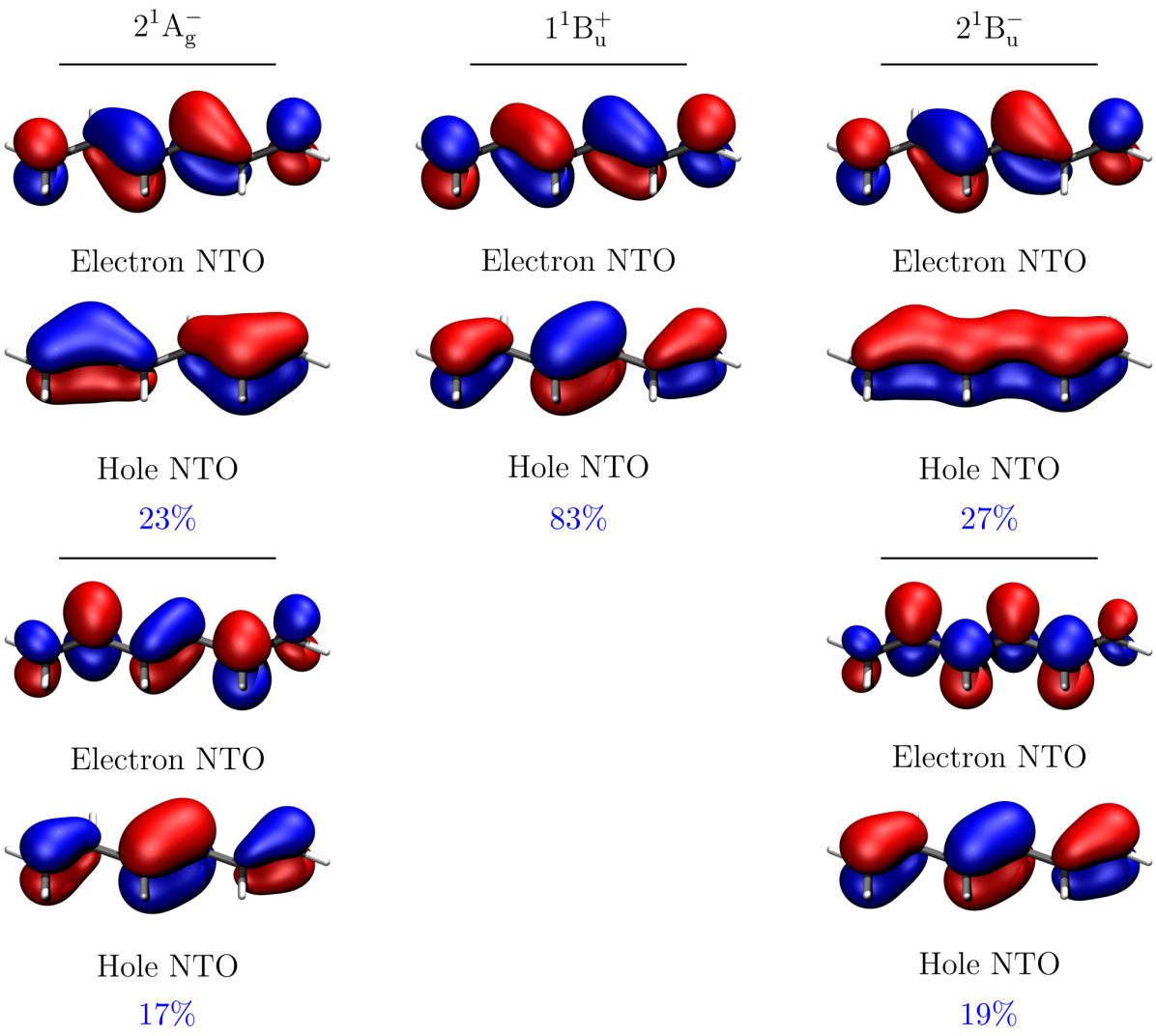

FIGURE B.6 – Natural transition orbitals (isovalue: ±0.05 a.u.). The dominant pair of natural transition orbitals and their contribution to the excitation are shown for the $2^1A_g^-$, $1^1B_u^+$, and $2^1B_u^-$ states of hexatriene.

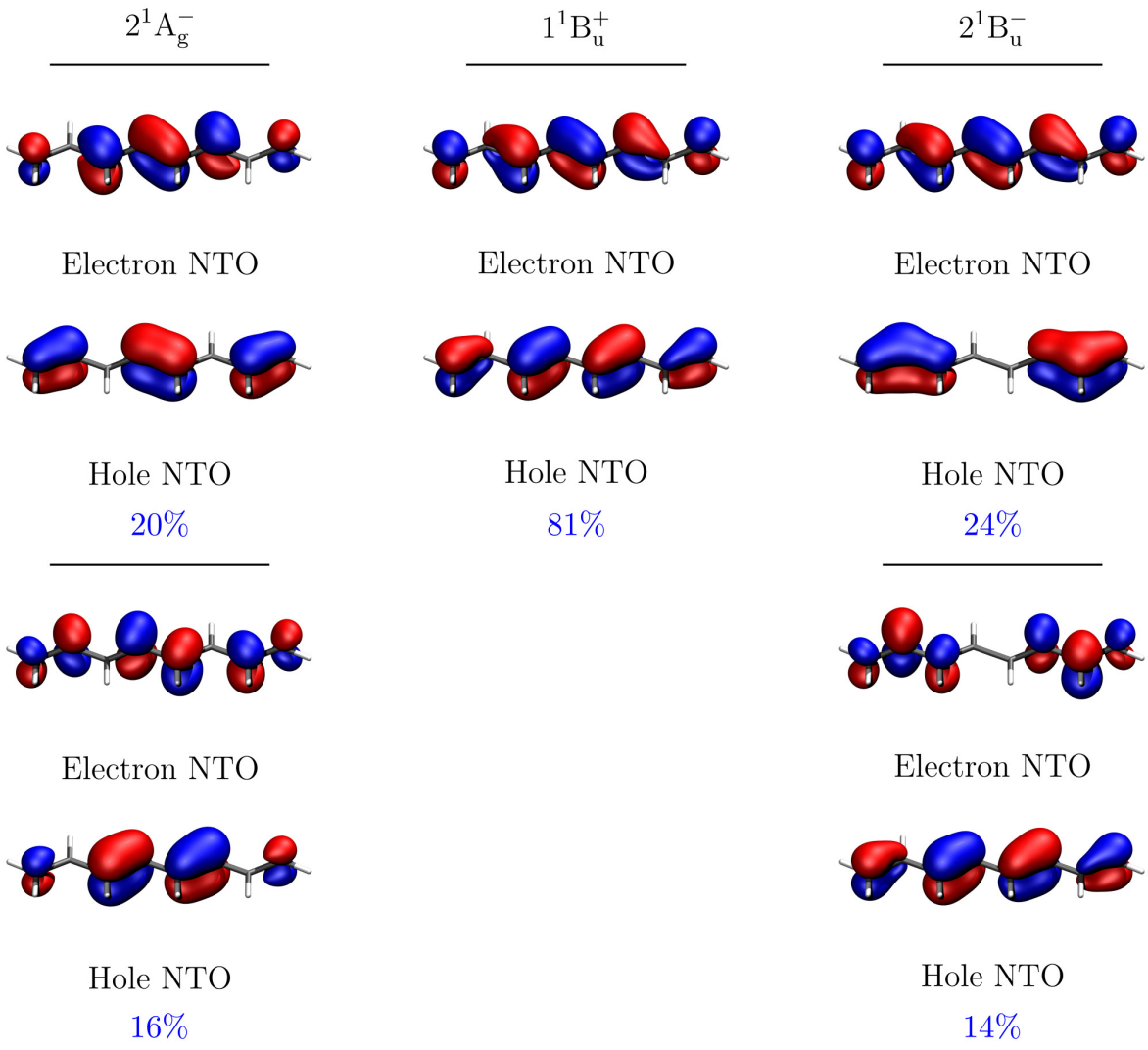

FIGURE B.7 – Natural transition orbitals (isovalue: ±0.05 a.u.). The dominant pair of natural transition orbitals and their contribution to the excitation are shown for the $2^1A_g^-$, $1^1B_u^+$, and $2^1B_u^-$ states of octatetraene.

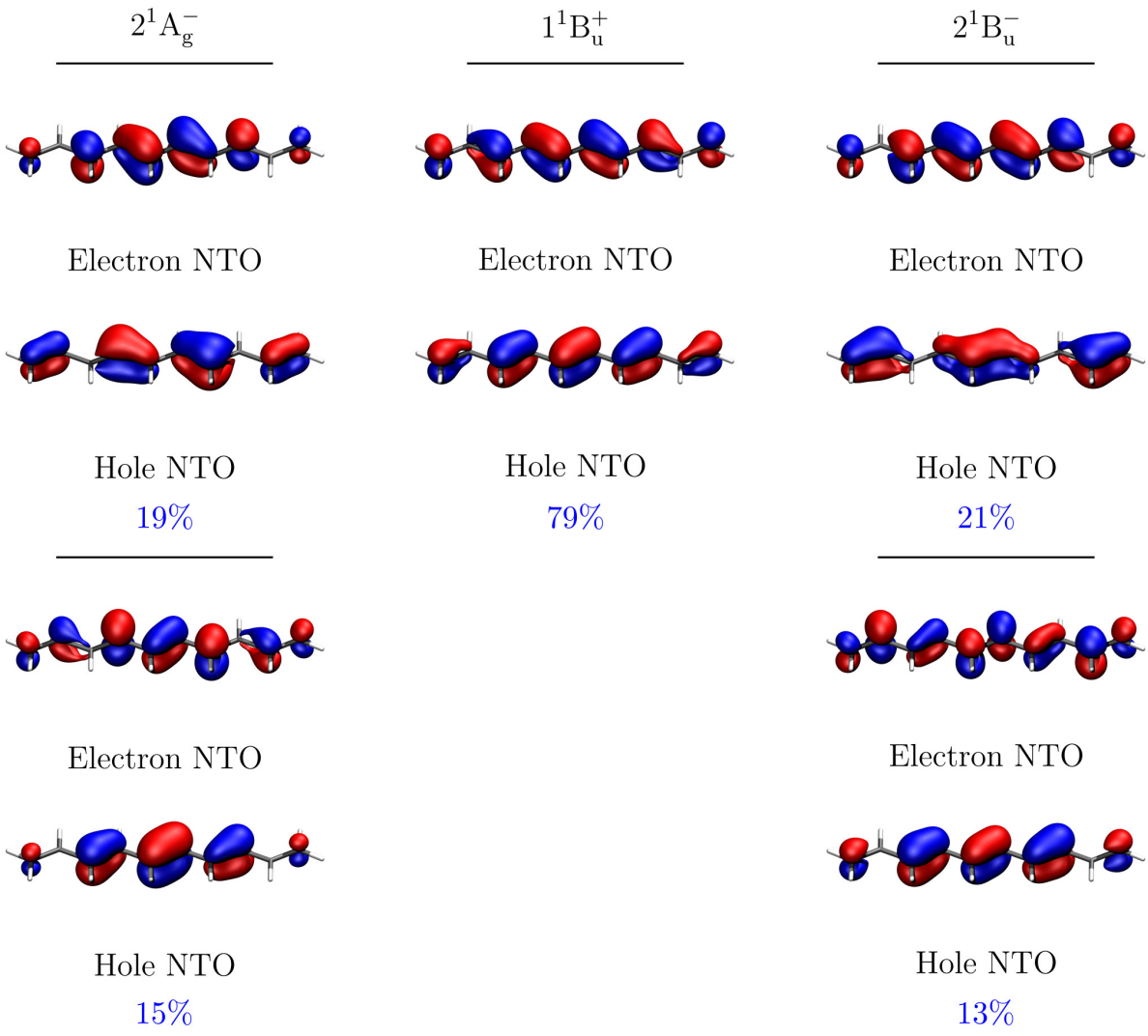

FIGURE B.8 – Natural transition orbitals (isovalue: ±0.05 a.u.). The dominant pair of natural transition orbitals and their contribution to the excitation are shown for the $2^1A_g^-$, $1^1B_u^+$, and $2^1B_u^-$ states of decapentaene.

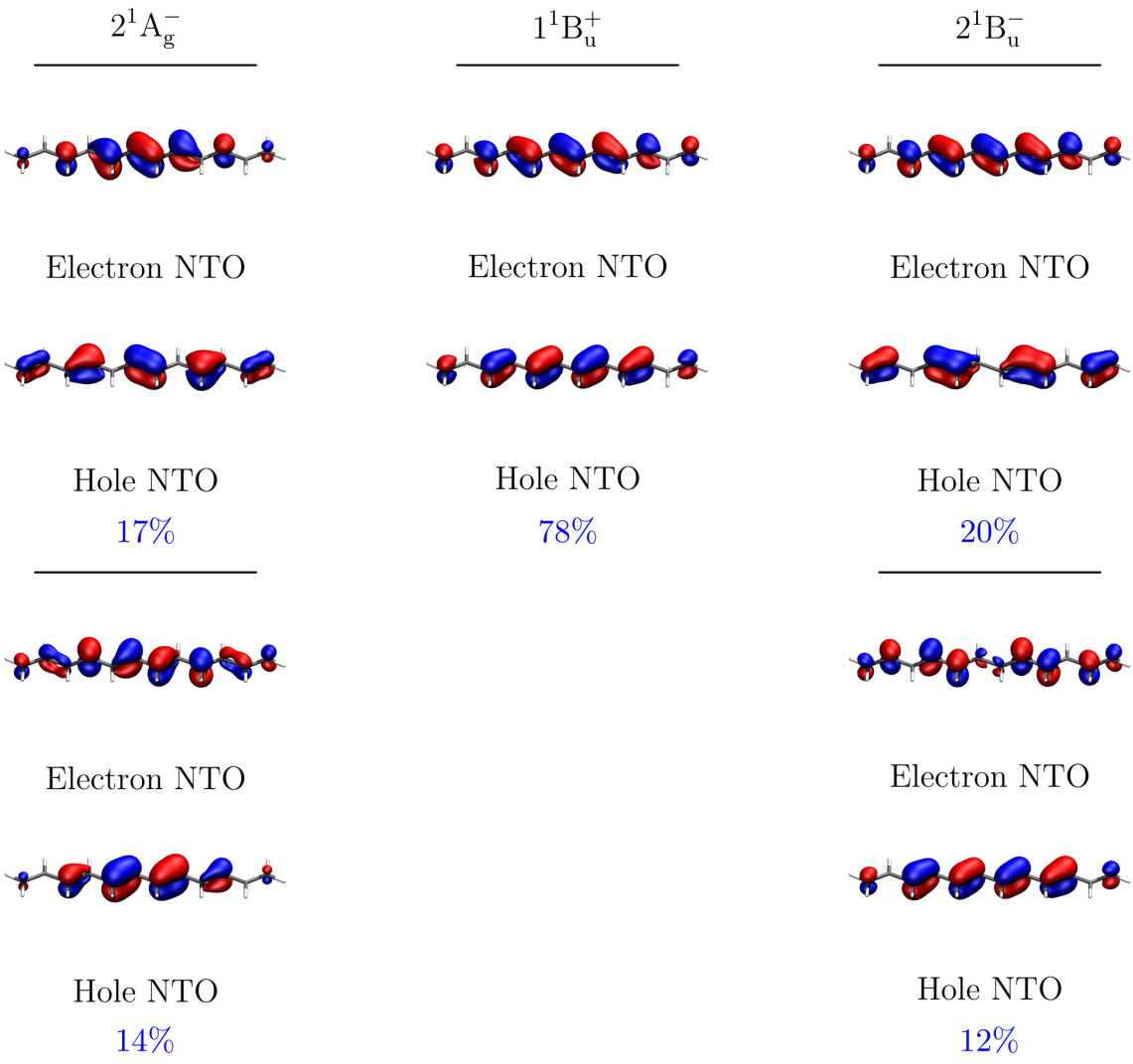

FIGURE B.9 – Natural transition orbitals (isovalue: ±0.05 a.u.). The dominant pair of natural transition orbitals and their contribution to the excitation are shown for the $2^1A_g^-$, $1^1B_u^+$, and $2^1B_u^-$ states of dodecahexaene.

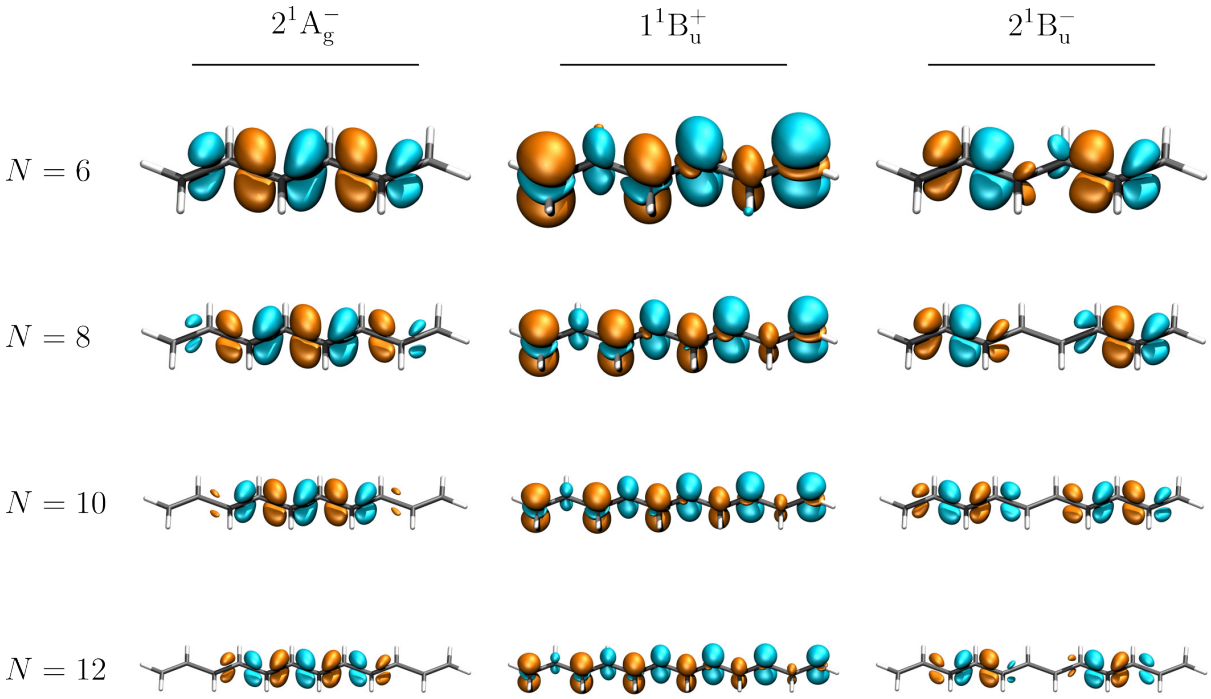

FIGURE B.10 – Transition densities (isovalue: ±0.002 a.u.) of the excited states $2^1A_g^-$, $1^1B_u^+$, and $2^1B_u^-$ of polyenes with N π-electrons calculated with respect to the ground state at the MR-CISD level of theory.

TABLE B.5 – Transition dipole moment, $\vec{\mu}_{0I}$, (e·bohr) and oscillator strength, f, for the transition from $1A_g^-$ to $2^1A_g^-$, $1^1B_u^+$, and $2^1B_u^-$ calculated using CASSCF and MR-CISD.

N	CASSCF		MR-CISD	
	$\vec{\mu}_{0I}$	f	$\vec{\mu}_{0I}$	f
		$2^1A_g^-$		
6	0.000000	0.000000	0.000000	0.000000
8	0.000000	0.000000	0.000000	0.000000
10	0.000000	0.000000	0.000000	0.000000
12	0.000000	0.000000	0.000000	0.000000
		$1^1B_u^+$		
6	2.788669	1.449741	2.851668	1.277410
8	3.310041	1.856344	3.489630	1.713239
10	3.766966	2.241605	4.072724	2.158272
12	4.171382	2.610051	4.605338	2.586742
		$2^1B_u^-$		
6	0.014323	0.000035	0.110412	0.002104
8	0.019647	0.000059	0.095771	0.001426
10	0.034695	0.000167	0.092181	0.001215
12	0.035388	0.000160	0.047863	0.000302

B.5 Transition charges

Transition charge (q_M^{t}) on each atom, calculated as the sum over the diagonal elements of the one-electron transition density matrix (1TDM) between the states of interest and the ground state for hexatriene, octatetraene, decapentaene, and dodecahexaene. Results were obtained at the MR-CISD/cc-pVDZ level of theory.

Hexatriene			
	$2A_g^-$	$1B_u^+$	$2B_u^-$
C	-0.02166	0.20236	-0.02192
C	-0.02166	-0.20236	0.02192
C	0.01845	-0.04893	0.01487
C	0.01845	0.04893	-0.01487
C	0.00327	0.14398	0.01994
C	0.00327	-0.14398	-0.01994
H	0.00051	0.01467	0.00023
H	0.00051	-0.01467	-0.00023
H	-0.00048	0.01403	-0.00047
H	-0.00048	-0.01403	0.00047
H	0.00009	0.00556	-0.00043
H	0.00009	-0.00556	0.00043
H	-0.00019	0.00628	-0.00068
H	-0.00019	-0.00628	0.00068

Octatetraene			
	$2A_g^-$	$1B_u^+$	$2B_u^-$
C	0.01004	-0.08974	-0.01294
C	0.01004	0.08974	0.01294
C	-0.00566	0.13612	0.01807
C	-0.00566	-0.13612	-0.01807
C	0.01223	-0.02572	0.01748
C	0.01223	0.02572	-0.01748
C	-0.01624	0.15206	-0.02435
C	-0.01624	-0.15206	0.02435
H	-0.00004	-0.00060	-0.00002
H	-0.00004	0.00060	0.00002
H	-0.00017	0.00773	0.00005
H	-0.00017	-0.00773	-0.00005
H	0.00000	0.00581	0.00002
H	0.00000	-0.00581	-0.00002
H	-0.00042	0.01037	-0.00050
H	-0.00042	-0.01037	0.00050
H	0.00026	0.01146	0.00041
H	0.00026	-0.01146	-0.00041

Decapentaene			
	$2A_g^-$	$1B_u^+$	$2B_u^-$
C	-0.01088	-0.12008	-0.01974
C	-0.01088	0.12008	0.01974
C	0.00762	0.01559	0.01342
C	0.00762	-0.01559	-0.01342
C	-0.00820	-0.11789	0.00445
C	-0.00820	0.11789	-0.00445
C	0.00936	0.05925	0.00059
C	0.00936	-0.05925	-0.00059
C	0.00250	-0.09716	0.02085
C	0.00250	0.09716	-0.02085
H	0.00007	-0.00937	0.00014
H	0.00007	0.00937	-0.00014
H	-0.00027	-0.00823	-0.00039
H	-0.00027	0.00823	0.00039
H	-0.00002	-0.00480	0.00006
H	-0.00002	0.00480	-0.00006
H	-0.00014	-0.00727	0.00009
H	-0.00014	0.00727	-0.00009
H	-0.00002	-0.00121	0.00006
H	-0.00002	0.00121	-0.00006
H	-0.00001	-0.00344	0.00002
H	-0.00001	0.00344	-0.00002

Dodecahexaene			
	$2A_g^-$	$1B_u^+$	$2B_u^-$
C	0.00831	-0.09883	-0.01461
C	0.00831	0.09883	0.01461
C	-0.00523	0.01204	0.00955
C	-0.00523	-0.01204	-0.00955
C	0.00783	-0.10063	-0.00262
C	0.00783	0.10063	0.00262
C	-0.00778	0.04196	0.00643
C	-0.00778	-0.04196	-0.00643
C	0.00115	-0.09678	0.01761
C	0.00115	0.09678	-0.01761
C	-0.00482	0.07479	-0.01301
C	-0.00482	-0.07479	0.01301
H	0.00023	-0.00654	-0.00029
H	0.00023	0.00654	0.00029
H	0.00000	-0.00766	0.00013
H	0.00000	0.00766	-0.00013
H	0.00004	-0.00404	0.00005
H	0.00004	0.00404	-0.00005
H	0.00015	-0.00630	0.00007
H	0.00015	0.00630	-0.00007
H	0.00005	-0.00205	0.00010
H	0.00005	0.00205	-0.00010
H	0.00009	-0.00435	0.00018
H	0.00009	0.00435	-0.00018
H	-0.00002	0.00123	0.00000
H	-0.00002	-0.00123	0.00000

B.6 Equilibrium geometries

Equilibrium geometries (Å) obtained at the ωB97X-D/cc-pVTZ level of theory for hexatriene, octatetraene, decapentaene, and dodecahexaene.

Hexatriene			
C	1.199785	2.813176	0.000000
C	1.199785	1.483143	0.000000
C	-0.001156	0.668414	0.000000
C	0.001156	-0.668414	0.000000
C	-1.199785	-1.483143	0.000000
C	-1.199785	-2.813176	0.000000
H	2.120872	3.378561	0.000000
H	0.273669	3.375164	0.000000
H	2.145268	0.949588	0.000000
H	-0.950722	1.196588	0.000000
H	0.950722	-1.196588	0.000000
H	-2.145268	-0.949588	0.000000
H	-2.120872	-3.378561	0.000000
H	-0.273669	-3.375164	0.000000

Octatetraene			
C	0.002067	0.722228	0.000000
C	-0.002067	-0.722228	0.000000
C	1.112008	1.471079	0.000000
C	-1.112008	-1.471079	0.000000
C	1.112008	2.920760	0.000000
C	-1.112008	-2.920760	0.000000
C	2.212462	3.668584	0.000000
C	-2.212462	-3.668584	0.000000
H	-0.965580	1.216443	0.000000
H	0.965580	-1.216443	0.000000
H	2.081206	0.980083	0.000000
H	-2.081206	-0.980083	0.000000
H	0.140113	3.404728	0.000000
H	-0.140113	-3.404728	0.000000
H	3.197764	3.218273	0.000000
H	-3.197764	-3.218273	0.000000
H	2.162014	4.748277	0.000000
H	-2.162014	-4.748277	0.000000

Decapentaene			
C	2.398511	4.962720	0.000000
C	2.392909	3.631995	0.000000
C	1.191228	2.821795	0.000000
C	1.191228	1.482319	0.000000
C	-0.001340	0.670478	0.000000
C	0.001340	-0.670478	0.000000
C	-1.191228	-1.482319	0.000000
C	-1.191228	-2.821795	0.000000
C	-2.392909	-3.631995	0.000000
C	-2.398511	-4.962720	0.000000
H	3.322048	5.523983	0.000000
H	1.474714	5.528448	0.000000
H	3.336944	3.095691	0.000000
H	0.242564	3.351439	0.000000
H	2.142576	0.957164	0.000000
H	-0.953055	1.194701	0.000000
H	0.953055	-1.194701	0.000000
H	-2.142576	-0.957164	0.000000
H	-0.242564	-3.351439	0.000000
H	-3.336944	-3.095691	0.000000
H	-1.474714	-5.528448	0.000000
H	-3.322048	-5.523983	0.000000

Dodecahexaene			
C	0.080392	6.739396	0.000000
C	0.651879	5.537613	0.000000
C	-0.080392	4.286915	0.000000
C	0.500160	3.079561	0.000000
C	-0.223280	1.831635	0.000000
C	0.360806	0.623803	0.000000
C	-0.360806	-0.623803	0.000000
C	0.223280	-1.831635	0.000000
C	-0.500160	-3.079561	0.000000
C	0.080392	-4.286915	0.000000
C	-0.651879	-5.537613	0.000000
C	-0.080392	-6.739396	0.000000
H	-0.997217	6.850054	0.000000
H	0.669422	7.645568	0.000000
H	1.735021	5.463469	0.000000
H	-1.164771	4.353107	0.000000
H	1.584980	3.017966	0.000000
H	-1.307984	1.891932	0.000000
H	1.445625	0.564353	0.000000
H	-1.445625	-0.564353	0.000000
H	1.307984	-1.891932	0.000000
H	-1.584980	-3.017966	0.000000
H	1.164771	-4.353107	0.000000
H	-1.735021	-5.463469	0.000000
H	0.997217	-6.850054	0.000000
H	-0.669422	-7.645568	0.000000

B.7 Analytical harmonic frequencies

Analytical harmonic frequencies (cm^{-1}) obtained at the ωB97X-D/cc-pVTZ level of theory for hexatriene, octatetraene, decapentaene, and dodecahexaene.

Hexatriene		
95.1336	150.7519	211.5209
255.9578	358.0191	449.7425
552.9187	623.9102	723.5179
922.7781	955.8464	956.0392
961.8523	985.5939	990.8484
1040.3897	1066.1807	1161.3261
1227.9621	1291.7130	1328.4505
1340.8802	1345.6464	1446.5141
1473.9792	1671.2505	1723.0189
1746.7017	3149.7507	3150.2842
3154.8230	3156.4427	3164.5415
3165.1372	3249.6232	3249.6284

Octatetraene		
58.0065	89.0457	146.4513
175.5533	227.9791	240.0637
344.6555	354.0860	398.7137
551.7074	580.3276	652.7047
695.0033	888.7538	938.3310
955.8429	956.6633	958.9506
976.4411	980.2533	1011.2405
1049.5024	1064.4052	1166.2661
1168.0533	1222.3243	1266.3935
1319.7383	1330.9599	1335.5178
1349.4858	1354.2800	1454.1398
1471.3191	1661.5676	1705.9223
1734.7093	1739.2413	3148.1013
3148.7343	3149.8237	3153.2998
3155.0322	3157.3526	3163.2744
3163.2856	3248.6255	3248.6352

Decapentaene		
39.4430	57.8961	102.6391
135.8017	153.3818	188.0334
236.1301	280.1418	280.8487
288.1648	399.2763	422.3690
496.9841	558.7764	611.5585
664.1020	682.5410	866.8573
917.9226	944.6001	954.3713
957.4848	968.9806	969.7571
970.2775	994.8173	1026.4846
1054.9110	1064.4060	1152.0253
1174.2786	1183.1725	1218.5637
1253.4684	1294.2542	1326.8542
1334.1048	1339.2740	1340.2768
1351.3754	1369.1895	1458.2054
1468.7348	1654.9311	1692.9295
1722.7413	1726.9375	1741.5269
3147.5963	3148.5767	3150.0570
3150.2509	3153.3100	3155.4337
3156.7557	3158.7931	3164.1468
3164.2666	3250.2006	3250.2055

Dodecahexaene		
27.6903	41.0313	74.1112
109.8725	111.5806	144.5454
191.3733	205.0345	236.7164
242.8161	250.2331	318.1396
338.1497	422.0856	423.0473
458.9032	527.6242	598.2838
614.5657	669.4709	677.4618
852.4118	899.0680	930.3173
947.2338	955.0495	956.3252
964.1880	967.9921	971.4348
983.6979	1008.9724	1035.8579
1057.4033	1063.7771	1154.2571
1156.0488	1184.5556	1188.2643
1215.0575	1244.8060	1277.1561
1313.3899	1330.6529	1333.0156
1338.0394	1344.1399	1345.3504
1352.6804	1382.8629	1460.6322
1467.4463	1649.8524	1683.0881
1712.0727	1714.6204	1736.3313
1737.6193	3148.3766	3148.5279
3149.7143	3150.0582	3150.6570
3153.3075	3154.9248	3156.1179
3157.9038	3159.9644	3163.9478
3164.0574	3248.9081	3248.9105

Appendix C - Supplementary Information for Chapter 6

C.1 Adiabatic excitation energies

Based on the optimized geometry of each state obtained via analytical energy gradients based on the MR-CISD wavefunction using the cc-pVDZ basis set, MR-CISD+P single point calculations were performed to analyze the effect of the basis set on adiabatic excitation energies (Table C.1).

TABLE C.1 – Adiabatic excitation energies (eV) of polyenes with N π electrons computed at the MR-CISD+P level. Values computed using the cc-pVDZ basis set (ΔE_D), cc-pVTZ basis set (ΔE_T), as well as values extrapolated from double-zeta to triple-zeta (ΔE_{DT}^{∞}), are presented. All values are based on the minimum of each state obtained via analytical energy gradients based on the MR-CISD wavefunction using the cc-pVDZ basis set.

N	State	ΔE_D	ΔE_T	ΔE_{DT}^{∞}
6	$2^1A_g^-$	4.365	4.439	4.471
	$1^1B_u^+$	5.335	5.239	5.199
8	$2^1A_g^-$	3.645	3.718	3.748
	$1^1B_u^+$	4.698	4.761	4.787
10	$2^1A_g^-$	3.122	3.193	3.222
	$1^1B_u^+$	4.236	4.205	4.192

C.2 Vertical excitation energies

Based on the optimized geometry of the ground state obtained via analytical energy gradients based on the MR-CISD wavefunction using the cc-pVDZ basis set, MR-CISD+P single point calculations were performed to analyze the effect of the basis set on vertical excitation energies (Table C.2).

TABLE C.2 – Vertical excitation energies (eV) of singlet states in polyenes with N π-electrons computed at the MR-CISD+P level. The ground-state geometry was optimized via analytic energy gradients based on the MR-CISD wavefunction using the cc-pVDZ basis set. Reference theoretical values and experimental data are provided for comparison.

N	State	MR-CISD+P			CASPT2	Exp.
		ΔE_D	ΔE_T	ΔE_{DT}^{∞}		
6	$2^1A_g^-$	5.422	5.382	5.365	5.420[a]; 5.09[b]	-
	$1^1B_u^+$	5.635	5.499	5.442	5.363[a]; 5.10[b]	4.93[d]; 4.93[e]
8	$2^1A_g^-$	4.648	4.623	4.613	4.46[c]; 4.47[b]	4.1[f]
	$1^1B_u^+$	4.968	4.867	4.825	4.35[c]; 4.66[b]	4.40[g]; 4.41[h]; 4.41[i]; 4.41[j]
10	$2^1A_g^-$	4.087	4.066	4.057	3.65[b]	3.5[k]
	$1^1B_u^+$	4.479	4.398	4.364	4.05[b]	3.98[l]

[a] Ground-state geometry optimized at CASSCF/NEVPT2 level; single-point energy at CASPT2 level.[1]

[b] Ground-state geometry optimized at CASSCF level; single-point energy at CASPT2 level.[2]

[c] Ground-state geometry optimized at CASSCF level; single-point energy at CASPT2 level.[3]

[d] Absorption band maximum of the spectrum for the isolated compound.[4]

[e] Absorption band maximum of the spectrum for the jet-cooled compound.[5]

[f] Estimated assuming mirror symmetry between absorption and emission. 0-0 excitation energy from Table 2 and emission band maximum from Table 3.

[g] Absorption band maximum of the spectrum for the isolated compound.[6]

[h] Absorption band maximum of the spectrum for the isolated compound.[7]

[i] Absorption band maximum of the spectrum for the jet-cooled compound.[8]

[j] Absorption band maximum of the spectrum for the jet-cooled compound.[9]

[k] Estimated assuming mirror symmetry between absorption and emission. 0-0 excitation data from Table 2 and emission band maximum data from Table 3.

[l] Absorption band maximum in condensed phase, corrected to gas phase using solvent shift theory.[10]

Note that the accuracy of experimental data for each state differs significantly due to their accessibility in one-photon processes. Experimental estimates for the vertical excitation energies of the $2^1A_g^-$ state rely on the mirror-image symmetry assumption, which posits that the energy difference between the (0-0) and vertical excitation energies is equal to the difference between the (0-0) and fluorescence intensity maximum−i.e., vertical excitation energies are estimated as $(0-0)+[(0-0)-\lambda_{\mathrm{emi}}^{\mathrm{max}}]$. On the other hand, for the $1^1B_u^+$ state, which is dipole-allowed and easily accessible in one-photon processes, the 0-0 excitation band also corresponds to the most intense absorption band.[11] We can also estimate the vertical excitation energy based on a mirror-image approximation using the MR-CISD+P values for adiabatic excitation (Table 2) and vertical emission energy (Table 3). This yields values of 5.10 eV for hexatriene, 4.33 eV for octatetraene, and 3.74 eV for decapentaene. For the two largest members, this represents an overestimation of approximately 0.2 eV with respect to the experimental estimate obtained via the mirror-image approximation.

C.3 Equilibrium geometries

CC bond lengths

The carbon numbering system is shown in Figure C.1. The CC bond lengths of the studied systems in the ground and excited states, at their relaxed geometries obtained via analytical energy gradients based on the MR-CISD wavefunction, are presented in Table C.3.

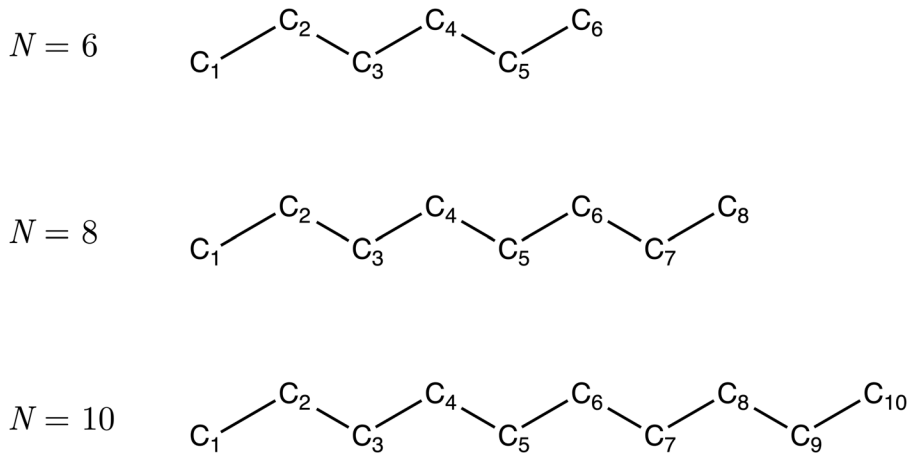

FIGURE C.1 – Atom numbering system used to label bonds in the studied polyenes with N π-electrons.

TABLE C.3 – Calculated CC bond lengths (Å) in polyenes with N π-electrons in the ground and excited states at their relaxed geometries, obtained via analytical energy gradients based on the MR-CISD wavefunction under the C_{2h} symmetry constraint. Atom numbering follows Figure C.1. Values within parenthesis obtained at the CASSCF level.[2]

State	N	Bond				
		C_1–C_2	C_2–C_3	C_3–C_4	C_4–C_5	C_5–C_6
$1^1A_g^-$	6	1.353 (1.338)	1.458 (1.469)	1.360 (1.345)	–	–
	8	1.351 (1.345)	1.454 (1.457)	1.361 (1.351)	1.450 (1.451)	–
	10	1.350 (1.346)	1.450 (1.454)	1.359 (1.351)	1.445 (1.450)	1.362 (1.352)
$2^1A_g^-$	6	1.468 (1.445)	1.390 (1.383)	1.447 (1.427)	–	–
	8	1.439 (1.432)	1.380 (1.369)	1.441 (1.432)	1.396 (1.390)	–
	10	1.413 (1.407)	1.381 (1.375)	1.439 (1.434)	1.389 (1.385)	1.426 (1.415)
$1^1B_u^+$	6	1.392 (1.395)	1.410 (1.397)	1.423 (1.423)	–	–
	8	1.377 (1.379)	1.417 (1.413)	1.407 (1.401)	1.400 (1.395)	–
	10	1.370 (1.369)	1.422 (1.430)	1.394 (1.406)	1.400 (1.406)	1.403 (1.425)

Equilibrium geometries (Å) of the states $1^1A_g^-$, $2^1A_g^-$, and $1^1B_u^+$ of hexatriene, octatetraene, and decapentaene, obtained via analytical gradients based on the MR-CISD wavefunction, are presented below.

Hexatriene

$1^1A_g^-$			
C	1.212244	2.846199	0.000000
C	-1.212244	-2.846199	0.000000
C	1.209667	1.493113	0.000000
C	-1.209667	-1.493113	0.000000
C	-0.000222	0.679762	0.000000
C	0.000222	-0.679762	0.000000
H	2.141056	3.410545	0.000000
H	-2.141056	-3.410545	0.000000
H	0.282941	3.413640	0.000000
H	-0.282941	-3.413640	0.000000
H	2.160163	0.958195	0.000000
H	-2.160163	-0.958195	0.000000
H	-0.954033	1.210056	0.000000
H	0.954033	-1.210056	0.000000

$2^1A_g^-$			
C	1.233633	2.938021	0.000000
C	-1.233633	-2.938021	0.000000
C	1.193689	1.470122	0.000000
C	-1.193689	-1.470122	0.000000
C	0.021076	0.723259	0.000000
C	-0.021076	-0.723259	0.000000
H	2.180707	3.465976	0.000000
H	-2.180707	-3.465976	0.000000
H	0.313851	3.515505	0.000000
H	-0.313851	-3.515505	0.000000
H	2.146903	0.942481	0.000000
H	-2.146903	-0.942481	0.000000
H	-0.933263	1.251796	0.000000
H	0.933263	-1.251796	0.000000

$1^1B_u^+$			
C	1.218192	2.879558	0.000000
C	-1.218192	-2.879558	0.000000
C	1.194535	1.487753	0.000000
C	-1.194535	-1.487753	0.000000
C	0.017830	0.711052	0.000000
C	-0.017830	-0.711052	0.000000
H	2.158063	3.422557	0.000000
H	-2.158063	-3.422557	0.000000
H	0.296328	3.457034	0.000000
H	-0.296328	-3.457034	0.000000
H	2.146105	0.954783	0.000000
H	-2.146105	-0.954783	0.000000
H	-0.939243	1.235209	0.000000
H	0.939243	-1.235209	0.000000

Octatetraene

$1^1A_g^-$			
C	-0.000898	0.725026	0.000000
C	0.000898	-0.725026	0.000000
C	1.126034	1.487443	0.000000
C	-1.126034	-1.487443	0.000000
C	1.120340	2.941139	0.000000
C	-1.120340	-2.941139	0.000000
C	2.235944	3.702764	0.000000
C	-2.235944	-3.702764	0.000000
H	-0.972102	1.219853	0.000000
H	0.972102	-1.219853	0.000000
H	2.098279	0.994667	0.000000
H	-2.098279	-0.994667	0.000000
H	0.145078	3.426970	0.000000
H	-0.145078	-3.426970	0.000000
H	3.226755	3.254049	0.000000
H	-3.226755	-3.254049	0.000000
H	2.180137	4.786974	0.000000
H	-2.180137	-4.786974	0.000000

$2^1A_g^-$			
C	-0.018907	0.697631	0.000000
C	0.018907	-0.697631	0.000000
C	1.153315	1.535873	0.000000
C	-1.153315	-1.535873	0.000000
C	1.119347	2.914973	0.000000
C	-1.119347	-2.914973	0.000000
C	2.286381	3.757313	0.000000
C	-2.286381	-3.757313	0.000000
H	-0.990206	1.190646	0.000000
H	0.990206	-1.190646	0.000000
H	2.123120	1.038485	0.000000
H	-2.123120	-1.038485	0.000000
H	0.146787	3.405382	0.000000
H	-0.146787	-3.405382	0.000000
H	3.282008	3.325100	0.000000
H	-3.282008	-3.325100	0.000000
H	2.193969	4.836871	0.000000
H	-2.193969	-4.836871	0.000000

$1^1B_u^+$			
C	-0.008571	0.699762	0.000000
C	0.008571	-0.699762	0.000000
C	1.142383	1.509457	0.000000
C	-1.142383	-1.509457	0.000000
C	1.127138	2.926565	0.000000
C	-1.127138	-2.926565	0.000000
C	2.252001	3.720900	0.000000
C	-2.252001	-3.720900	0.000000
H	-0.977814	1.198178	0.000000
H	0.977814	-1.198178	0.000000
H	2.112351	1.012203	0.000000
H	-2.112351	-1.012203	0.000000
H	0.150922	3.410943	0.000000
H	-0.150922	-3.410943	0.000000
H	3.248495	3.286620	0.000000
H	-3.248495	-3.286620	0.000000
H	2.173945	4.802826	0.000000
H	-2.173945	-4.802826	0.000000

Decapentaene

$1^1A_g^-$			
C	2.416384	5.002357	0.000000
C	-2.416384	-5.002357	0.000000
C	2.407503	3.652414	0.000000
C	-2.407503	-3.652414	0.000000
C	1.201562	2.846971	0.000000
C	-1.201562	-2.846971	0.000000
C	1.198528	1.487893	0.000000
C	-1.198528	-1.487893	0.000000
C	0.000309	0.680776	0.000000
C	-0.000309	-0.680776	0.000000
H	3.346030	5.561345	0.000000
H	-3.346030	-5.561345	0.000000
H	1.491757	5.573495	0.000000
H	-1.491757	-5.573495	0.000000
H	3.354588	3.115529	0.000000
H	-3.354588	-3.115529	0.000000
H	0.250404	3.377439	0.000000
H	-0.250404	-3.377439	0.000000
H	2.151363	0.960277	0.000000
H	-2.151363	-0.960277	0.000000
H	-0.953089	1.207124	0.000000
H	0.953089	-1.207124	0.000000

$2^1A_g^-$			
C	2.435702	5.057419	0.000000
C	-2.435702	-5.057419	0.000000
C	2.386735	3.645427	0.000000
C	-2.386735	-3.645427	0.000000
C	1.224197	2.900480	0.000000
C	-1.224197	-2.900480	0.000000
C	1.189830	1.461896	0.000000
C	-1.189830	-1.461896	0.000000
C	0.019737	0.712862	0.000000
C	-0.019737	-0.712862	0.000000
H	3.382080	5.584119	0.000000
H	-3.382080	-5.584119	0.000000
H	1.524219	5.646151	0.000000
H	-1.524219	-5.646151	0.000000
H	3.333840	3.108202	0.000000
H	-3.333840	-3.108202	0.000000
H	0.269870	3.424637	0.000000
H	-0.269870	-3.424637	0.000000
H	2.142878	0.936197	0.000000
H	-2.142878	-0.936197	0.000000
H	-0.931644	1.242232	0.000000
H	0.931644	-1.242232	0.000000

$1^1B_u^+$			
C	2.422001	5.018231	0.000000
C	-2.422001	-5.018231	0.000000
C	2.393339	3.648412	0.000000
C	-2.393339	-3.648412	0.000000
C	1.206515	2.865054	0.000000
C	-1.206515	-2.865054	0.000000
C	1.184692	1.471007	0.000000
C	-1.184692	-1.471007	0.000000
C	0.015114	0.701291	0.000000
C	-0.015114	-0.701291	0.000000
H	3.361133	5.559740	0.000000
H	-3.361133	-5.559740	0.000000
H	1.505474	5.601302	0.000000
H	-1.505474	-5.601302	0.000000
H	3.339408	3.109365	0.000000
H	-3.339408	-3.109365	0.000000
H	0.253591	3.392427	0.000000
H	-0.253591	-3.392427	0.000000
H	2.138762	0.945738	0.000000
H	-2.138762	-0.945738	0.000000
H	-0.939000	1.226661	0.000000
H	0.939000	-1.226661	0.000000

Bibliography

1 GUARESCHI, Riccardo; ANGELI, Celestino. The lowest singlet states of hexatriene revisited. **Theoretical Chemistry Accounts**, Springer Science and Business Media Deutschland GmbH, v. 142, n. 12, p. 127, Dec. 2023.

2 NAKAYAMA, Kenichi; NAKANO, Haruyuki; HIRAO, Kimihiko. Theoretical study of the $\pi\pi^*$ excited states of linear polyenes: The energy gap between 11Bu+ and 21Ag states and their character. **International Journal of Quantum Chemistry**, John Wiley & Sons, Inc, v. 66, n. 2, p. 157–175, 1998.

3 ANGELI, Celestino; PASTORE, Mariachiara. The lowest singlet states of octatetraene revisited. **The Journal of Chemical Physics**, v. 134, n. 18, May 2011.

4 GAVIN, R. M.; RISEMBERG, Salomon; RICE, Stuart A. Spectroscopic properties of polyenes. I. The lowest energy allowed singlet-singlet transition for cis- and trans-1,3,5-hexatriene. **The Journal of Chemical Physics**, v. 58, n. 8, p. 3160–3165, Apr. 1973.

5 LEOPOLD, D. G. et al. Direct absorption spectroscopy of jet-cooled polyenes. II. The $1^1B_u^+ \leftarrow 1^1A_g^-$ transitions of butadienes and hexatrienes. **The Journal of Chemical Physics**, v. 81, n. 10, p. 4218–4229, Nov. 1984.

6 GAVIN, R. M. et al. Spectroscopic properties of polyenes. III. 1,3,5,7-Octatetraene. **The Journal of Chemical Physics**, v. 68, n. 2, p. 522–529, Jan. 1978.

7 BOUWMAN, Wim G. et al. Fluorescence of gaseous tetraenes and pentaenes. **The Journal of Physical Chemistry**, v. 94, n. 19, p. 7429–7434, Sept. 1990.

8 LEOPOLD, D. G.; VAIDA, V.; GRANVILLE, Mark F. Direct absorption spectroscopy of jet-cooled polyenes. I. The $1^1B_u^+ \leftarrow 1^1A_g^-$ transition of trans,trans-1,3,5,7-octatetraene. **The Journal of Chemical Physics**, v. 81, n. 10, p. 4210–4217, Nov. 1984.

9 HEIMBROOK, Lou Ann; KOHLER, Bryan E.; LEVY, Irvin J. Fluorescence from the 1^1B_u state of trans,trans-1,3,5,7-octatetraene in a free jet. **The Journal of Chemical Physics**, v. 81, n. 4, p. 1592–1597, Aug. 1984.

10 D'AMICO, Kevin L.; MANOS, Christopher; CHRISTENSEN, Ronald L. Electronic energy levels in a homologous series of unsubstituted linear polyenes. **Journal of the American Chemical Society**, v. 102, n. 6, p. 1777–1782, Mar. 1980.

11 CHAGAS, Julio C. V. et al. Low-lying excited states of linear all-trans polyenes: the σ–π electron correlation and the description of ionic states. **Physical Chemistry Chemical Physics**, v. 27, n. 15, p. 7916–7928, 2025.

FOLHA DE REGISTRO DO DOCUMENTO

1. CLASSIFICAÇÃO/TIPO	2. DATA	3. DOCUMENTO Nº	4. Nº DE PÁGINAS
TD	25 de junho de 2025	DCTA/ITA/TD-016/2025	204

5. TÍTULO E SUBTÍTULO:

Electronic Structure of Conjugated Organic Molecules: From Aromaticity to Excited-State Dynamics

6. AUTOR(ES):

Julio Cesar Verli Chagas

7. INSTITUIÇÃO(ÕES)/ÓRGÃO(S) INTERNO(S)/DIVISÃO(ÕES):

Instituto Tecnológico de Aeronáutica – ITA

8. PALAVRAS-CHAVE SUGERIDAS PELO AUTOR:

Electronic structure of molecules; Atomic and molecular physics; Computational and theoretical chemistry.

9. PALAVRAS-CHAVE RESULTANTES DE INDEXAÇÃO:

Estrutura eletrônica; Estados excitados; Estrutura molecular; Química computacional; Física atômica; Física molecular; Química.

10. APRESENTAÇÃO: (**X**) **Nacional** ( ) **Internacional**

ITA, São José dos Campos. Curso de Doutorado. Programa de Pós-Graduação em Física. Área de Física Atômica e Molecular. Orientador: Prof. Dr. Francico Bolivar Correto Machado; coorientador: Dr. Hans Lischka. Defesa em 09/06/2025. Publicada em 2025.

11. RESUMO:

This thesis presents a comprehensive investigation into the electronic structure of conjugated organic molecules, spanning from aromaticity in benzene derivatives to the complex excited-state dynamics of linear all-trans polyenes. In the first study, a detailed multi-component analysis reveals how substituents influence the aromatic character of mono- and disubstituted benzene derivatives. The findings provide the reader with a conceptual toolkit to modulate aromaticity. We show that appropriate π-electron-donating and π-electron-accepting substituents, with suitable size and symmetry, can interact with the ring's π-system and significantly affect π-electron delocalization. The second and third studies focus on the spectroscopic properties of linear polyenes—structures that form the backbone of many chromophores. Particular attention is given to the covalent $2^1A_g^-$ and ionic $1^1B_u^+$ excited states. Using high-level multireference methods, we demonstrate in the second study that while nondynamic correlation is sufficient to describe the covalent state, accurately treating the ionic state requires addressing basis set effects, size-extensivity errors, and, most critically, σ–π electron correlation. This analysis offers the reader a clear prescription for the appropriate multireference treatment of covalent and ionic excited states. In the third study, analytic gradients based on a multireference wavefunction are employed to compute refined adiabatic transition and emission energies, allowing close comparison with experimental results. The insights deepen our understanding of the intricate electronic landscape of polyenes and underscore the challenges involved in bridging theoretical predictions with experimental spectroscopy. Taken together, the results offer detailed insight into how electronic structure evolves across different conjugated systems and electronic states, thereby fulfilling the central aim of this work: to explore the Electronic Structure of Conjugated Organic Molecules: From Aromaticity to Excited-State Dynamics.

12. GRAU DE SIGILO:

(**X**) **OSTENSIVO** ( ) **RESERVADO** ( ) **SECRETO**